1995

Experimental evaluation of the behavior of spirally-reinforced high-strength concrete columns

Annette M. Pieroni
Lehigh University

AUTHOR:

Pieroni, Annette M.

TITLE:

Experimental Evaluation of the Behavior of Spirally-Reinforced High-Strength Concrete Columns

DATE: May 28, 1995

Experimental Evaluation of the Behavior of Spirally-Reinforced High-Strength Concrete Columns

by

Annette M. Pieroni

A Thesis

Presented to the Graduate and Research Committee

of Lehigh University

in Candidacy for the Degree of

Master of Science

in

Civil Engineering

Lehigh University

May 9, 1995

This thesis is accepted and approved in partial fulfillment of the requirements for the Master of Science.

5/9/95
Date

Dr. Stephen Pessiki, Thesis Advisor

Dr. Le-Wu Lu, Chairman
Department of Civil and
Environmental Engineering

Dedicated to my family...

Dad, Mom, Laura, Lisa, Michael, and Renee.

ACKNOWLEDGEMENTS

The research described in this report was sponsored by the National Science Foundation, and was conducted at the Engineering Research Center for Advanced Technology for Large Structural Systems (ATLSS). The ATLSS Center is directed by Dr. John W. Fisher, and is affiliated with the Department of Civil and Environmental Engineering, chaired by Dr. Le Wu-Lu.

I would like to thank Dr. Stephen Pessiki for his enthusiasm and guidance during the research and writing of this thesis. Appreciation is also extended to the technical staff at both the ATLSS and Fritz Laboratories. Also, I am grateful to Keith Webb who assisted in various phases of this project. Great appreciation is given to John Abruzzo for all his technical advice during my entire graduate career.

I extend special thanks to all the friends I have made during my educational experience at Lehigh University, especially; Bill Bruin, Kali Wyncott, Javier Escobedo, and Jim Van Dien.

Finally, I would like to thank my family; Laura, Lisa, Michael, Renee, Mom and Dad, for their never ending love, support, and encouragement. Special appreciation must be given to my brother Michael who introduced me to my first shear and moment diagrams and sparked my interest in structural engineering.

Annette M. Pieroni

May 1995

TABLE OF CONTENTS

LIST OF TABLES

LIST OF FIGURES

ABSTRACT

The concept of using spiral reinforcement to improve the strength and ductility of concrete columns is well understood. As the concrete in a column is compressed axially, it expands laterally. Spiral reinforcement acts to resist this lateral expansion, and both the deformation capacity and strength of the concrete are enhanced.

The present ACI 318 Code approach to the design of spirally reinforced concrete columns is to equate the loss of the strength associated with the spalling of the cover concrete to the strength enhancement of the core provided by the spiral reinforcement. The objective of the code is to provide a more ductile member. This approach was developed for columns made with low or medium strength concretes. However the use of high-strength concrete has become increasingly more popular, and little is known about the structural performance of these high-strength members.

This research investigated the behavior of large-scale spirally-reinforced high-strength concrete columns. A total of 8 specimens of 559 mm (22 in) diameter were designed according to ACI 318 Code and tested in concentric axial compression. These specimens were made with concrete compressive strengths ranging from 34.5 MPa to 69 MPa (5 ksi to 10 ksi). The influence of concrete strength, longitudinal reinforcement, and spiral reinforcement size/pitch on the strength and ductility of the confined column was evaluated.

The tests revealed that the higher strength concrete columns displayed less ductility than the lower strength concrete columns. For the columns tested in this study, an increase in the spiral size and pitch, while maintaining a constant volume of spiral reinforcement lead to an increase in the column ductility. Columns with a higher longitudinal reinforcement ratio were able to maintain peak resistance for a large displacement, but, overall exhibited less ductility as compared to columns with a relatively lower longitudinal reinforcement ratio. First cracking of the cover concrete was observed at a lower load relative to the peak load in the high-strength concrete columns. Two failure modes were observed in the 8 specimens tested. The low-strength concrete columns exhibited bulging type failure mode, and the higher strength concrete columns exhibited an inclined failure plane.

CHAPTER 1

INTRODUCTION

1.1 INTRODUCTION

The concept of using spiral reinforcement to improve the strength and ductility of concrete columns is well understood. As the concrete in a column is compressed axially, it expands laterally. Spiral reinforcement acts to resist this lateral expansion, thereby subjecting the core concrete to a state of multi-axial compression. In this state of multi-axial compression, both the deformation capacity and strength of the concrete are enhanced.

The present ACI 318 Code (1989) approach to the design of spirally-reinforced concrete columns is to equate the loss of the strength associated with the spalling of the cover concrete to the strength enhancement of the core provided by the spiral reinforcement. The objective of the ACI approach is to provide a tougher and more ductile member. This approach was developed for columns made with what today might be considered low- or medium- strength concretes.

The use of high-strength concrete has become increasingly more popular in the last decade. High-strength concrete allows smaller cross-sections and reduced dead loads which is favorable in columns of tall concrete buildings. However, little is known about the structural performance of these members,

particularly whether or not they exhibit adequate toughness to satisfy the intended ACI design concept.

As will be explained in Chapter 2, much of the early research leading to the present understanding of the behavior of spirally-reinforced high-strength concrete columns was obtained from tests of small concrete cylinders. Small specimens were tested due to the limitation of force capacity of the testing machines. The results of these earlier tests suggest that specimens of higher strength concrete possess less ductility than specimens of lower strength concrete. Following this work on high-strength cylinders, additional research has been performed on medium-scale column specimens (cross-section dimensions up to 300x500 mm (11.8x19.7 in)).

1.2 OBJECTIVE

The objective of this research is to study the behavior of large-scale, spirally-reinforced high-strength concrete columns subjected to concentric axial load. The experimental program was developed to specifically evaluate the role of concrete compressive strength and reinforcement details (longitudinal steel and spiral steel) on the strength and ductility of the confined column. The specific objectives follow:

1. Evaluate the influence of high-strength concrete on the ductility of spirally-reinforced concrete columns.

2. Evaluate the influence of longitudinal reinforcement on the ductility of high-strength concrete columns. As described in Chapter 2, the presence of an additional amount of longitudinal reinforcement may increase the column ductility. However, there are conflicting findings on the effectiveness of the longitudinal reinforcement in this role.

3. Evaluate the influence of the spiral reinforcement size/pitch on the strength and ductility of high-strength concrete columns. As described in Chapter 2, reducing the pitch of the spiral reinforcement while maintaining a constant volume of spiral steel may more effectively confine the concrete core. This may produce a column with greater strength and ductility than a similar column with the same amount of spiral reinforcement, but larger pitch.

4. Evaluate the effectiveness of an existing empirical equation for predicting the strength of the confined core of high-strength concrete columns. The equation evaluated in this report is based on the research performed by Martinez et al. (1982) and is presented in Chapter 2.

1.3 SUMMARY OF APPROACH

This research involved 8 tests of large-scale, spirally-reinforced concrete columns in concentric axial compression. The tests were performed in a 22.2 MN

(5000 kip) universal testing machine. The specimens were 559 mm (22 in) in diameter and 2235 mm (88 in) tall. The concrete compressive strengths ranged from 34.5 MPa (5 ksi) to 69 MPa (10 ksi). All the specimens were designed according to the requirements of the ACI 318 Code. The amount of longitudinal steel reinforcement as well as the spacing of the spiral reinforcement was varied within the 8 specimens.

1.4 RESEARCH SIGNIFICANCE

A situation exists today where the practical use of high-strength concrete extends beyond full knowledge of its behavior. This may lead to uncertain margins of safety in structures built with this material. Continuing advances in the production of higher strength concretes, coupled with an increasing willingness by designers to make use of these higher strength materials, further exacerbates the situation.

Much of the research upon which the present understanding of spirally-reinforced concrete columns is based was performed on columns made with low- to medium- strength concrete. Recent tests on columns made with high-strength concrete were made on small- or medium-scale specimens. These tests revealed possible shortcomings in the toughness and ductility of these members. This research will explore the validity of these earlier studies through a program that includes large-scale testing.

Addressing the issue of spirally-confined high-strength concrete columns will provide much needed information to practicing engineers engaged in the design of structures, and may avoid a possible future need for expensive retrofit of inadequate structures. The ACI Committee 363 High-Strength Concrete has identified the ductility of high-strength concrete columns as a priority research need (1984, 1992).

1.5 SCOPE OF REPORT

As mentioned earlier, Chapter 2 presents the background information which explains the concept behind spiral reinforcement and discusses past and recent research performed on confined concrete columns.

Chapter 3 explains the experimental program. A description of the test plan, fabrication of specimens, and instrumentation is provided in this chapter.

Chapter 4 describes the individual specimen tests. An explanation of the general loading procedure is presented along with a summary of observations made during each of the specimen tests.

Chapter 5 presents the results of the tests performed on the 8 columns. The conclusions from these results are also presented.

Chapter 6 summarizes the findings and conclusions from this study. This chapter also outlines areas for future research.

1.6 NOTATION

The following is a list of notation used in this report:

A_c = core area of a spirally reinforced column measured to outside diameter of spiral, mm^2 (in^2);

A_g = gross area of column, mm^2 (in^2);

A_{st} = total area of longitudinal reinforcement, mm^2 (in^2);

A_{sp} = area of a spiral reinforcement bar, mm^2 (in^2);

A_b = area of a longitudinal reinforcement bar, mm^2 (in^2);

d_c = diameter of core of spirally reinforced column measured to outside diameter of spiral, mm (in);

d_g = gross diameter of column, mm (in);

d_{sp} = diameter of a spiral reinforcement bar, mm (in);

d_b = diameter of a longitudinal reinforcement bar, mm (in);

E_c = modulus of elasticity of concrete, MPa (ksi);

E_s = modulus of elasticity of steel, MPa (ksi);

f_c' = compressive strength of concrete, MPa (ksi);

$f_{c\text{-}28}$ = 28-day compressive strength of wet-cured cylinders, MPa (ksi);

$f_{c\text{-}field}$ = compressive strength of field-cured cylinders, MPa (ksi);

$f_{c\text{-}core}$ = compressive strength of cored cylinders, MPa (ksi);

f_{cc} = compressive strength of confined core, MPa (ksi);

f_2 = lateral confinement stress in core concrete produced by spiral reinforcement, MPa (ksi);

f_{ys} = yield strength of spiral reinforcement, MPa (ksi);

f_{yl} = yield strength of longitudinal reinforcement, MPa (ksi);

P_{max} = experimental maximum load sustained by column, MN (kips);

P_n = predicted nominal axial capacity of column, MN (kips);

P_c = predicted axial capacity of confined concrete core based on compressive strength of field cured cylinders, MN (kips);

P_{ccore} = predicted axial capacity of confined concrete core based on compressive strength of cored cylinders, MN (kips);

R_{SF} = ratio of column ductilities defined at first spiral fracture;

R_{85} = ratio of column ductilities defined at 85% of maximum load;

s = pitch of spiral reinforcement, mm (in);

Δ_1 = limiting axial displacement in the linear elastic range of the column response, mm (in);

Δ_{SF} = axial displacement of column at first spiral fracture, mm (in);

Δ_{85} = axial displacement of column at 85% of P_{max}, mm (in);

ρ_s = volumetric steel ratio, computed as the ratio of volume of spiral reinforcement to total volume of core;

ρ_l = longitudinal steel ratio, computed as the ratio of area of longitudinal reinforcement to gross area of concrete;

μ_{SF} = ductility of the column at first spiral fracture, computed as the ratio of the axial displacement at the first spiral fracture to the limiting axial displacement;

μ_{85} = ductility of the column at 85% of maximum load, computed as the ratio of the axial displacement at 85% of maximum load to the limiting axial displacement.

CHAPTER 2

BACKGROUND

2.1 INTRODUCTION

This chapter provides a summary of the literature on confined high-strength concrete columns subjected to concentric axial load. The concept of spiral reinforcement is presented in Section 2.2. Section 2.3 summarizes the research and findings on small-scale, high-strength concrete cylinders, and Section 2.4 details the results of more recent research performed on larger high-strength specimens. Section 2.5 describes the results of an exploratory large-scale, high-strength column test, and Section 2.6 addresses the current ACI 318 Code requirements for spirally confined columns.

In this report the following definitions are adopted: low- strength concretes have compressive strengths less than 41.4 MPa (6 ksi); medium strength concretes have strengths that range from 41.4 to 55.2 MPa (6 to 8 ksi); and, high-strength concretes have strengths that exceed 55.2 MPa (8 ksi).

2.2 STRENGTH ENHANCEMENT PROVIDED BY TRANSVERSE REINFORCEMENT

The concept of using spiral reinforcement in concrete columns has existed for over 90 years. First introduced by Considere in 1899, the idea was explored by many engineers around the turn of the century.

In 1928, Richart, Brandtzaeg, and Brown (1928) reported the results of tests made of 101x203 mm (4x8 in) normal weight concrete cylinders loaded under the action of axial force and various intensities of lateral fluid pressure. They reported that the axial strength and ductility of concrete increased with an increase in lateral fluid pressure. The following equation was presented to predict the axial compressive strength f_c of a cylinder of unconfined strength f_c', under a lateral pressure f_p:

$$f_c = f_c' + 4.1 f_p \qquad (2.1)$$

In a subsequent study, Richart, Brandtzaeg, and Brown (1929) tested a series of 254x1016 mm (10x40 in) spirally-reinforced normal-weight concrete columns under axial compression. The concrete strengths ranged from 13.8 to 20.7 MPa (2 to 3 ksi). The compressive strength of the confined column was related to the lateral confinement stress produced by the spiral steel as:

$$f_c = f_c' + 4.1 f_2 \qquad (2.2)$$

where f_2 is the lateral stress produced by the confining reinforcement. This confinement stress is computed as:

$$f_2 = \frac{2A_{sp}f_{sp}}{d_c s} \qquad (2.3)$$

where A_{sp} is the area of the spiral bar, f_{sp} is the stress in the spiral steel at maximum column load, and d_c and s are the outside diameter and pitch, respectively, of the spiral reinforcement.

Since this early work, other researchers have explored the effects of spiral confinement on column behavior. Chan (1955) reported the test results of 152x305 mm (6x12 in) cylinders constructed with spiral reinforcement and with concrete strengths that ranged from 20.7 to 27.6 MPa (3 to 4 ksi). Chan observed large strength and ductility gains in the cylinders, and credited this to the presence of the spiral reinforcement. Spirals were found to provide about twice as much confinement as an equal volume of rectilinear ties, demonstrating the efficiency of spirals over ties. Chan also reported that the core concrete arched across the gaps of adjacent loops in the spiral reinforcement, and that failure occurred due to excessive deformation of the lateral reinforcement. Iyengar, Desayi, and Reddy (1970) reported the results of a study of 100x200 mm (3.9x7.9 in) and 150x300 mm (5.9x11.8 in) cylinders tested in axial compression. Spiral pitches varied from 30 to 120 mm (1.2 to 4.7 in) and concrete strengths ranged from 13.8 to 34.5 MPa (2 to 5 ksi). Based on their results, Iyengar et al. presented an equation, which can be written in the following form, to represent the increased strength in the core due to the presence of spiral reinforcement:

$$f_c = f'_c + 4.6 f_2 (1 - \frac{s}{d_c}) \quad (2.4)$$

Here the confining stress f_2, computed assuming the spiral steel yields at the maximum column load, is multiplied by the term in parentheses which shows that the confinement becomes less effective as the spiral pitch increases. Essentially, the confinement becomes ineffective as the pitch of the spiral approaches the diameter of the core.

In all of the studies cited above, the concrete strength did not exceed 34.5 MPa (5 ksi). Lack of information about the behavior of spirally reinforced concrete columns made with higher concrete strengths prompted the studies described Section 2.3.

2.3 SMALL-SCALE TESTS OF HIGH-STRENGTH CONCRETE CONFINED BY SPIRAL REINFORCEMENT

Most of the present understanding about the behavior of spirally-reinforced high-strength concrete is based upon studies by Ahmad and Shah (1982a) and Martinez, Nilson, and Slate (1982, 1984).

The earliest tests of high-strength concrete confined by spiral reinforcement were reported by Ahmad and Shah (1982a). Cylinders measuring 76x152 mm (3x6 in) and 76x305 mm (3x12 in) made with concrete strengths ranging from 20.7 to 69 MPa (3 to 10 ksi) were tested in axial compression. Specimens were made

without longitudinal reinforcement or concrete cover. Variables considered included concrete strength, and spacing and yield strength of the spiral reinforcement.

Martinez, Nilson and Slate (1982, 1984) presented the results of an extensive study of spirally-reinforced columns made with both normal weight and lightweight low-, medium-, and high-strength concretes, loaded in axial compression. As with the Ahmad and Shah study, the Martinez et al. study was made on small cylindrical specimens rather than on full-scale columns. Most of the tests were performed on 101x203 mm, 101x406 mm, and 127x610 mm (4x8 in, 4x16 in, and 5x24 in) specimens without concrete cover. In addition, a series of tests were conducted on 152x610 mm (6x24 in) specimens with a protective cover. Concrete strengths ranged from 20.7 to 69 MPa (3 to 10 ksi). None of the specimens contained longitudinal reinforcement. Strains in the spiral reinforcement were measured with strain gages.

The following sections summarize the findings that were obtained from the Ahmad and Shah (1982a) and Martinez, Nilson and Slate (1982, 1984) studies. Included are discussions of the influence of concrete strength, the influence of concrete density, the behavior of spiral reinforcement, the behavior beyond peak resistance, and the observed modes of failure.

2.3.1 Influence of Concrete Strength

Ahmad and Shah evaluated the effectiveness of confinement in terms of two parameters, k_1 and k_2, as follows:

$$f_{oc} = f_o + k_1 (f_r)_p \tag{2.5}$$

$$\epsilon_{oc} = \epsilon_o + k_2 (f_r)_p \tag{2.6}$$

where

f_o, ε_o = stress and strain at peak resistance, respectively, for unconfined specimens;

f_{oc}, ε_{oc} = stress and strain at peak resistance, respectively, for spirally-confined specimens;

$(f_r)_p$ = confining pressure at peak resistance, computed assuming that the spiral reinforcement yielded at peak resistance.

Based on a comparison of k_1 and k_2 values for specimens with a range of concrete strengths and similar confinement, Ahmad and Shah found that the effectiveness of the spiral reinforcement at peak resistance decreased with an increase in concrete strength (k_1 and k_2 values decreased with an increase in concrete strength). However, Ahmad et al. noted that the spiral reinforcement may not have yielded in columns made with higher strength concrete, and that this assumption resulted in lower values of k_1 and k_2 at peak column resistance for these columns.

Based on confining stresses computed from measurements of the strain in spiral reinforcement, Martinez et al. found that the compressive strength of normal weight spirally-confined concrete columns could be computed as

$$f_{cc} = 0.85 f_c' + 4.0 f_2 (1 - \frac{s}{d_c}) \qquad (2.7)$$

which is similar to Equation 2.4. Equation 2.7 was found to be valid for the entire range of concrete strengths considered in the study, including the high-strength concrete. Thus, the effectiveness of spiral reinforcement as a means of enhancing column strength was not diminished for high-strength concrete. However, high-strength concrete did affect many other aspects of behavior as discussed more fully in the sections that follow.

2.3.2 Behavior of the Spiral Reinforcement

Martinez et al. presented a description of the behavior of a spirally-reinforced column divided into three stages. In the first stage, at loads below about 30 percent of the unconfined column strength, the concrete remained essentially elastic, lateral expansion of the concrete was due mostly to the Poisson's effect, and the confining effect of the spiral reinforcement was small. In the second stage, plastic deformation of the concrete lead to a more rapid increase in the spiral steel stress. This continued up to about the unconfined strength of

the column. At this point began the third stage, in which further loading caused a rapid disintegration of the concrete and a great increase in the spiral steel stress.

Martinez et al. observed that both normal weight and lightweight low-strength columns showed all three stages listed above, and that the spiral steel stress in these columns generally reached yield before the column attained peak resistance. In contrast, the spiral steel stress in normal weight high-strength concrete columns was observed to increase almost linearly as load was applied up to the unconfined column strength. Beyond this point, a gradual increase in spiral steel stress was observed. The rate of increase of spiral steel stress in the high-strength columns was less than the rate of increase found in the low-strength concrete columns. Martinez et al. suggested that this behavior was associated with the mode of failure of these columns. As discussed in the next section, failure in the normal weight high-strength concrete columns occurred by the development of a single shear plane rather than by a bulging mechanism.

An analytical model presented by Ahmad and Shah (1982a) predicted that the spiral steel stresses at peak column resistance were lower in columns made with high-strength concrete as compared to columns made with lower strength concrete. This was attributed to a smaller lateral strain in the high-strength concrete at peak resistance as compared to lower strength concrete [Ahmad and Shah (1982b)]. In the experiments performed by Ahmad and Shah (1982a), strain gages were not placed on the spiral reinforcement to confirm this finding. However, strain measurements made in the tests reported by Martinez et al.

support this prediction. Specifically, Martinez et al. found that none of the spiral steel stresses reached yield at maximum column resistance in the high-strength concrete columns.

Martinez et al. reported that lightweight, high-strength concrete columns exhibited similar behavior to the normal weight high-strength columns, except that the spiral steel stress increased rapidly at loads close to the peak resistance. Similar to the normal weight, high-strength concrete columns, the stresses in the spiral steel at peak resistance were below yield in the lightweight, high-strength concrete columns.

2.3.3 Behavior Beyond Peak Resistance

Ahmad and Shah reported that the slope of the post peak portion of the load deformation plot was steeper for columns made with higher strength concrete as compared to columns made with lower strength concrete.

Experimental axial stress-strain curves obtained from tests of 101x406 mm (4x16 in) normal weight columns by Martinez et al. are shown in Figure 1. These specimens were made without concrete cover. Three groups of curves corresponding to low-, medium-, and high-strength concrete specimens are identified in each figure. Each group is comprised of three sets of curves corresponding to three different amounts of spiral reinforcement. Indicated in each set of curves is the average unconfined cylinder strength f_c'. It is important to note that in each

strength group, the columns with the least confinement have the amount of spiral reinforcement that would be required by the ACI 318 Code.

This figure shows very clearly the rapid decrease in resistance that occurred beyond the peak resistance for normal weight high-strength columns of all strengths. The high-strength concrete columns showed a rapid decrease in load after the maximum load was obtained even when confined effectively by high amounts of spiral reinforcement. In contrast, the low-strength concrete columns displayed a great amount of plastic deformation without significant decrease in load.

2.3.4 Failure Modes

Three different modes of failure were observed in the tests reported by Martinez et al.:

1. bulging of the column at a location along its length followed by rupture of one or more spirals;

2. excessive lateral bending of the column; and,

3. formation of an inclined failure plane through the column.

These 3 failure modes were found to be dependent upon many factors, most notably the concrete strength.

In the tests of 152x610 mm (6x24 in) columns made with protective cover, Martinez et al. observed that the behavior of low-strength concrete columns were characterized by a gradual spalling of the concrete shell, and a continued increase in the strain in the spiral reinforcement. In contrast, the concrete covers of medium-strength concrete columns were observed to fail rather suddenly. For both the low-and medium-strength concrete columns, failure ultimately occurred in either mode 1 or mode 2, and both failure modes were gradual.

Under the action of axial compression, concrete covers in high-strength concrete columns were observed to fail in a rather sudden and brittle manner, similar to the medium strength concrete columns. As additional load was applied to these columns, failure was observed to occur in mode 3, the formation of a shear plane through the column.

Martinez et al. concluded that the failure of normal weight spirally-reinforced columns is controlled by a compression-shear mechanism, regardless of concrete strength. They further state that the bulging failure observed in the low strength concrete columns may actually have been a network of failure planes rather than a single distinct failure plane as found in the high-strength concrete columns. The limited ductility observed in high-strength concrete columns is due in part to the unique failure mode in these members.

2.4 LARGE-SCALE AXIAL LOAD TESTS OF CONFINED HIGH-STRENGTH CONCRETE COLUMNS

The work reviewed in Section 2.3 was limited to tests of spirally confined cylinders (no longitudinal reinforcement) with a maximum diameter size of 152 mm (6 in). This section of the report summarizes previous research on the axial load behavior of large-scale, confined, high-strength concrete columns. The summary focusses primarily on spirally confined and tied columns. Results of tests of columns with compressive strengths up to 124 MPa (18 ksi) and cross sections as large as 300x500 mm (11.8x19.7 in) are included in this summary.

A recent paper by Razvi and Saatcioglu (1994) reports on the strength and deformability of confined high-strength concrete columns based on available experimental data. This paper will be used as the basis of this summary, however this review will only summarize those findings dealing with columns tested under concentric axial load. Topics included in the summary include, influence of concrete strength, influence of longitudinal reinforcement, influence of spiral reinforcement size/pitch, behavior of concrete cover, observed failure modes, and size effects of test specimens.

2.4.1 Influence of Concrete Strength

The compressive strength, strain at maximum stress, and ductility are known to increase with an increase in lateral confinement (Galeota et al. 1992).

However, the amount of this increase was observed to be less in high-strength concrete than in normal-strength concrete.

Saatcioglu and Razvi (1993) performed tests on 250x250 mm (9.8x9.8 in) tied columns ranging in concrete strength from 81 to 124 MPa (11.8 to 18.0 ksi). Comparisons were made between columns with the same amount of lateral and longitudinal reinforcement, but with varying concrete strengths. These tests showed that although there is an improvement in the deformability of the column, it is not proportional to the increase in the volumetric ratio of lateral reinforcement; a significantly higher volumetric ratio is required for high-strength concrete columns in order to achieve deformations usually expected from normal-strength concrete columns.

Bjerkeli, Tomaszewicz, and Jensen (1990) also reported on a reduced effectiveness of spiral reinforcement in high-strength concrete. Bjerkeli et al. performed tests on 21 small-scale circular columns 150 mm (5.9 in) in diameter with concrete strengths ranging from 62.5 MPa (9.1 ksi) to 99.6 MPa (14.4 ksi). The volumetric ratio was varied from 1.1% to 3.1%. Bjerkeli et al. reported that there was no significant increase in column ductility when only a 1.1% volumetric ratio was used, but a 3.1% volumetric ratio did increase the column ductility.

Galeota and Giametteo (1992) performed tests on 150 mm (5.9 in) square columns with a concrete compressive strength of 65 MPa (9.4 ksi). The columns were reinforced with three amounts of lateral reinforcement (rectilinear steel ties); 0.01, 0.015, and 0.03. The results from these tests showed an increase in the

compressive strength and ductility of the confined core as the degree of confinement increased as compared to the unconfined concrete. However, the increase in compressive strength and ductility in the high-strength concrete with the same degrees of confinement was less than for lower strength concrete.

Azizinamini, Paultre, and Saatcioglu (1993) have summarized the findings of Cusson and Paultre and Nagashima, Sugano, Kimura, and Ichikawa. Cusson et al. and Nagashima et al. have found similar results to Saatcioglu et al. (1993) and Bjerkeli et al. (1990) relating to the influence of concrete strength.

2.4.2 Influence of Longitudinal Reinforcement

Studies have been performed to determine whether or not longitudinal reinforcement plays a role in the ductility of high-strength concrete columns. Conflicting views exist concerning the beneficial effect of increasing the longitudinal steel ratio. The longitudinal steel ratio can be increased by either increasing the diameter of the bars or by increasing the number of bars.

Saatcioglu et al. (1993) compared columns with varying longitudinal steel, eight bar and twelve bar configurations. As long as the longitudinal reinforcement was adequately distributed and laterally supported, they reported a noticeable improvement in both the peak strength and ductility of high-strength concrete columns.

Bjerkeli et al. (1990) also studied the effects of longitudinal reinforcement on column ductility. The effects of increasing the number of bars and the effects

of increasing the bar diameter were studied in two separate comparisons. These columns were 300 x 500 mm (11.8 x 19.7 in) and ranged from 83.1 to 107.6 MPa (12 to 15.6 ksi). Specimens reinforced with 12 longitudinal bars were compared to specimens with 18 longitudinal bars. Bjerkeli et al. reported a significant influence on the ductility of large-scale columns due to the number of longitudinal bars. Those reinforced with more bars sustained the ultimate load, whereas the axial load of the specimens with 12 longitudinal bars decreased immediately after peak load. However, there was no significant effect on the stress-strain behavior of the confined concrete core due to the different longitudinal bar diameters.

Itakura and Yagenji (1992) compared specimens with and without longitudinal reinforcement. These specimens were 218 mm (8.6 in) square with a concrete compressive strength of 74 MPa (10.7 ksi). The columns which were longitudinally reinforced exhibited a strength decrease at lower levels of strain as compared to the columns which were not reinforced. The lateral reinforcement fractured at the locations of buckled longitudinal bars. This buckling of the longitudinal bars was reported as the primary cause of the decrease in strain capacity.

Nagashima, Sugano, Kimura, and Ichikawa (1992) reported on 225 mm (8.86 in) square columns ranging in concrete strength from 59 MPa to 118 MPa (8.6 ksi to 17.1 ksi). No significant difference in the strength and ductility for specimens reinforced with 12, 8, or 6 longitudinal bars was found.

2.4.3 Influence of Spiral Reinforcement

As stated earlier in Section 2.2, the reduction of spiral spacing increases the effectiveness of the confining reinforcement which increases the compressive strength of the confined core. Nagashima et al. (1992) compared columns with the same amount of confinement reinforcement but with varying tie spacing. These tests showed a strength increase in the core of the columns with closer spaced ties, however there was no apparent difference in the ductilities of these specimens.

2.4.4 Behavior of Concrete Cover

A phenomena observed in high-strength concrete column tests has been the early failure of the cover concrete. Saatcioglu et al. (1993) reported that spalling of the cover concrete occurred at approximately 70% of the unconfined concrete strength. This failure is more pronounced in columns with closely spaced spiral reinforcement, because the reinforcement physically separates the cover concrete from the core concrete. This is explained as an instability of the shell concrete at high compressive stresses. The peak strains developed in the cover concrete at the time when the contribution of the cover concrete is negligible are much lower than the strains associated with crushing of concrete. Therefore, it is suggested that while $0.85f_c'$ may be accurate to determine the force in the core concrete, it overestimates the contribution of the shell (Razvi et al. 1994).

In the summary by Azizinamini et al. (1993) Cusson and Paultre tested thirty 235 mm (9.25 in) square columns with concrete strengths ranging from 55.6 MPa to 113.6 MPa (8.1 ksi to 16.5 ksi). Cusson et al. reported a sudden failure of the cover concrete to be characteristic of the high-strength concrete columns. This lead to a reduced axial capacity in the column before the lateral confinement became effective.

2.4.5 Failure Modes

In recent tests a formation of a single failure plane in high-strength columns as reported by Martinez et al. (1984) was also observed by Bjerkeli et al. (1990), and Nagashima et al. (1992). In the tests performed by Nagashima et al. all the specimens with concrete strengths greater than 98 MPa (14.2 ksi) had buckled longitudinal bars and fractured spirals which defined a diagonal failure plane.

However, this failure mechanism also existed in columns with lower strength concrete. Mander, Priestley, and Park (1988) tested 500 mm (19.7 in) diameter columns with concrete compressive strengths of 28 MPa (4.0 ksi). Mander reported a "strongly defined diagonal failure plane" characteristic of columns with small amounts of spiral reinforcement (a volumetric ratio ρ_s less than 0.02). Columns with a volumetric ratio greater than this lacked a well defined failure plane.

2.4.6 Size Effects

Ahmad and Fattah (1991) proposed a model for the strength enhancement which included effects due to specimen size. In their model, as the diameter of the specimen increases, the strength enhancement factor decreases. Ahmad et al. suggests that the beneficial effects of lateral confinement seen in test cylinders may be less for large columns. Even though a concern exists regarding size effects, most of the research reported on high-strength concrete is based on tests conducted on small-scale specimens.

An exploratory test performed by Mielich and Pessiki (1991) involved one 508 mm (20 in) diameter column with a concrete compressive strength of 66.2 MPa (9.6 ksi) designed according to ACI 318 code provisions. Results from this test indicated that the strength lost due to the spalling of the shell was not replaced by an equivalent strength enhancement of the core due to the confining action of the spirals. The following section discusses in more detail the results from this exploratory test.

2.5 EXPLORATORY LARGE-SCALE TEST OF SPIRALLY-REINFORCED HIGH-STRENGTH CONCRETE COLUMNS

The large-scale column tested by Mielich and Pessiki (1991) was treated as a 2/3-scale model and designed according to ACI 318 Code provisions for spiral reinforcement. The specimen was reinforced with 12-#8 longitudinal bars and a #3 spiral at 38 mm (1.5 in) pitch.

Contrary to observations made on small-scale specimens, spalling of the concrete cover occurred in a rather gradual manner. The cover had completely spalled away from the core prior to peak resistance of the column. Failure of the column occurred due to an abrupt formation of a single failure plane along an inclined axis through the column. Continued loading caused sliding of the column along this failure plane, accompanied by buckling of the longitudinal reinforcing bars where they intersected this plane.

Results from this single exploratory test indicate that the strength of the concrete core is not increased due to confinement as predicted by equations presented in Section 2.2. The strength loss due to the spalling of the concrete cover was not replaced by an equivalent strength enhancement of the column core. This analysis of the test results was based on concrete compressive strengths obtained from tests of field-cured cylinders.

In addition to the lack of strength enhancement, the column displayed a lack of ductility. After the formation of the failure plane, a large decrease in the axial load capacity of the column occurred. This large decrease in resistance occurred at an axial displacement of about 13 mm (0.5 in).

2.6 DISCUSSION OF CURRENT ACI 318 CODE REQUIREMENTS

Equations 2.8 and 2.9 from the ACI 318 Code are used to design spirally reinforced concrete columns. The nominal capacity of the column is computed

using Equation 2.8, and the minimum amount of spiral reinforcement is calculated using Equation 2.9.

$$P_n = 0.85 f'_c (A_g - A_{st}) + A_{st} f_{yl} \tag{2.8}$$

$$\rho_s = 0.45 \left(\frac{A_g}{A_c} - 1\right) \frac{f'_c}{f_{ys}} \tag{2.9}$$

Martinez et al. concluded that the current equations in the ACI 318 Code adequately predicted the strength of spirally-reinforced normal weight concrete columns for the range of concrete strengths examined. In fact, the equations were found to under predict the axial strength of low strength concrete columns because the shell concrete had not spalled away completely and therefore remained somewhat effective in carrying vertical compression. However, because spiral reinforcement designed according to code provisions is intended to increase member ductility, the current equations appear to be inadequate.

It is important to note that the current edition of the ACI 318 Code and Commentary (1989) makes no mention of the reduced ductility likely to be found in high-strength concrete columns. Instead, the Commentary states that tests of columns provided with spiral reinforcement as specified by the Code "exhibit considerable toughness and ductility." This statement is not supported by the experimental evidence reviewed in Sections 2 and 3 on high-strength concrete

columns. Accordingly, the continued use of normal weight high-strength concrete in spirally-reinforced columns may be regarded as inconsistent with the intent of the Code.

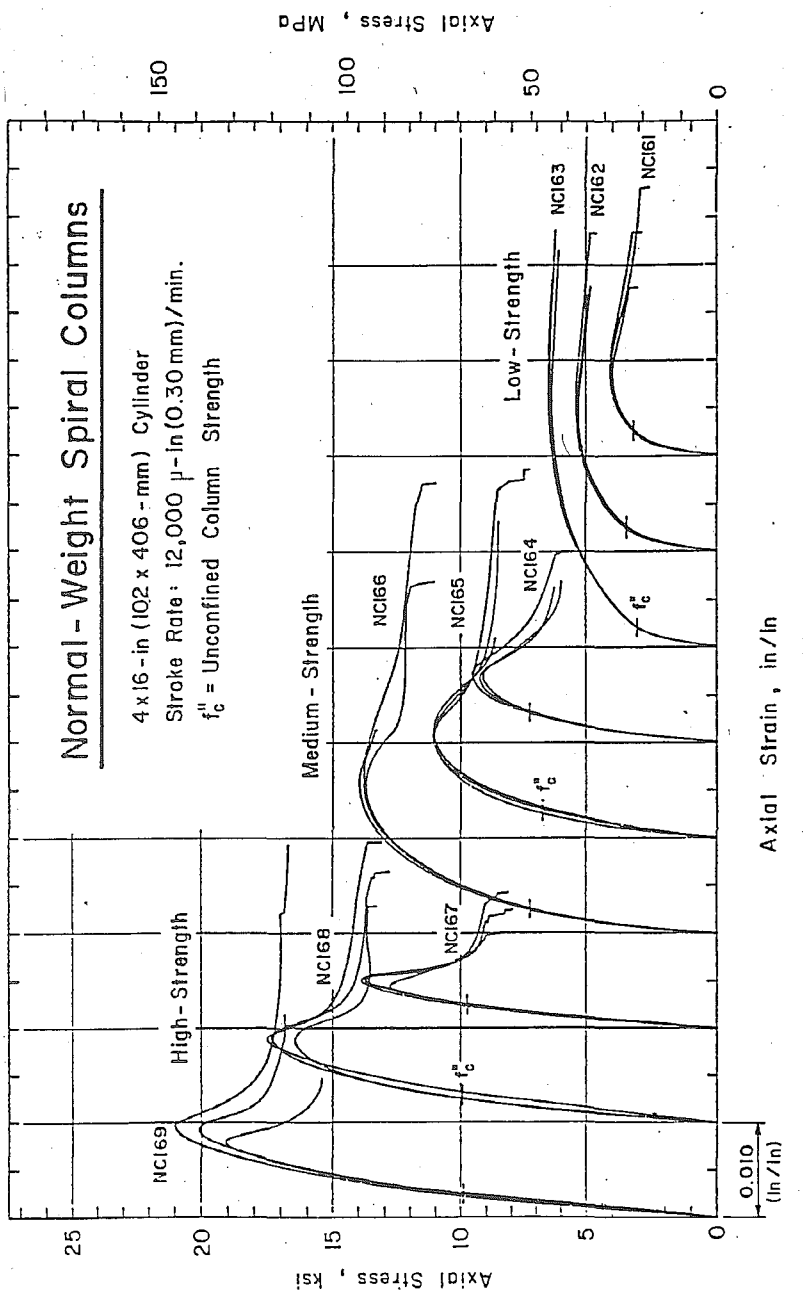

Figure 2.1 Axial stress-strain curves for normal weight concrete [Martinez et al. (1982)].

CHAPTER 3

DESCRIPTION OF EXPERIMENTAL PROGRAM

3.1 INTRODUCTION

This chapter provides a detailed description of the experimental program. Section 3.2 reviews the research objective and presents the test matrix. Section 3.3 describes the specimen details, and Section 3.4 describes the instrumentation used to evaluate the behavior of the column. Specimen fabrication details are discussed in Section 3.5, and Section 3.6 summarizes the material properties.

3.2 TEST PROGRAM

3.2.1 Review of Objective

The objective of this research, as previously stated in Chapter 1, is to study the behavior of spirally-reinforced, high-strength concrete columns subjected to concentric axial load. The experimental program was developed to specifically evaluate the role of concrete compressive strength and reinforcement details (longitudinal reinforcement and spiral reinforcement) on column ductility.

3.2.2 Test Matrix

The test matrix is presented in Table 3.1. A total of 8 columns were tested in this research. The primary variables included concrete compressive strength, longitudinal steel ratio, and spiral steel size/pitch. The prefixes "L", "M", and "H"

denote in a relative sense low, medium, and high concrete compressive strengths. Two specimens were designed in the L-Series, L1 and L2, and 3 specimens in each of the M- and H-Series, M1, M2, and M3 and H1, H2, and H3, respectively.

All of the specimens were designed according to ACI 318 Code requirements for spiral reinforcement with nominal design material strengths (actual material strengths deviated from the nominal design material strengths as discussed later in Section 3.6). Two different longitudinal steel ratios were considered. The design yield strength for the longitudinal and spiral steel was 414 MPa (60 ksi). Specimens L1 and L2 were designed for a concrete compressive strength of 34.5 MPa (5 ksi). Specimens M1, M2, and M3 were designed for a concrete compressive strength of 69 MPa (10 ksi). Unfortunately the actual concrete strength for Specimens M1, M2, and M3 was much lower than the intended design strength. Consequently, for the purpose of this study, these specimens are treated as "medium" strength concrete specimens (M-Series). Three additional specimens, H1, H2, and H3 were designed for a concrete strength of 69 MPa (10 ksi).

As previously discussed, the test matrix was arranged in order to evaluate the influence of concrete compressive strength, longitudinal steel ratio, and spiral steel size/pitch upon the strength and ductility of high-strength concrete columns. Table 3.2 summarizes the specimens which can be compared to help evaluate the influence of each of these variables on the behavior of the columns. Three major comparisons can be made:

1. The influence of concrete strength can be evaluated by comparing the specimens with similar longitudinal configurations (i.e. the results of L1, M1, and H1; and the results of L2, M2, M3, H2, H3).

2. The influence of longitudinal steel ratio ρ_l on column ductility for a given f_c' and ρ_s can be evaluated by comparing Specimens L1 and L2, M1 and M2, and H1 and H2.

3. The role of spiral steel size/pitch for a given ρ_s, f_c', and ρ_l can be evaluated by comparing Specimens M2 and M3 and Specimens H2 and H3.

When comparing the results of these eight column tests, it must be kept in mind that the amount of spiral reinforcement provided for the M-Series specimens is greater than that required by the ACI 318 Code. This is because the actual concrete strength in this series was approximately 25% lower than the nominal design concrete strength.

3.3 SPECIMEN DETAILS

As noted earlier, each column was designed according to ACI 318 Code requirements. Two different longitudinal steel ratios were considered. The longitudinal and spiral reinforcement provided in each specimen is summarized in

Table 3.3. Figures 3.1 (a) and (b) show the two different longitudinal reinforcement configurations and the column cross-sectional dimensions. The 8-#8 bars provided a ρ_l equal to 1.65% and the 16-#9 bars provided a ρ_l equal to 4.20%.

Two different spiral steel sizes/pitches were also considered. Within the M- and H-Series, Specimens M3 and H3 had a reduced spiral steel size/pitch as compared to Specimens M2 and H2. The volume of spiral steel and the amount of longitudinal steel in these specimens remained constant.

3.4 INSTRUMENTATION

Electrical resistance strain gages and linear variable differential transformer (LVDT) displacement transducers were used to evaluate the behavior of the columns. The strain gages were used to monitor strains in the longitudinal and spiral reinforcement, and the displacement transducers were used to monitor axial deformations. Two different instrumentation plans were used, referred to here as plan A and plan B. The L- and M-Series specimens were tested with instrumentation plan A, and the H-Series specimens were tested with instrumentation plan B.

For instrumentation purposes the total height of each column was divided into 5 sections as shown in Figure 3.2. The 5 sections included two 280 mm (11 in) sections at each end of the column, and three 559 mm (22 in) sections in the middle region of 1676 mm (66 in). As shown in Figure 3.2, each section was numbered 1 through 5 from bottom to top, respectively. The cross section of the column is divided by two axes labelled North, South, East, and West.

3.4.1 Instrumentation Plan A

The L- and M-Series specimens were tested with instrumentation plan A. A total of 12 strain gages and 15 displacement transducers were used in this plan. A schematic of the layout of the gages is presented in Figure 3.3. Four gages were located on the longitudinal reinforcement and 8 gages were located on the spiral reinforcement. The longitudinal bars were gaged at mid-height of the column on diametrically opposite bars and labelled L1 through L4. The gages were placed here to detect first yielding of the longitudinal bars at mid-height of the column. The first 4 spiral gages were equally spaced around the circumference of the spiral cage at mid-height of the column, and labelled S1 through S4. These gages measured tensile strains that developed in the spiral reinforcement due to the dilation of the concrete core. The remaining 4 gages were located on the north face on the spirals at 559 mm (22 in), 838 mm (33 in), 1397 mm (55 in), and 1676 mm (66 in), and labelled S5, S6, S7, and S8 respectively. The strains measured by these gages showed the variation of the tensile strains in the spiral reinforcement along the height of the column.

Figure 3.4 shows the layout of the LVDTs on the column. As shown in Figure 3.5, the LVDTs were held in wooden blocks which were clamped together with brass bolts. These blocks were then mounted to the threaded bars via an aluminum plate. Five LVDTs were placed at each of the five sections on the north face, and were thus labelled DN1, DN2, DN3, DN4, DN5. These 5 LVDTs measured axial deformations within their respective sections. The remaining 3

faces, south, east, and west, were instrumented at the middle 3 regions only. The remaining LVDT measured overall head travel of the testing machine, and was labelled DHT.

3.4.2 Instrumentation Plan B

The three H-Series specimens were tested using instrumentation plan B. These specimens had a total of 7 LVDTs and 19 strain gages. Figure 3.6 shows the strain gage locations and nomenclature for instrumentation plan B. Ten gages were placed on 2 longitudinal bars diametrically opposite of one another. Each bar was gaged at 5 locations along the height of the bar. L1 and L6 were placed at 305 mm (12 in), L2 and L7 were placed at 711 mm (28 in), L3 and L8 were placed at 1118 mm (44 in), L4 and L9 were placed at 1524 mm (60 in), and L5 and L10 were placed at 1930 mm (76 in). The increase in the number of longitudinal strain gages from plan A to plan B was intended to help capture any localized yielding in the longitudinal reinforcement along the height of the column. The remaining 9 gages were placed on the spiral reinforcement. These gages were located on the north face starting at 305 mm (12 in) from the bottom and at every 203 mm (8 in) to 1930 mm (76 in). The gages were labelled S1 through S9, bottom to top, as shown in Figure 3.6. Again these spiral strain gages were placed here to measure the tensile strain that developed in the spiral reinforcement as the column core expanded laterally.

Figure 3.7 shows the layout of the displacement transducers for instrumentation plan B. These LVDTs were also mounted to the threaded bars via an aluminum plate as shown in Figure 3.5. Six of the displacement transducers were used to measure axial deformation over the middle 3 regions of both the east and west faces. Again the remaining LVDT was used to measure test machine head travel displacement, i.e. total axial displacement.

3.4.3 Instrumentation Protection

Several measures were taken to protect the strain gages from damage during concrete placement, and to protect the LVDTs from falling debris during testing of the column.

The protection system applied to the strain gages prior to concrete placement was as follows. After the gages were bonded to the reinforcement and the lead wires were attached, the gages were coated with poly-urethane. Next, a coat of liquid rubber was applied generously over the entire gage area, then mastic tape was placed over the gage and lead wires. A strip of foil tape was then placed around the mastic tape and reinforcing bar. This foil tape was then sealed at the ends with an epoxy.

Aluminum plates were used to armor the instrumentation as shown in Figure 3.8. These plates were 152 mm (6 in) wide and 1930 mm (76 in) long, and shielded the LVDTs from concrete debris. The plates were slotted to allow free

movement past the threaded bars anchored in the column. Additional measures were taken to protect the instrumentation from debris, as described in Section 3.5.

3.4.4 Data Acquisition System

A schematic drawing of the data acquisition system is presented in Figure 3.9. The data acquisition system consisted of the strain gages and displacement transducers, power supplies, strain gage signal conditioners, analog to digital (A/D) converter, computer, and monitor. The output signals from the signal conditioners and the displacement transducers were wired to 2 high speed, programmable data acquisition boards which translated the information from an analog signal to a digital signal. Each channel's reading was an average of 20 high speed samples. The information was then processed by a computer program and displayed to a computer monitor which allowed the user to monitor the column behavior during testing. Specimen information displayed to the computer monitor was updated every 3 seconds.

A computer program was written in BASIC programming language to retrieve, process, display, and save data during testing. The program allowed the user to balance channels, save data to the hard drive at specified time intervals or command, change the time interval between data saves, and toggle between display screens. Two display screens were created to display all the necessary channels, and allowed the behavior of the column to be easily monitored during testing. A photograph of the computer monitor during testing is presented in

Figure 3.10. The screens allowed the user to monitor specific channels during testing, and permitted real-time plotting of 3 separate graphs: load versus deflection; load versus longitudinal steel strain and load versus spiral steel strain.

3.5 SPECIMEN FABRICATION DETAILS

3.5.1 Construction of Reinforcement Cages

Each coil of spiral reinforcement was comprised of one complete helical spiral, i.e. without any lapped splices. The appropriate longitudinal bars were wire tied to the spiral reinforcement to complete the cages. The pitch of the spiral reinforcement at each end of the cage was reduced to provide extra confinement in an attempt to prevent premature failure in the end regions. At one end the longitudinal bars were welded to a 914 x 914 x 19 mm (36 x 36 x 3/4 in) steel base plate. The base plate provided stability to the column during handling and concrete placement. Several completed cages are shown in Figure 3.11.

Circular cardboard forms were used to construct the columns. After the base plate and cage construction was complete, the circular formwork was lowered over the top of the steel cage by a crane, and 4 wooden staffs 2.44 m (8 ft) long acted to guide the form over the cage. A photograph of the preparation of the formwork for placement over the steel cage is shown in Figure 3.12. As it was lowered, the lead wires to the strain gages were carefully pulled through pre-drilled holes in the formwork. The wooden staffs were later removed and replaced by short lengths of 38 mm (1.5 in) chairs. After the form was securely in place, 38

mm (1.5 in) long plastic sheaths were slipped over the strain gage lead wires and fitted inside the drilled holes. These sheaths were used to protect the lead wires during testing, as the wires were able to slip through the sheath as the concrete cover spalled from the column.

In addition to the sheaths described above, polystyrene inserts were also cast into the concrete around each threaded bar. The 50.8 mm (2 in) diameter, 25.4 mm (1 in) thick inserts were located within the cover concrete and created a pocket around each threaded bar (Figure 3.5). This was done in an attempt to protect the threaded bars from deflecting under heavy pieces of cover concrete. However, this protection system proved to be largely ineffective, and axial displacement measurements beyond the point when significant spalling of the cover concrete occurred, are not considered to be very reliable, except for the measurement of head travel.

3.5.2 Concrete Placement

All columns were oriented in a vertical position during casting, and concrete was placed in the column in approximately 4 or 5 lifts. The concrete was placed with a bucket, and the columns were consolidated with an electrically powered internal submersion vibrator at each of the lifts.

Three separate pours were made, one each for the L-, M-, and H-Series specimens. Ready-mixed concrete was used in all cases. Table 3.4 summarizes the mixture proportions provided by the ready-mix supplier.

The L-Series and M-Series columns were cured in the cardboard formwork for 14 days, during which time the tops of the columns were covered with wet burlap and plastic sheeting. After this time period the formwork was removed. The H-Series columns were cured in a similar manner except that the formwork remained in place for 21 days after casting.

3.5.3 Placement of Columns in the Testing Machine

All the columns were tested in concentric compression in a 22.2 MN (5000 kip) capacity universal testing machine. The steel base plate of each specimen rested against the steel base in the testing machine. The tops of the columns were grouted in place with hydrostone, however a plastic sheet was placed between the hydrostone and machine head before the machine head was lowered against the specimen. The tops of two of the columns (Specimens H2 and H3) were considered too uneven to allow proper capping with hydrostone. Instead a high-strength epoxy-based grout was placed on the tops of these columns to level the surface. The grout had a 1-day strength of 76 MPa (11 ksi). The tops of the columns were then grouted in place with hydrostone. When these columns were grouted in place, Specimen H2 had a thin steel plate placed between the hydrostone and the machine head. This specimen failed in a region very near the top of the column, and it was unclear whether the capping system may have contributed to the observed failure in this specimen. Similar failures were

observed in some of the small-scale specimens tested by Martinez et al. Specimen H3 was grouted directly to the machine head without a thin steel plate.

3.6 MATERIAL PROPERTIES

3.6.1 Reinforcement Steel Properties

Table 3.5 summarizes the material properties of the longitudinal and spiral reinforcement. Tension tests were performed on the longitudinal bars to determine yield and ultimate strengths. The tests were conducted on a 133 KN (300 kip) load-controlled testing machine. In each test, reinforcement bars with a clear distance between machine grips of approximately 254 mm (10 in) were loaded to failure, and a load-deflection plot was generated. The yield load and ultimate load were taken from this plot.

Material properties for the spiral reinforcement are listed in Table 3.6, and are as provided on mill test reports from the reinforcement supplier. Tension tests were also made on short lengths of spiral reinforcement that were cut and straightened from the coiled spiral. These tests were inconclusive, and it was decided that the mill tests would be used for the reinforcement properties of the spirals.

3.6.2 Concrete Properties

Concrete compressive strengths were determined by performing compression tests on 3 different types of cylindrical specimens: wet-cured prepared

cylinders ($f_{c\text{-}28}$), field-cured prepared cylinders ($f_{c\text{-}field}$), and cores ($f_{c\text{-}core}$), as illustrated in Figure 3.13. The wet-cured prepared cylinders were used to determine the 28-day compressive strengths of the different concrete mixtures. The field-cured cylinders and cores were intended to be more representative of the actual concrete in the columns.

The wet-cured and field-cured cylinders measured 152 mm (6 in) in diameter and 305 mm (12 in) high and were made according to ASTM C-31 procedures. These cylinders were cast in plastic cylinder molds and covered with wet burlap and plastic sheeting for the first 24 hours after casting. The wet-cured cylinders were stripped from their molds after about 24 hours after casting and placed in lime-saturated curing baths. The field-cured cylinders were stripped from their molds at the same time the columns were stripped from their forms. The field cured cylinders were tested at approximately the same age as the columns were tested.

The core specimens were extracted from a plain concrete column that was cast along with each set of reinforced columns. Procedures as outlined by ASTM C-42 were approximately followed to extract these cores. The cores were cut from the column with an electric coring machine, and the ends of the cores were then saw cut to obtain smooth and parallel ends. Figure 3.14 shows the locations at which the cores were extracted from the columns. The cores were tested at approximately the same age as the columns were tested.

It is thought that of the three types of concrete strength specimens (wet-cured, field-cured, and cored cylinders), the concrete in the cored cylinders better represented the concrete in the columns, because they both underwent the same consolidation and experienced the same moisture and temperature histories. As shown schematically in Figure 3.13, a thermocouple was placed in the plain column and a field cured cylinder to monitor temperatures. Figure 3.15 shows the variations in temperature between the different strength concretes and different size specimens.

All the cylinders were tested in compression in a 3584 KN (800 kip) displacement-controlled testing machine. The cylinders were capped with a sulfur mortar compound according to ASTM C-617 specifications and tested according to ASTM C-39. All cylinders were tested at a displacement rate of 1.4 mm/min (0.055 in/min), which is approximately equal to the ASTM prescribed rate of 1.5 mm/min (0.05 in/min).

In reporting the concrete compressive strengths, a length to diameter correction factor was applied to the cored cylinders. The correction factor for the normal-strength cored cylinders was based on ASTM C-42 provisions. These provisions are only good for concrete strengths less than or equal to 41.4 MPa (6.0 ksi). The correction factor for the higher strength concretes was based on a study by Bartlett et al. (1994). Equation 3.1 was found to accurately predict the length to diameter correction factor for concrete compressive strengths up to 96.5 MPa (14 ksi).

$$CF = 1 + (-0.144 + 0.027 Z_{wd} + 0.003 \frac{f_{c\text{-}NS}}{1000})(2 - \frac{l}{d})^2 \qquad (3.1)$$

where Z_{wd} = indicator variable for core moisture condition, =0 for air dried, =1 for soaked, =0.5 for sealed. (cores were air dried).

$f_{c\text{-}NS}$ = average strength of concrete core specimens with constant length to diameter ratio between 1 and 2.

l = length of cored specimen.

d = diameter of cored specimen.

The compressive strengths of the cored cylinders with the corresponding correction factors are tabulated separately in Table 3.6. The average concrete compressive strengths of the wet-cured, field-cured, and cored cylinders are presented in Table 3.8.

The specimen details with actual material properties are summarized in Table 3.9. The volumetric ratio of the spiral reinforcement reported is the based on the actual amount of spiral steel provided in the specimen. The actual pitch

values were rounded-off to the nearest 1 mm (0.04 in) from the design pitch values required by the ACI 318 Code (Equation 2.9). Two concrete strengths are reported, namely the day of column test field-cured cylinder strengths and the cored cylinder strengths.

	Reinforcement			
Concrete Strength	Longitudinal Steel Ratio		Spiral Steel size/pitch	
	4.20%	1.65 %	#5/64 mm	#4/41 mm
low	L1	L2	-----	-----
medium	M1	M2, M3	M2	M3
high	H1	H2, H3	H2	H3

25.4 mm=1 in

Table 3.1 Test matrix.

	TEST VARIABLES							
	Concrete Strength		Longitudinal Steel			Spiral Steel		
Specimen	ρ_l		f_c'			f_c'		
	4.20%	1.65%	Low	Medium	High	Low	Medium	High
L1	A		C					
L2		B	C					
M1	A			D				
M2		B		D			F	
M3		B		D			F	
H1	A				E			
H2		B			E			G
H3		B			E			G

Table 3.2 Comparison of specimens to evaluate the influence of test variables.

Table 3.3 Summary of reinforcement provided in each specimen.

Specimen	Spiral Reinforcement				Longitudinal Reinforcement			
	bar size	A_{sp} (mm^2)	s (mm)	ρ_s %	bar size	No. of bars	A_{st} (cm^2)	ρ_l %
L1	#3	71	44	1.32	#9	16	103	4.20
L2	#3	71	44	1.32	#8	8	40.8	1.65
M1	#5	200	64	2.61	#9	16	103	4.20
M2	#5	200	64	2.61	#8	8	40.8	1.65
M3	#4	129	41	2.59	#8	8	40.8	1.65
H1	#5	200	64	2.61	#9	16	103	4.20
H2	#5	200	64	2.61	#8	8	40.8	1.65
H3	#4	129	41	2.59	#8	8	40.8	1.65

25.4 mm=1 in
645 mm^2=1 in^2
64.5 cm^2=1 in^2

	Low	Medium	High
Cement-Type I (m^3)	0.0865	0.1087	0.1155
Coarse Aggregate (m^3)	0.2905	0.2600	0.2600
Fine Aggregate (m^3)	0.2290	0.2088	0.2003
Fly Ash (m^3)	----	0.0380	0.0380
Silica Fume (m^3)	----	0.0102	0.0196
Air Entrainment (%)	1.35	0.68	0.68
w/c ratio	0.45	0.27	0.23
Slump (mm)	152	152	152
Total Volume (m^3)	0.7661	0.7661	0.7661

25.4 mm=1 in
0.02837 m^3 =1 ft^3

Table 3.4 Mixture proportions of concrete as reported by ready-mix supplier.

Specimen Series	Bar Size	Area of Bar (mm^2)	Yield Load (kN)	Ultimate Load (kN)	Yield Stress (MPa)
L- & M-	#8[a]	510	237	365	465
	#9[b]	645	339	480	525
H-	#8[b]	510	206	343	405
	#9[b]	645	316	448	490

4.448 kN=1 kip
6.895 MPa=1 ksi
645 mm^2=1 in^2
[a]Loads and stresses reported for these bars are an average of 6 tests
[b]Loads and stresses reported for these bars are an average of 4 tests

Table 3.5 Longitudinal steel properties.

Specimen Series	Spiral Size	Yield Stress (MPa)
L-	#3	490
M-	#4	496
	#5	511
H-	#4	476
	#5	537

6.895 MPa=1 ksi

Table 3.6 Spiral steel yield strengths as provided by mill test reports.

CONCRETE STRENGTH	CORE No.	L/D RATIO	ASTM correction factor	Bartlett correction factor [a]	$f_{c\text{-}core}$ (MPa)
LOW	1	1.896	0.99	****	37.6
	2	1.896	0.99	****	36.3
	3	1.896	0.99	****	35.2
	4	1.896	0.99	****	36.3
	5	1.896	0.99	****	36.4
	6	1.896	0.99	****	34.5
	7	1.896	0.99	****	34.6
	8	1.896	0.99	****	38.3
MEDIUM	1	1.896	****	1.00	50.7
	2	1.896	****	1.00	45.0[b]
	3	1.896	****	1.00	40.9
	4	1.896	****	1.00	41.1
	5	1.896	****	1.00	43.5
	6	1.771	****	0.99	6.72
	7	1.604	****	0.98	45.2
	8	1.938	****	1.00	41.0
HIGH	1	1.375	****	0.95	55.2
	2	1.927	****	1.00	59.7
	3	1.938	****	1.00	63.6
	4	1.938	****	1.00	63.6[b]
	5	1.708	****	0.99	62.8
	6	1.792	****	0.99	58.7
	7	1.781	****	0.99	68.5
	8	1.760	****	0.99	61.3

6.895 MPa=1 ksi
[a]Bartlett et al. (1994)
[b]Small piece of reinforcement or threaded bar contained within cylinder specimen

Table 3.7 Compressive strengths of cored cylinders.

Specimen	Wet-Cured[a] $f_{c\text{-}28}$ (MPa)	Field-Cured[b] $f_{c\text{-}field}$ (MPa)	Cored[c] $f_{c\text{-}core}$ (MPa)
L1	37.9	35.8	36.2
L2	37.9	35.8	36.2
M1	51.9	52.7	44.7
M2	51.9	52.7	44.7
M3	51.9	52.7	44.7
H1	84.7	76.0	61.4
H2	84.7	81.3	61.4
H3	84.7	83.0	61.4

6.895 MPa=1 ksi
[a]Average of 4 cylinders
[b]Average of 3 cylinders
[c]Average of 8 cylinders

Table 3.8 Average compressive strengths of cylinders.

Table 3.9 Specimen details with actual material properties and spiral steel size/pitch.

Specimen	Concrete Strength		Spiral Reinforcement				Longitudinal Reinforcement		
	field-cured (MPa)	cored (MPa)	f_{ys} (MPa)	A_{sp} (mm^2)	s (mm)	ρ_s %	f_{yl} (MPa)	A_{st} (cm^2)	ρ_l %
L1	35.8	36.2	490	71	44	1.32	525	103	4.20
L2	35.8	36.2	490	71	44	1.32	465	40.8	1.65
M1	52.7	44.7	511	200	64	2.61	525	103	4.20
M2	52.7	44.7	511	200	64	2.61	465	40.8	1.65
M3	52.7	44.7	496	129	41	2.59	465	40.8	1.65
H1	76.0	61.4	537	200	64	2.61	490	103	4.20
H2	81.3	61.4	537	200	64	2.61	405	40.8	1.65
H3	83.0	61.4	476	129	41	2.59	405	40.8	1.65

25.4 mm=1 in
645 mm^2=1 in^2
64.5 cm^2=1 in^2
6.895 MPa=1 ksi

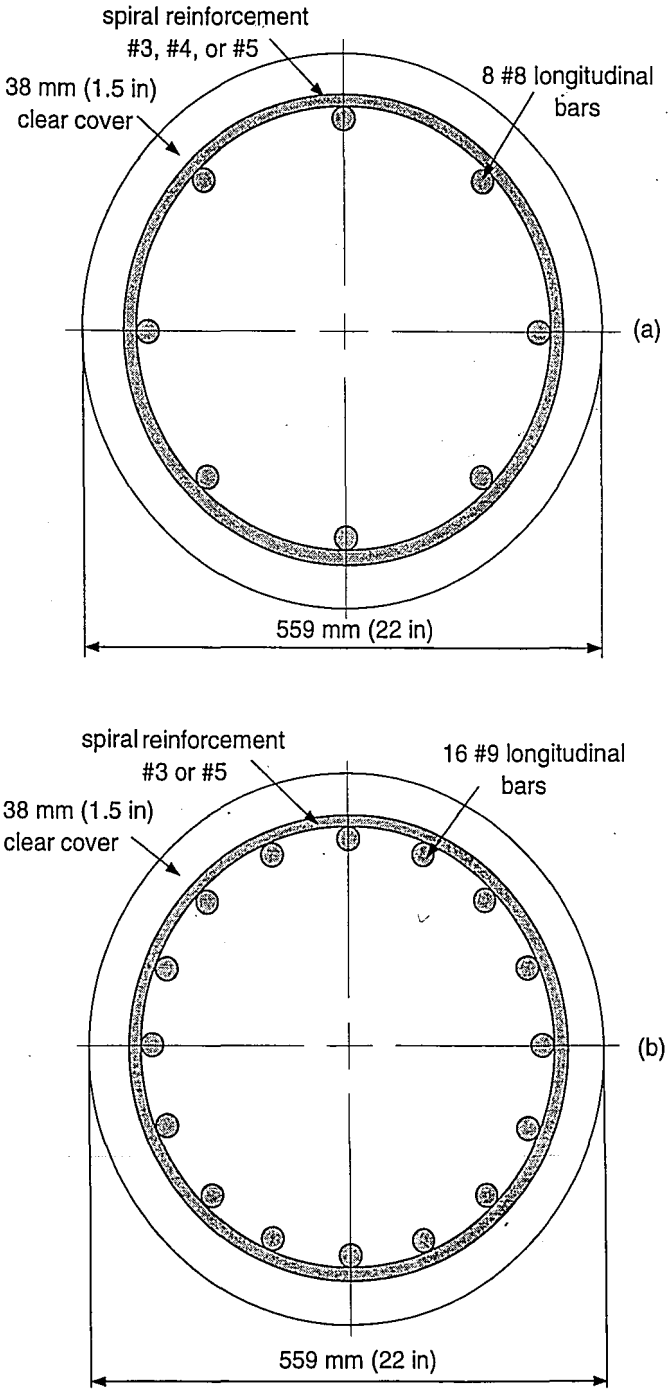

Figure 3.1 Cross-sectional view of column (a) 8-#8 bar configuration; (b) 16-#9 bar configuration.

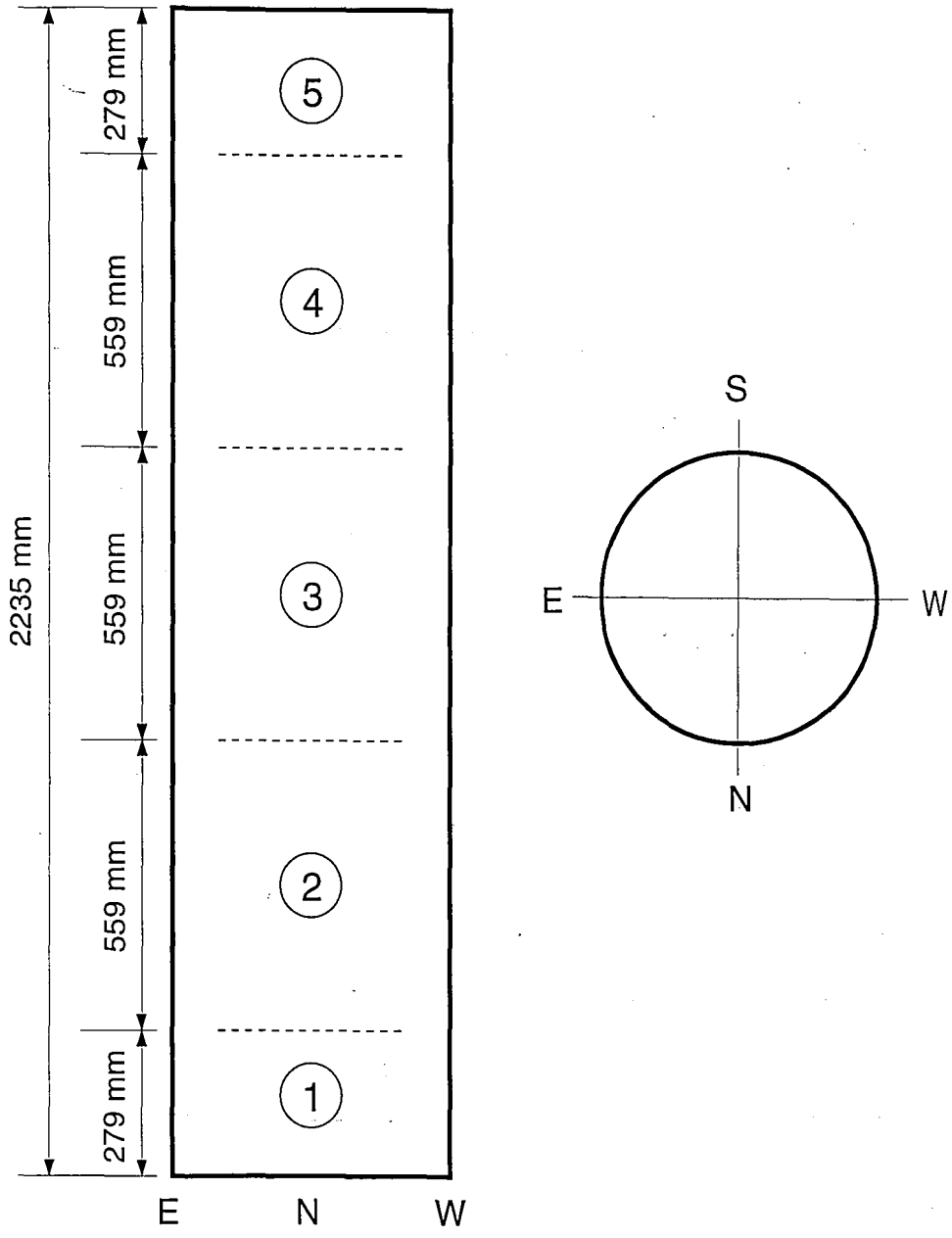

Figure 3.2 Division of column into sections for instrumentation purposes.

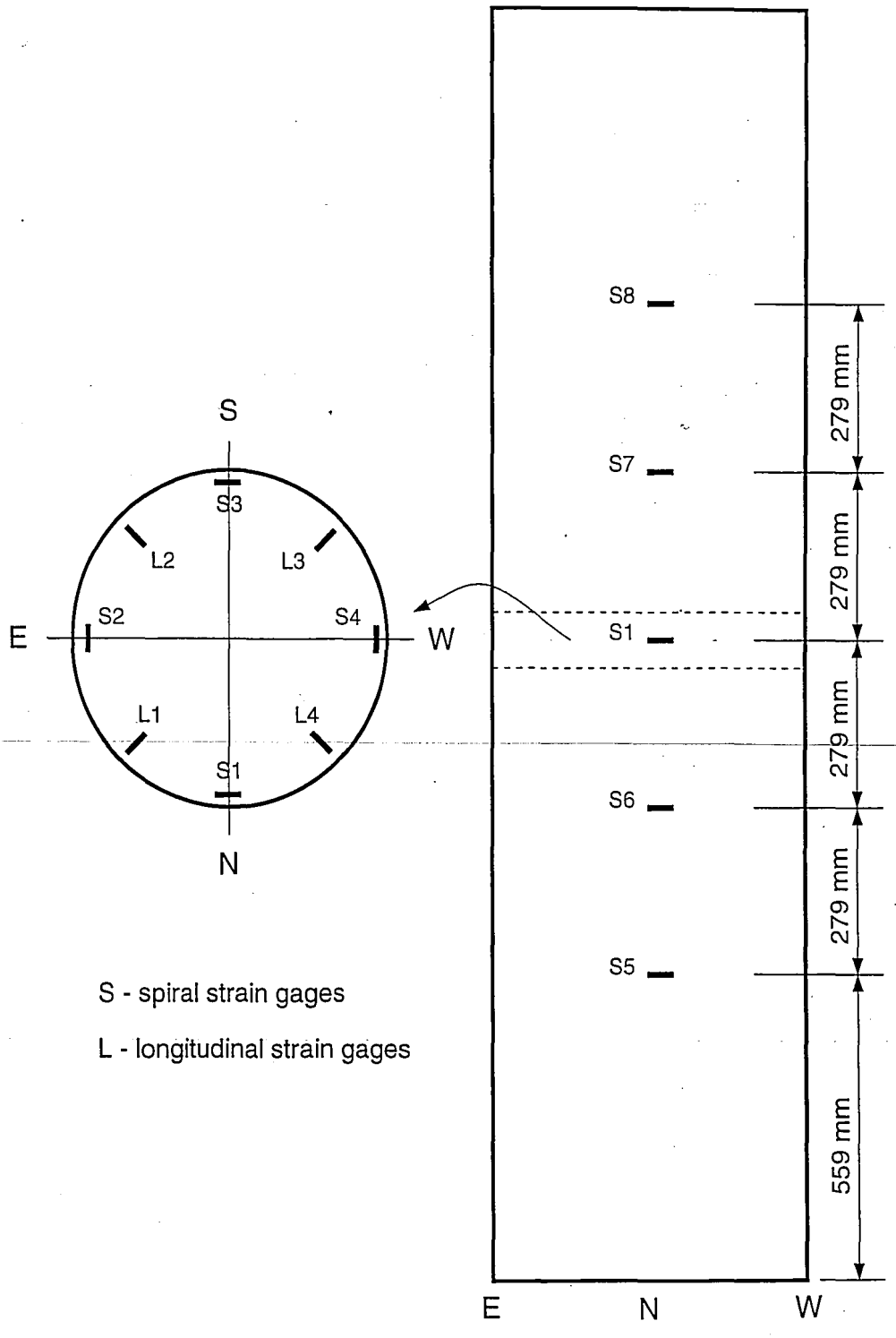

Figure 3.3 Instrumentation Plan A - Layout of strain gages.

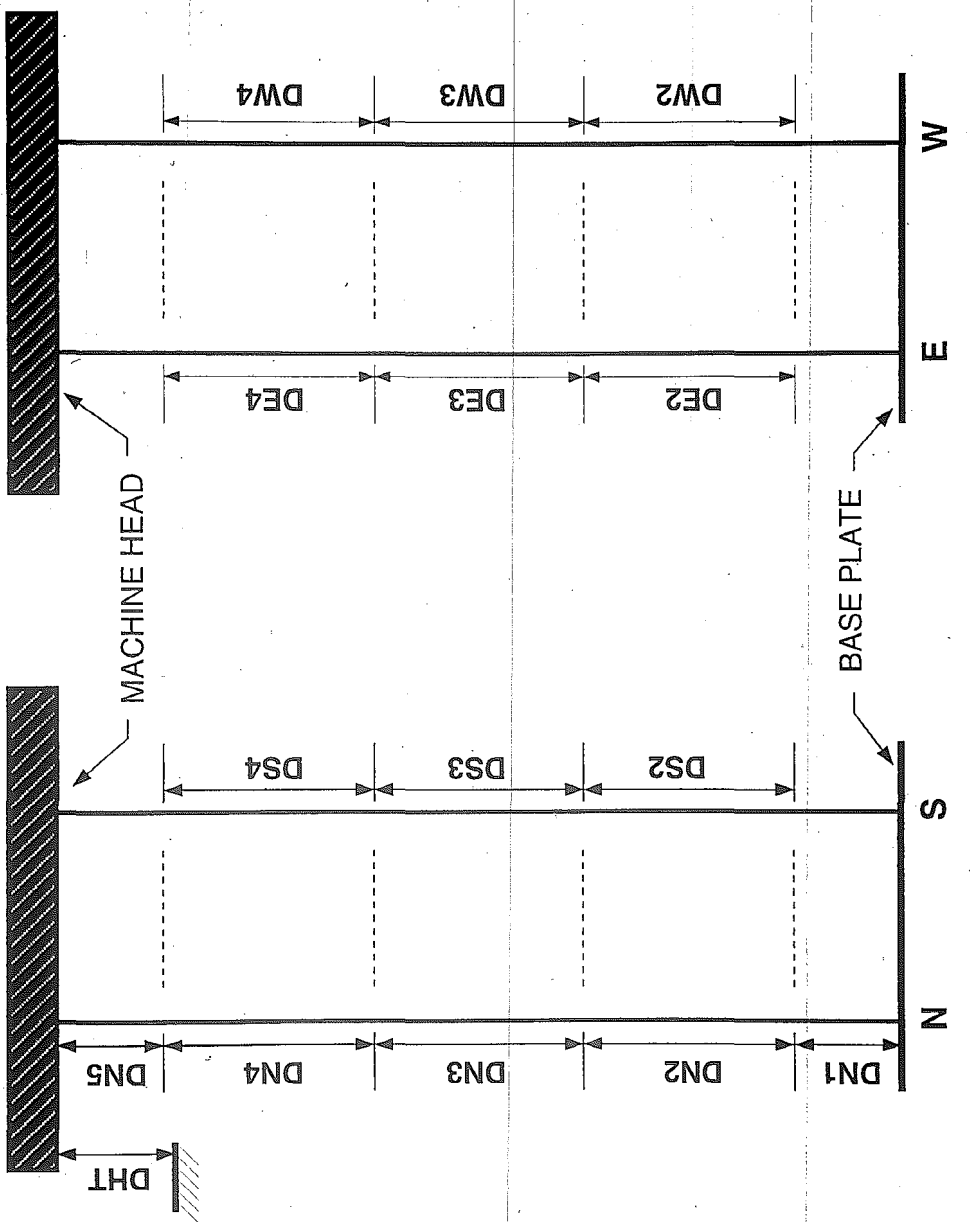

Figure 3.4 Instrumentation Plan A - Layout of displacement transducers.

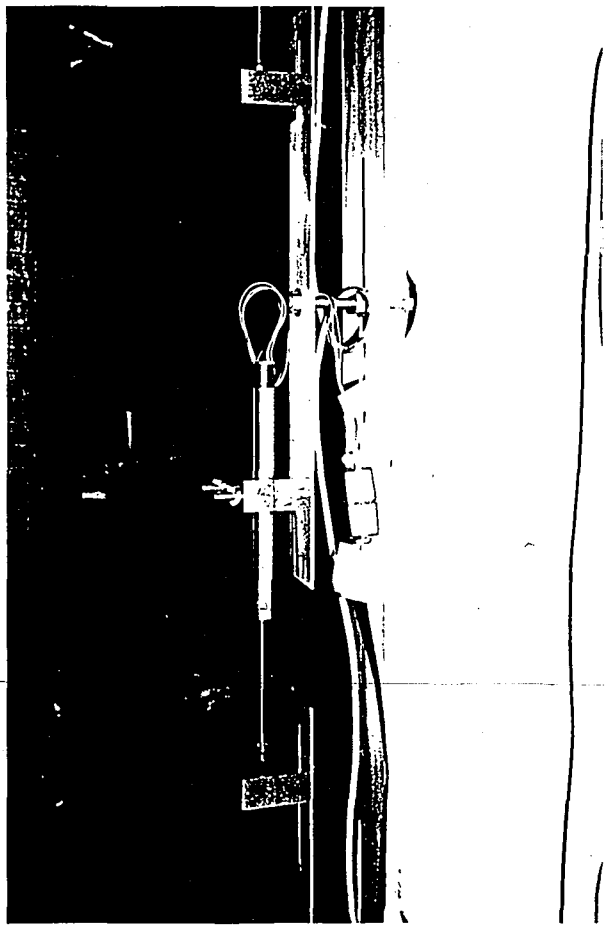

Figure 3.5 LVDT mounted to threaded bars via an aluminum plate.

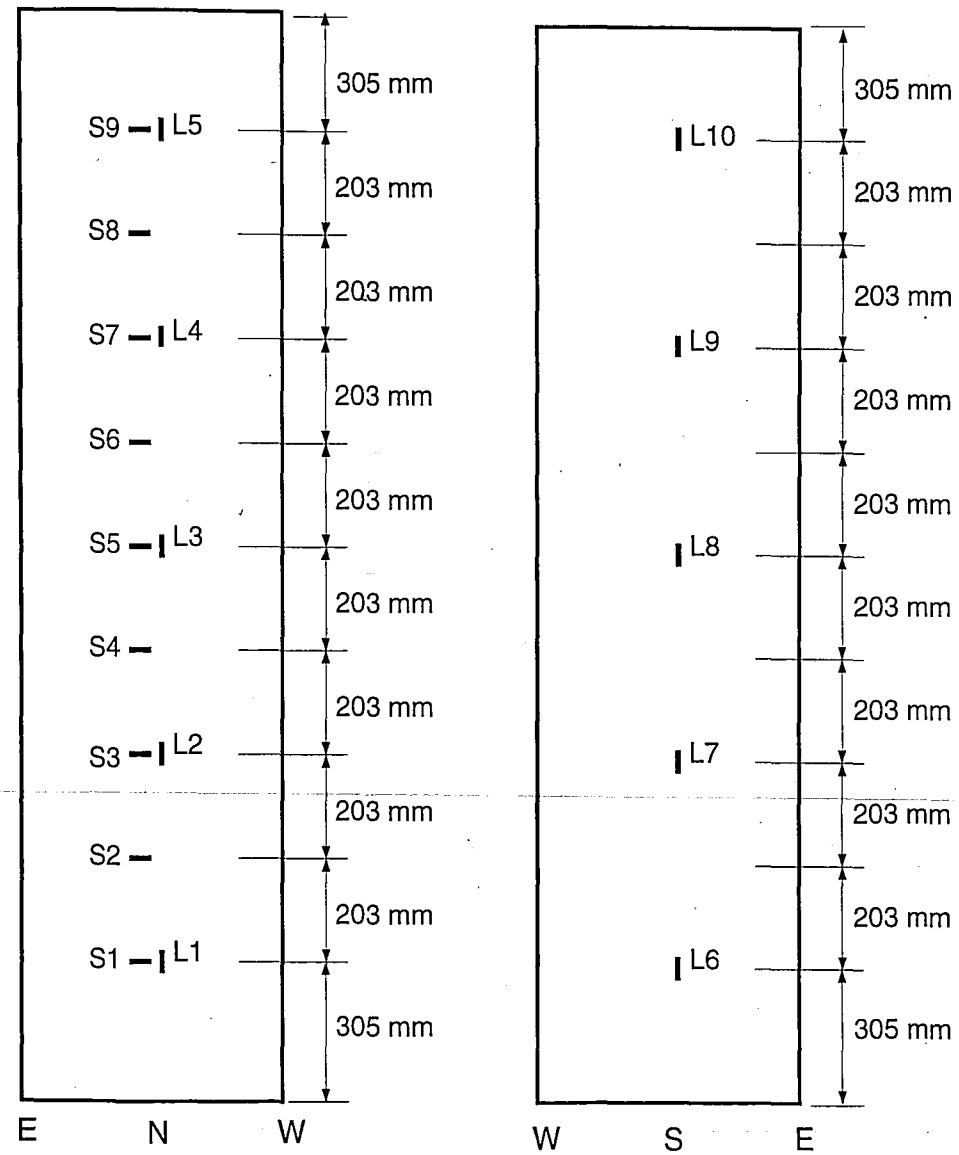

Figure 3.6 Instrumentation Plan B - Layout of strain gages.

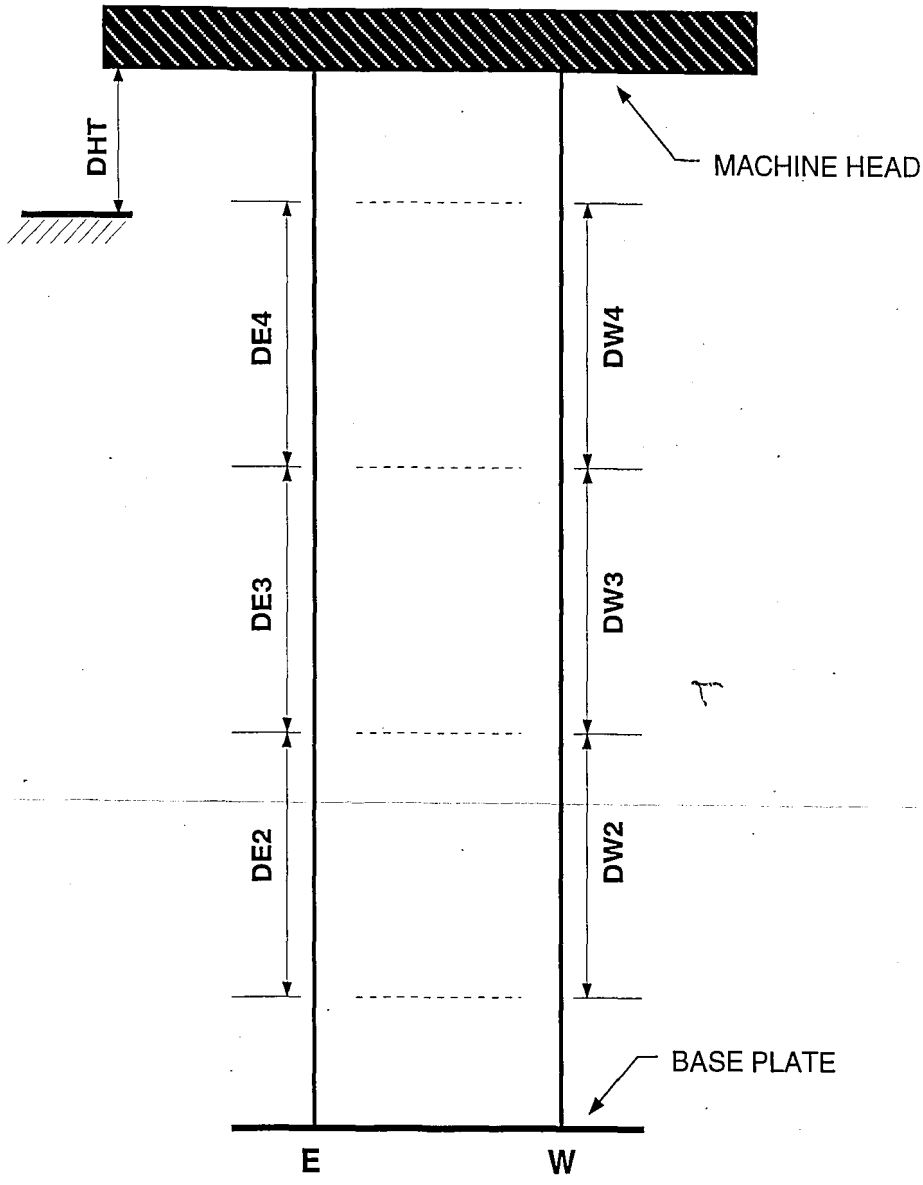

Figure 3.7 Instrumentation Plan B - Layout of displacement transducers.

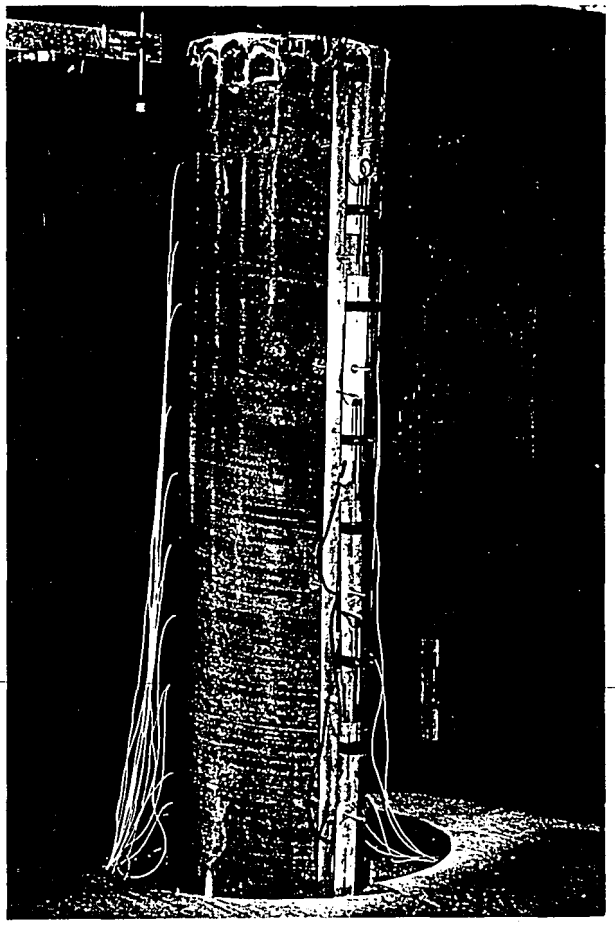

Figure 3.8 Aluminum hardware to protect instrumentation.

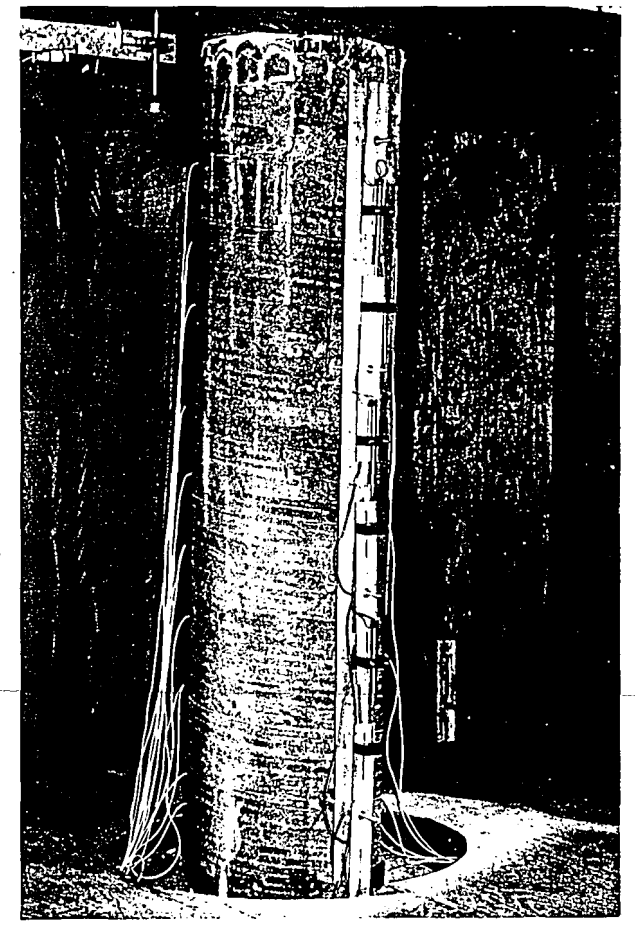

Figure 3.8 Aluminum hardware to protect instrumentation.

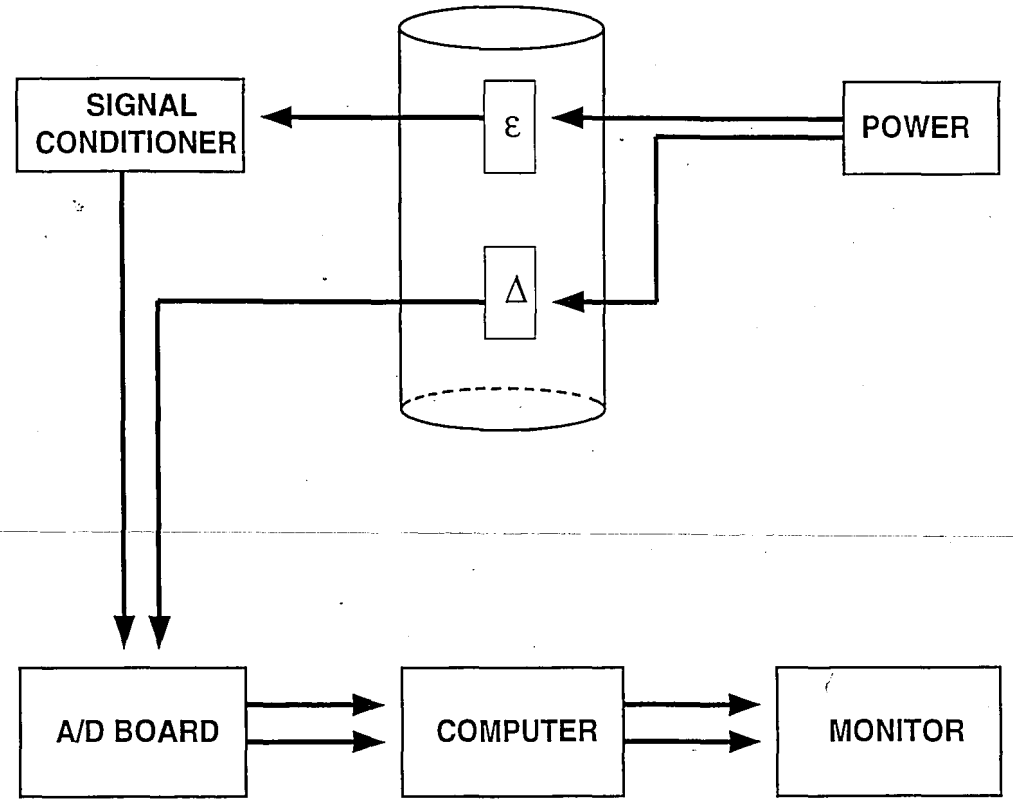

Figure 3.9 Schematic of data acquisition system.

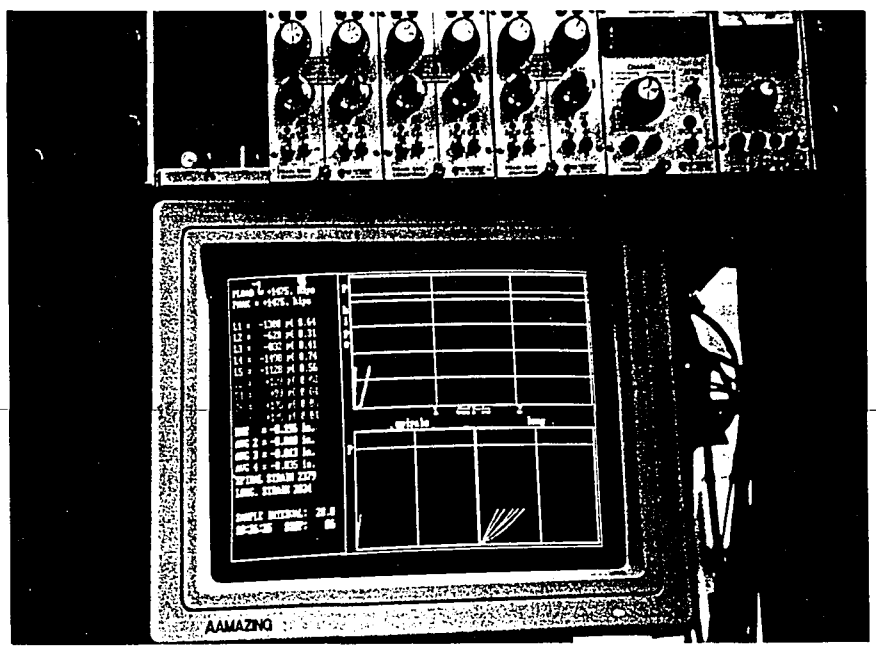

Figure 3.10 Computer monitor during testing.

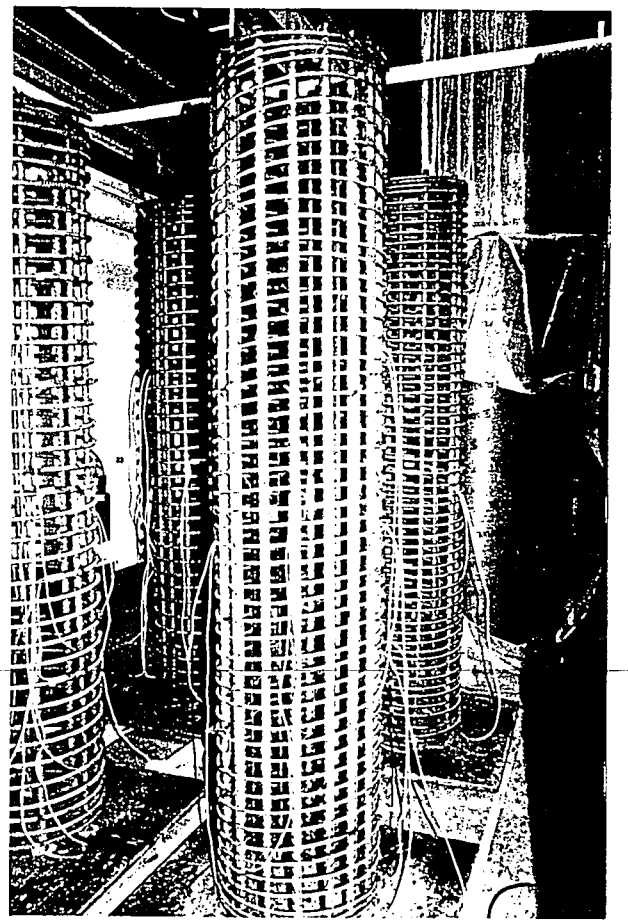

Figure 3.11 Completed reinforcement cages.

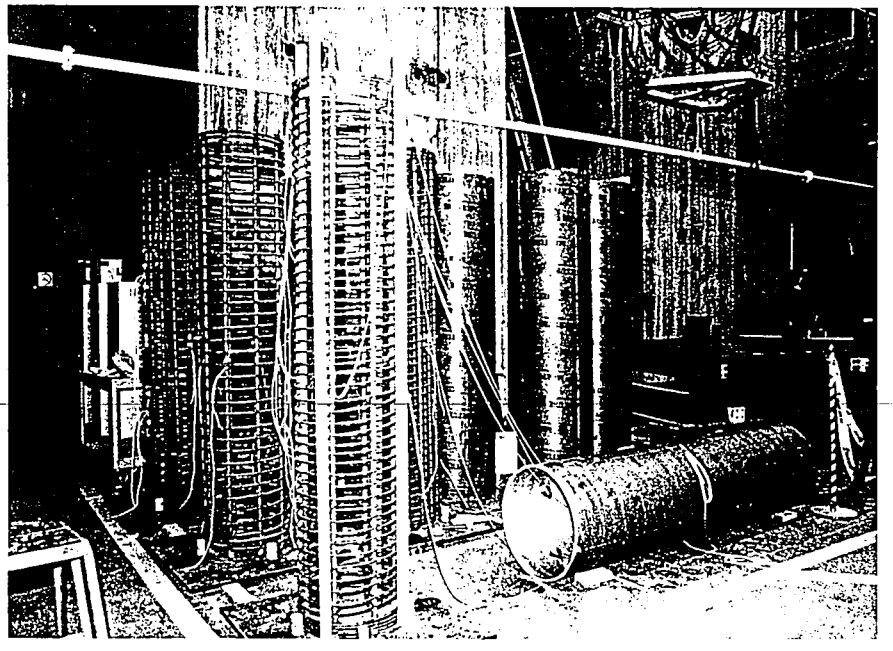

Figure 3.12 Preparation of formwork for placement over steel cages.

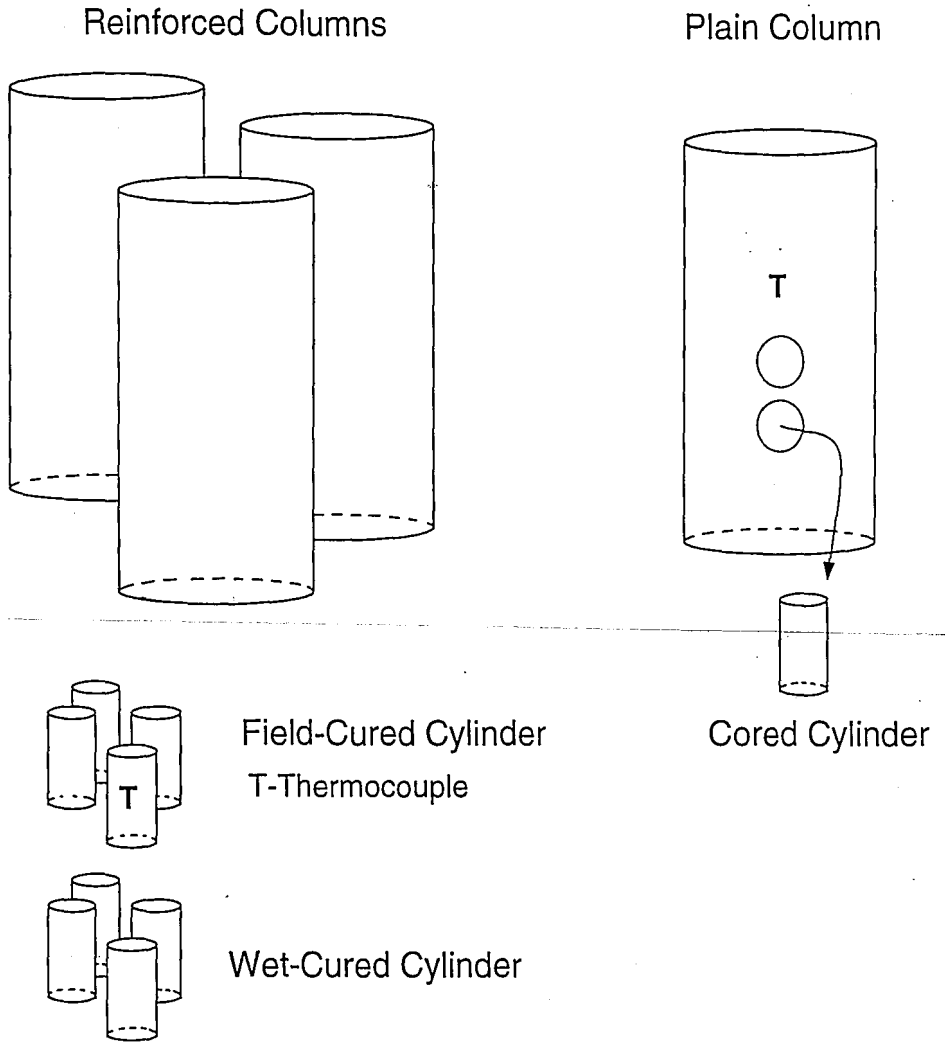

Figure 3.13 Illustration of the different 152x305 mm (6x12 in) cylindrical specimens used to determine concrete compressive strength.

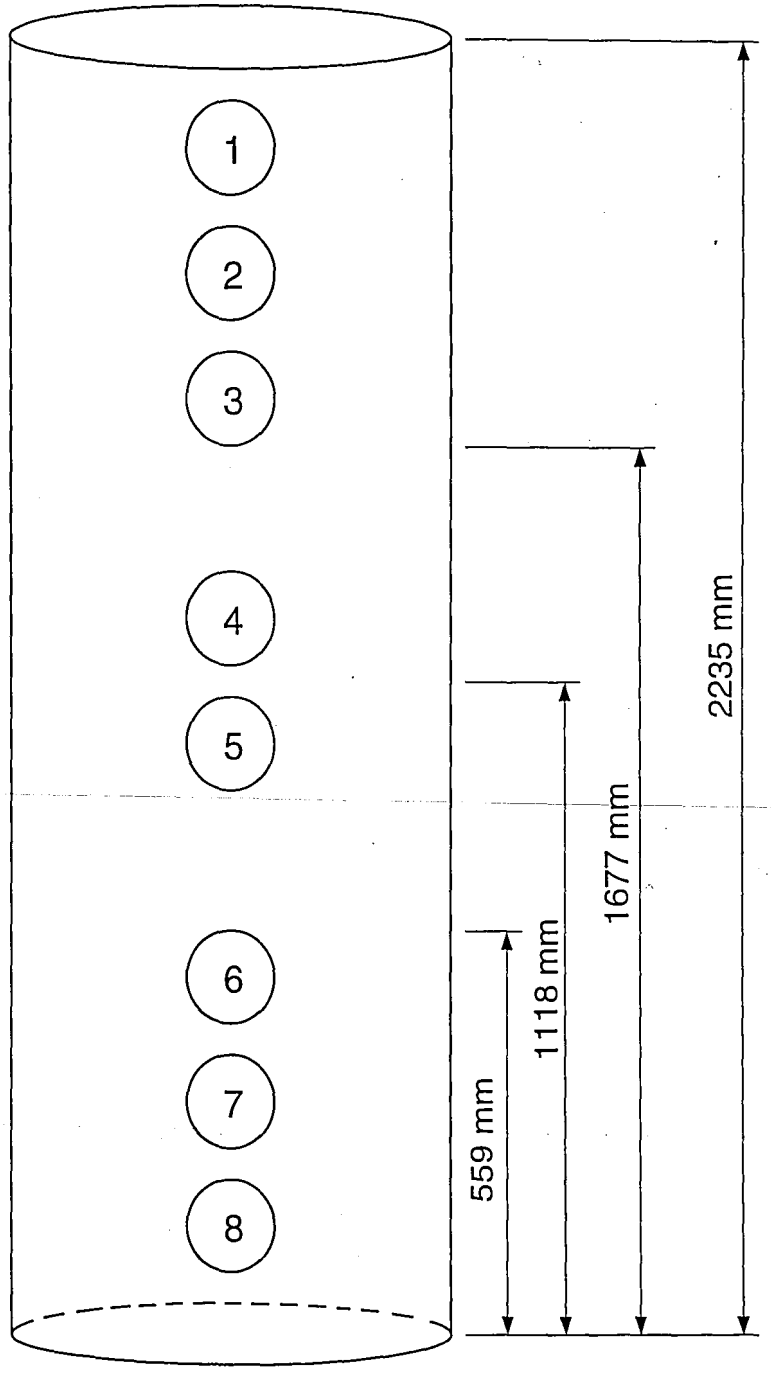

Figure 3.14 Locations at which cores were extracted.

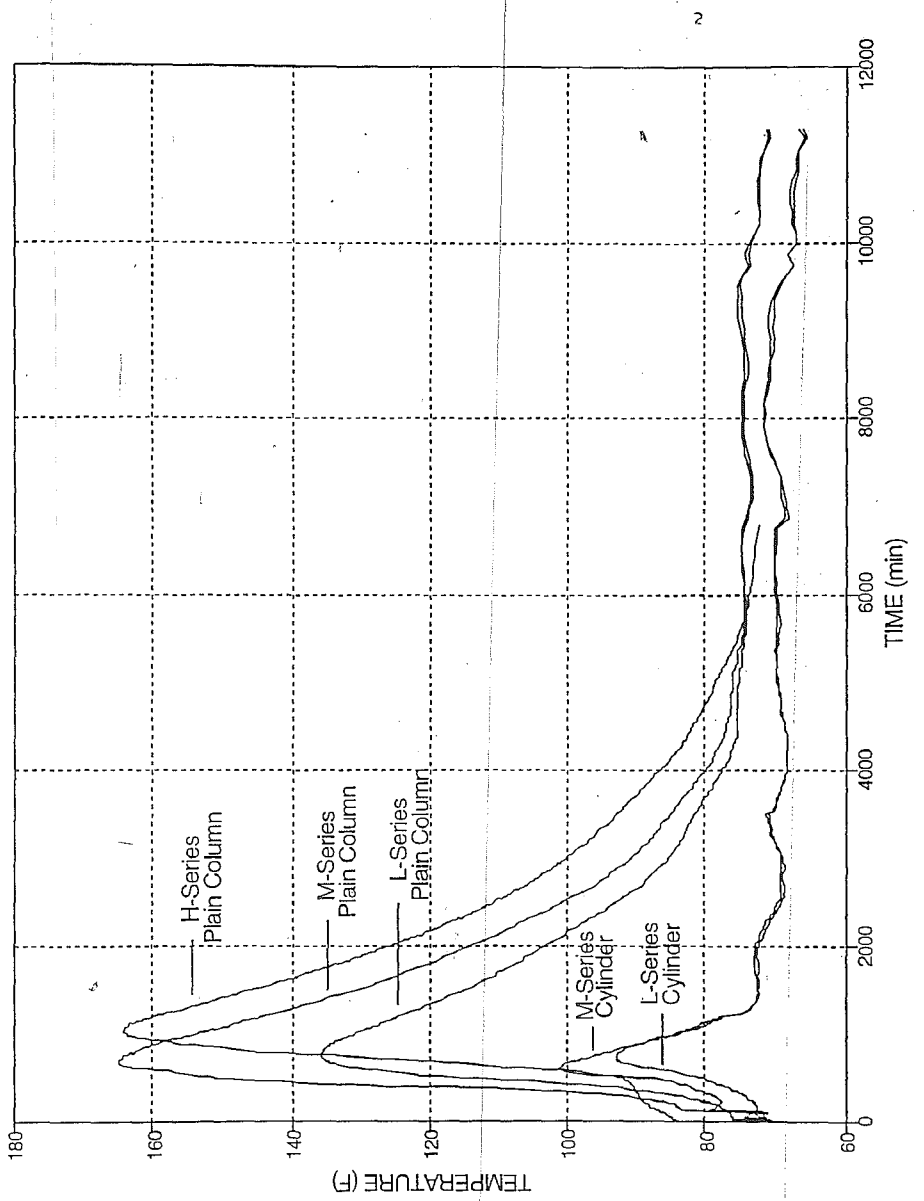

Figure 3.15 Temperature variations of different strength concretes and different size specimens.

CHAPTER 4

INDIVIDUAL TEST SUMMARIES

4.1 INTRODUCTION

This chapter provides a detailed description of the results of each individual column test. Section 4.2 explains the general loading procedure used for each test, and Section 4.3 describes in detail the observations made during each test. A comparison and discussion of these results is given in Chapter 5.

4.2 GENERAL LOADING PROCEDURE

Each column was tested in concentric compression in a 22.2 MN (5000 kip) capacity universal test machine. The test machine operator monitored the applied load, the load rate, and displacement rate (rate of head travel).

All columns were subjected to an initial cycle of load of 1334 kN (300 kips) at a rate of about 222 kN/min (50 kips/min), and then completely unloaded. This initial load cycle was made to ensure that the instrumentation and data acquisition were functioning properly.

Actual testing of each column also began at a load rate of 222 kN/min (50 kips/min). For each column, the initial load rate corresponded to a displacement rate between 0.18 mm/min (0.007 in/min) and 0.20 mm/min (0.008 in/min). As the columns became damaged and decreased in stiffness, this load rate would decrease. Continued testing of each column was then performed at a desired

displacement rate. After first cracking appeared in the cover concrete, this displacement rate was incremented approximately 0.051 mm/min (0.002 in/min). The faster displacement rate was maintained until the column began to sustain a relatively constant load with increasing displacement. During this period, the displacement rate was periodically increased until spiral fractures began to occur. The maximum displacement rates of each column were between 0.64 mm/min (0.025 in/min) and 0.76 mm/min (0.03 in/min).

4.3 INDIVIDUAL TEST SUMMARIES

This section summarizes the observations made during each test. All the individual test summaries are presented in the same general format which includes the following:

1. A summary of the reinforcement in the specimen and concrete strengths.

2. A detailed description of the observations made during testing.

3. One table that summarizes the predicted axial strength of the confined column and the experimentally observed strength. The table presents calculations of the column strength based on the concrete compressive strength of the day of test field-cured cylinders $f_{c\text{-}field}$, and the concrete

compressive strength of the cored cylinders $f_{c\text{-}core}$. The following predicted strength values are summarized in each table:

$$P_c = f_{cc}A_c + A_{st}f_{yl} \quad (4.1)$$

$$P_{ccore} = f_{cc}A_c + A_{st}f_{yl} \quad (4.2)$$

P_c -The axial strength of the confined core based on actual material properties, $f_{c\text{-}field}$, and the equation for the compressive strength of the confined concrete, Equation 2.7 (Martinez et al.). This value is plotted as a dashed line on each load-displacement graph.

P_{ccore} -The axial strength of the confined core based on actual material properties, $f_{c\text{-}core}$, and the equation for the compressive strength of the confined concrete, Equation 2.7 (Martinez et al.). This value is plotted as a dashed line on each load-displacement graph.

4. A graph of axial load versus axial displacement. This graph is annotated with the following symbols.

L#Y -L#Y indicates yielding of the longitudinal reinforcement at the location of strain gage number #.

S#Y -S#Y indicates yielding of the spiral reinforcement at the location of the spiral steel strain gage number #.

SF# -SF indicates a point in the test at which a spiral fracture was observed. The # symbol indicates the number sequence in which the spirals fractured.

P_{max} -maximum load sustained by the column

FCR - first observed cracking of cover concrete.

Δ_1 -axial displacement corresponding to the intersection of the maximum load (P_{max}) and the linear elastic portion of the load-displacement curve.

Δ_{SF} -axial displacement at first spiral fracture (SF1)

Δ_{85} -axial displacement corresponding to the intersection of the descending portion of the load-displacement curve and 85% of P_{max}.

5. Graphs of axial load versus longitudinal reinforcement strains.

6. Graphs of axial load versus spiral reinforcement strains.

7. A set of key photographs taken during and after the experiment.

Note that all of the graphs are plotted to the same scales which were determined by the columns that experienced the largest axial load, axial displacement, and reinforcement strain.

4.3.1 Specimen L1

-#3 spiral at 44 mm (1.75 in) pitch

-16-#9 longitudinal bars

-$f_{c\text{-field}}$ = 35.8 MPa (5.19 ksi)

-$f_{c\text{-core}}$ = 36.2 MPa (5.25 ksi)

The location of strain gages and the location of displacement transducers for Specimen L1 are detailed in Figure 3.3 and Figure 3.4, respectively. First cracking (FCR) was observed in the concrete cover at an axial load of 10.85 MN (2461 kips) and an axial displacement of 5.4 mm (0.213 in). This is 94% of the maximum load. These cracks were a series of small cracks which initiated at the top of the column on the east face. The graph of axial load versus axial displacement (Figure 4.1) shows that the column exhibited an approximately linear load displacement response from the beginning of the test to first cracking in the cover concrete. At a load around 11.56 MN (2600 kips) a series of longitudinal splitting cracks, approximately 610 mm (2 ft) in length, existed at the top of the column on the northwest, northeast, and southwest face. The northeast face is pictured in Figure 4.5(a). The column reached a peak load of 11.60 MN (2608 kips), and the axial displacement at this load was 6.5 mm (0.256 in).

As the cover began separating from the core at the top of the column, the cover concrete became less effective in sustaining load. The axial resistance of the column decreased approximately 356 kN (80 kips), then began to increase again. As shown in Figure 4.1, the column sustained a constant load of about 11.68 MN (2625 kips). The maximum load (P_{max}) of the column was 11.70 MN (2630 kips) at an axial displacement of 13.6 mm (0.534 in).

During this period of increasing displacement at a constant load, additional cracking developed in the concrete cover. At an axial displacement of 11.7 mm (0.459 in) the longitudinal splitting cracks extended approximately 914 mm (3 ft) down from the top of the column. The cover concrete at the very top of the column began disintegrating, as shown in Figure 4.5(b). By a deformation of about 12.7 mm (0.5 in) the cracks on the south face of the column widened due to the lateral expansion of the core concrete. The extensive lateral deformation elongated the instrumented threaded rods causing rotation in the top row of LVDTs. As the lateral deformation increased further, sections of cover concrete fell away from the column exposing the spiral reinforcement. The damage in the column was concentrated in the top 1/3 region.

The first two spiral fractures (SF1, SF2) occurred simultaneously at an axial displacement of Δ_{SF}=27.6 mm (1.086 in), shown in Figure 4.1. This was accompanied by a decrease in column resistance from 10.56 MN (2373 kips) to 6.51 MN (1465 kips). The third spiral fracture (SF3) occurred at an axial displacement of 32.2 mm (1.268 in). This was accompanied by a 2.15 MN (483 kips) decrease in

column axial force. At this point the load on the column was 32% of the maximum load. The column was then unloaded at a rate of 222 kN/min (50 kips/min).

Figure 4.2 is a graph of axial load versus strain in the longitudinal reinforcement. First yielding of the longitudinal bars was recorded on strain gages L2 and L4 at an axial load of 11.68 MN (2626 kips) and an axial displacement of 13.1 mm (0.514 in) (L2Y and L4Y on Figure 4.1). Longitudinal strain gage L1 yielded at an axial load of 11.62 MN (2613 kips) and an axial displacement of 15.4 mm (0.606 in). Strain gage L3 approached yield strain but never reached it. Due to the location of the gages, yielding of the longitudinal reinforcement occurred very late. The longitudinal bars were instrumented at mid-height of the column, and the failure was contained within the top 1/3 of the column. The variation of strain in the spiral reinforcement along the height of the column is illustrated in Figure 4.4. As shown in this figure, strain gage S8 was the only gage to yield. This gage yielded (S8Y) around 11.28 MN (2537 kips) (Figure 4.1).

At the end of the test the column was completely unloaded, and the separated regions of concrete cover were carefully removed to expose the core and spiral reinforcement (Figures 4.5(c)-(d)). Three spiral fractures were noted. All of the spiral fractures occurred at the location of buckled longitudinal bars. The failure region was characterized by a bulging of the column at the top 1/3 region (Figure 4.5(e)). All of the spiral breaks were contained within this region.

Experimental Axial Capacity	Predicted Axial Capacity	
P_{max} (MN)	P_c (MN)	P_{ccore} (MN)
11.70	12.70	12.76

0.004448 MN=1 kip

Table 4.1 Specimen L1-predicted strengths and experimentally observed strengths.

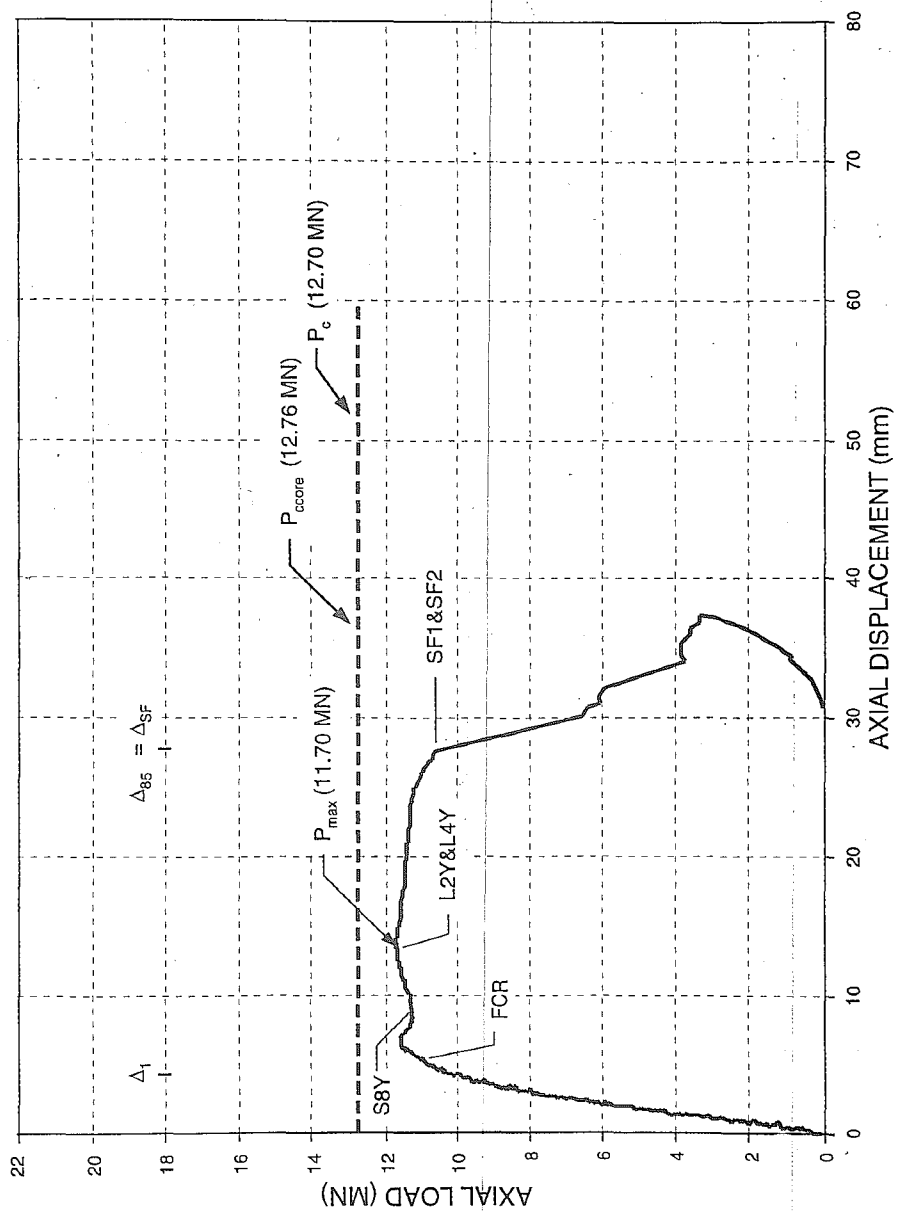

Figure 4.1 Specimen L1-axial load versus axial displacement.

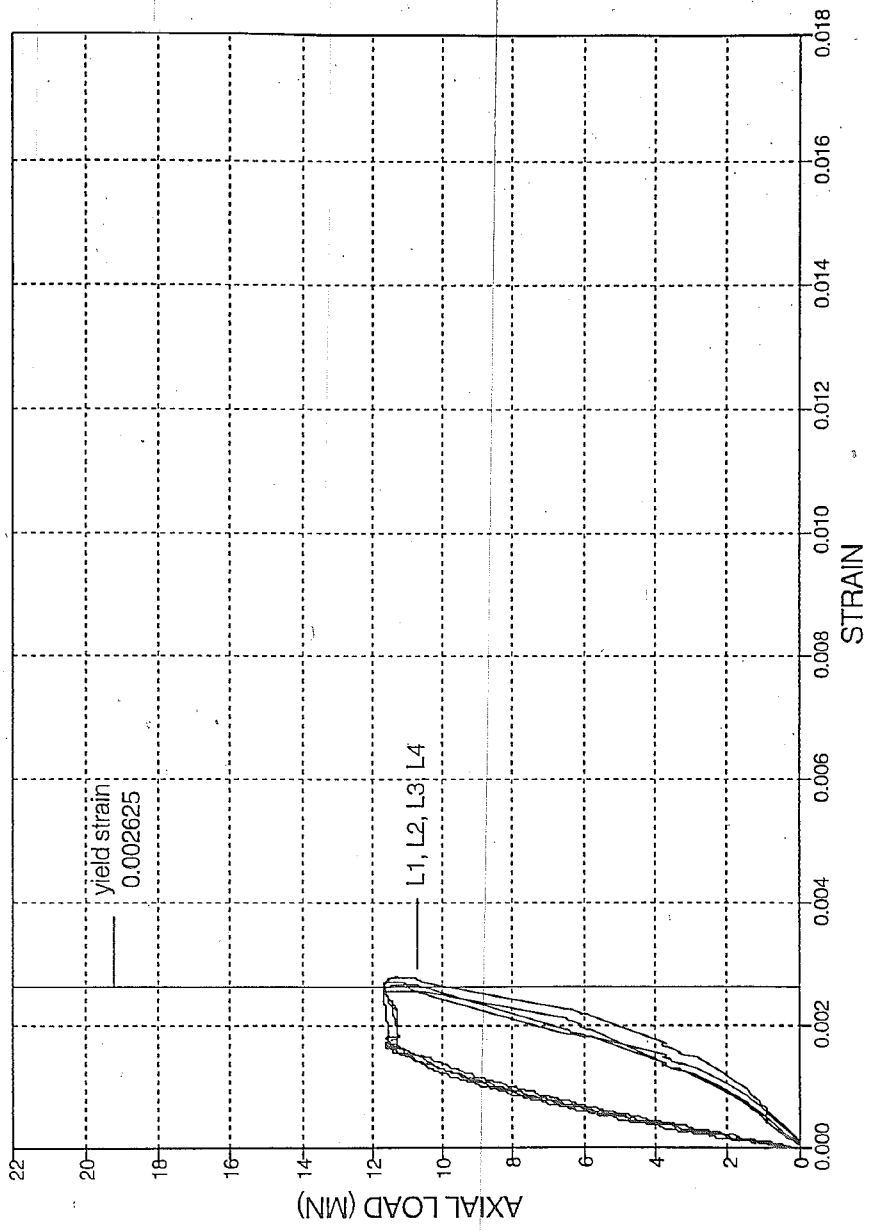

Figure 4.2 Specimen L1-axial load versus longitudinal reinforcement strains, gages L1, L2, L3, L4.

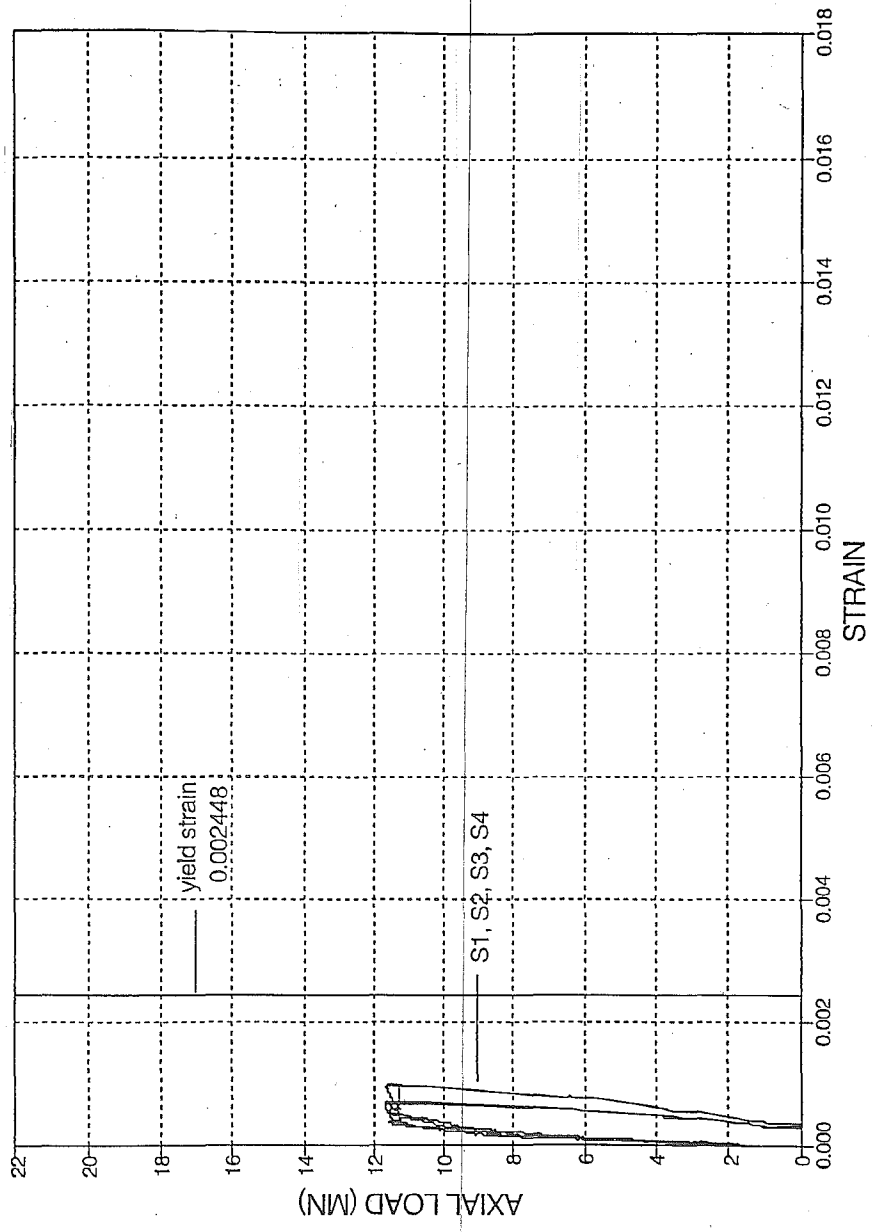

Figure 4.3 Specimen L1-axial load versus spiral reinforcement strains, gages S1, S2, S3, S4.

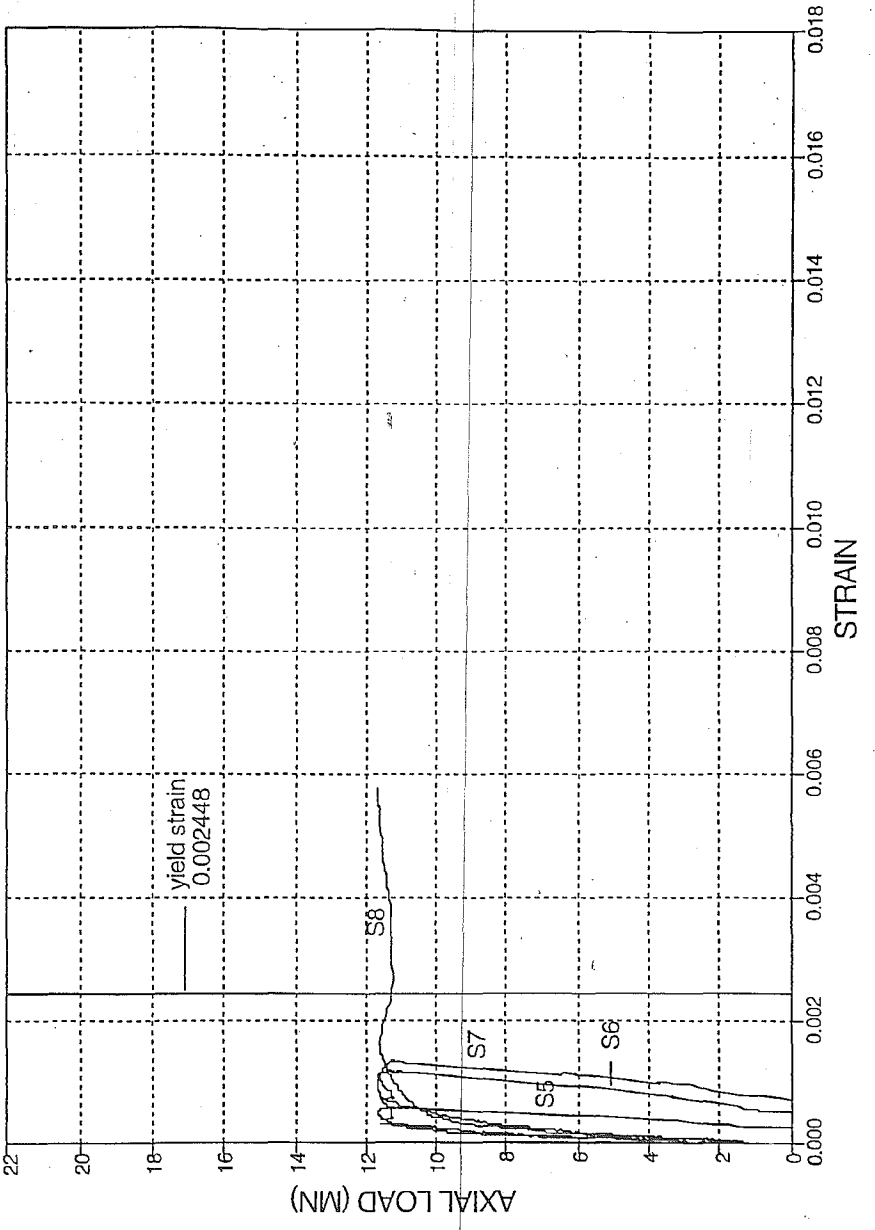

Figure 4.4 Specimen L1-axial load versus spiral reinforcement strains, gages S5, S6, S7, S8.

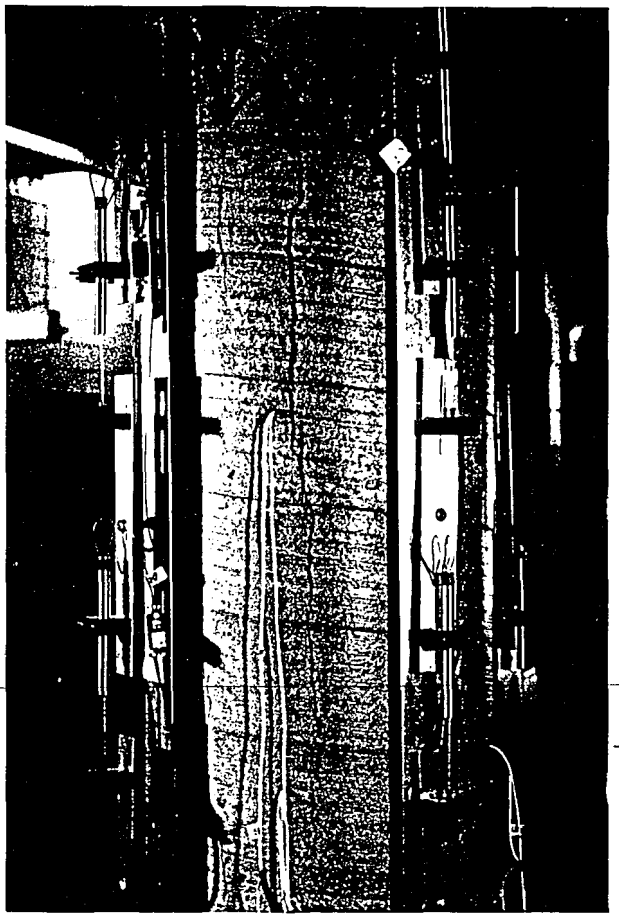

Figure 4.5(a) Specimen L1-series of key photographs; (a) initial cracking.

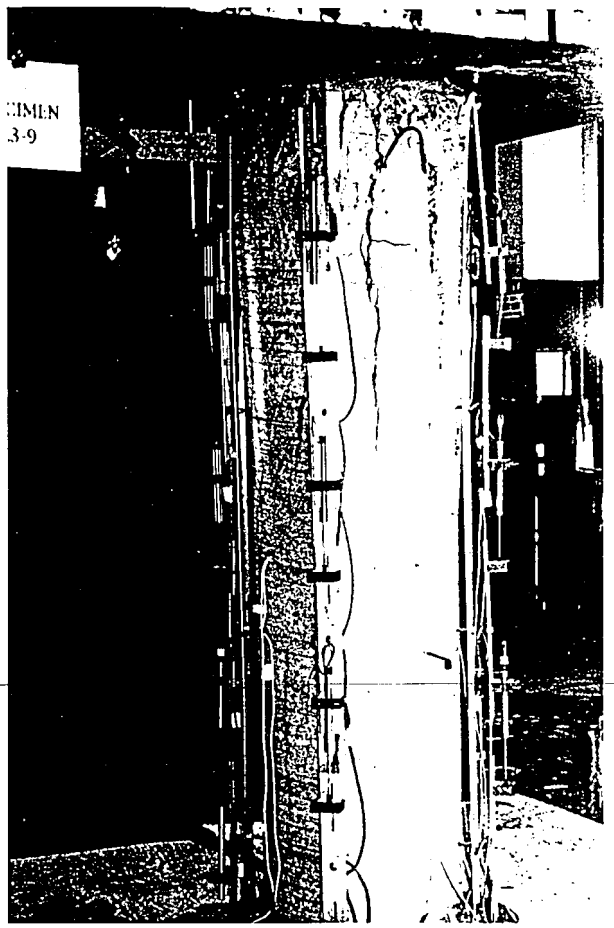

Figure 4.5(b) Specimen L1-series of key photographs; (b) spalling of cover concrete.

Figure 4.5(c) Specimen L1-series of key photographs; (c) fractured spiral.

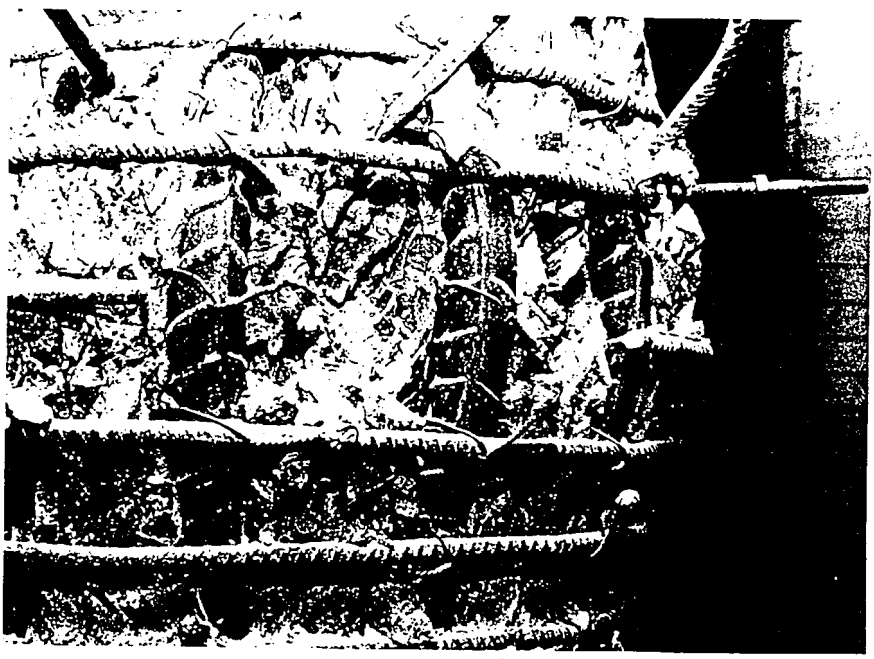

Figure 4.5(d) Specimen L1-series of key photographs; (d) fractured spiral.

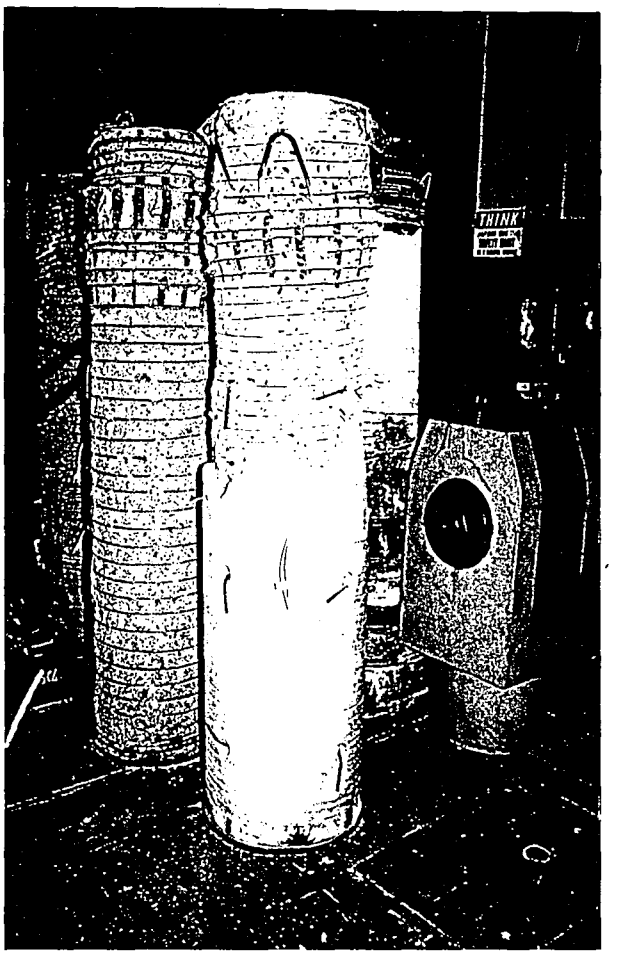

Figure 4.5(e) Specimen L1-series of key photographs; (e)post-test photograph showing the bulged failure region.

4.3.2 Specimen L2

-#3 spiral at 44 mm (1.75 in) pitch

-8-#8 longitudinal bars

-$f_{c\text{-}field}$ = 35.8 MPa (5.19 ksi)

-$f_{c\text{-}core}$ = 36.2 MPa (5.25 ksi)

The location of strain gages and the location of displacement transducers for Specimen L2 are detailed in Figure 3.3 and Figure 3.4, respectively. First cracking (FCR) was observed in the concrete cover at an axial load of 8.53 MN (1918 kips) and an axial displacement of 4.2 mm (0.165 in). This is 90% of the maximum load. This crack initiated at the top of the east face and propagated approximately 254 mm (10 in) down the column. The graph of axial load versus axial displacement (Figure 4.6) shows that the column exhibited an approximately linear load displacement response from the beginning of the test to first cracking in the cover concrete. At a load of 9.50 MN (2135 kips) the cover concrete at the top of the column began disintegrating, as shown in Figure 4.10(a). The maximum load (P_{max}) occurred at a load of 9.53 MN (2142 kips), and the axial displacement at this load was 6.0 mm (0.237 in).

As the cover began separating from the core at the top of the column, the cover concrete became less effective in sustaining load. As shown in Figure 4.6, the axial resistance of the column decreased approximately 890 kN (200 kips), and the column continually decreased resistance with increased axial displacement.

Over an axial displacement of 19.0 mm (0.747 in), the axial load of the column decreased from 8.64 MN (1942 kips) to 7.57 MN (1703 kips).

During this period of increasing deformation and decreasing resistance, additional cracking developed in the concrete cover. At an axial displacement of 11.7 mm (0.46 in) the longitudinal splitting cracks propagated approximately 914 mm (3 ft) down from the top of the column. By a deformation of 17.9 mm (0.705 in) the crack on the northwest face of the column widened to 6 mm (0.25 in), due to the lateral expansion of the core concrete. The extensive lateral deformation elongated the instrumented threaded rods causing rotation in the top row of LVDTs. As the lateral deformation further increased, sections of cover concrete fell away from the column exposing the spiral reinforcement. The damage in the column was concentrated at the top 1/3 region.

The first spiral fracture (SF1) occurred at an axial displacement of Δ_{SF}=29.2 mm (1.148 in), shown on Figure 4.6. This was accompanied by a decrease in column resistance from 7.57 MN (1703 kips) to 7.00 MN (1573 kips). The column then exhibited increased axial displacement at an approximately constant load of 6.67 MN (1500 kips). The second spiral fracture (SF2) occurred at an axial displacement of 32.3 mm (1.271 in). This was accompanied by another 680 kN (153 kips) decrease in column axial load. At a displacement of about 35.2 mm (1.384 in) the third spiral fracture (SF3) occurred, and the load on the column decreased by a value of 909 kN (437 kips). At this point the load on the column

was 33% of the maximum load. The column was then unloaded at a rate of 222 kN/min (50 kips/min).

Figure 4.7 is a graph of axial load versus strain in the longitudinal reinforcement. Due to the location of the longitudinal strain gages (Figure 3.3), yielding of the longitudinal bars was not recorded. The longitudinal bars were instrumented at mid-height of the column, however the failure was contained within the top 1/3 of the column. The variation of strain in the spiral reinforcement along the height of the column is illustrated in Figure 4.9. As shown in this figure, strain gage S8 was the only gage to yield. This gage yielded (S8Y) at 9.39 MN (2110 kips) prior to the maximum load (Figure 4.6).

At the end of the test the column was completely unloaded, the separated regions of cover concrete were carefully removed to expose the core and spiral reinforcement. Three spiral fractures were noted. All of the spiral fractures were on the west and the northwest faces, and occurred at the location of buckled longitudinal bars. The failure region was characterized by a bulging of the column in the top 1/3 region (Figure 4.10(b)). All of the spiral breaks were contained within this region.

Experimental Axial Capacity	Predicted Axial Capacity	
P_{max} (MN)	P_c (MN)	P_{ccore} (MN)
9.53	9.44	9.58

0.004448 MN=1 kip

Table 4.2 Specimen L2-predicted strengths and experimentally observed strengths.

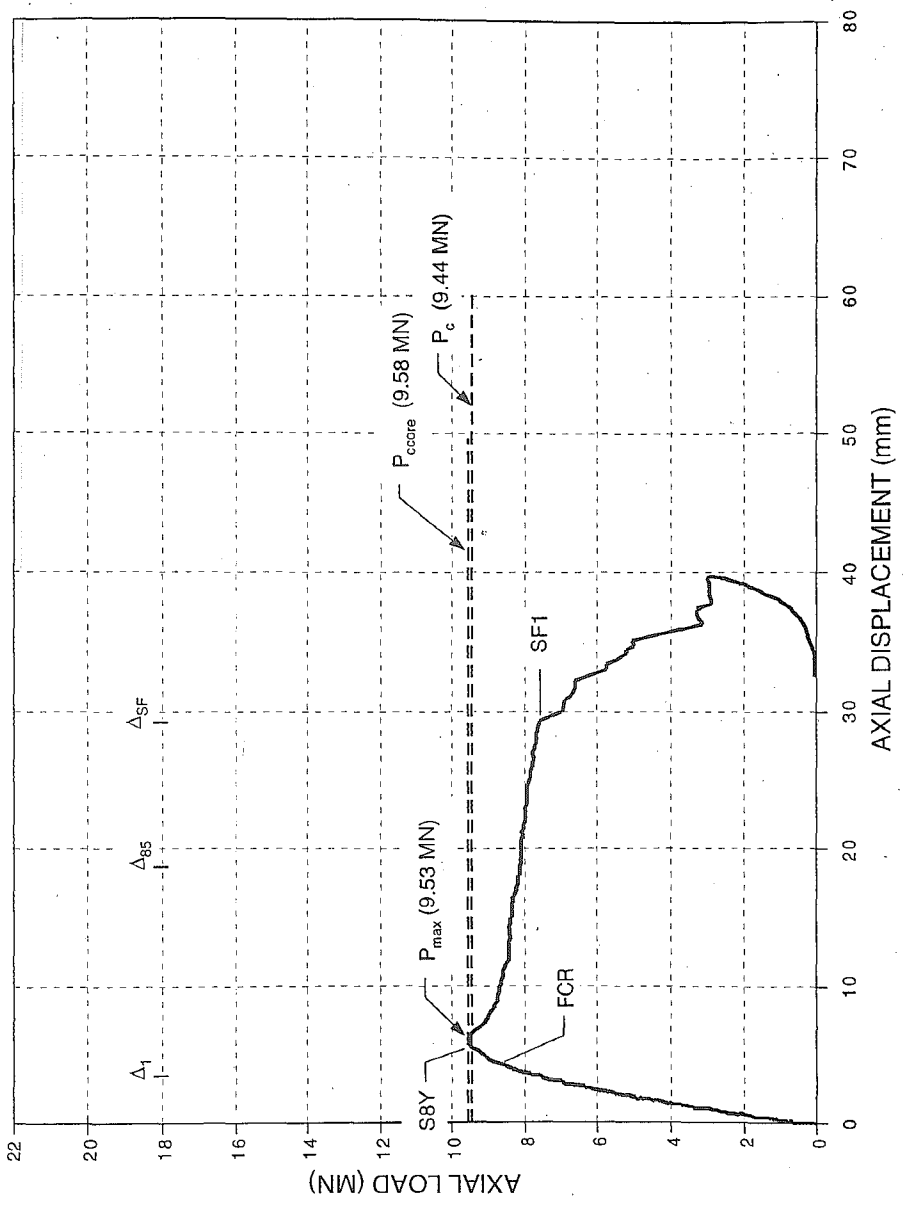

Figure 4.6 Specimen L2-axial load versus axial displacement.

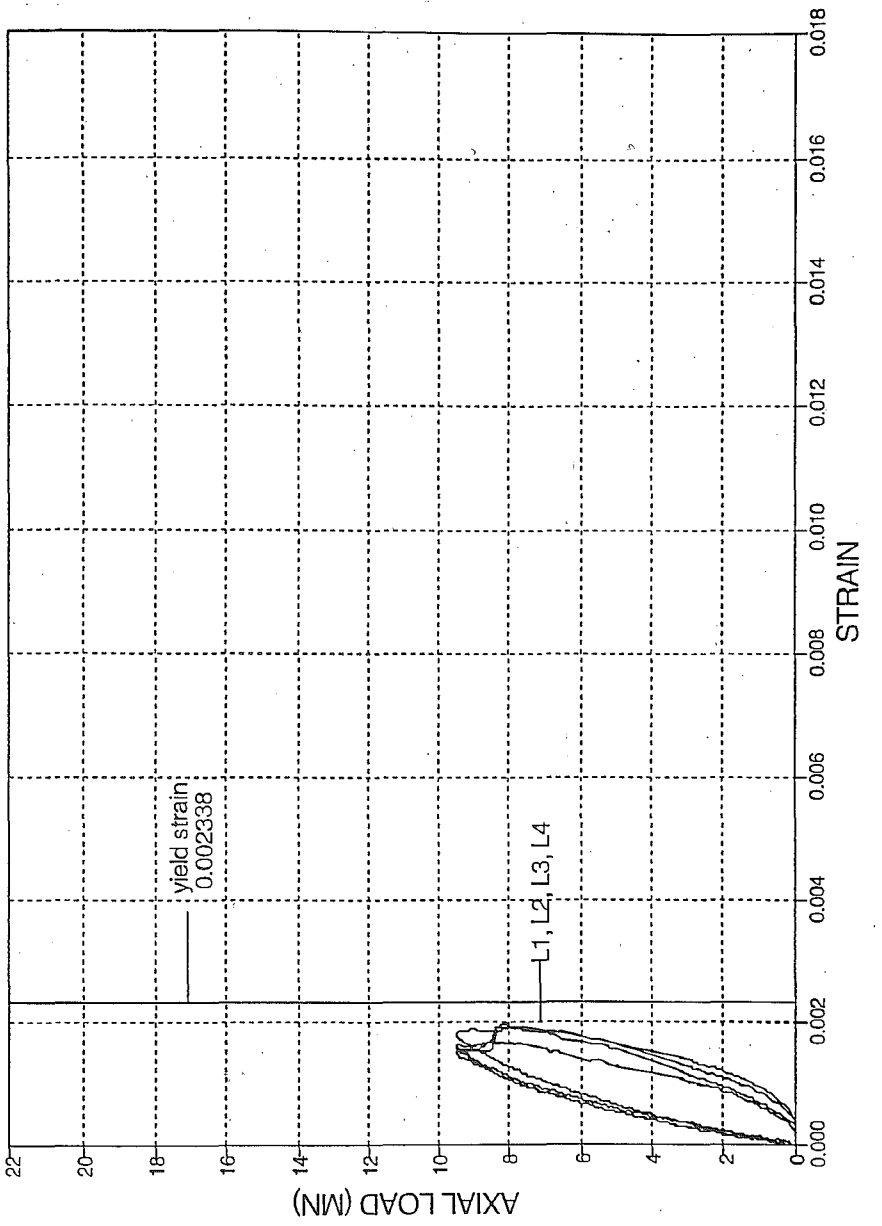

Figure 4.7 Specimen L2-axial load versus longitudinal reinforcement strains, gages L1, L2, L3, L4.

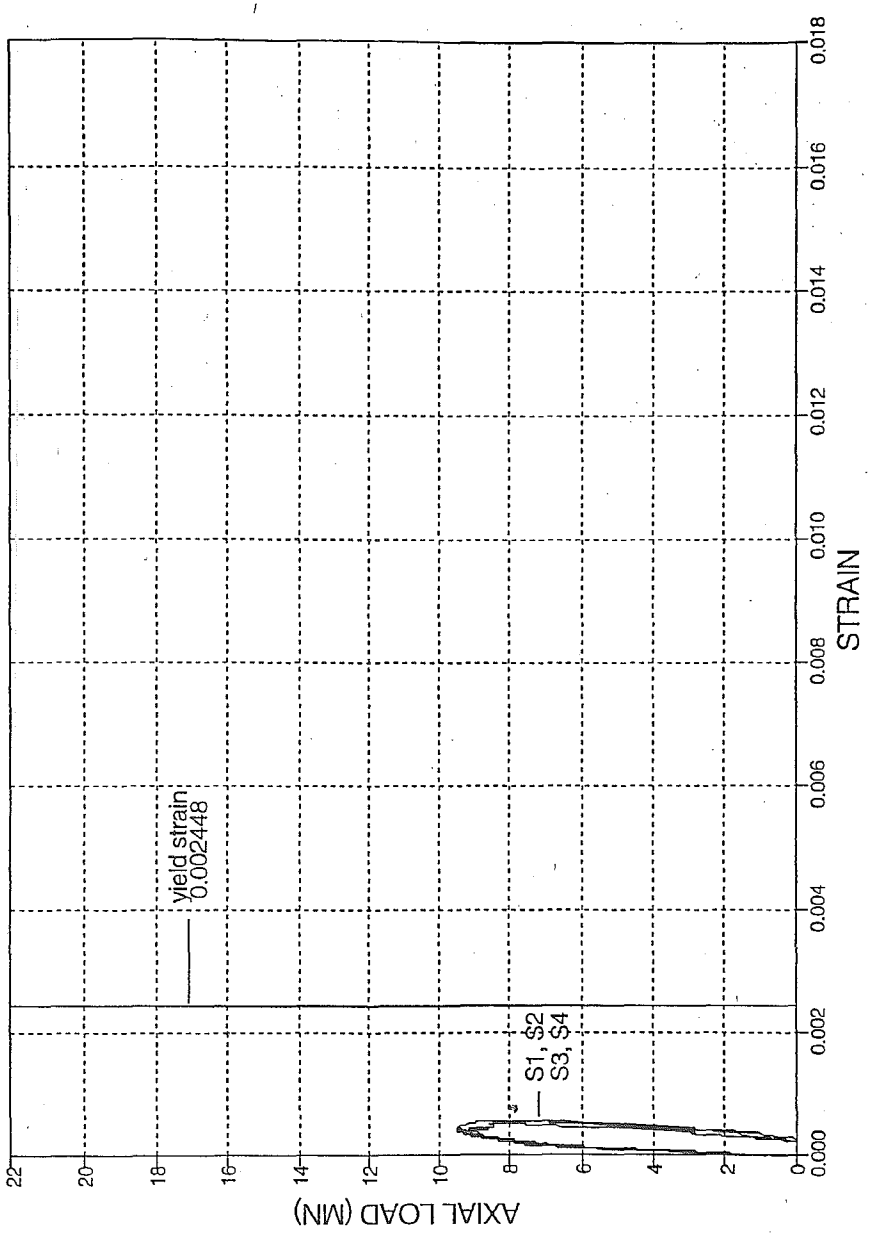

Figure 4.8 Specimen L2-axial load versus spiral reinforcement strains, gages S1, S2, S3, S4.

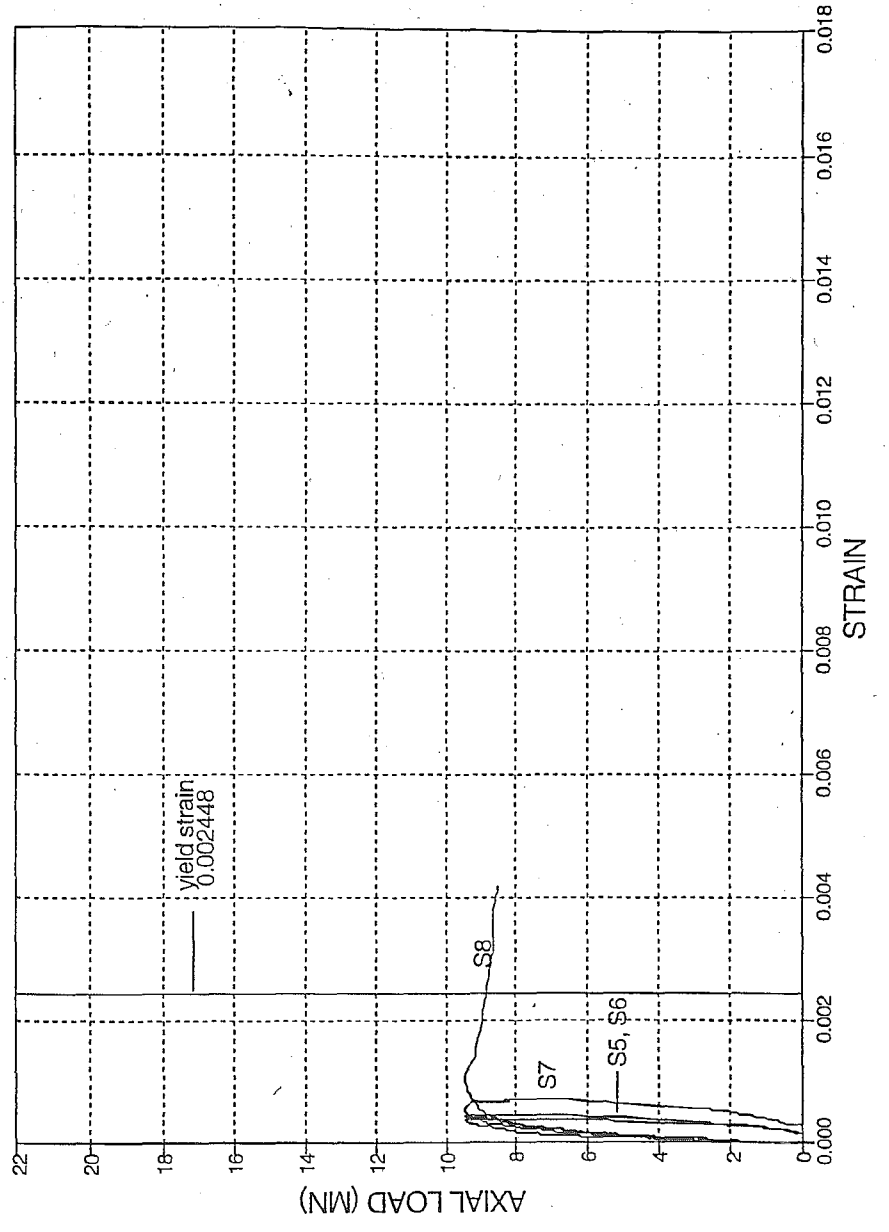

Figure 4.9 Specimen L2-axial load versus spiral reinforcement strains, gages S5, S6, S7, S8.

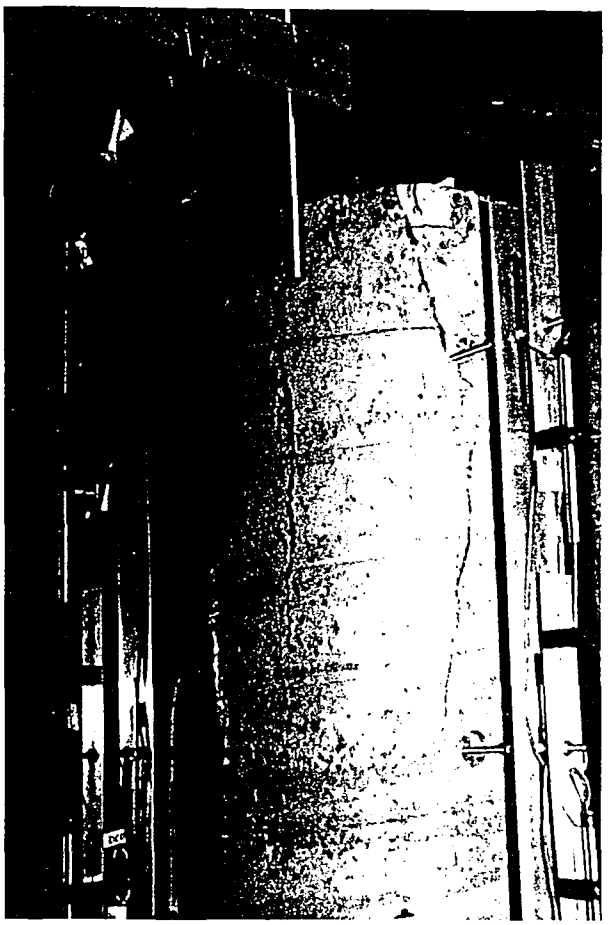

Figure 4.10(a) Specimen L2-series of key photographs; (a) initial cracking.

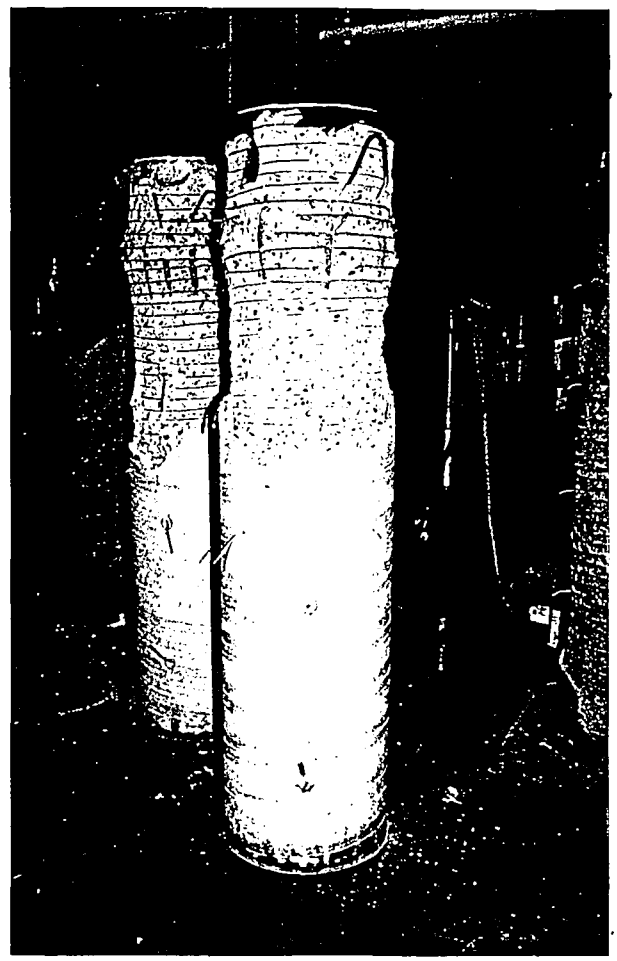

Figure 4.10(b) Specimen L2-series of key photographs; (b) post-test photograph showing the bulged failure region.

4.3.3 Specimen M1

-#5 spiral at 64 mm (2.5 in) pitch

-16-#9 longitudinal bars

-$f_{c\text{-field}}$ = 52.7 MPa (7.64 ksi)

-$f_{c\text{-core}}$ = 44.7 MPa (6.48 ksi)

The location of strain gages and the location of displacement transducers for Specimen M1 are detailed in Figure 3.3 and Figure 3.4, respectively. First cracking (FCR) was observed in the concrete cover at an axial load of 11.45 MN (2574 kips) and at an axial displacement of 5.0 mm (0.195 in). This is 67% of the maximum load. This crack initiated at the top of the column on the east face and was approximately 127 mm (5 in) long. The graph of axial load versus axial displacement (Figure 4.11) shows that the column exhibited an approximately linear load displacement response from the beginning of the test to first cracking in the cover concrete. At a load around 14.81 MN (3330 kips) a series of longitudinal splitting cracks, approximately 610 mm (2 ft) in length, existed at the top of the column on the northwest, and west face. The load peaked at about 15.2 MN (3410 kips), and the axial displacement at this load was 8.6 mm (0.339 in).

As the column was loaded more cracks developed in the cover concrete, and the existing cracks lengthened and widened. Figure 4.15(a) shows the southeast face at an axial load of 16.46 MN (3700 kips). The cover concrete began separating from the core and became less effective in sustaining load. The axial load of the column decreased approximately 400 kN (90 kips), then began

to increase again. As shown if Figure 4.11, the column sustained a constant load of about 16.90 MN (3800 kips). The maximum load (P_{max}) of the column was 16.99 MN (3820 kips) at an axial displacement of 20.3 mm (0.799 in).

During this period of increasing deformation at a constant load, additional cracking developed in the concrete cover. At an axial displacement of 34.2 mm (1.345 in) the longitudinal splitting cracks on the northwest face extended the full length of the column (Figure 4.15(b)). By an axial displacement of about 38.0 mm (1.495 in), the cracks on the southeast face of the column widened to about 19 mm (0.75 in) due to the lateral expansion of the core concrete. The extensive lateral deformation elongated the instrumented threaded rods causing rotation in the top row of LVDTs. As the lateral deformation further increased, the cover concrete separated from the core concrete in long sheets (Figure 4.15(c)).

The first spiral fracture (SF1) occurred at an axial displacement of Δ_{SF}=51.3 mm (2.019 in), as shown on Figure 4.11. This was accompanied by a decrease in column resistance from 16.1 MN (3614 kips) to 13.2 MN (2962 kips). The second spiral fracture (SF2) occurred at an axial displacement of 57.0 mm (2.245 in). This was accompanied by a 1.0 MN (225 kips) decrease in column axial force. A third spiral fracture (SF3) occurred at an axial displacement of 58.5 mm (2.302 in). The axial load on the column decreased 5.77 MN (1297 kips) when the fourth spiral fracture occurred. At this point the load on the column was 12% of the maximum load. The column was then unloaded at a rate of 222 kN/min (50 kips/min). Figures 4.15(d)-(f) reveal the column after the spiral fractures occurred.

Figure 4.12 is a graph of axial load versus strain in the longitudinal reinforcement. First yielding of the longitudinal bars was indicated by strain gages L1 and L2 at an axial load of 15.08 MN (3390 kips) and an axial displacement of 8.9 mm (0.349 in) (L1Y and L2Y on Figure 4.11). The variation of strain in the spiral reinforcement along the height of the column is illustrated in Figure 4.14. As shown in this figure and Figure 4.13, all the spiral strain gages yielded. First yielding in the spirals was indicated by strain gage S4 at an axial displacement of 12.24 mm (0.482 in) and an axial load of 16.11 MN (3596 kips) (S4Y on Figure 4.11).

At the end of the test the column was completely unloaded, and the separated regions of cover concrete were carefully removed to expose the core and spiral reinforcement (Figure 4.15(g)). Four spiral fractures were noted. All of the spiral fractures occurred at the location of buckled longitudinal bars. The failure region was characterized by an inclined failure plane concentrated in the top 1/3 of the column (Figure 4.15(h)). All of the spiral fractures were contained within this region.

Experimental Axial Capacity	Predicted Axial Capacity	
P_{max} (MN)	P_c (MN)	P_{ccore} (MN)
16.99	17.14	15.97

0.004448 MN=1 kip

Table 4.3 Specimen M1-predicted strengths and experimentally observed strengths.

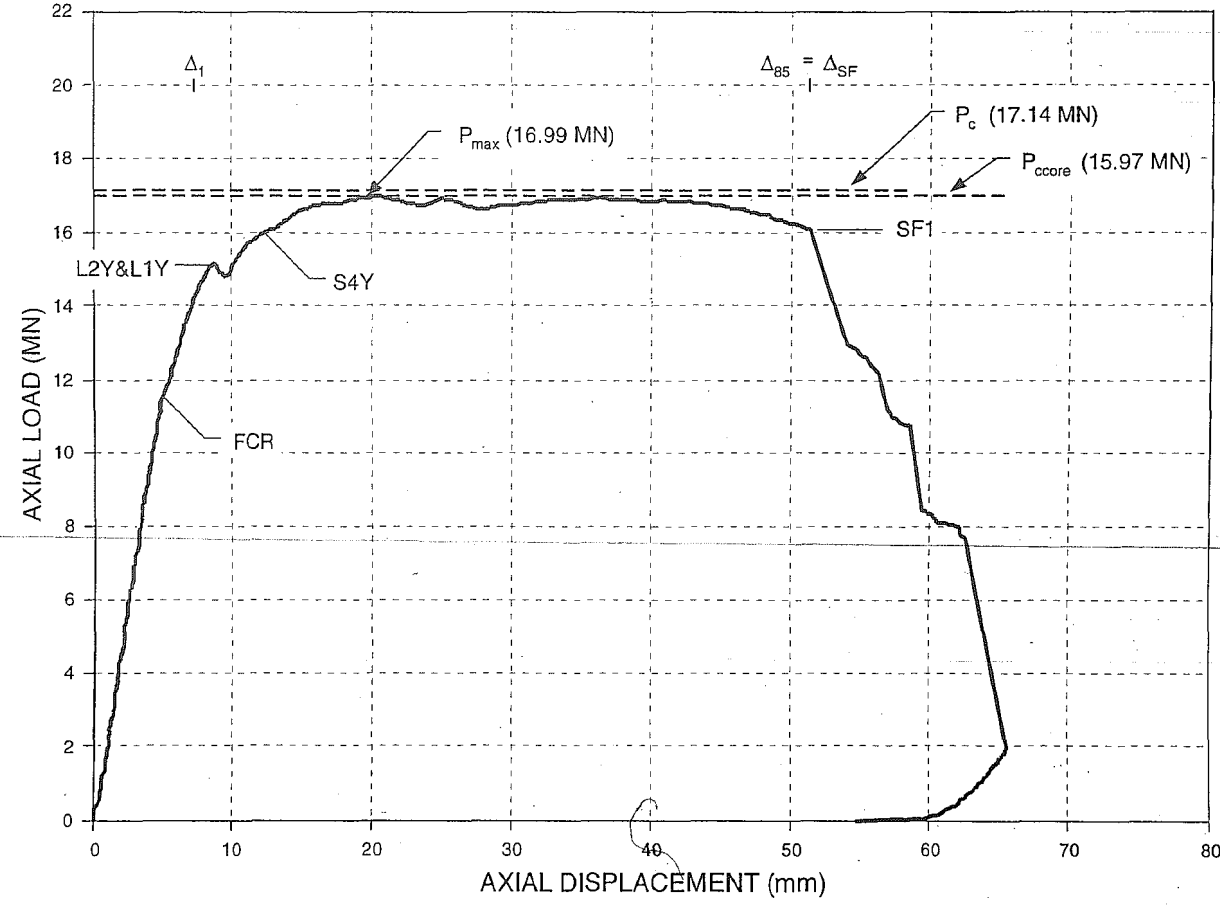

Figure 4.11 Specimen M1-axial load versus axial displacement.

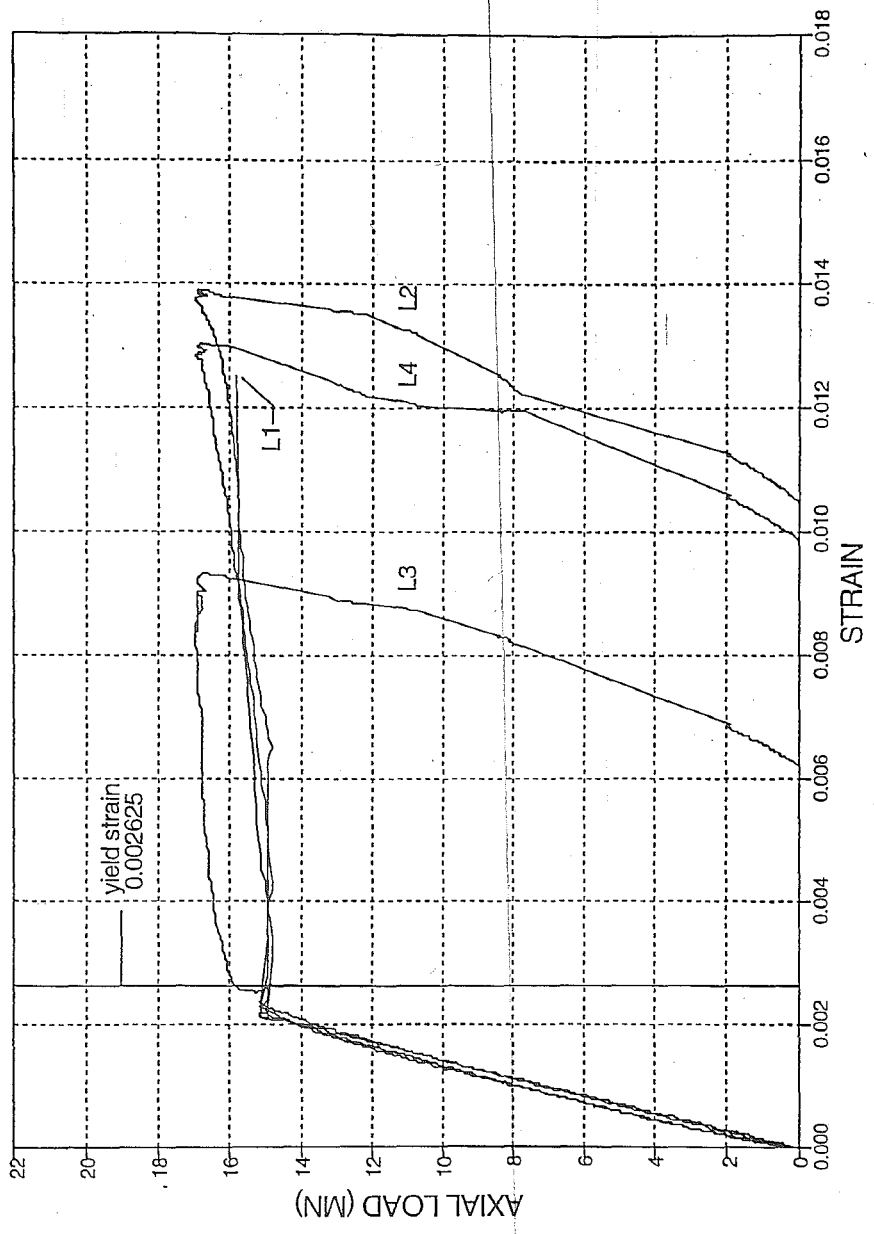

Figure 4.12 Specimen M1-axial load versus longitudinal reinforcement strains, gages L1, L2, L3, L4.

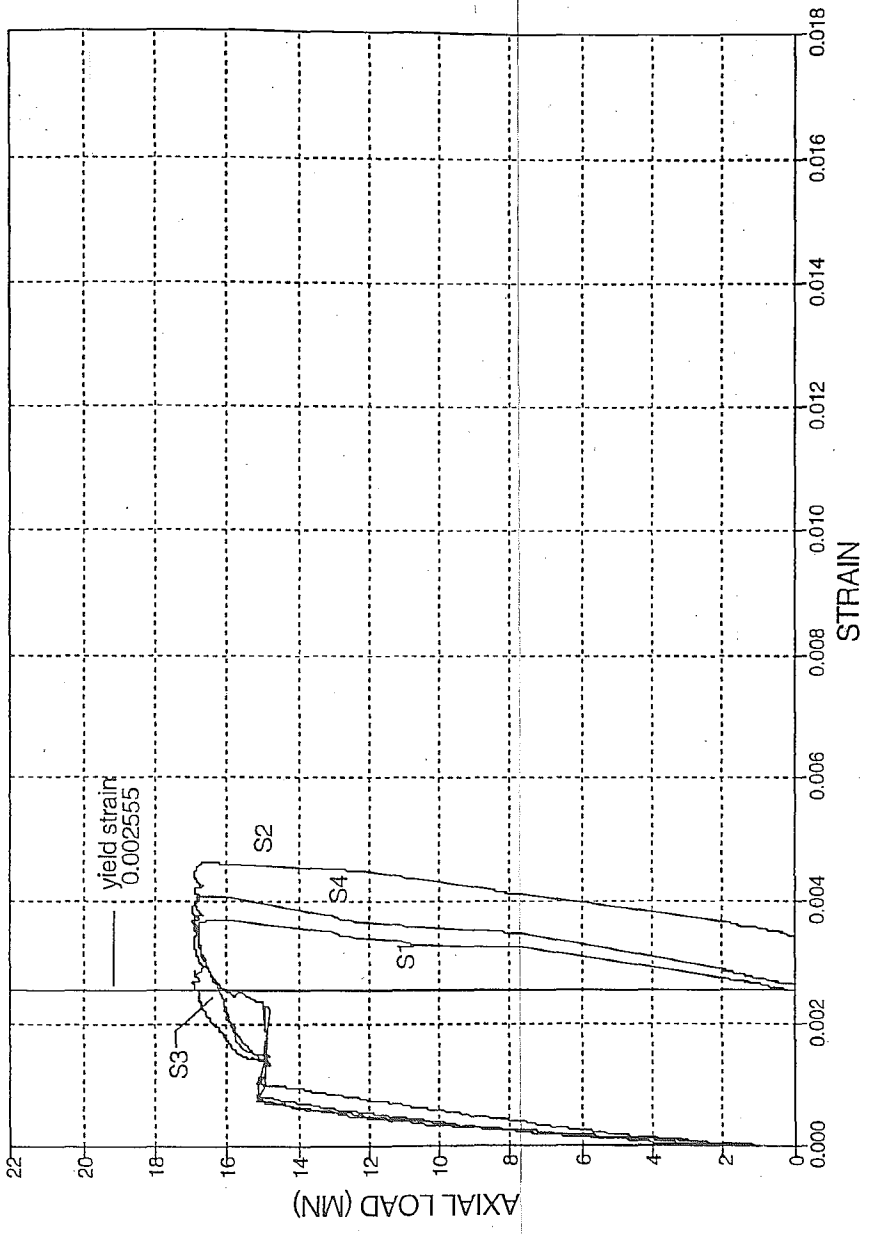

Figure 4.13 Specimen M1-axial load versus spiral reinforcement strains, gages S1, S2, S3, S4.

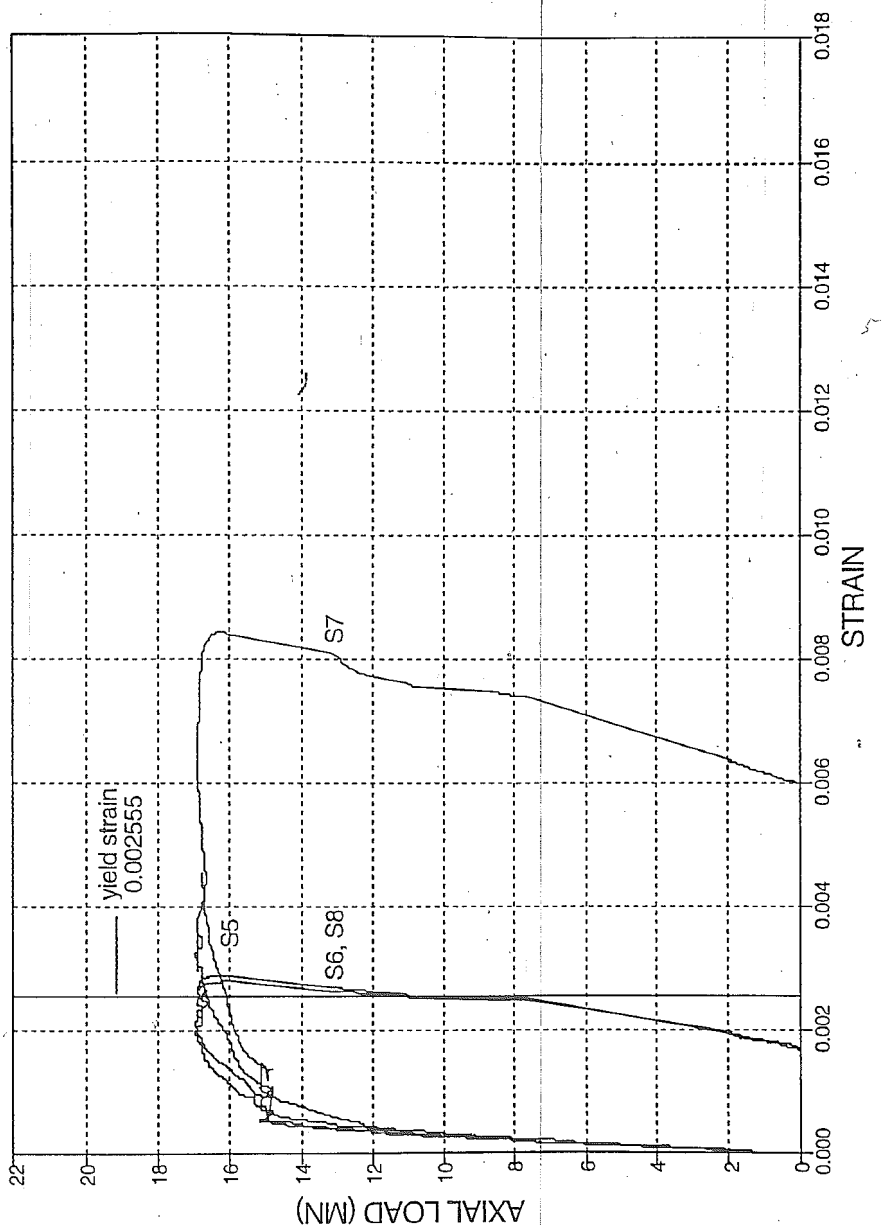

Figure 4.14 Specimen M1-axial load versus spiral reinforcement strains, gages S5, S6, S7, S8.

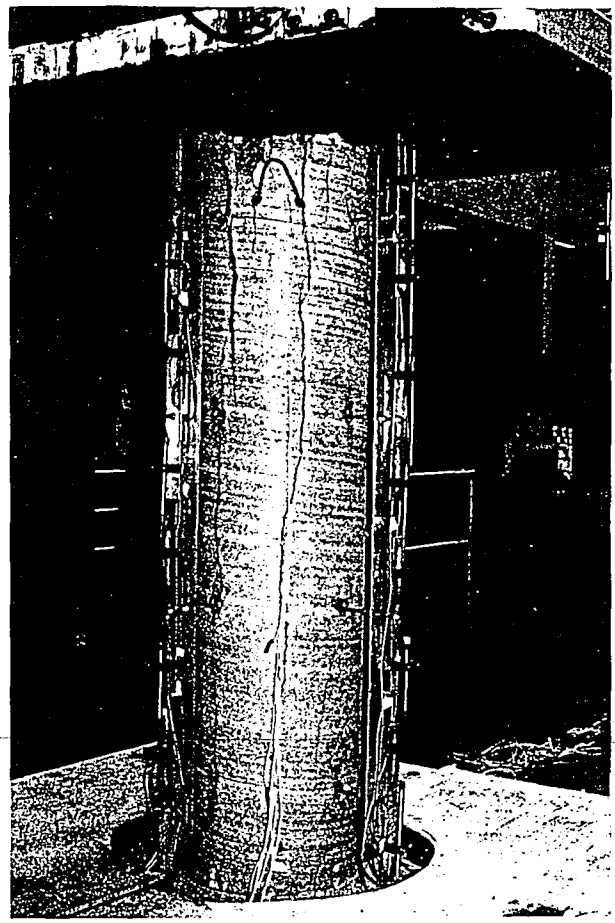

Figure 4.15(a) Specimen M1-series of key photographs; (a) longitudinal splitting cracks.

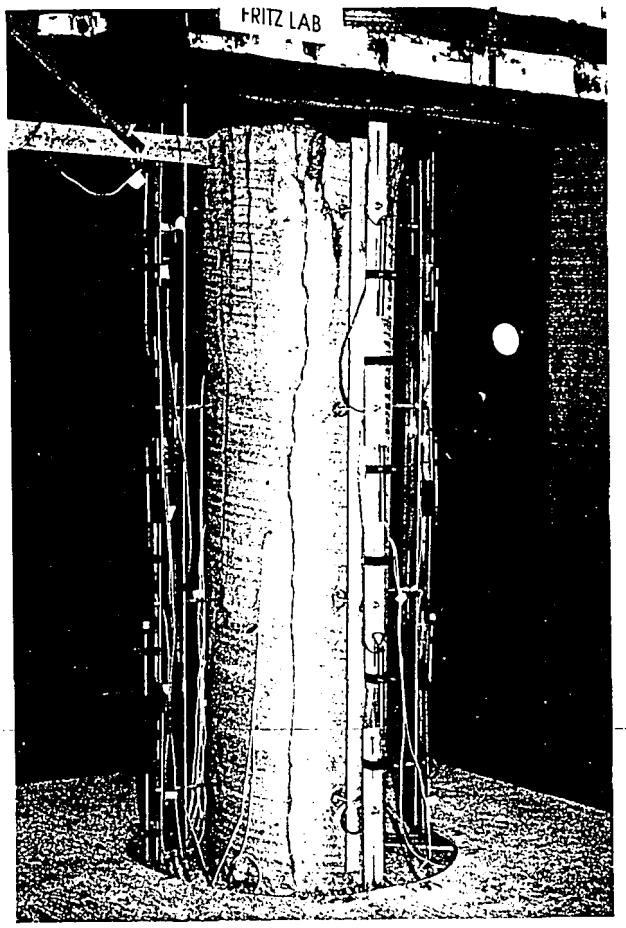

Figure 4.15(b) Specimen M1-series of key photographs; (b) longitudinal splitting cracks propagating the length of the column.

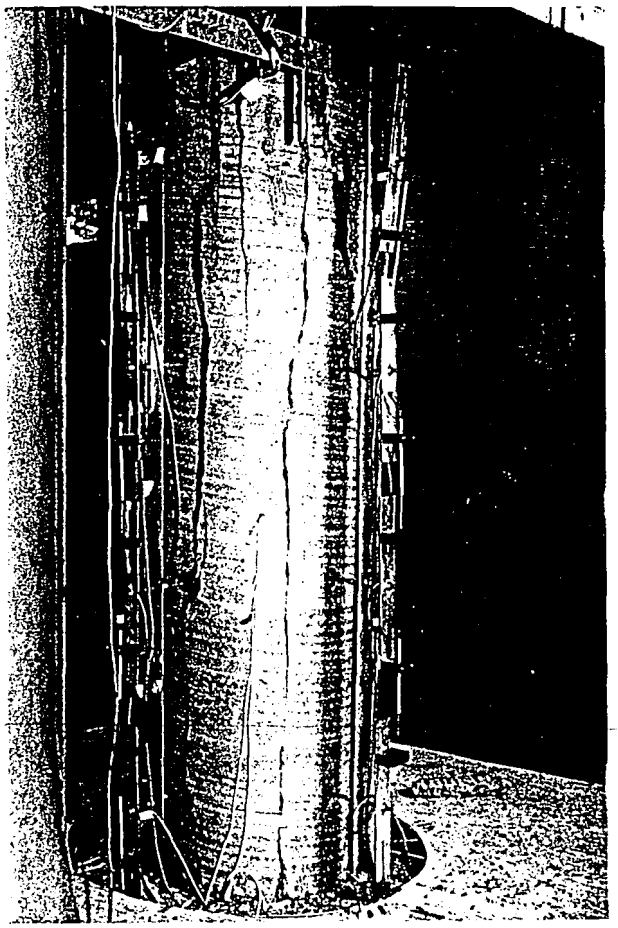

Figure 4.15(c) Specimen M1-series of key photographs; (c) separation of cover concrete into long sheets.

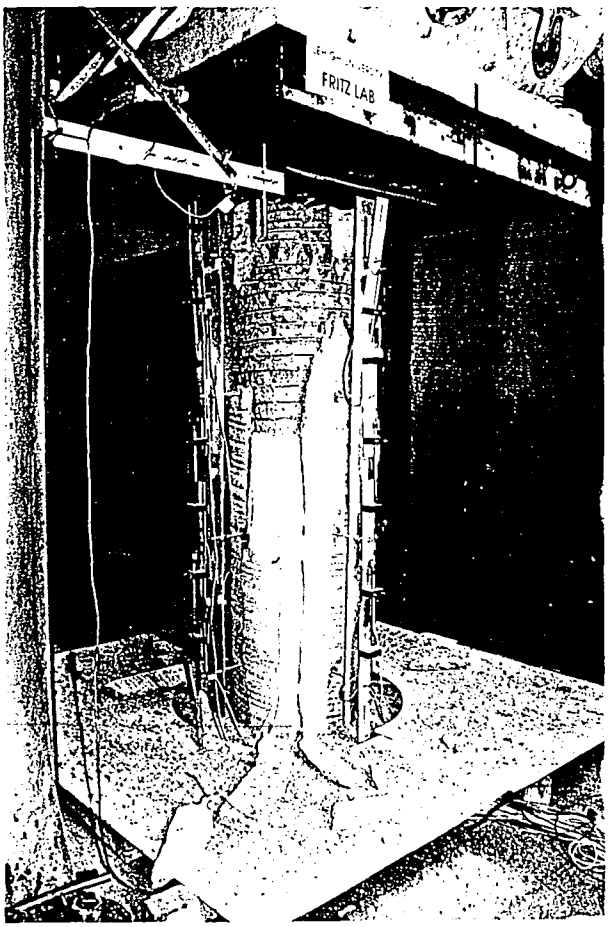

Figure 4.15(d) Specimen M1-series of key photographs; (d) exposed spiral reinforcement after spiral fractures.

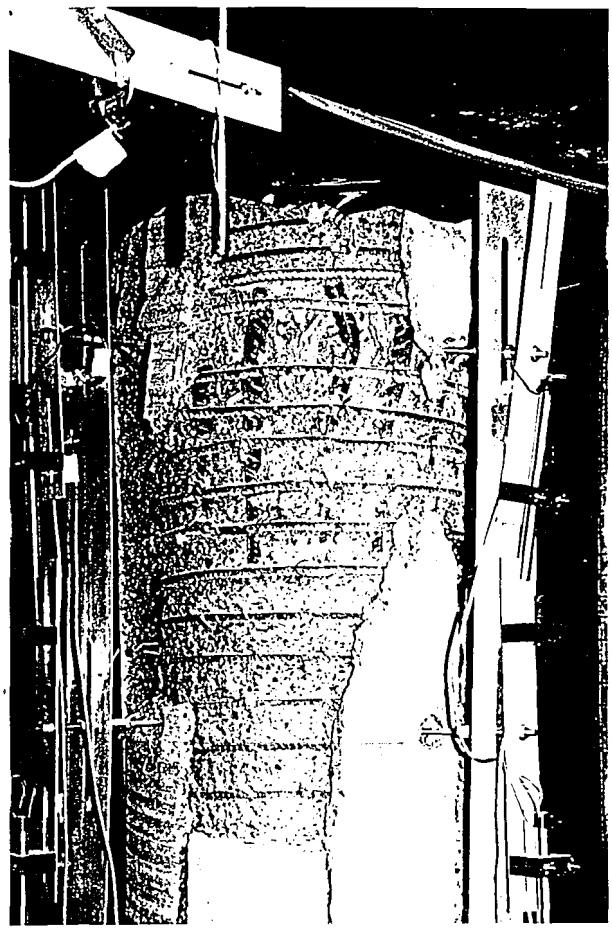

Figure 4.15(e) Specimen M1-series of key photographs; (e) exposed spiral reinforcement after spiral fractures.

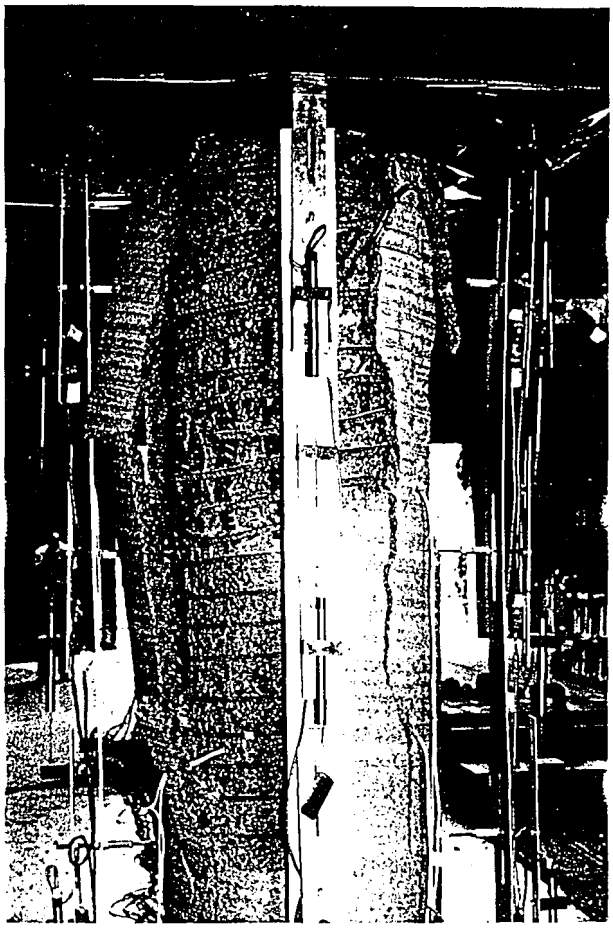

Figure 4.15(f) Specimen M1-series of key photographs; (f) exposed spiral reinforcement after spiral fractures.

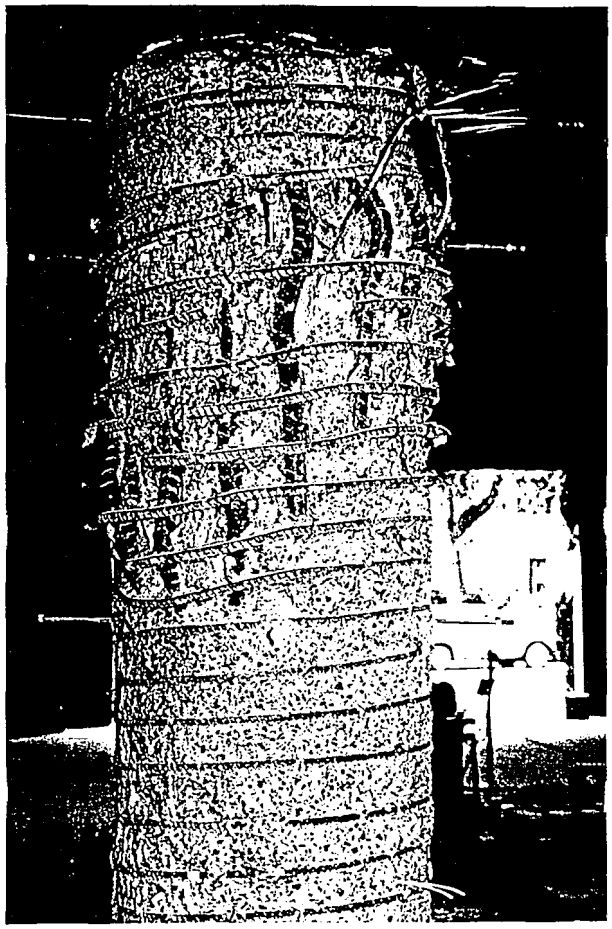

Figure 4.15(g) Specimen M1-series of key photographs; (g) spiral fractures at location of buckled longitudinal bars.

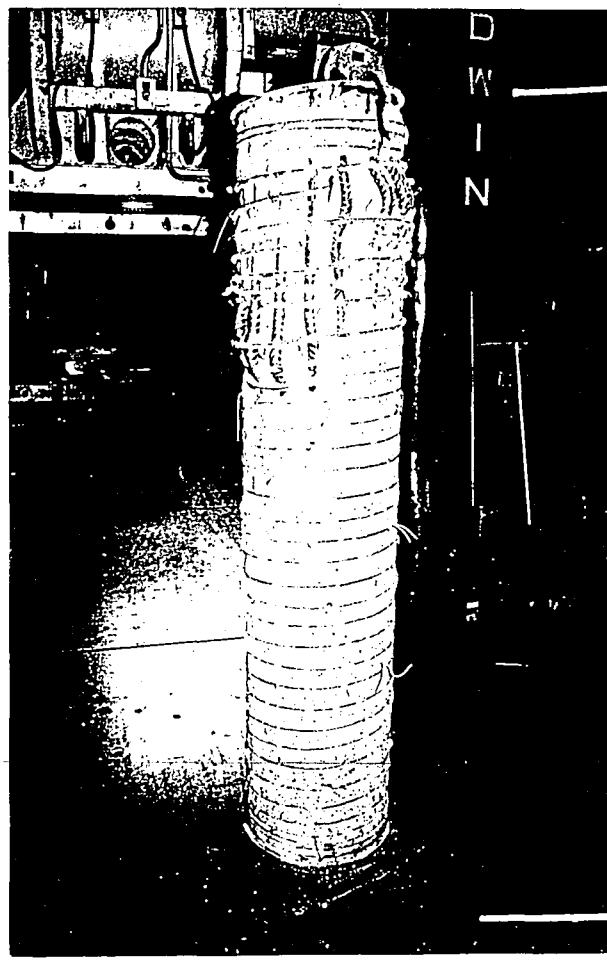

Figure 4.15(h) Specimen M1-series of key photographs; (h) post-test photograph showing the inclined failure plane.

4.3.4 Specimen M2

-#5 spiral at 64 mm (2.5 in) pitch

-8-#8 longitudinal bars

-$f_{c\text{-}field}$ = 52.7 MPa (7.64 ksi)

-$f_{c\text{-}core}$ = 44.7 MPa (6.48 ksi)

The location of strain gages and the location of displacement transducers for Specimen M2 are detailed in Figure 3.3 and Figure 3.4, respectively. First cracking (FCR) was observed in the concrete cover at an axial load of 10.20 MN (2294 kips) and at an axial displacement of 5.3 mm (0.208 in). This is 74% of the maximum load. A series of cracks initiated at the top of the column on the northeast, north, and northwest faces and were approximately 254 mm (10 in) long. The graph of axial load versus axial displacement (Figure 4.16) shows that the column exhibited an approximately linear load displacement response from the beginning of the test to first cracking in the cover concrete. At a load of around 14.81 MN (3330 kips) the longitudinal splitting crack on the southeast face was approximately 3.18 mm (0.125 in) wide. A peak in the load occurred at 12.33 MN (2772 kips), and the axial displacement at this load was 8.5 mm (0.334 in).

The cover concrete began separating from the core and became less effective in sustaining load. The axial resistance of the column decreased approximately 280 kN (63 kips), then began to increase again. As the column increased load more cracks developed in the cover concrete, and the existing cracks lengthened and widened. Figure 4.20(a) shows the southeast face at an axial load

of 12.61 MN (2836 kips) and at an axial displacement of 11.0 mm (0.434 in). The maximum load (P_{max}) of the column was 13.86 MN (3115 kips) at an axial displacement of 17.7 mm (0.696 in). As shown in Figure 4.16, the axial load on the column then began to decrease again with an increase in axial displacement. The axial load on the column decreased approximately 1.78 MN (400 kips) over a change in axial displacement of 17.3 mm (0.683 in). By a displacement of 24.8 mm (0.977 in) all the cracks extended the entire length of the column. The column then sustained a constant load of about 12.05 MN (2710 kips).

During this period of increasing deformation at a constant load, the existing cracks on the northeast face widened (Figure 4.20(b)). The extensive lateral deformation elongated the instrumented threaded rods causing rotation in the top row of LVDTs. As the lateral deformation further increased, the cover concrete separated from the core concrete in long sheets. These sheets of concrete slid along the plane formed between the core concrete and the cover concrete. As the concrete slid, it rested on the threaded rods and deformed them. At an axial displacement of 41.5 mm (1.632 in) a long and narrow section of the cover concrete fell from the column (Figure 4.20(c)).

The first spiral fracture (SF1) occurred at an axial displacement of Δ_{SF}=56.8 mm (2.236 in), shown in (Figure 4.16). This was accompanied by a decrease in column resistance from 11.78 MN (2650 kips) to 9.06 MN (2037 kips). The second spiral fracture (SF2) occurred at an axial displacement of 57.0 mm (2.442 in). This was accompanied by a 1.98 MN (445 kips) decrease in column axial

force. The column then exhibited increased axial displacement at an approximately constant load of 6.18 MN (1380 kips). A third spiral fracture (SF3) occurred at an axial displacement of 69.2 mm (2.724 in). At this point the load on the column was 36% of the maximum load. The column was then unloaded at a rate of 222 kN/min (50 kips/min). Figure 4.20(d) reveals the column after the spiral fractures occurred.

Figure 4.17 is a graph of axial load versus strain in the longitudinal reinforcement. First yielding of the longitudinal bars was indicated by strain gage L3 at an axial load of 10.90 MN (2450 kips) and an axial displacement of 6.3 mm (0.249 in) (L3Y on Figure 4.16). The variation of strain in the spiral reinforcement along the height of the column is illustrated in Figure 4.19. First yielding of the spirals was indicated by strain gage S3 at and axial displacement of 13.0 mm (0.546 in) and an axial load of 13.18 MN (2964 kips).

At the end of the test the column was completely unloaded, and the separated regions of cover concrete were carefully removed to expose the core and spiral reinforcement. Deformation in the spiral reinforcement was visible (Figure 4.20(e)). Three spiral fractures were noted. All of the spiral fractures occurred at the location of buckled longitudinal bars. The failure region was characterized by an inclined failure plane concentrated in the top 1/2 of the column (Figure 4.20(f)). The plane extended from the top of the south face to the middle of the north face. All of the spiral fractures were contained within this region.

Experimental Axial Capacity	Predicted Axial Capacity	
P_{max} (MN)	P_c (MN)	P_{ccore} (MN)
13.86	14.05	12.83

0.004448 MN=1 kip

Table 4.4 Specimen M2-predicted strengths and experimentally observed strengths.

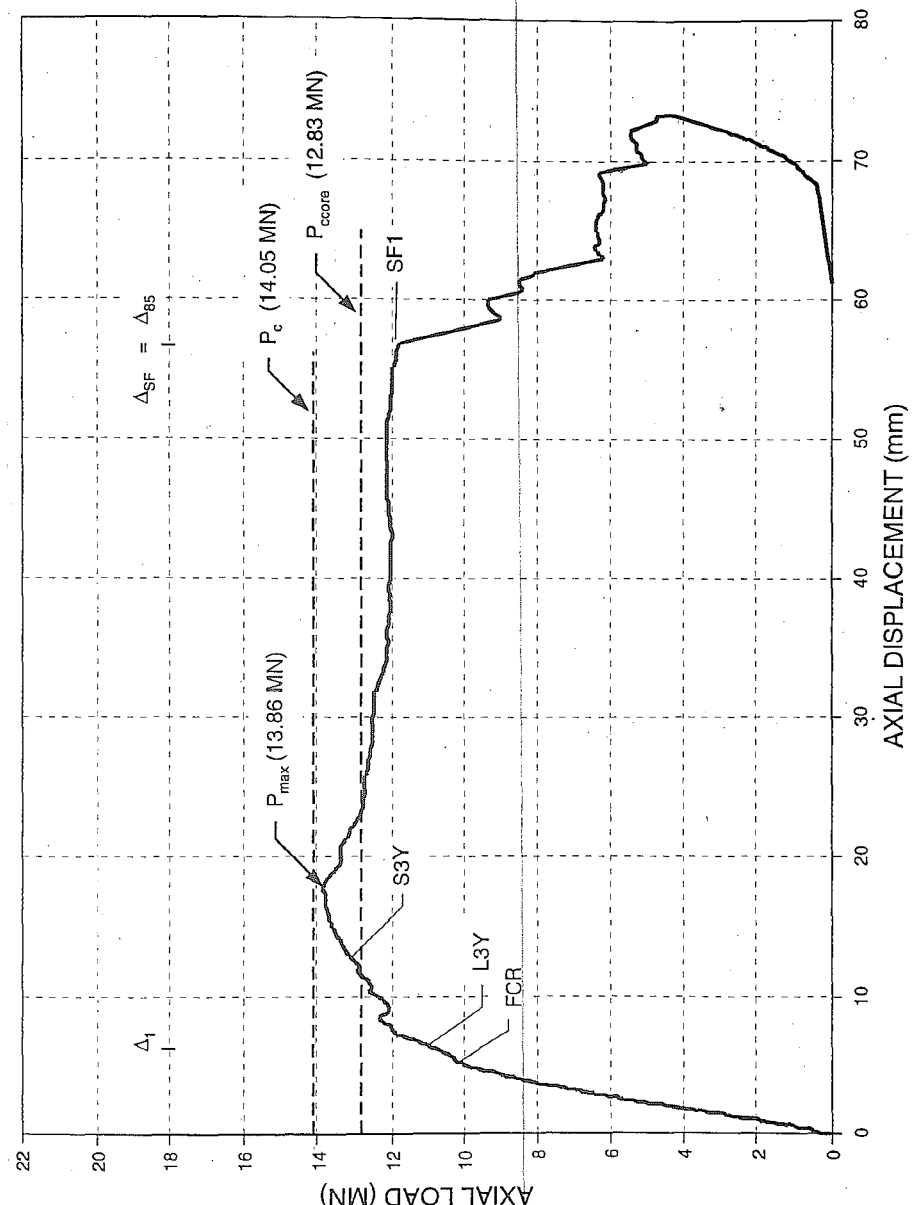

Figure 4.16 Specimen M2-axial load versus axial displacement.

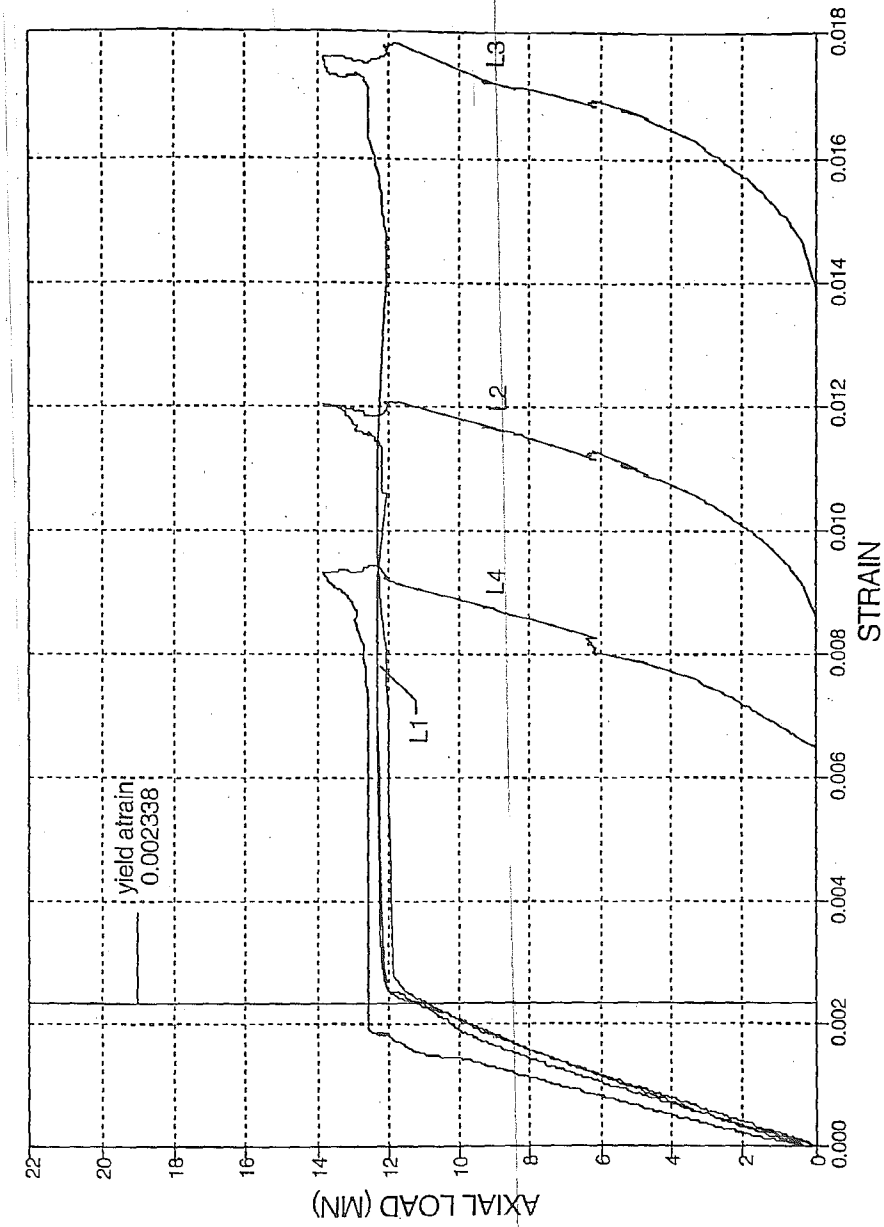

Figure 4.17 Specimen M2-axial load versus longitudinal reinforcement strains, gages L1, L2, L3, L4.

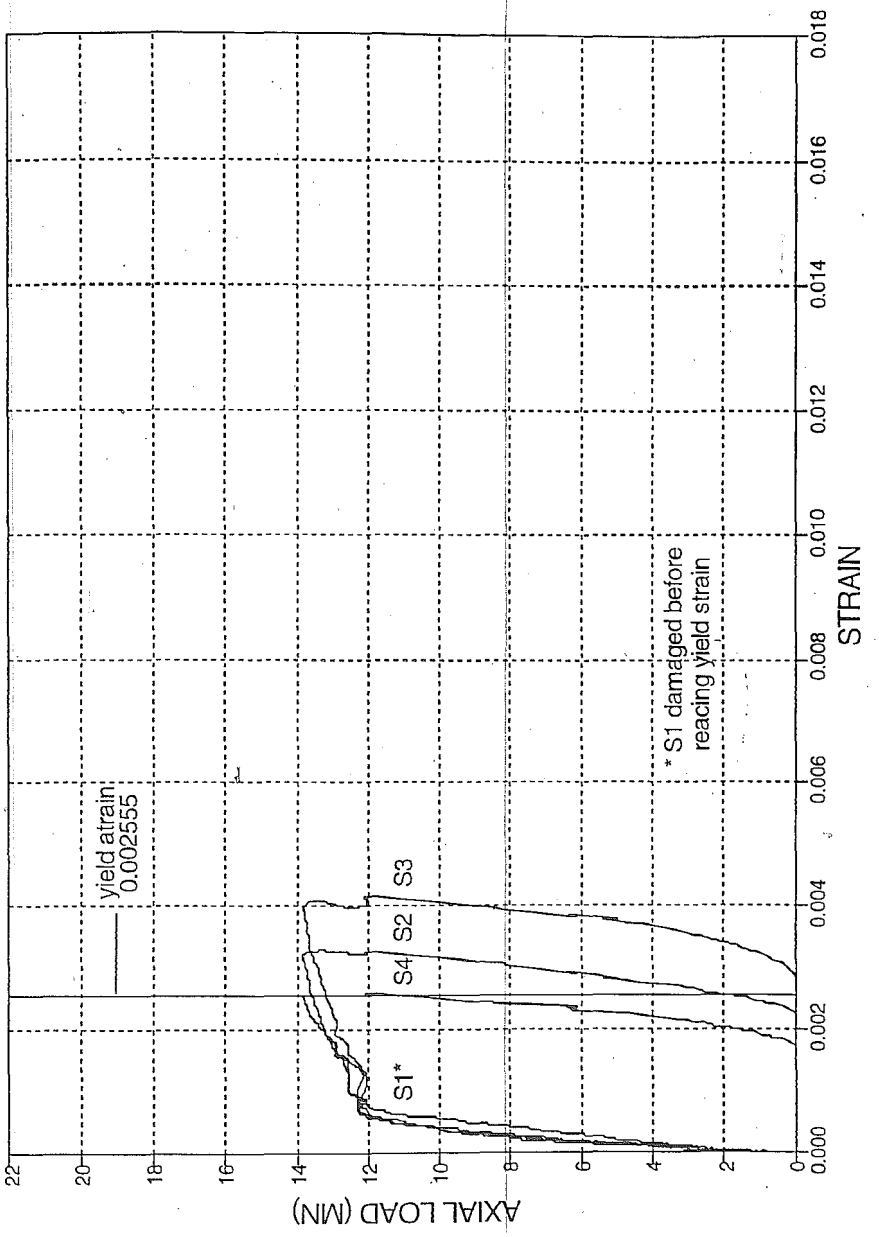

Figure 4.18 Specimen M2-axial load versus spiral reinforcement strains, gages S1, S2, S3, S4.

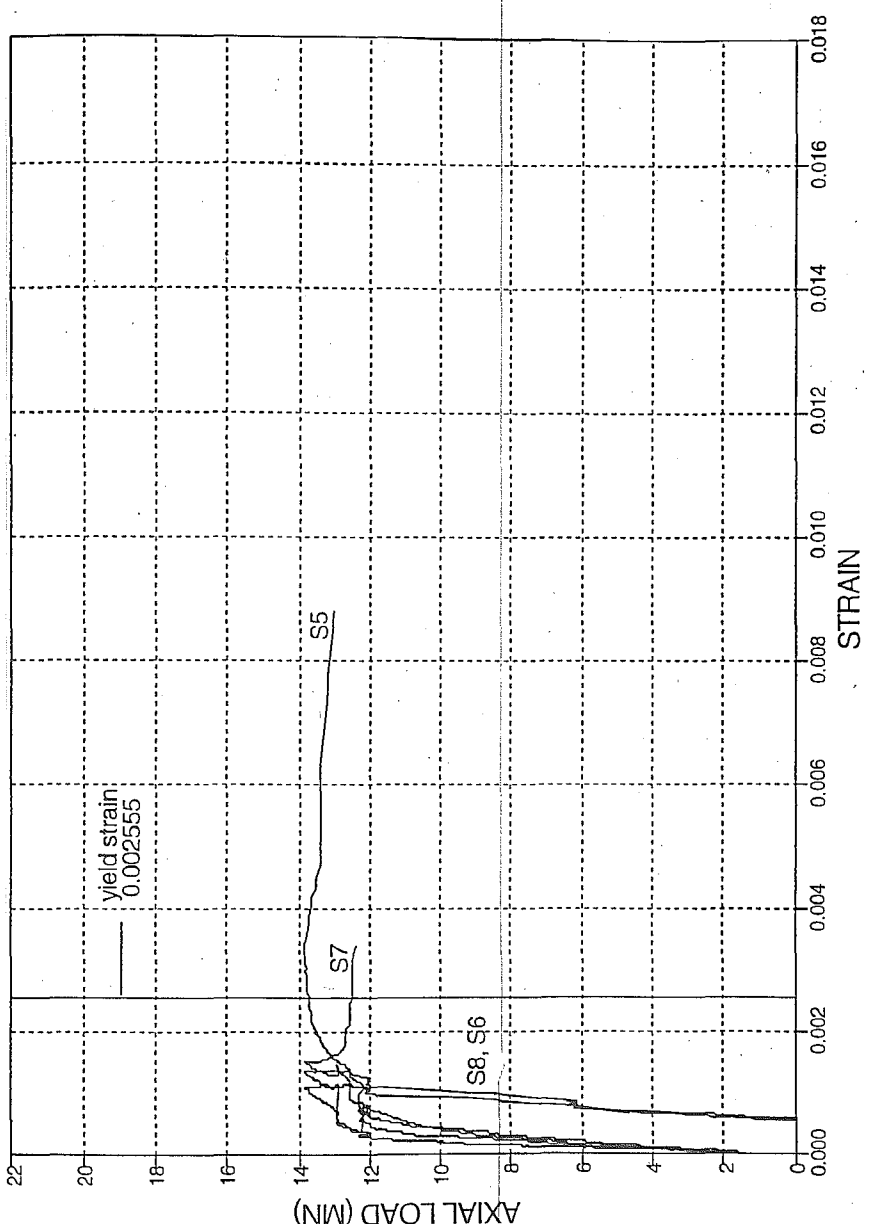

Figure 4.19 Specimen M2-axial load versus spiral reinforcement strains, gages S5, S6, S7, S8.

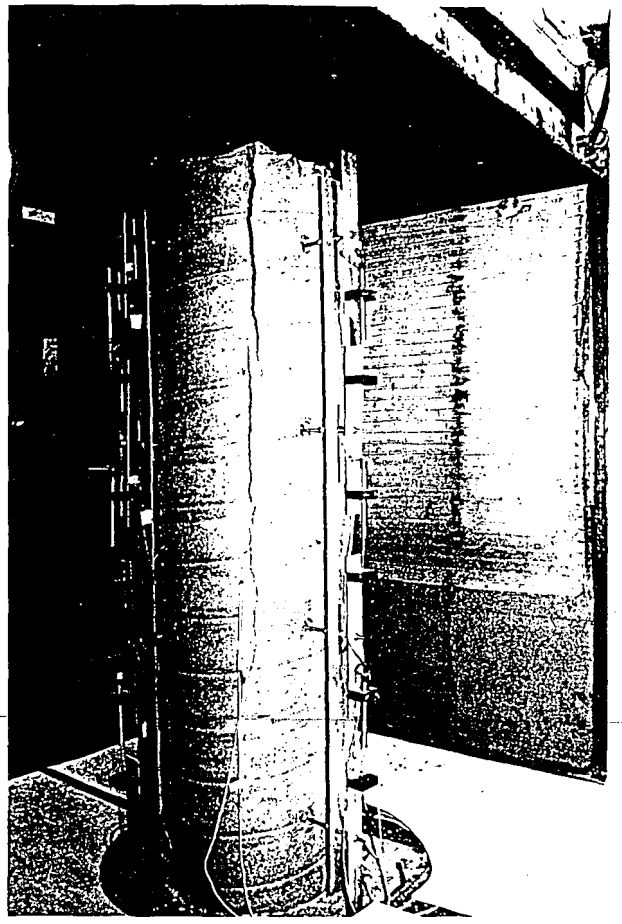

Figure 4.20(a) Specimen M2-series of key photographs; (a) longitudinal splitting crack on southeast face.

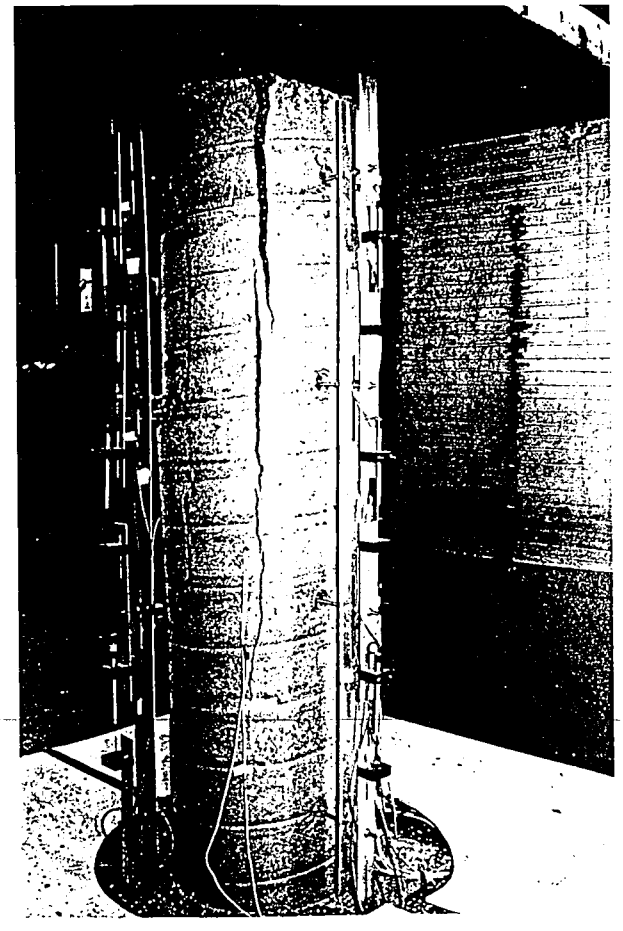

Figure 4.20(b) Specimen M2-series of key photographs; (b) widening of longitudinal splitting crack on southeast face.

Figure 4.20(c) Specimen M2-series of key photographs; (c) spalling of cover concrete in long sheets.

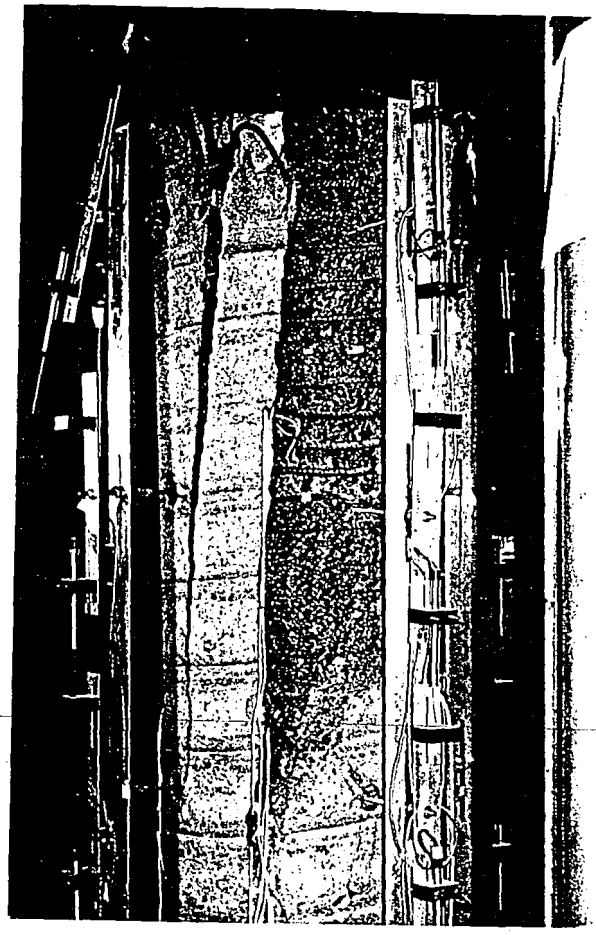

Figure 4.20(d) Specimen M2-series of key photographs; (d) exposed core concrete after fracture of spirals.

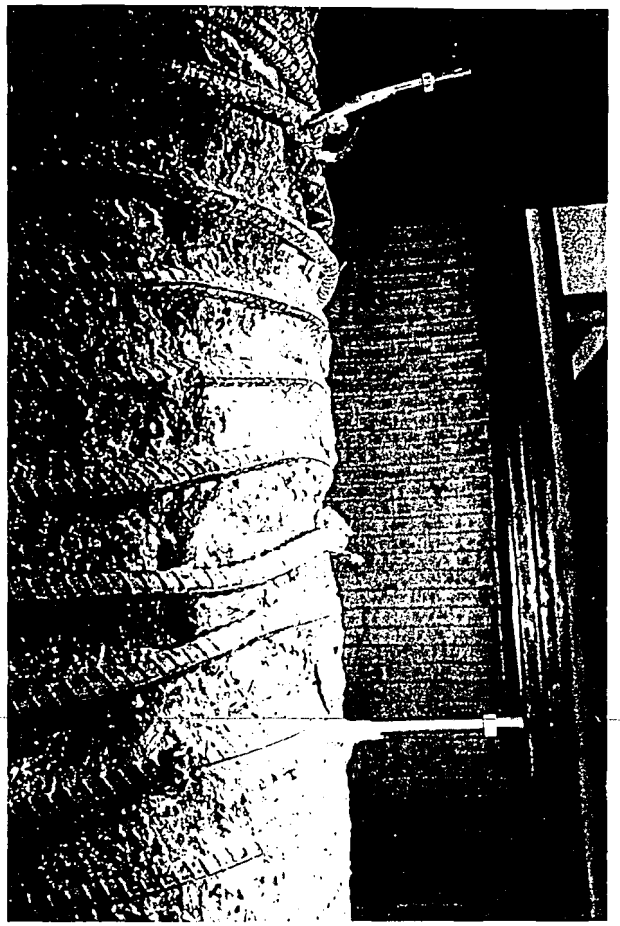

Figure 4.20(e) Specimen M2-series of key photographs; (e) deformation of the spiral reinforcement.

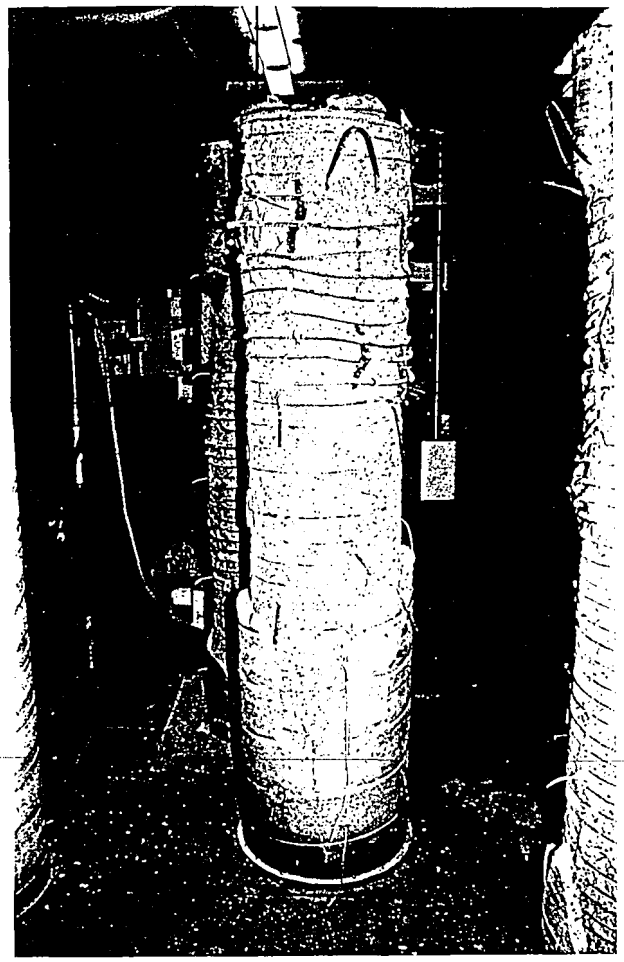

Figure 4.20(f) Specimen M2-series of key photographs; (f) post-test photograph showing the inclined failure plane.

4.3.5 Specimen M3

-#4 spiral at 41.3 mm (1.625 in) pitch

-8-#8 longitudinal bars

-$f_{c\text{-}field}$ = 52.7 MPa (7.64 ksi)

-$f_{c\text{-}core}$ = 44.7 MPa (6.48 ksi)

The location of strain gages and the location of displacement transducers for Specimen M3 are shown in Figure 3.3 and Figure 3.4, respectively. First cracking (FCR) was observed in the concrete cover at an axial load of 11.10 MN (2495 kips) and at an axial displacement of 5.7 mm (0.223 in). This is 77% of the maximum load. A series of hairline cracks initiated at the top of the column on the southeast face. The graph of axial load versus axial displacement (Figure 4.21) shows that the column exhibited an approximately linear load displacement response from the beginning of the test to first cracking in the cover concrete. At a load around 12.32 MN (2769 kips) the longitudinal splitting crack on the southeast face was approximately 1/3 the length of the column (Figure 4.25(a)) and cracks 254 mm (10 in) long formed at the top of the northwest and west faces. The column reached a peak load of 12.41 MN (2790 kips), and the axial displacement at this load was 6.7 mm (0.271 in).

Cracks quickly developed in the cover concrete, and it became less effective in sustaining load. The axial load of the column decreased approximately 400 kN (90 kips), then began to increase again. As the column increased load more cracks developed in the cover concrete, and the existing cracks on the northwest

and west faces propagated the entire length of the column. Figure 4.25(b) shows the cracks which developed on the northeast face. The maximum load (P_{max}) of the column was 14.50 MN (3258 kips) at an axial displacement of 16.2 mm (0.638 in). As shown in Figure 4.21, the axial load on the column then began to decrease with an increase in axial displacement. At an axial load of 12.79 MN (2875 kips), the load on the column suddenly decreased 1.13 MN (255 kips). The column then sustained a constant load around 11.79 MN (2650 kips).

During this period of increasing deformation at a constant load, extensive lateral deformation elongated and bent the instrumented threaded rods causing rotation in the top row of LVDTs. As the lateral deformation further increased, sections of cover concrete fell from the column on the west and northwest faces (Figure 4.25(c)). The cover concrete separated from the core concrete in long sheets (Figure 4.25(d)). These sheets of concrete slid along the plane formed between the core concrete and the cover concrete. As the concrete slid, it rested on the threaded rods and deformed them.

The first spiral fracture (SF1) occurred at an axial displacement of Δ_{SF}=50.3 mm (1.981 in), shown in Figure 4.21. This was accompanied by a decrease in column resistance from 11.57 MN (2602 kips) to 11.24 MN (2528 kips). Five successive spiral fractures then occurred and the axial load on the column decreased from 11.08 MN (2491 kips) to 9.32 MN (2096 kips). The axial load on the column continuously decreased as more spiral fractures occurred. The spiral fractures occurred as a series of several fractures. The axial load on the column

decreased to 3.95 MN (888 kips) which was 25% of the first peak load. The column was then unloaded at a rate of 222 kN/min (50 kips/min). Figure 4.25(e) reveals the column after the spiral fractures occurred.

Figure 4.22 is a graph of axial load versus strain in the longitudinal reinforcement. First yielding of the longitudinal bars was indicated by strain gage L3 at an axial load of 11.74 MN (2640 kips) and an axial displacement of 6.3 mm (0.247 in) (L3Y on Figure 4.21). The variation of strain in the spiral reinforcement along the height of the column is illustrated in Figure 4.24. As shown in Figure 4.21, first yielding of the spirals was indicated by strain gage S3 at an axial displacement of 10.7 mm (0.423 in) and an axial load of 12.92 MN (2904 kips).

At the end of the test the column was completely unloaded, and the separated regions of cover concrete were carefully removed to expose the core and spiral reinforcement. Deformation in the spiral reinforcement was visible (Figure 4.25(f)). Eighteen spiral fractures were counted. All of the spiral fractures occurred at the location of buckled longitudinal bars (Figures 4.25(g)-(i)). The failure region was characterized by an inclined failure plane concentrated in the top 1/2 of the column (Figure 4.25(g)). The plane extended from the top of the west face to the middle of the east face. All of the spiral breaks were contained within this region.

Experimental Axial Capacity	Predicted Axial Capacity	
P_{max} (MN)	P_c (MN)	P_{ccore} (MN)
14.50	14.10	12.89

0.004448 MN=1 kip

Table 4.5 Specimen M3-predicted strengths and experimentally observed strengths.

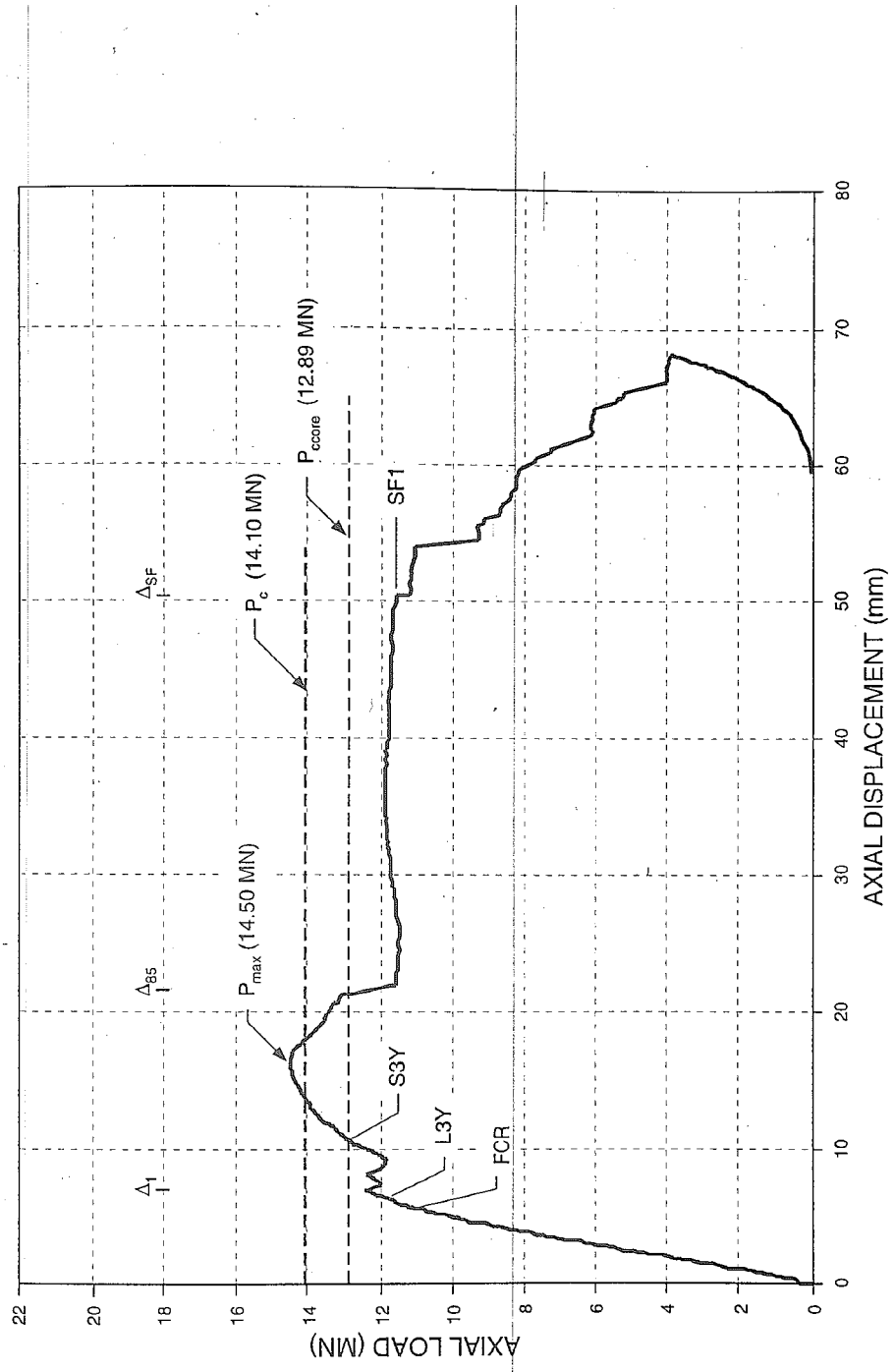

Figure 4.21 Specimen M3-axial load versus axial displacement.

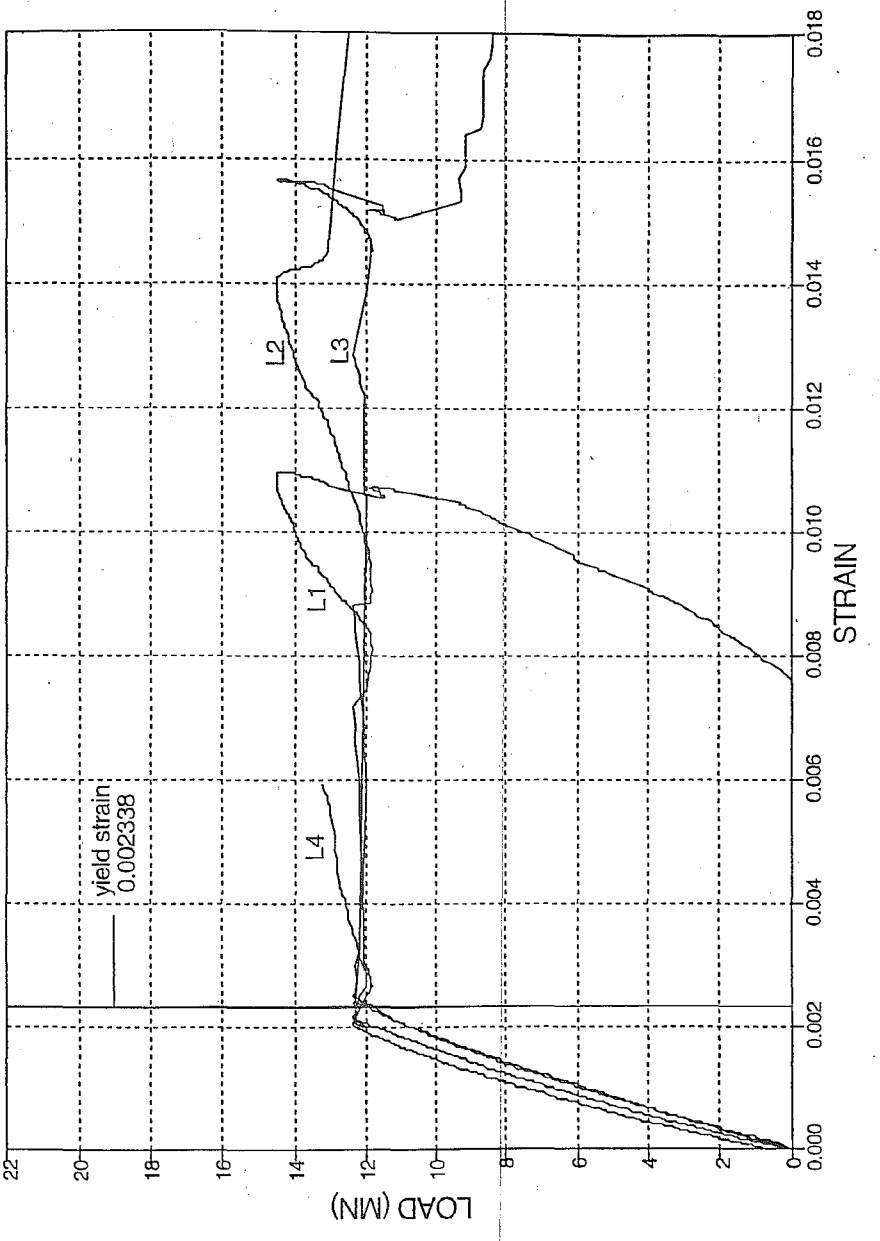

Figure 4.22 Specimen M3-axial load versus longitudinal reinforcement strains, gages L1, L2, L3, L4.

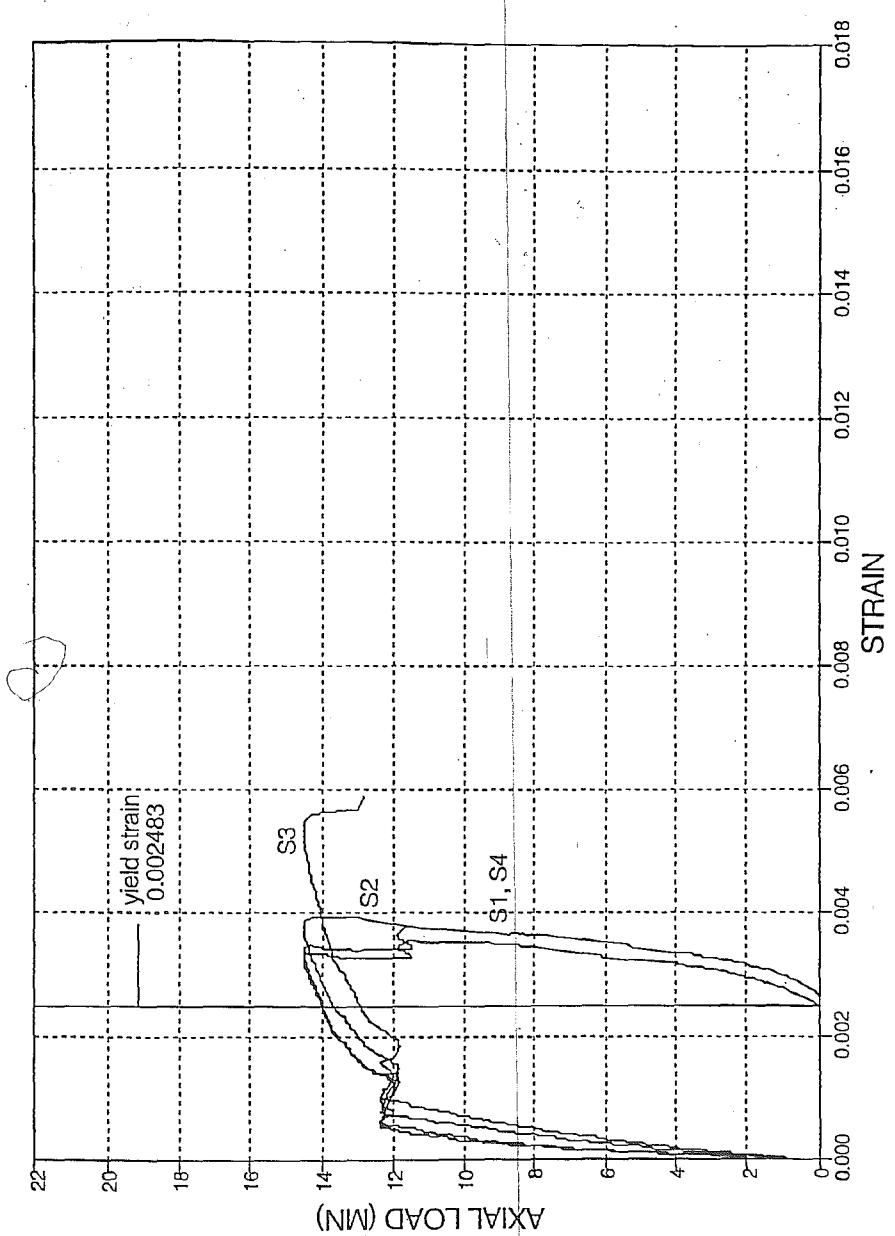

Figure 4.23 Specimen M3-axial load versus spiral reinforcement strains, gages S1, S2, S3, S4.

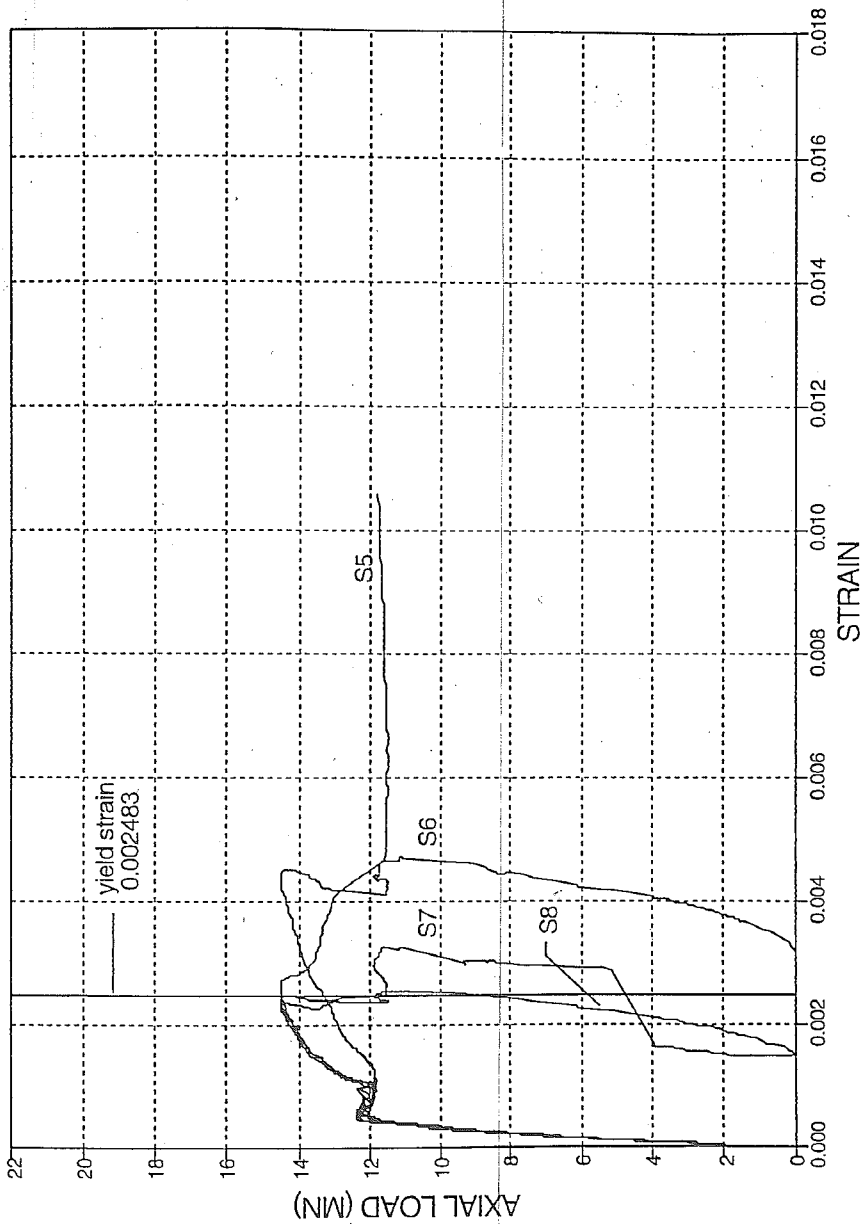

Figure 4.24 Specimen M3-axial load versus spiral reinforcement strains, gages S5, S6, S7, S8.

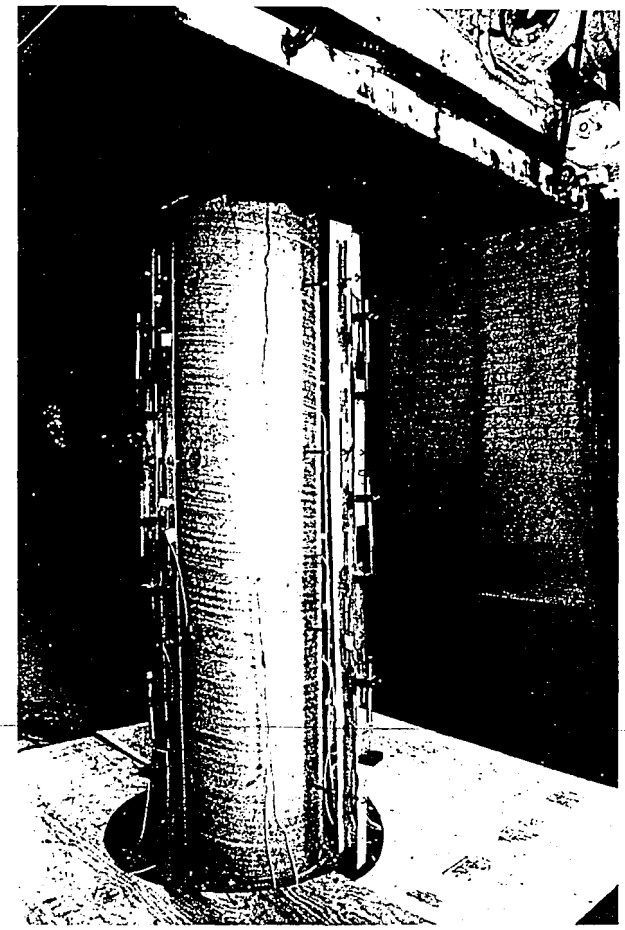

Figure 4.25(a) Specimen M3-series of key photographs; (a) longitudinal splitting crack on southeast face.

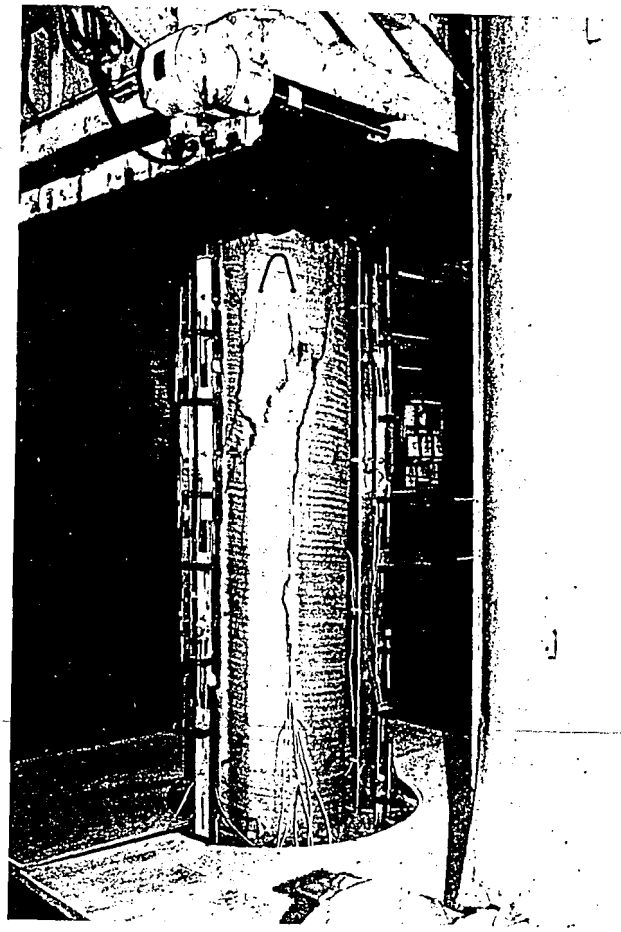

Figure 4.25(b) Specimen M3-series of key photographs; (b) longitudinal splitting crack on northeast face.

Figure 4.25(c) Specimen M3-series of key photographs; (c) separation of cover concrete in long sheets.

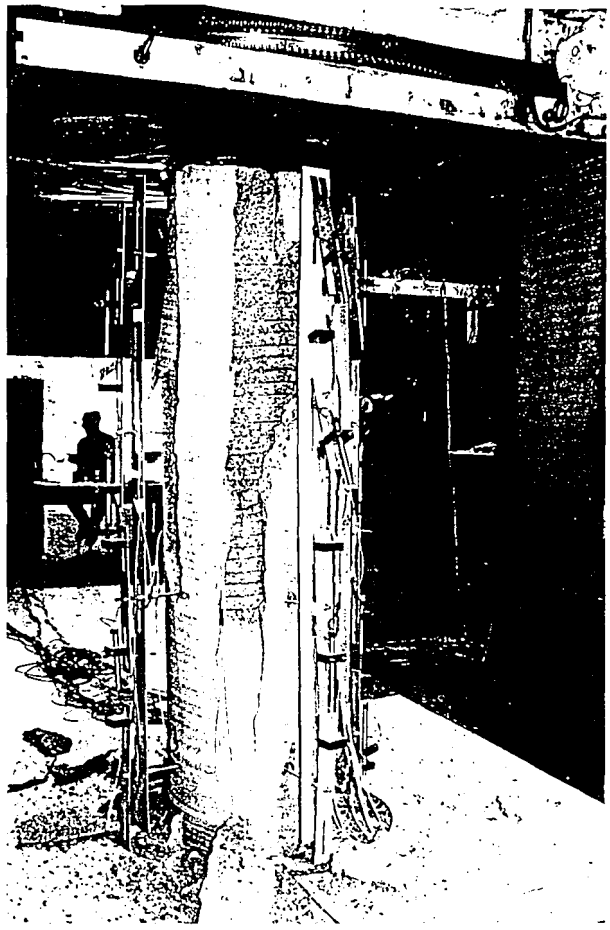

Figure 4.25(d) Specimen M3-series of key photographs; (d) separation of cover concrete in long sheets.

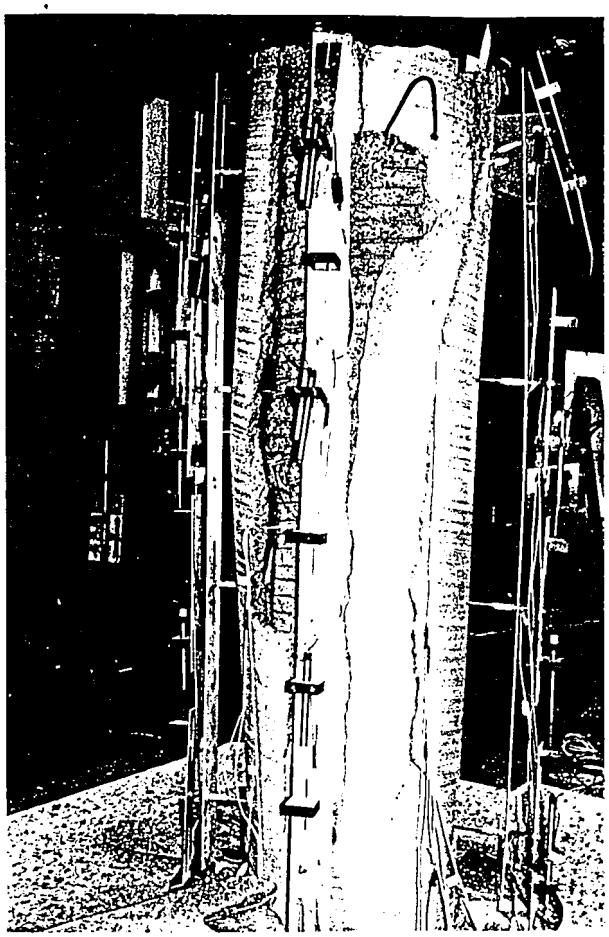

Figure 4.25(e) Specimen M3-series of key photographs; (e) exposed core concrete after fracture of spirals.

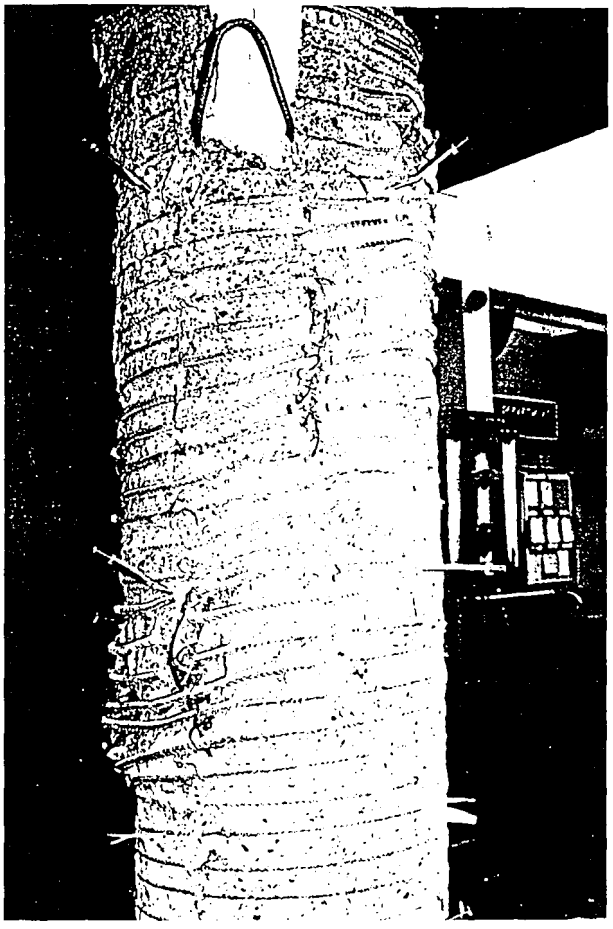

Figure 4.25(f) Specimen M3-series of key photographs; (f) deformation of spiral reinforcement.

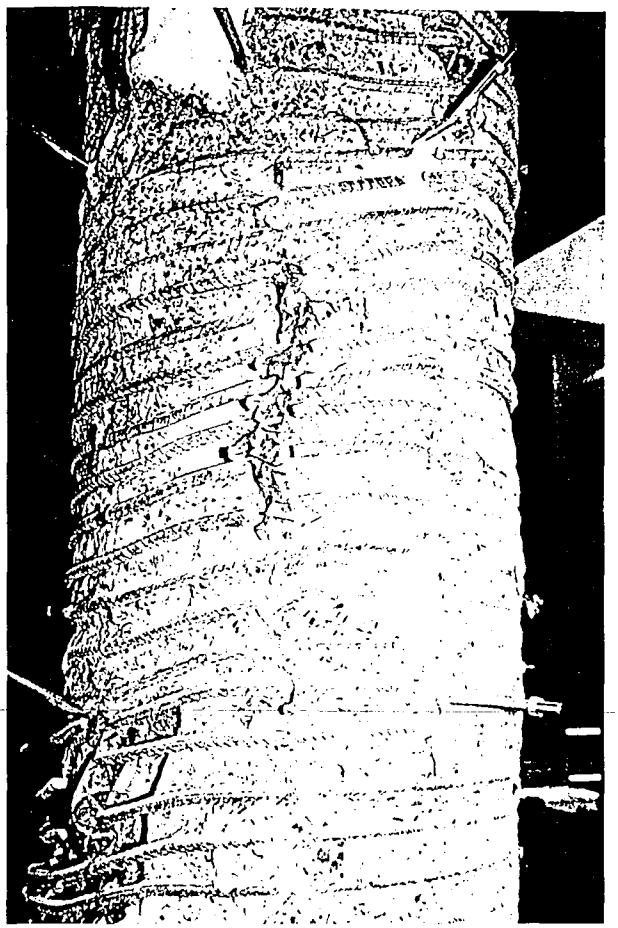

Figure 4.25(g) Specimen M3-series of key photographs; (g) spiral fractures at location of buckled longitudinal bars.

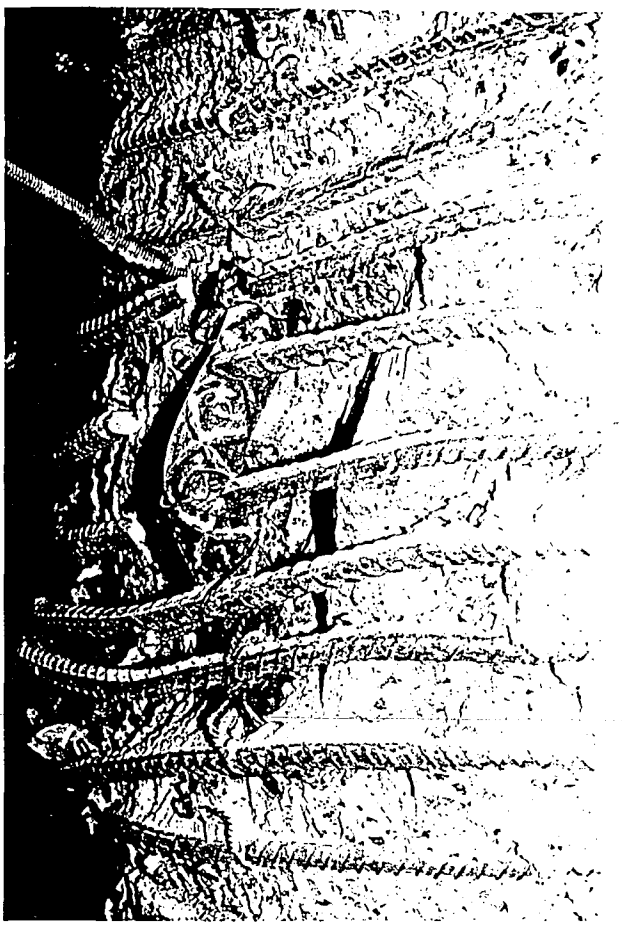

Figure 4.25(h) Specimen M3-series of key photographs; (h) spiral fractures at location of buckled longitudinal bars.

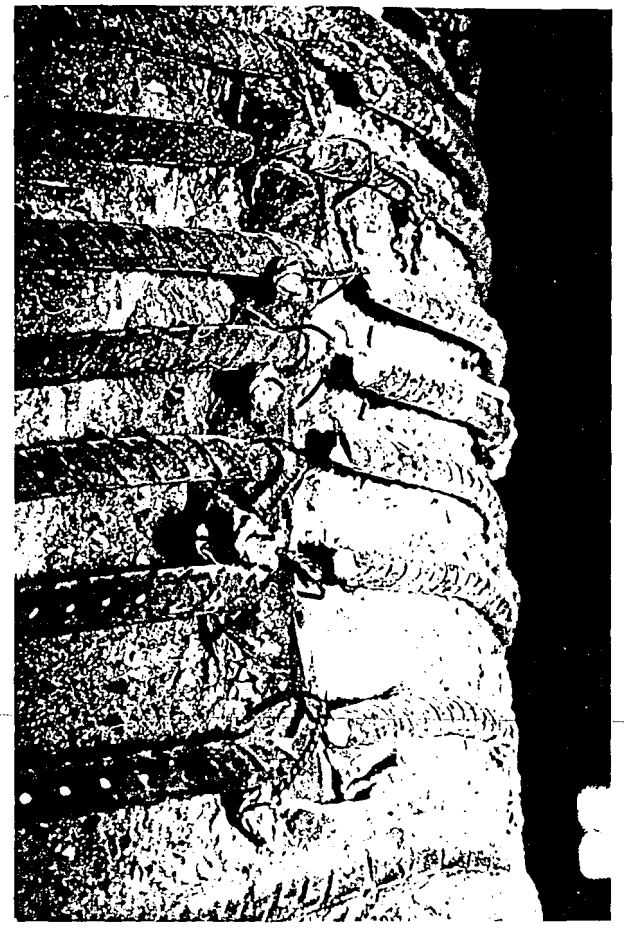

Figure 4.25(i) Specimen M3-series of key photographs; (i) spiral fractures at location of buckled longitudinal bars.

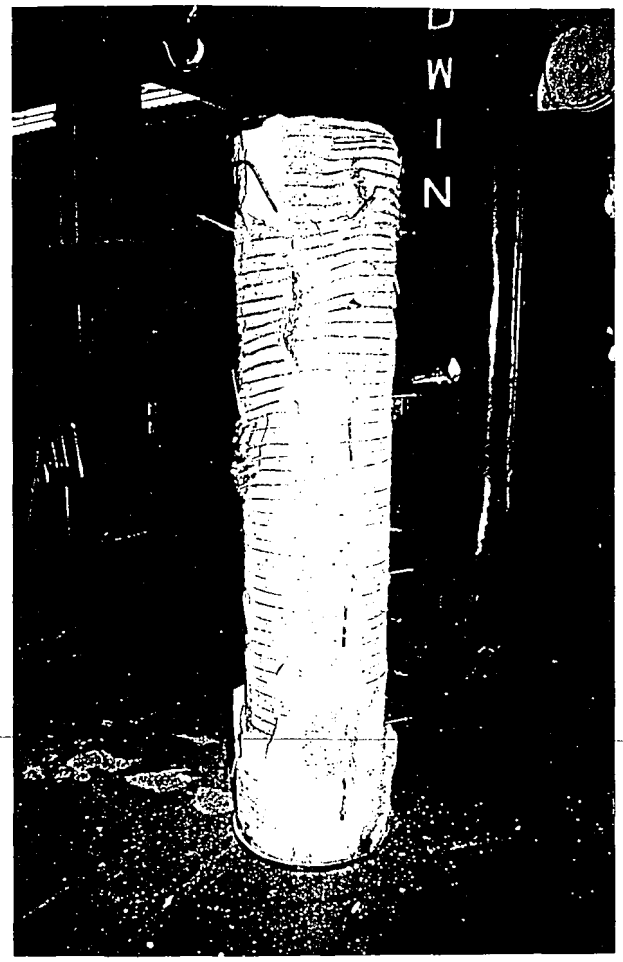

Figure 4.25(j) Specimen M3-series of key photographs; (j) post-test photograph showing the inclined failure plane.

4.3.6 Specimen H1

-#5 spiral at 64 mm (2.5 in) pitch

-16-#9 longitudinal bars

-$f_{c\text{-field}}$ = 76.0 MPa (11.02 ksi)

-$f_{c\text{-core}}$ = 61.4 MPa (8.91 ksi)

The location of strain gages and the location of displacement transducers for Specimen H1 are detailed in Figure 3.6 and Figure 3.7, respectively. First cracking (FCR) was observed in the concrete cover at an axial load of 11.26 MN (2533 kips) and an axial displacement of 7.00 mm (0.274 in). This is 65% of the maximum load. This crack initiated at the top of the column on the southeast face, and was approximately 152 mm (6 in) long. The graph of axial load versus axial displacement (Figure 4.26) shows that the column exhibited an approximately linear load deflection response from the beginning of the test to first cracking in the cover concrete. As the axial load increased, additional cracks developed on the southwest face which extended the entire length of the column, and a small section of cover concrete fell from the bottom of the south face (Figure 4.31(a)). By an axial load of 16.01 MN (3600 kips) the crack on the southwest face widened to about 25 mm (1 in) (Figure 4.31(b)). The maximum load of the column (P_{max}) was 17.45 MN (3924 kips), and the axial displacement at this load was 16.6 mm (0.651 in).

As more cracks developed in the cover concrete, the cover concrete became less effective in sustaining load. The axial resistance of the column

decreased approximately 672 kN (151 kips), then began to increase again. As shown in Figure 4.26, the column sustained a constant load around 17.12 MN (3850 kips).

During this period of increasing deformation at a constant load, the cover concrete separated from the core concrete. By an displacement around 25.4 mm (1.0 in), a large section of cover concrete broke away from the southwest face of the column exposing the spiral reinforcement, as shown in Figure 4.31(c).

The first spiral fracture (SF1) occurred at an axial displacement of Δ_{SF}=43.3 mm (1.705 in), shown in Figure 4.26. This was accompanied by a decrease in column resistance from 16.79 MN (3775 kips) to 16.21 MN (3645 kips). The second spiral fracture (SF2) occurred at an axial displacement of 45.2 mm (1.781 in). The third spiral fracture (SF3) occurred at an axial displacement of 48.7 mm (1.919 in). This was accompanied by a 7.67 MN (1724 kips) decrease in column axial force. At this point the load on the column was 38% of the maximum load. The column was then unloaded at a rate of 222 kN/min (50 kips/min).

Figures 4.27 and 4.28 are graphs of axial load versus strain in the longitudinal reinforcement. First yielding of the longitudinal reinforcement was indicated by strain gage L8 at an axial displacement of 5.82 mm (0.229 in) and an axial load of 9.74 MN (2189 kips) (L8Y in Figure 4.26). The variation of strain in the spiral reinforcement along the height of the column is illustrated in Figures 4.29 and 4.30. First yielding in the spirals was indicated by strain gages S9 at an axial displace-

ment of 12.8 mm (0.502 in) and an axial load of 15.85 MN (3564 kips), as shown in Figure 4.26.

At the end of the test the column was completely unloaded, and the separated regions of cover concrete were carefully removed to expose the core and spiral reinforcement. Three spiral fractures were noted. All of the spiral fractures occurred at the location of buckled longitudinal bars (Figures 4.31(d) and (e)). The failure region was characterized by an inclined failure plane which extended from the top of the west face to 2/3 the column height on the east face, shown in Figure 4.31(f). All of the spiral fractures were contained within this region.

Experimental Axial Capacity	Predicted Axial Capacity	
P_{max} (MN)	P_c (MN)	P_{ccore} (MN)
17.45	20.40	18.27

0.004448 MN=1 kip

Table 4.6 Specimen H1-predicted strengths and experimentally observed strengths.

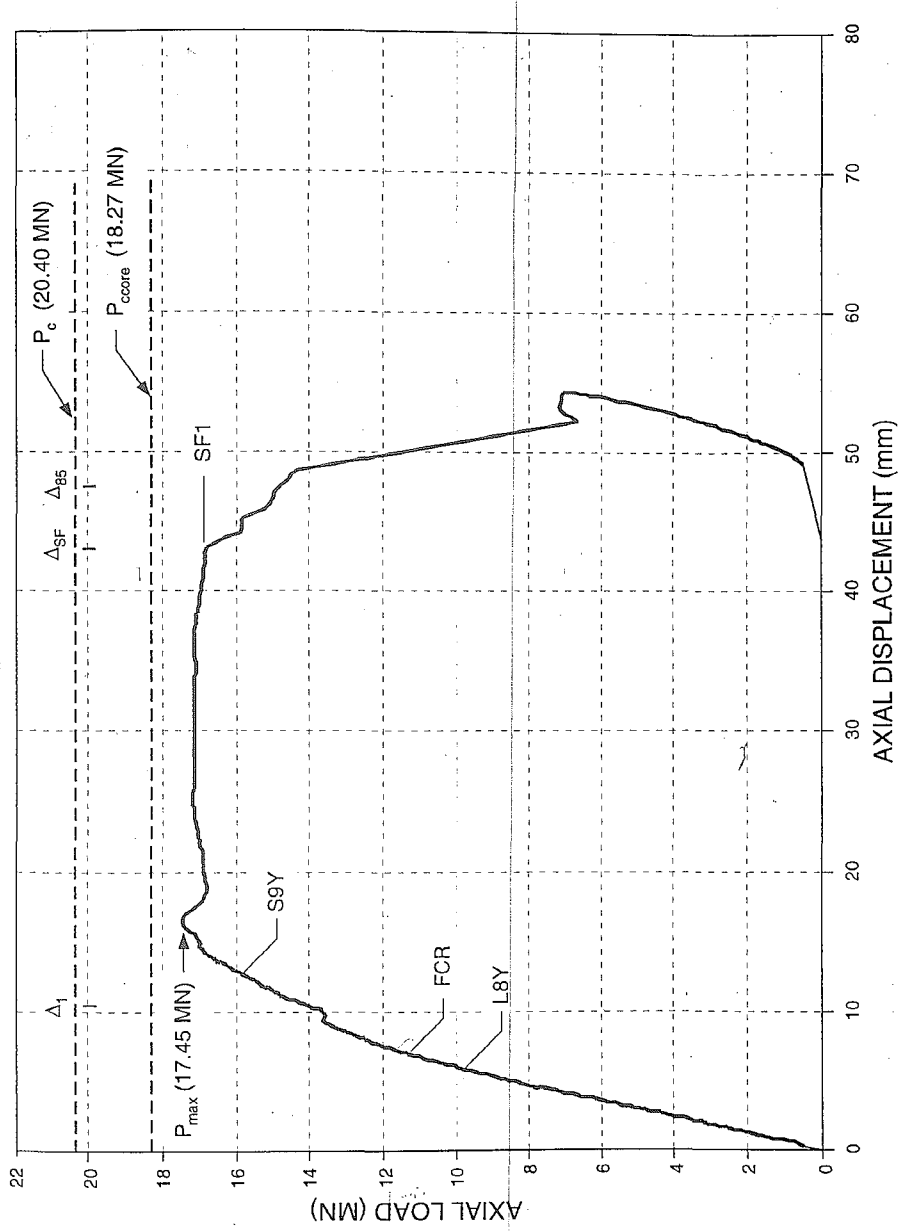

Figure 4.26 Specimen H1-axial load versus axial displacement.

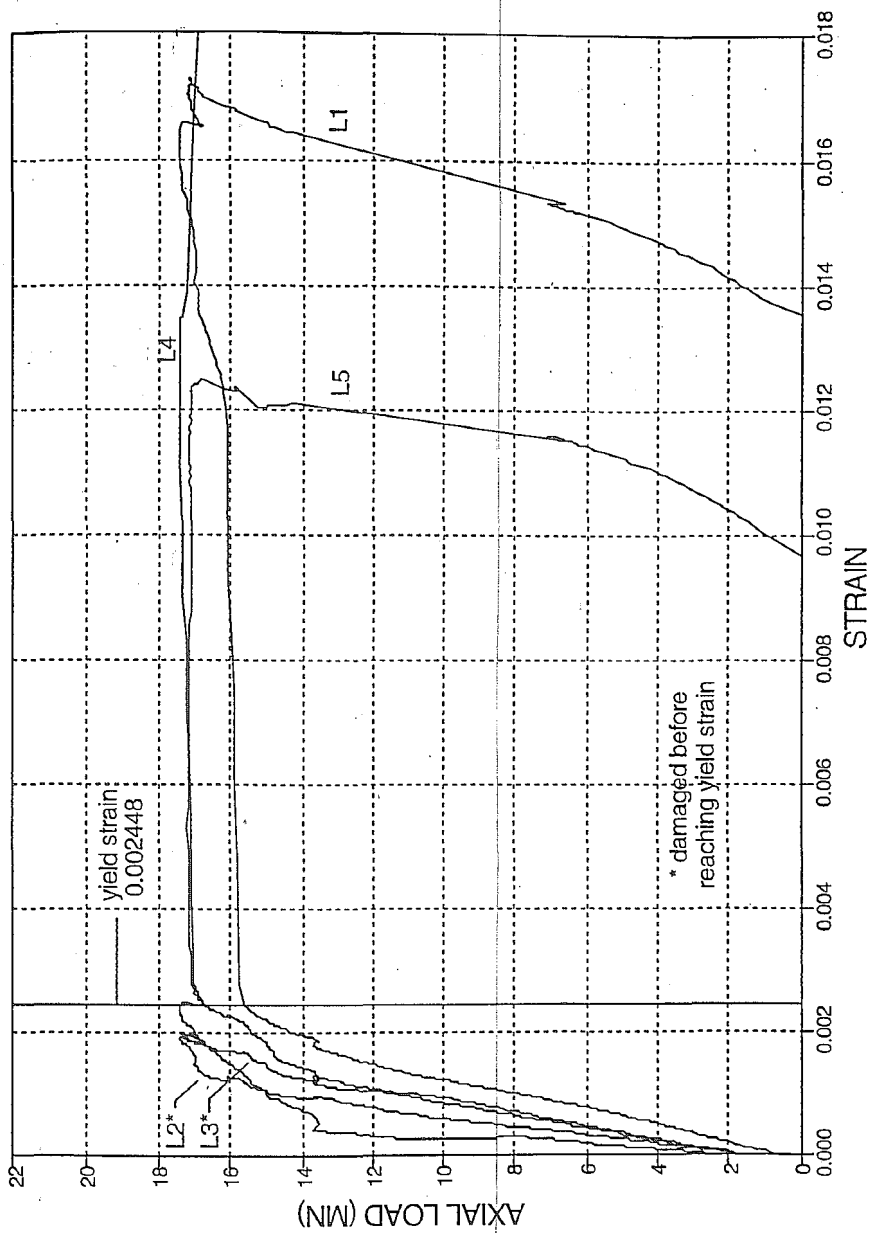

Figure 4.27 Specimen H1-axial load versus longitudinal reinforcement strains, gages L1, L2, L3, L4,L5.

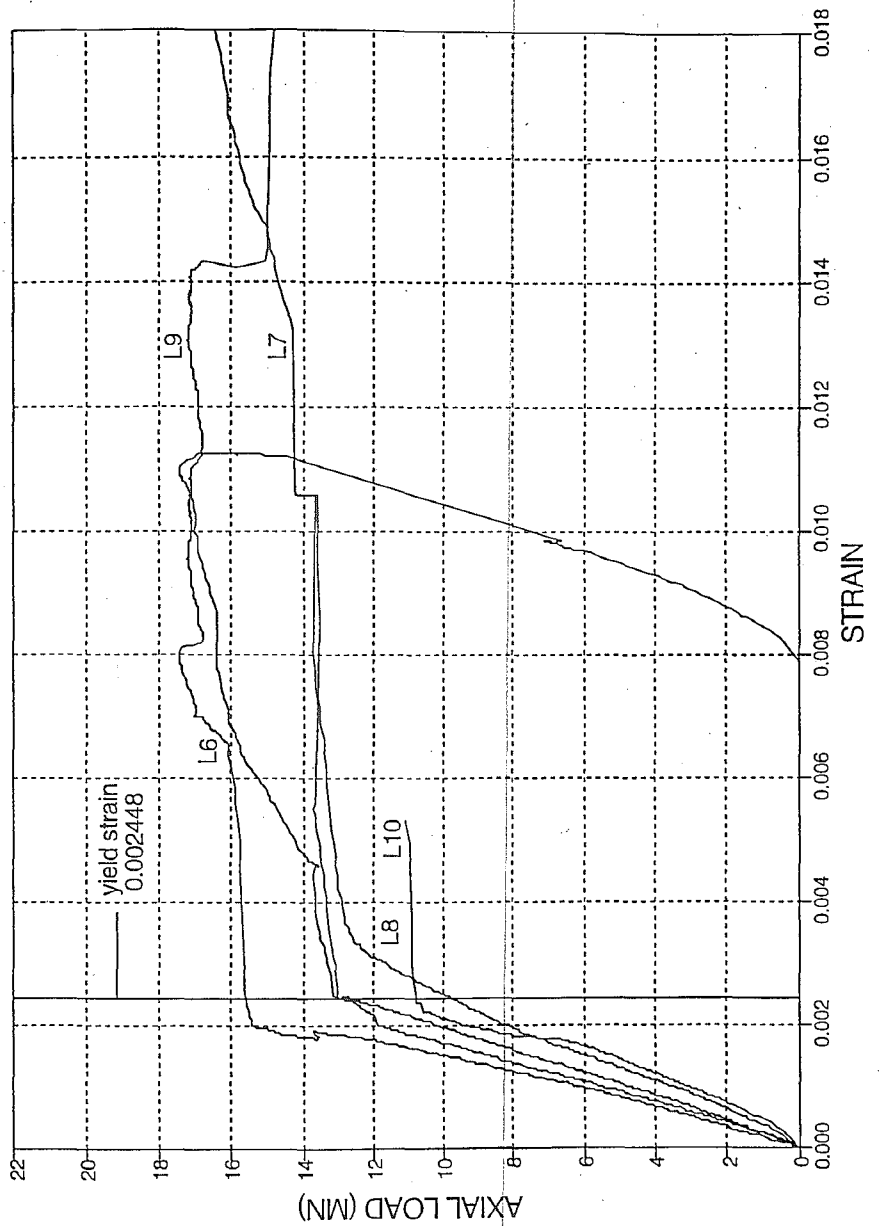

Figure 4.28 Specimen H1-axial load versus longitudinal reinforcement strains, gages L6, L7, L8, L9,L10.

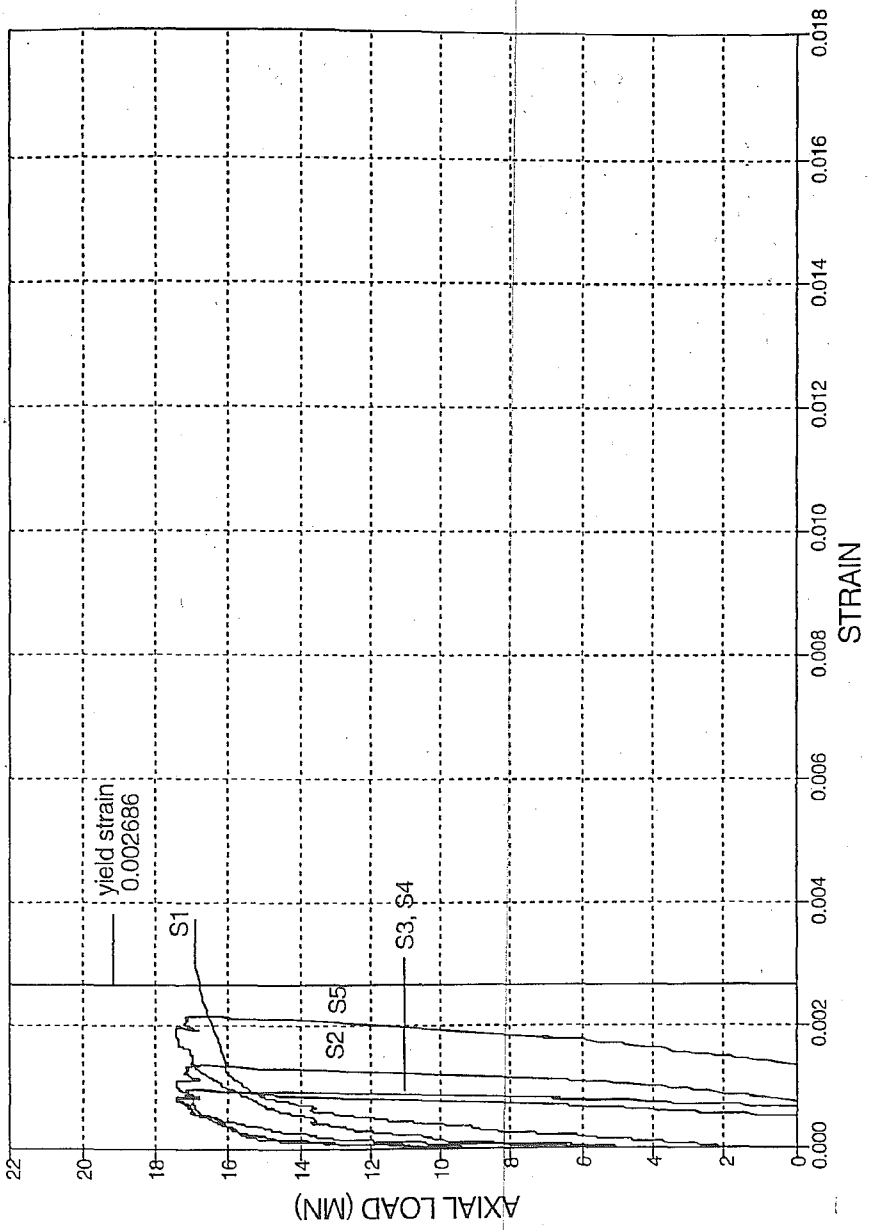

Figure 4.29 Specimen H1-axial load versus spiral reinforcement strains, gages S1, S2, S3, S4, S5.

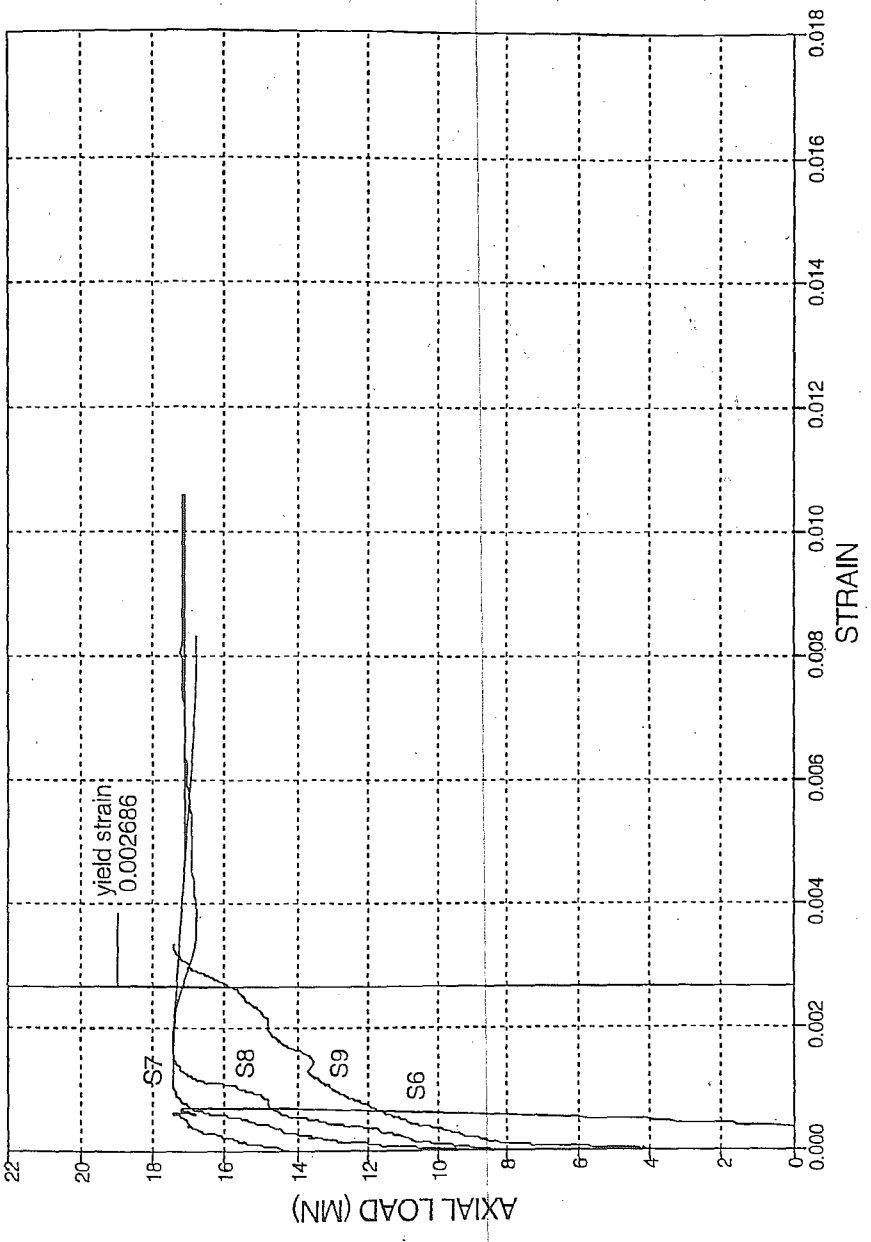

Figure 4.30 Specimen H1-axial load versus spiral reinforcement strains, gages S6, S7, S8, S9.

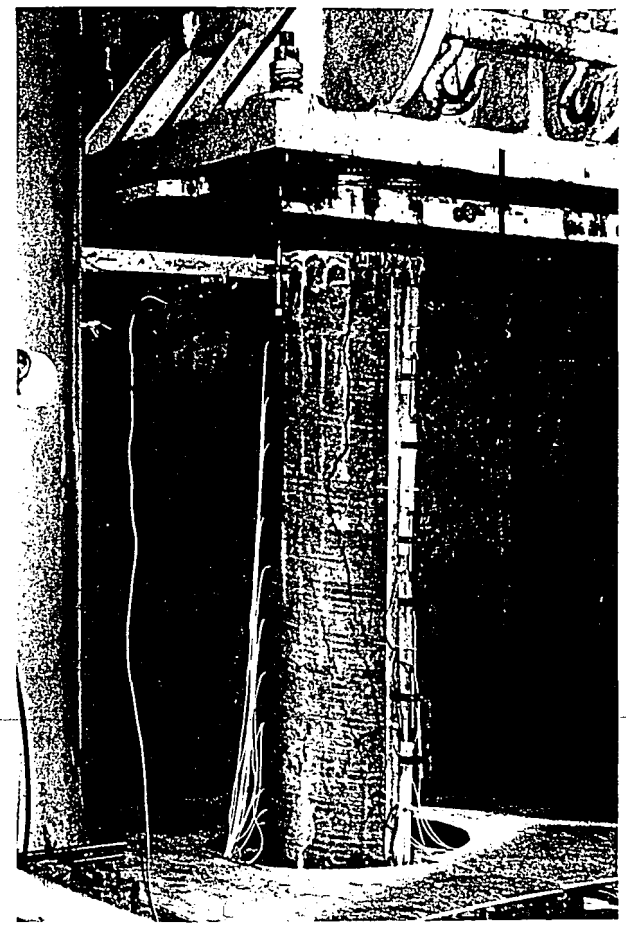

Figure 4.31(a) Specimen H1-series of key photographs; (a) longitudinal splitting cracks propagating the entire length of the column.

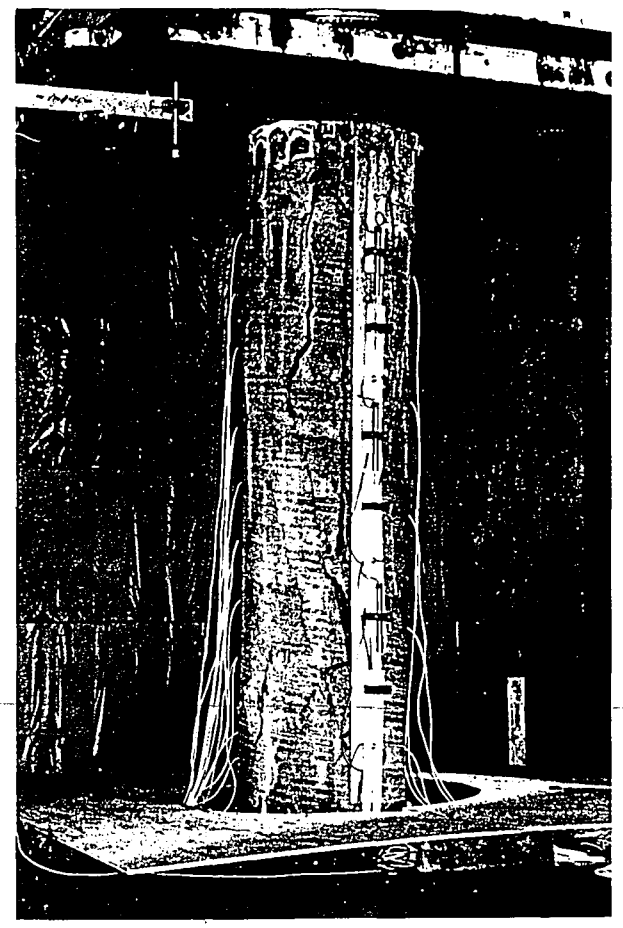

Figure 4.31(b) Specimen H1-series of key photographs; (b) widening of longitudinal splitting crack on southwest face.

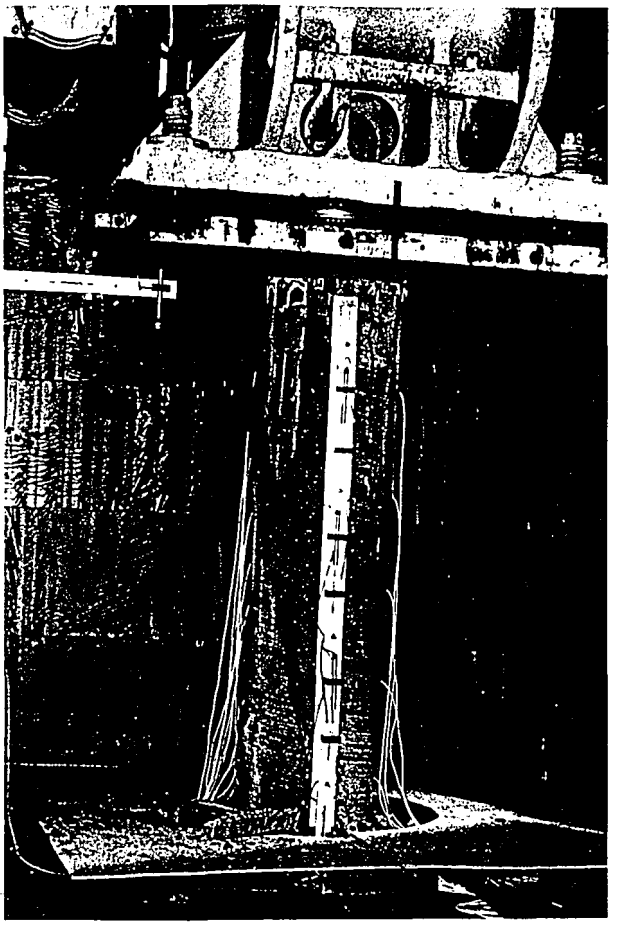

Figure 4.31(c) Specimen H1-series of key photographs; (c) exposed core concrete after spalling of cover concrete.

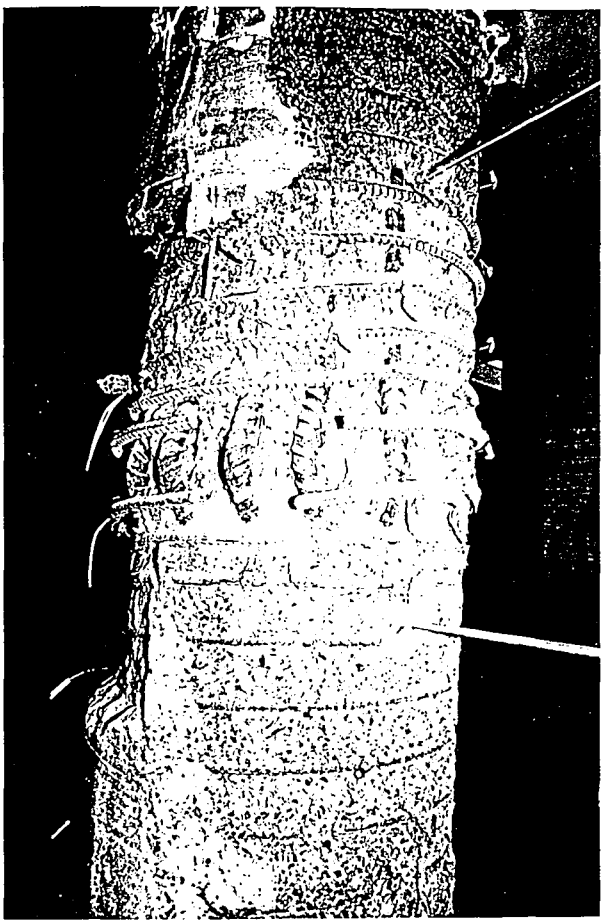

Figure 4.31(d) Specimen H1-series of key photographs; (d) spiral fractures at location of buckled longitudinal bars.

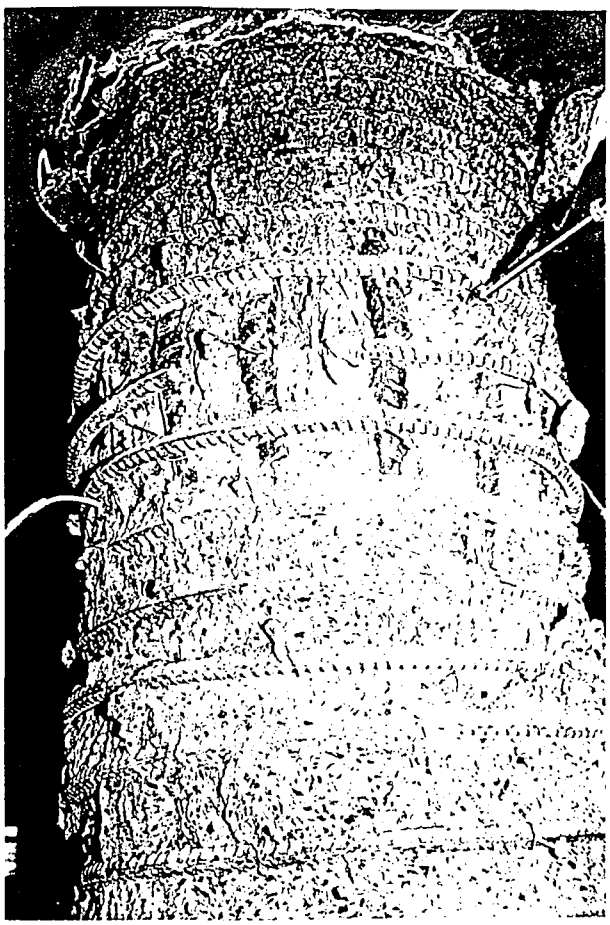

Figure 4.31(e) Specimen H1-series of key photographs; (e) spiral fractures at location of buckled longitudinal bars.

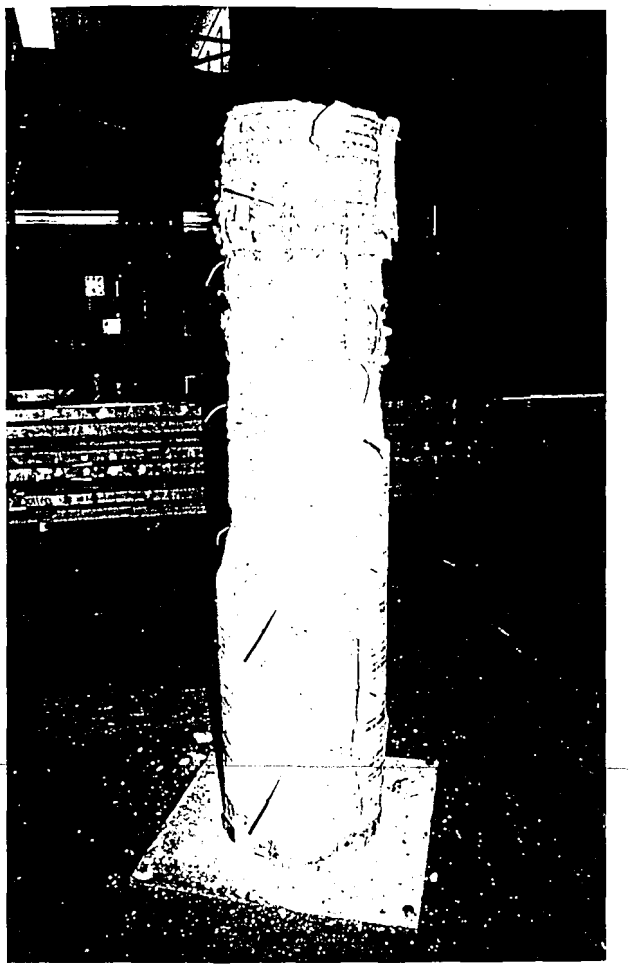

Figure 4.31(f) Specimen H1-series of key photographs; (f) post-test photograph showing the inclined failure plane.

4.3.3 Specimen H2

-#5 spiral at 64 mm (2.5 in) pitch

-8-#8 longitudinal bars

-$f_{c\text{-}field}$ = 81.3 MPa (11.79 ksi)

-$f_{c\text{-}core}$ = 61.4 MPa (8.91 ksi)

-51 mm (2 in) of epoxy grout compound, Figure 4.37(a)

The location of strain gages and the location of displacement transducers for Specimen H2 are detailed in Figure 3.6 and Figure 3.7, respectively. First cracking (FCR) was observed in the concrete cover at an axial load of 8.90 MN (2000 kips) and at an axial displacement of 5.5 mm (0.216 in). This is 68% of the maximum load. A series of cracks about 127 mm (5 in) apart formed on the west face. These cracks initiated at the top of the column and were approximately 152 mm (6 in) long. The graph of axial load versus axial displacement (Figure 4.32) shows that the column exhibited an approximately linear load deflection response from the beginning of the test to first cracking in the cover concrete. By an axial load of 11.87 MN (2668 kips), cracks began to form in the capping compound (Figure 4.37(b)). The maximum load (P_{max}) occurred at a load of 13.12 MN (2950 kips), and the axial displacement at this load was 13.1 mm (0.583 in).

As the column was further loaded more cracks developed in the cover concrete, and the existing cracks lengthened and widened. By an axial load of 12.81 MN (2880 kips) the cracks on the north face propagated 1/2 the length of the column, and the cover concrete separated from the west face of the column.

As cover concrete began separating from the core it became less effective in sustaining load. The axial resistance of the column decreased approximately 667 kN (150 kips). As shown in Figure 4.32, the column then sustained a relatively constant axial load of 12.45 MN (2800 kips).

During this period of increasing axial displacement at a relatively constant load the cover concrete separated from the core concrete. Figure 4.37(c) shows the west face of the column at an axial displacement of 34.0 mm (1.337 in) just after the cover concrete fell from the core concrete.

The first spiral fracture (SF1) occurred at an axial displacement of Δ_{SF}=41.2 mm (1.62 in) shown in Figure 4.32. This was accompanied by a decrease in column resistance from 12.15 MN (2732 kips) to 10.62 MN (2388 kips). The second spiral fracture (SF2) occurred at an axial displacement of 49.2 mm (1.938 in). This was accompanied by a 3.66 MN (823 kips) decrease in column axial force. A third spiral fracture (SF3) occurred at an axial displacement of 53.1 mm (2.089 in), and the axial load decreased 4.85 MN (1091 kips). At this point the load on the column was 22% of the maximum load. The column was then unloaded at a rate of 222 kN/min (50 kips/min).

Figures 4.33 and 4.34 are graphs of axial load versus strain in the longitudinal reinforcement. First yielding of the longitudinal bars was indicated by strain gage L5 at and axial displacement of 5.9 mm (0.232 in) and an axial load of 9.36 MN (2104 kips) (L5Y on Figure 4.32). The variation of strain in the spiral reinforcement along the height of the column is illustrated in Figures 4.33 and 4.34. As

shown in this figure spiral strain gage S9 was the only gage to reach yield strain. Shown in Figure 4.32, first yielding of this strain gage (S9Y) occurred at an axial displacement of 7.6 mm (0.300 in) and an axial load of 10.94 MN (2460 kips).

At the end of the test the column was completely unloaded, and the separated regions of cover concrete were carefully removed to expose the core and spiral reinforcement. Three spiral fractures were noted. The damage was concentrated at the very top of the column (Figures 4.37(d)). All of the spiral fractures were contained within this region.

Experimental Axial Capacity	Predicted Axial Capacity	
P_{max} (MN)	P_c (MN)	P_{ccore} (MN)
13.12	18.35	15.34

0.004448 MN=1 kip

Table 4.7 Specimen H2-predicted strengths and experimentally observed strengths.

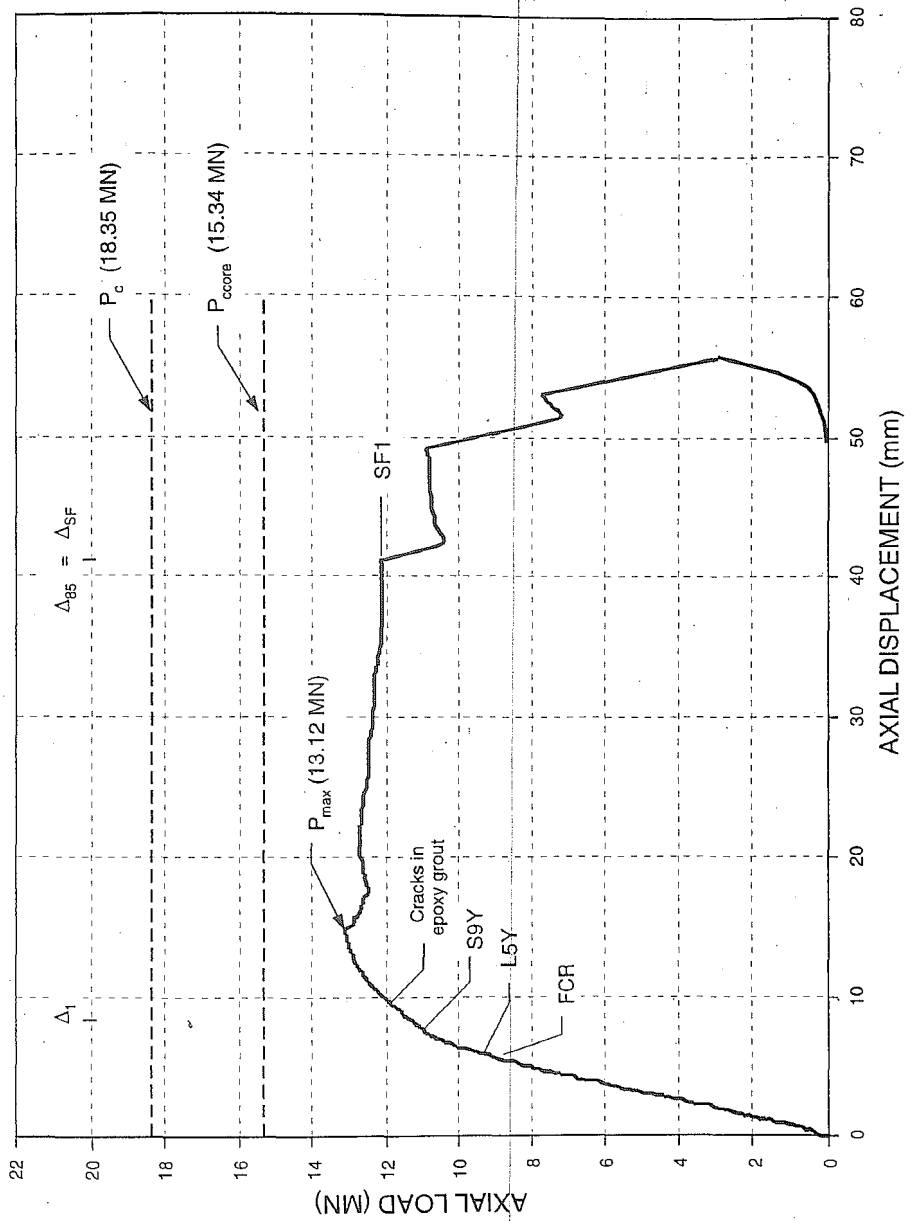

Figure 4.32 Specimen H2-axial load versus axial displacement.

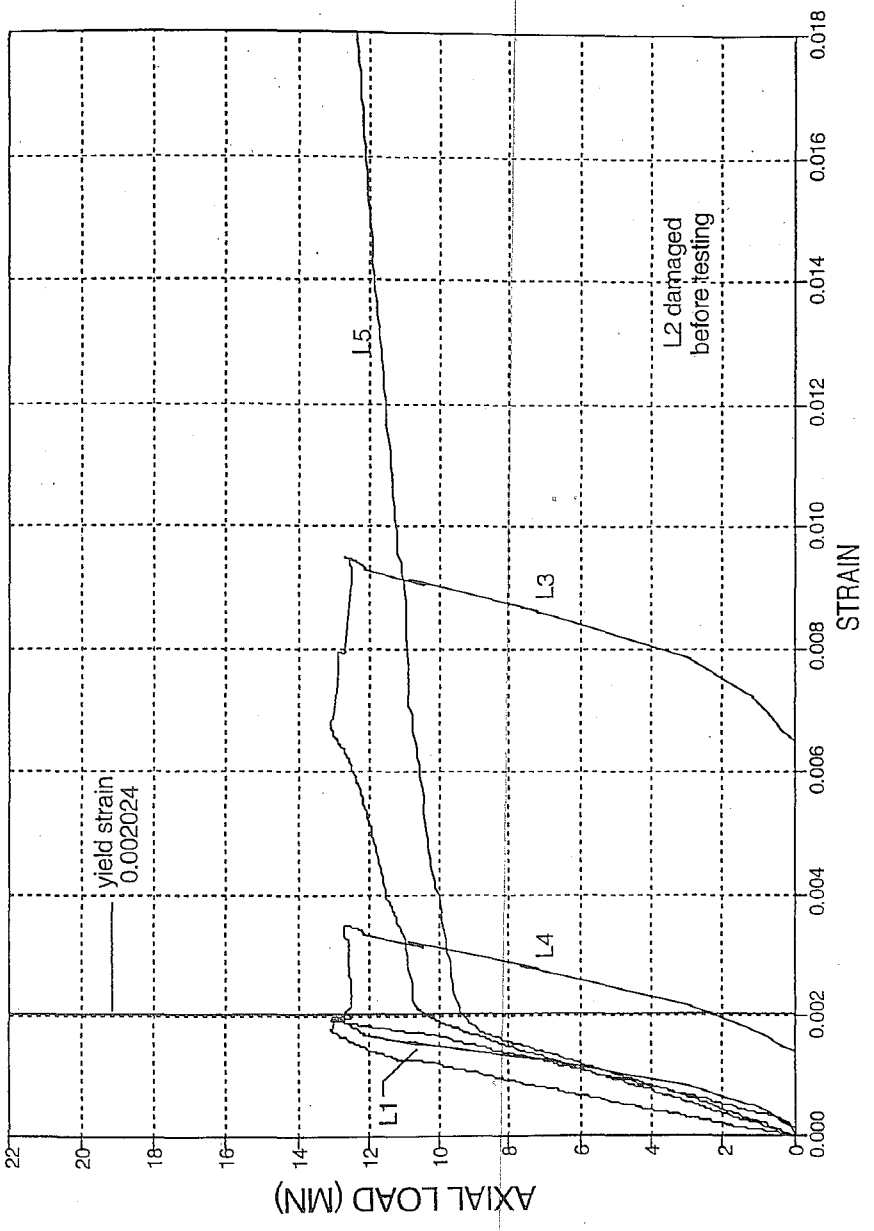

Figure 4.33 Specimen H2-axial load versus longitudinal reinforcement strains, gages L1, L2, L3, L4,L5.

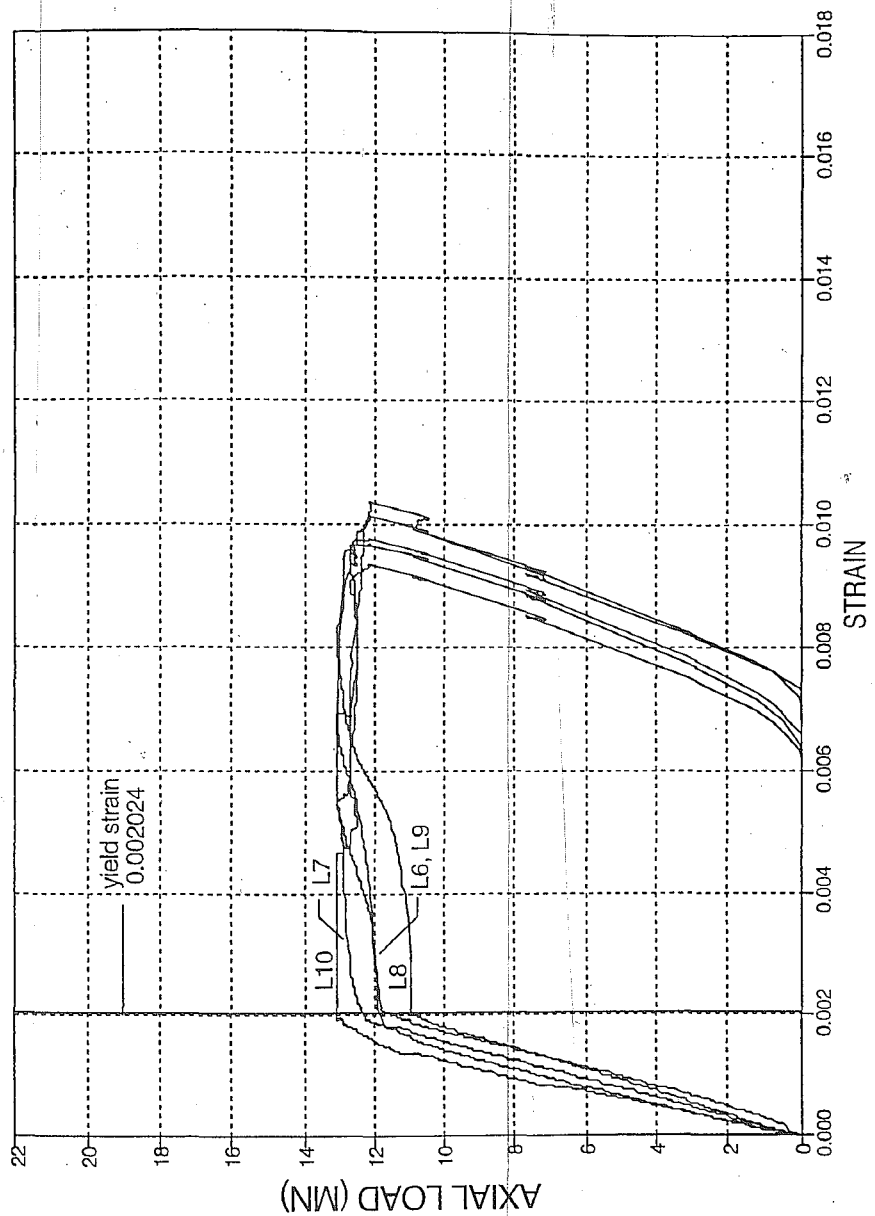

Figure 4.34 Specimen H2-axial load versus longitudinal reinforcement strains, gages L6, L7, L8, L9, L10.

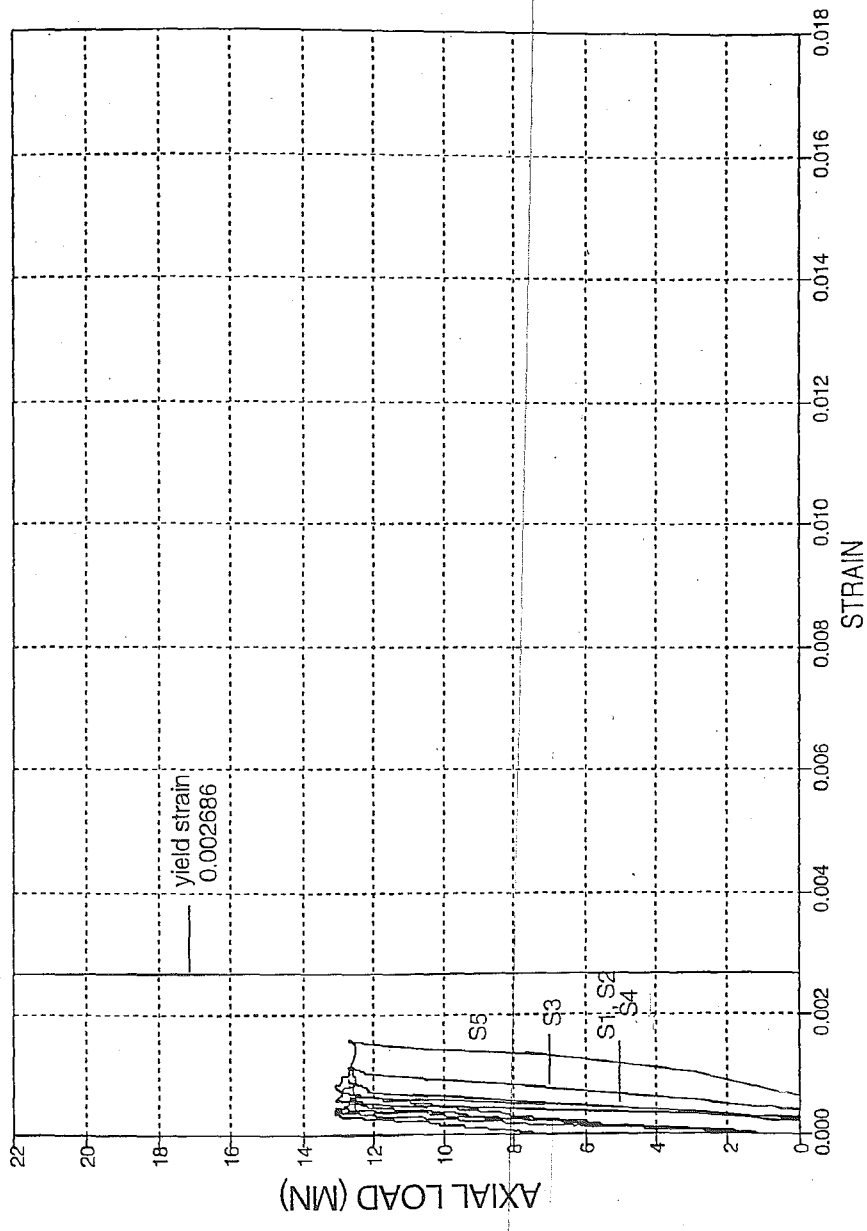

Figure 4.35 Specimen H2-axial load versus spiral reinforcement strains, gages S1, S2, S3, S4, S5.

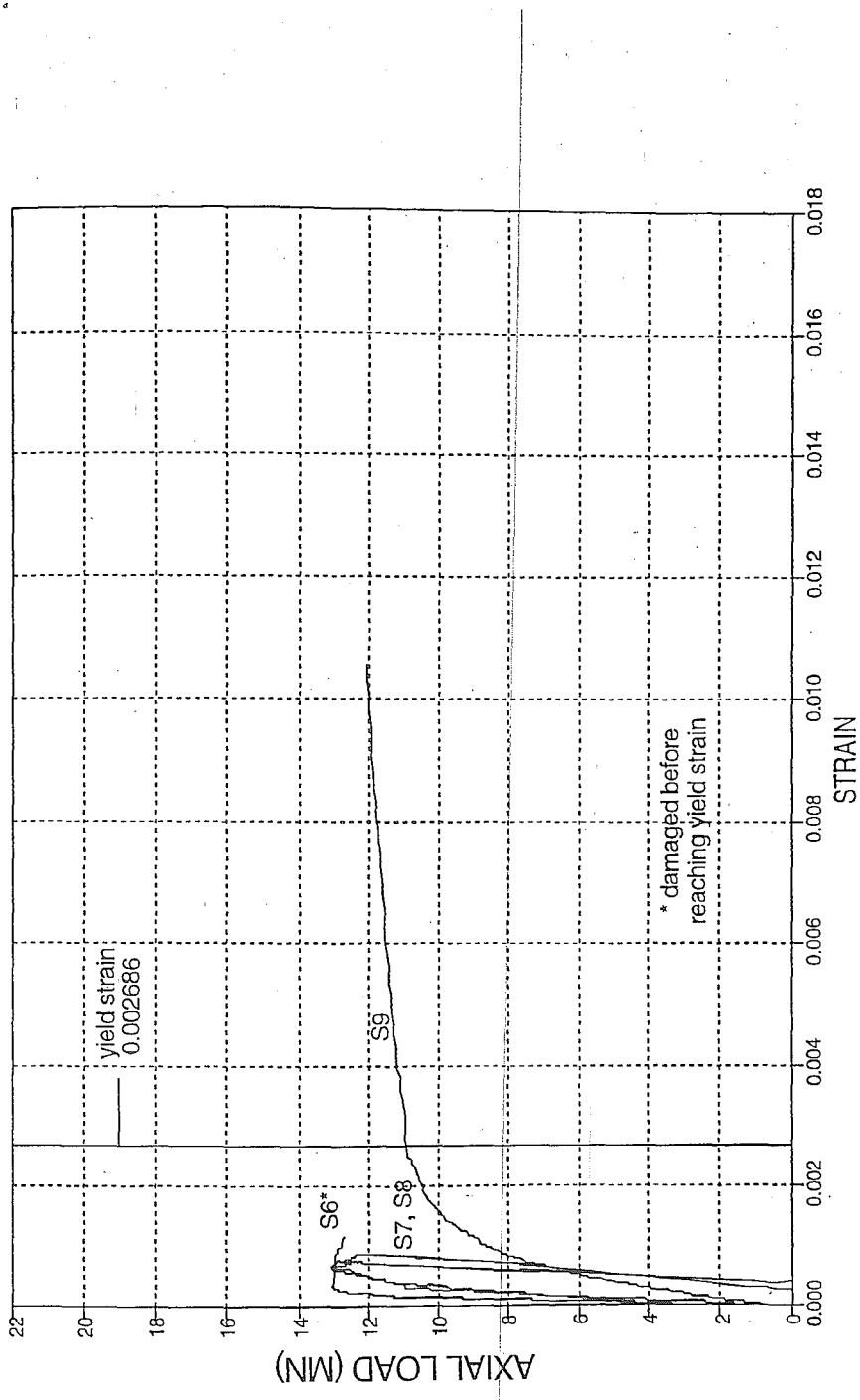

Figure 4.36 Specimen H2-axial load versus spiral reinforcement strains, gages S6, S7, S8, S9.

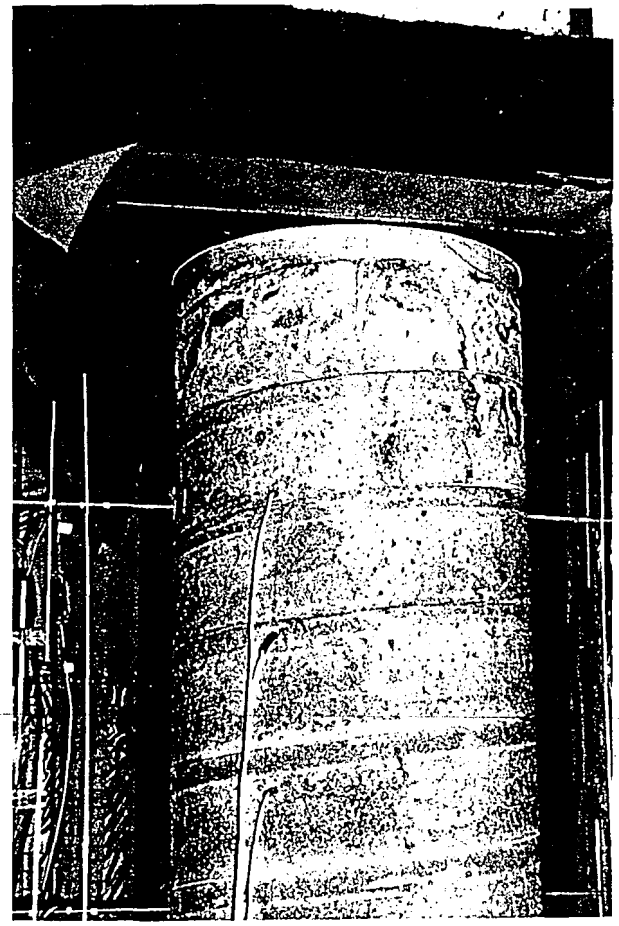

Figure 4.37(a) Specimen H2-series of key photographs; (a) capping compound.

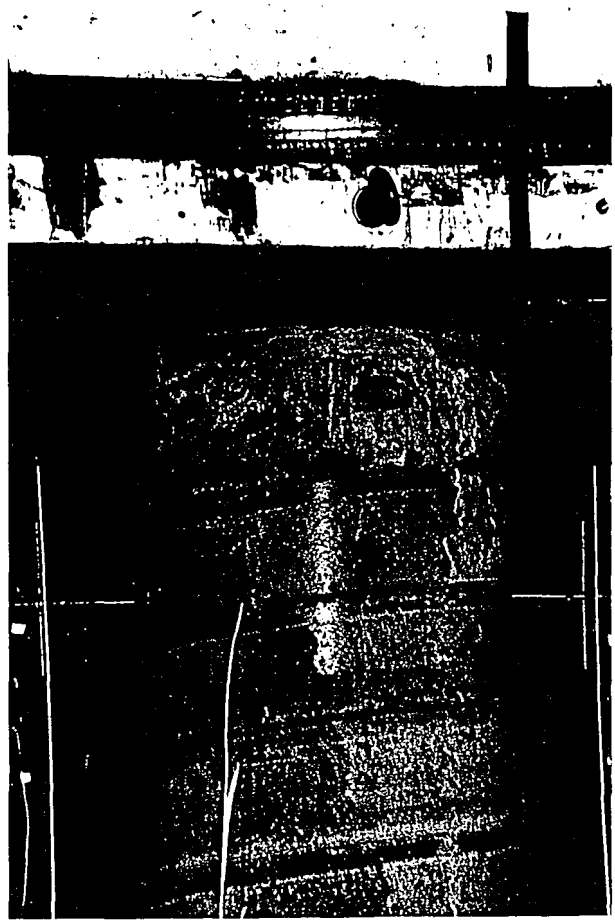

Figure 4.37(b) Specimen H2-series of key photographs; (b) cracks forming in capping compound.

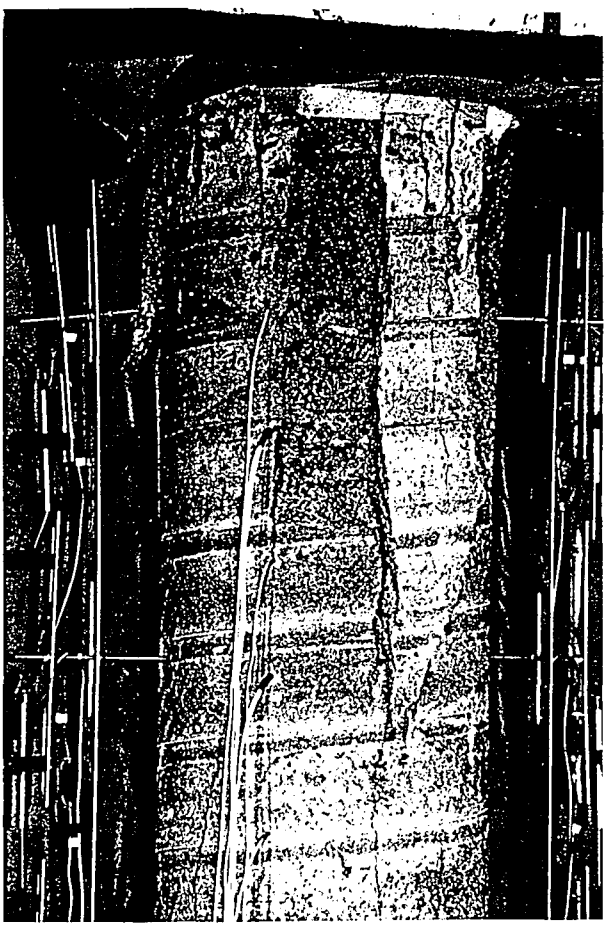

Figure 4.37(c) Specimen H2-series of key photographs; (c) spalling of cover concrete.

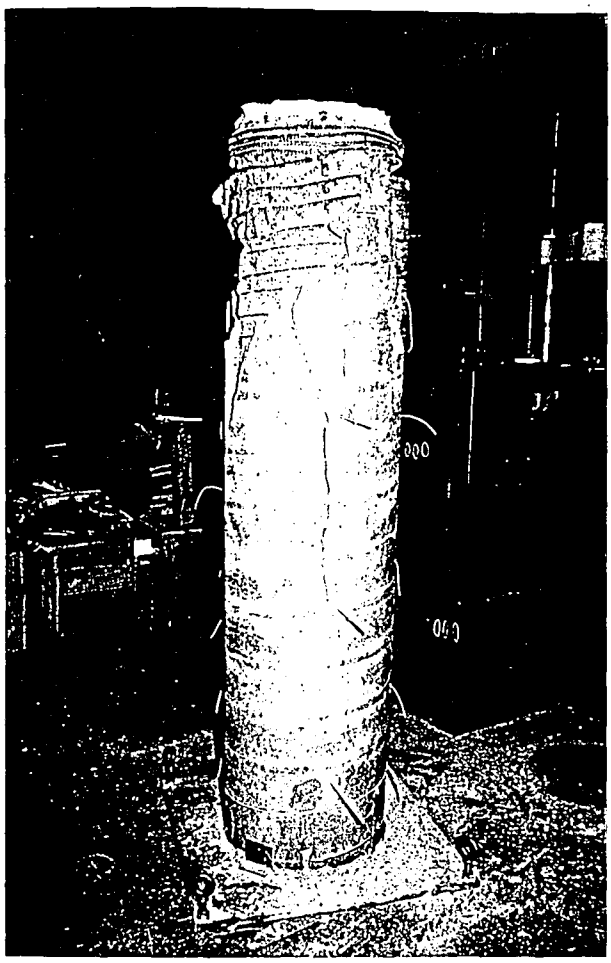

Figure 4.37(d) Specimen H2-series of key photographs; (d) post-test photograph showing the failure concentrated at the top of the column.

4.3.8 Specimen H3

-#4 spiral at 41.3 mm (1.625 in) pitch

-8-#8 longitudinal bars

-$f_{c\text{-}field}$ = 83.0 MPa (12.04 ksi)

-$f_{c\text{-}core}$ = 61.4 MPa (8.91 ksi)

-51 mm (2 in) of epoxy grout compound

The location of strain gages and the location of displacement transducers for Specimen H3 are detailed in Figure 3.6 and Figure 3.7, respectively. First cracking (FCR) was observed in the concrete cover at an axial load of 11.28 MN (2536 kips) and at an axial displacement of 5.7 mm (0.226 in). This is 74% of the maximum load. A series of hairline cracks initiated at the top of the column on the southwest face. The graph of axial load versus axial displacement (Figure 4.38) shows that the column exhibited an approximately linear load deflection response from the beginning of the test to first cracking in the cover concrete. The load-displacement graph peaked at a load of 13.89 MN (3122 kips), and the axial displacement at this load was 7.5 mm (0.297 in).

Cracks quickly developed in the cover concrete, and it likely became less effective in sustaining load. The axial resistance of the column decreased approximately 596 kN (134 kips), then began to increase again. The column reached a maximum load (P_{max}) of 15.21 MN (3421 kips), at an axial displacement of 13.3 mm (0.525 in). The axial load on the column began to rapidly decreased by 1.48 MN (333 kips). By an axial load of 15.0 MN (3375 kips) the cracks on the

northwest face widened to approximately 12.7 mm (0.5 in), and the cover concrete on the lower 1/2 of the column began to separate from the core concrete (Figure 4.43(a)). The column then sustained a relatively constant load around 12.58 MN (2830 kips).

During this period of constant load, the column continually increased in axial displacement. As the cover concrete separated form the core concrete, it slid onto the instrumented threaded bars and deflected the bars. The damage was concentrated in the lower 1/3 of the column (Figure 4.43(b)).

The first spiral fracture (SF1) occurred at an axial displacement of Δ_{SF}=40.4 mm (1.591 in), shown in Figure 4.38. This was accompanied by a decrease in column resistance from 12.42 MN (2792 kips) to 12.16 MN (2734 kips). The spiral fractures occurred as a series of several fractures in a row. The axial load on the column continuously decreased as more spiral fractures occurred. The axial load on the column decreased to 7.19 MN (1617 kips) which was 47% of the maximum load. The column was then unloaded at a rate of 222 kN/min (50 kips/min).

Figures 4.39 and 4.40 are a graphs of axial load versus strain in the longitudinal reinforcement. First yielding of the longitudinal bars was indicated by strain gage L4 at an axial displacement of 4.8 mm (0.188 in) and an axial load of 9.19 MN (2067 kips) (L4Y on Figure 4.38). The variation of strain in the spiral reinforcement along the height of the column is illustrated in Figures 4.41 and 4.42. First yielding of the spirals was indicated by strain gage S1 at an axial displace-

ment of 12.7 mm (0.5 in) and an axial load of 15.10 MN (3395 kips) (S1Y on Figure 4.38).

At the end of the test the column was completely unloaded, and the separated regions of cover concrete were carefully removed to expose the core and spiral reinforcement. Deformation in the spiral reinforcement was visible (Figure 4.43(c)). Ten spiral fractures were counted. All of the spiral fractures occurred at the location of buckled longitudinal bars (Figures 4.37(d)-(g)). The failure region was characterized by a shear plane concentrated in the bottom 1/2 of the column (Figures 4.37(h)). The plane extended from the middle of the north face to the bottom of the south face. All of the spiral breaks were contained within this region.

Experimental Axial Capacity	Predicted Axial Capacity	
P_{max} (MN)	P_c (MN)	P_{ccore} (MN)
15.21	18.27	15.01

0.004448 MN=1 kip

Table 4.8 Specimen H3-predicted strengths and experimentally observed strengths.

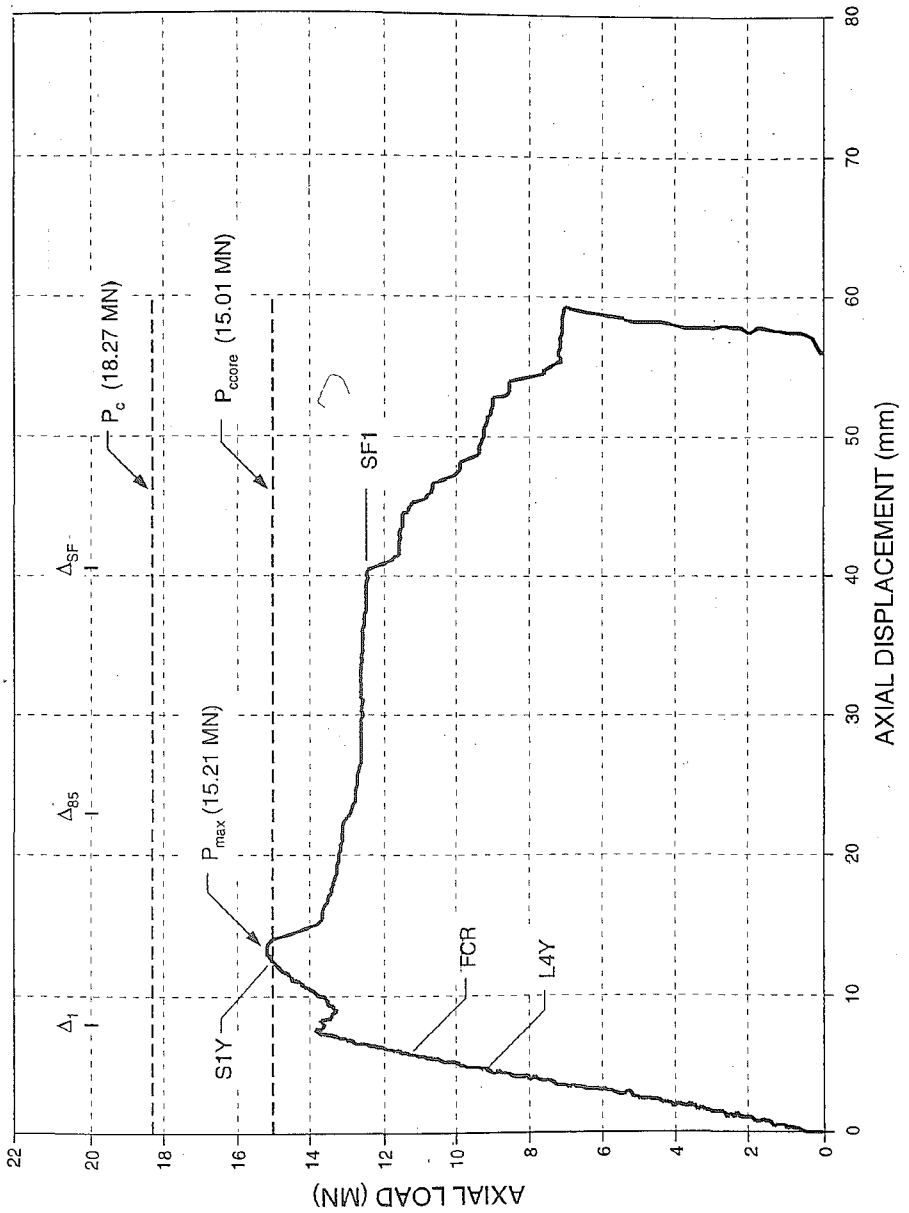

Figure 4.38 Specimen H3-axial load versus axial displacement.

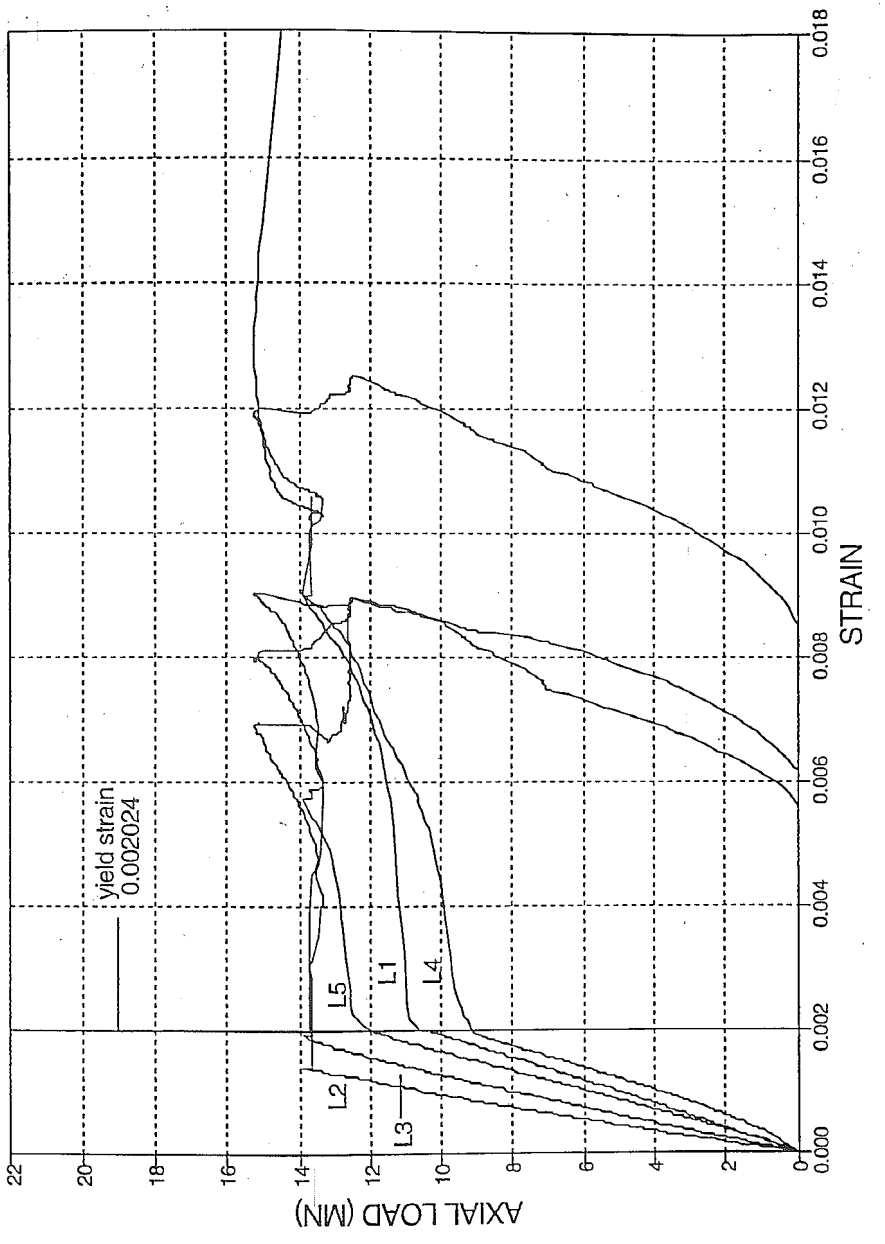

Figure 4.39 Specimen H3-axial load versus longitudinal reinforcement strains, gages L1, L2, L3, L4, L5.

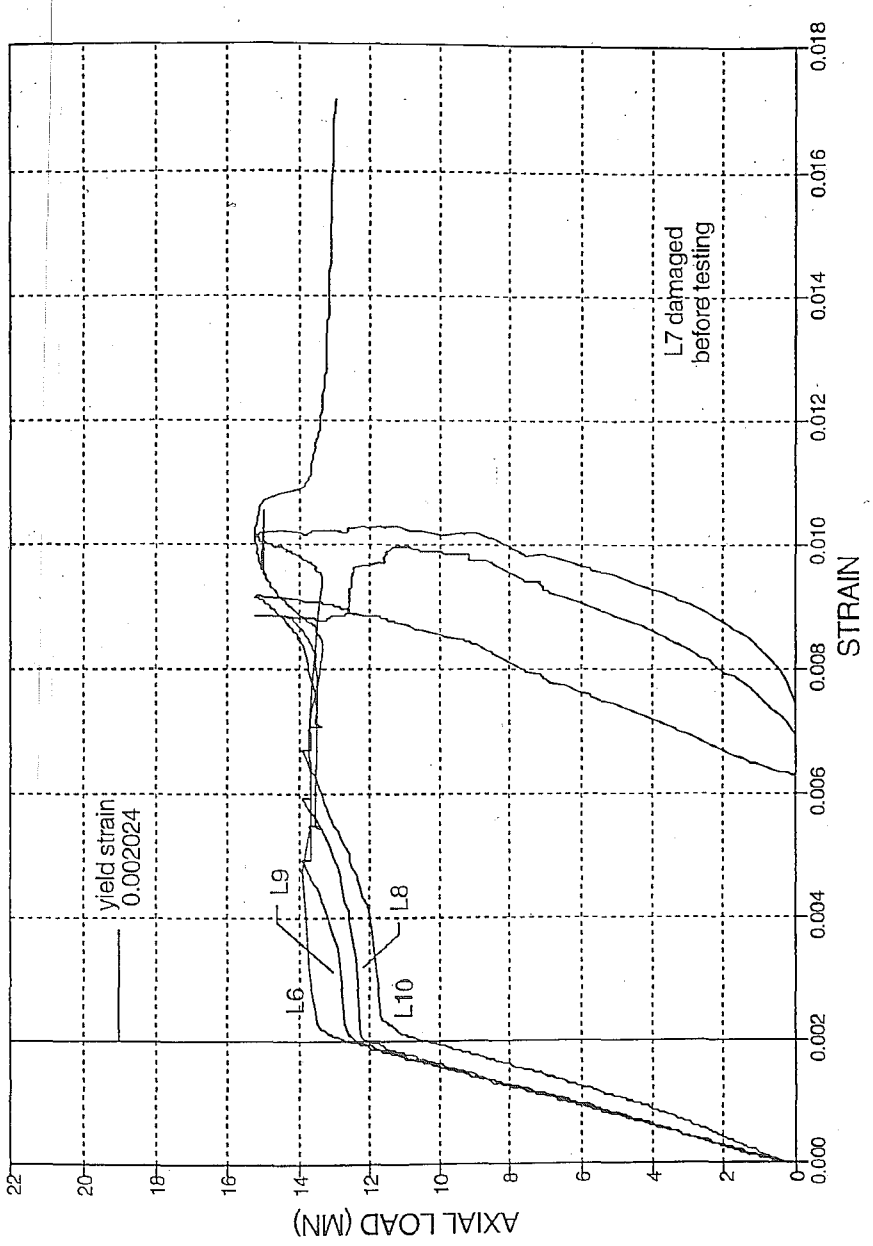

Figure 4.40 Specimen H3-axial load versus longitudinal reinforcement strains, gages L6, L7, L8, L9, L10.

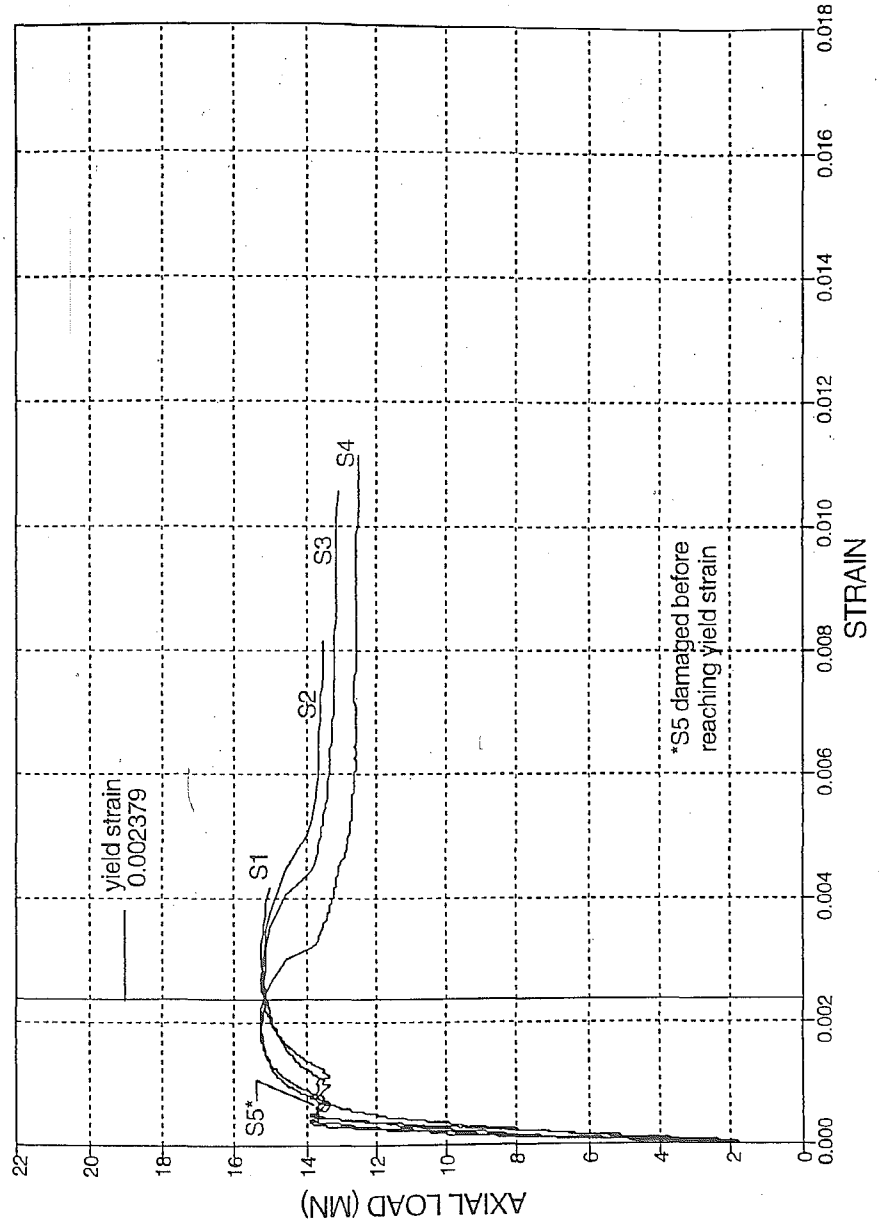

Figure 4.41 Specimen H3-axial load versus spiral reinforcement strains, gages S1, S2, S3, S4, S5.

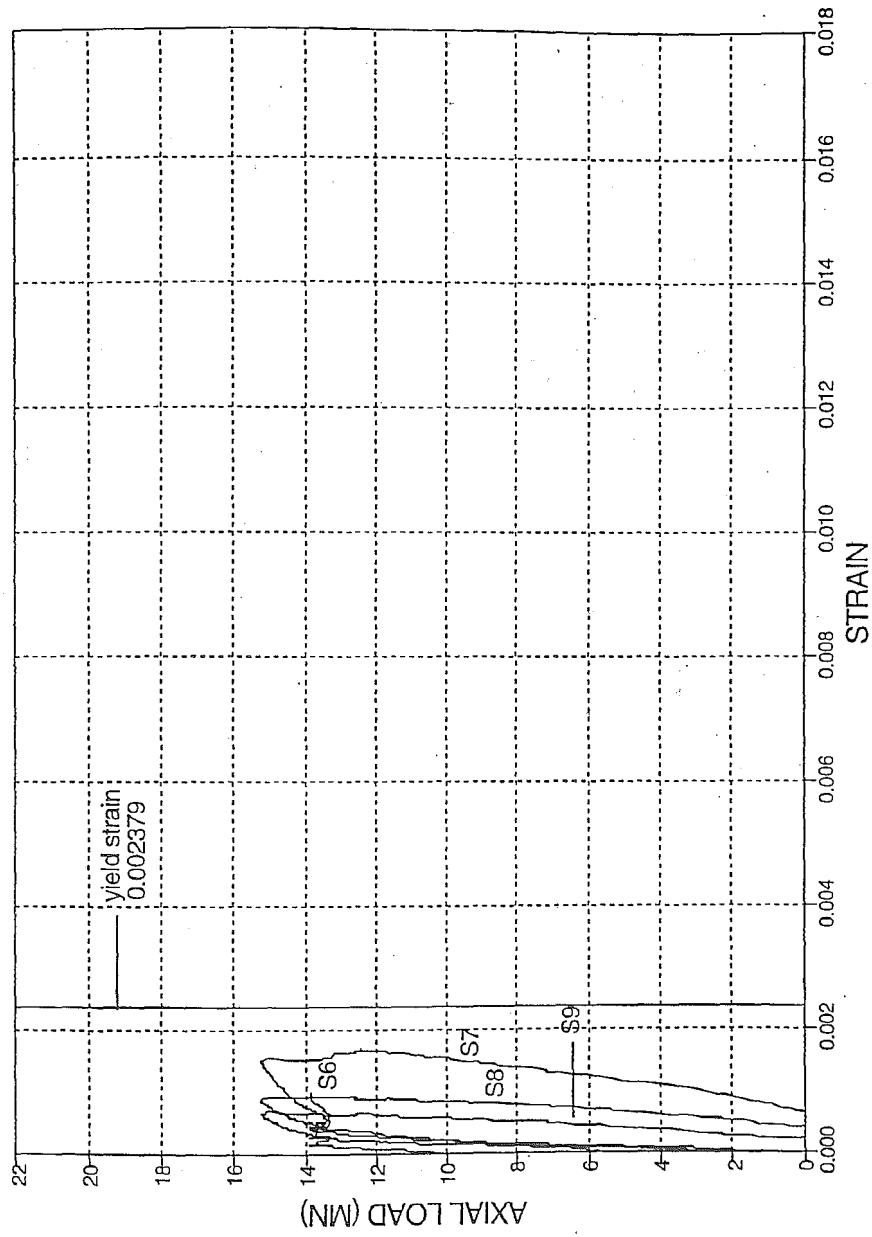

Figure 4.42 Specimen H3-axial load versus spiral reinforcement strains, gages S6, S7, S8, S9.

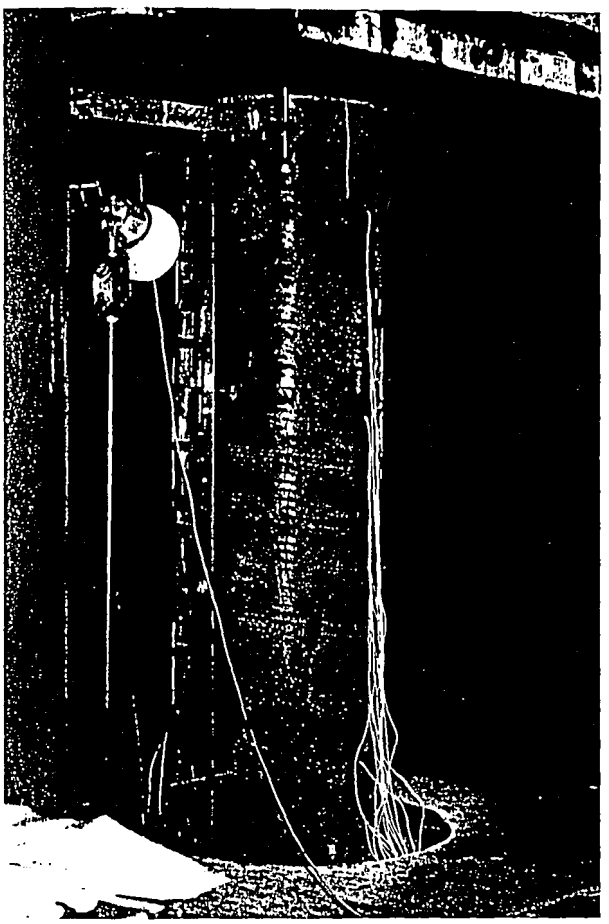

Figure 4.43(a) Specimen H3-series of key photographs; (a) spalling of cover concrete at bottom of column.

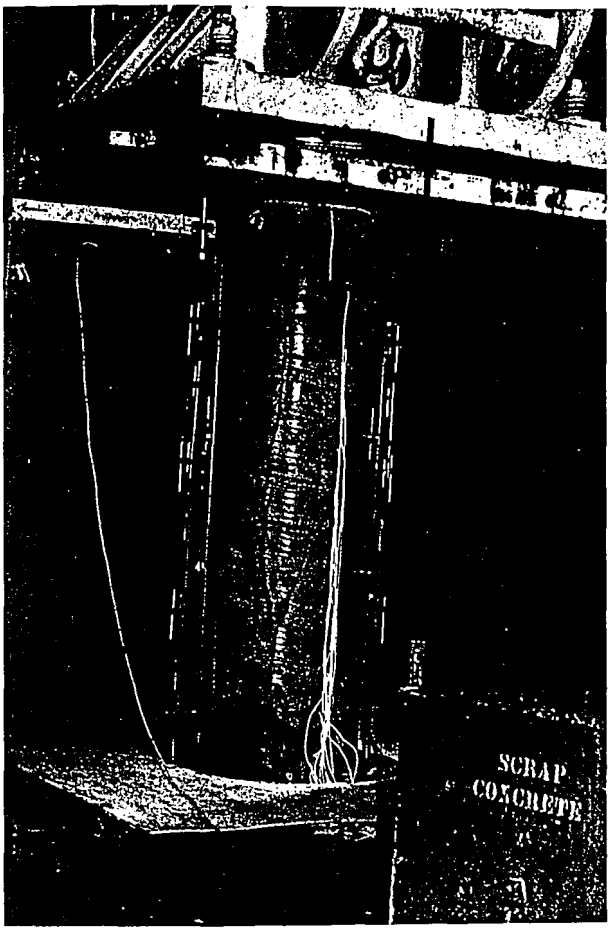

Figure 4.43(b) Specimen H3-series of key photographs; (b) concentration of damage in lower 1/3 of column.

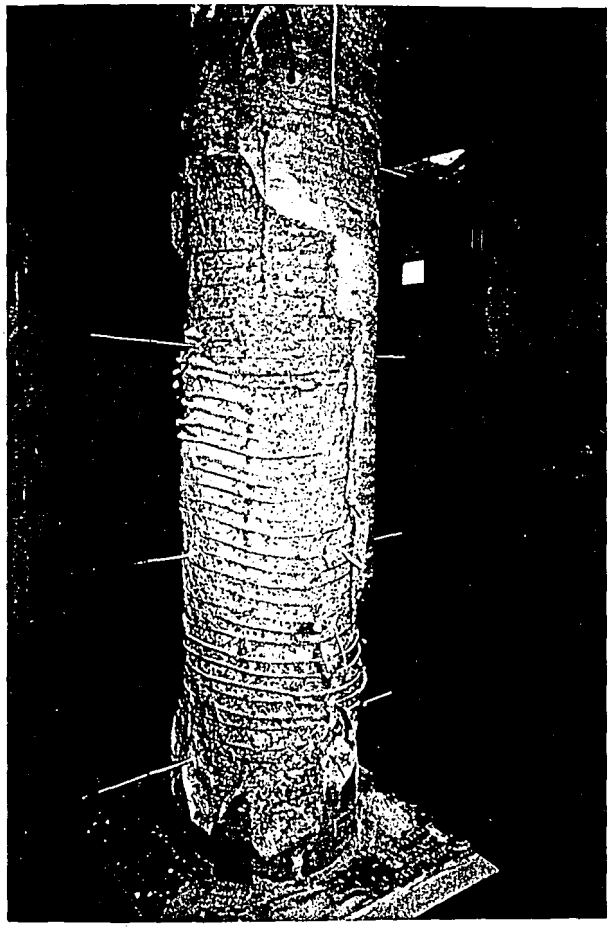

Figure 4.43(c) Specimen H3-series of key photographs; (c) deformation of spiral reinforcement.

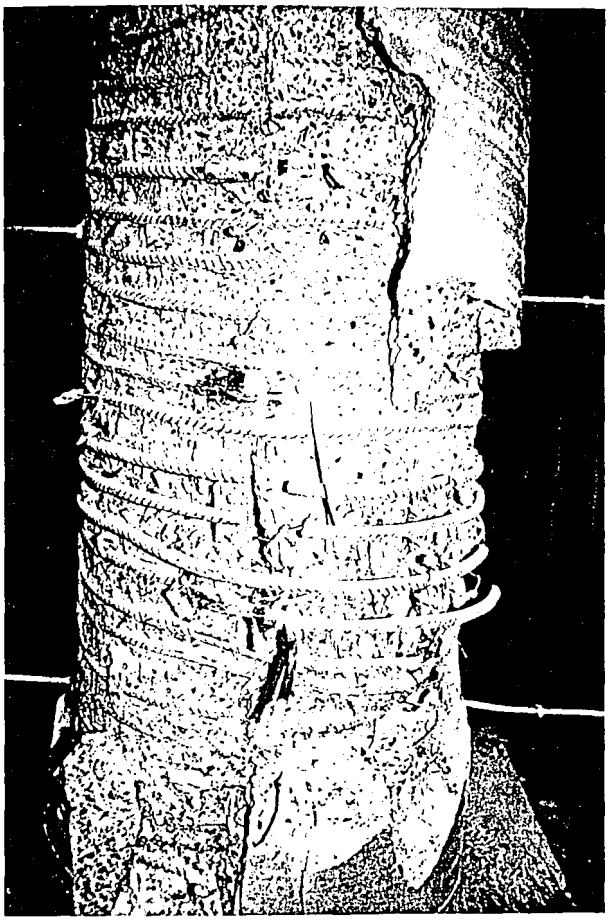

Figure 4.43(d) Specimen H3-series of key photographs; (d) spiral fractures at location of buckled longitudinal bars.

Figure 4.43(e) Specimen H3-series of key photographs; (e) spiral fractures at location of buckled longitudinal bars.

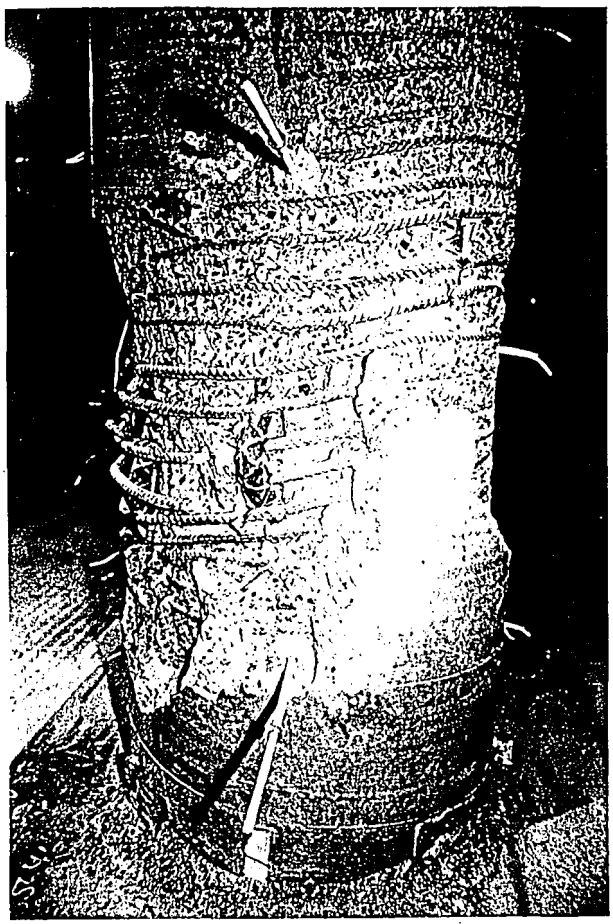

Figure 4.43(f) Specimen H3-series of key photographs; (f) spiral fractures at location of buckled longitudinal bars.

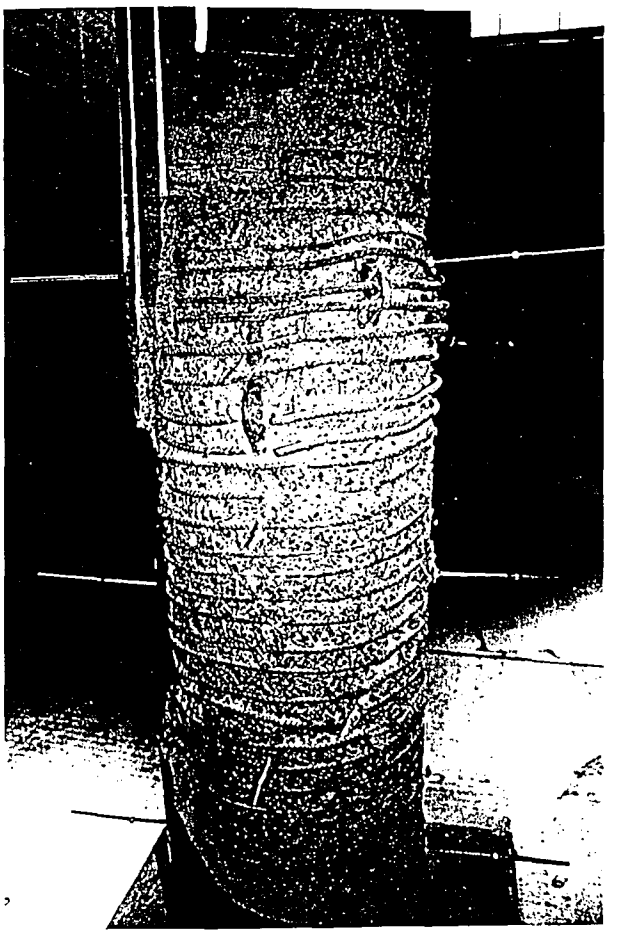

Figure 4.43(g) Specimen H3-series of key photographs; (g) spiral fractures at location of buckled longitudinal bars.

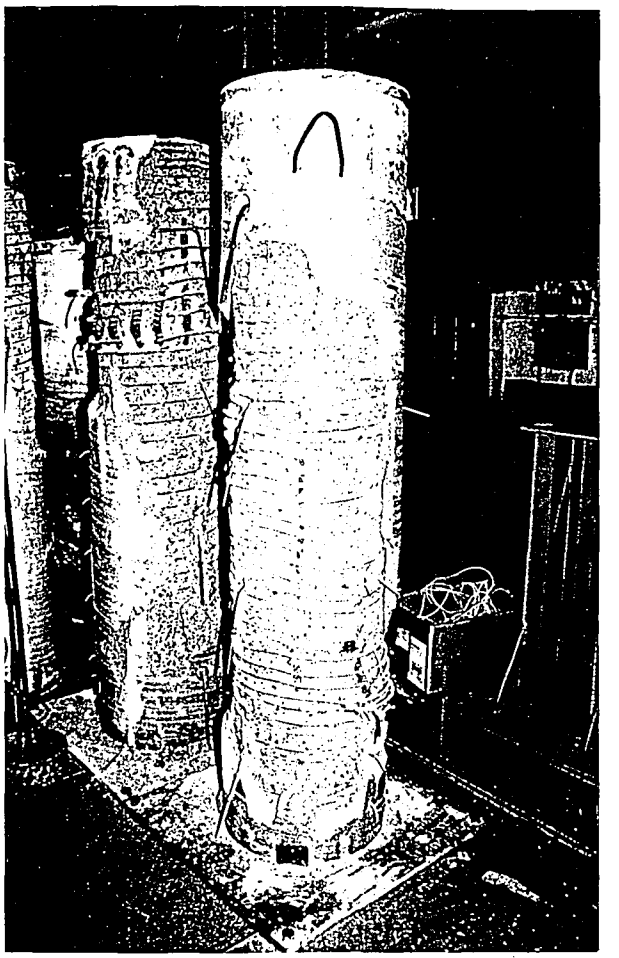

Figure 4.43(h) Specimen H3-series of key photographs; (h) post-test photograph showing the inclined failure plane.

CHAPTER 5

DISCUSSION OF RESULTS

5.1 INTRODUCTION

This chapter discusses the results from the eight column tests presented in Chapter 4. A comparison of observed and predicted column axial strengths is presented in Section 5.2. Section 5.3 discusses the column ductility with respect to the three test variables, namely concrete strength, longitudinal steel ratio, and spiral steel size/pitch. Sections 5.4, 5.5, and 5.6 discuss the behavior of the concrete cover, the load-deflection graphs, and the behavior of the spiral reinforcement, respectively. A description of the different types of failure modes observed in the tests is presented in Section 5.7. Finally, conclusions from the discussion are presented in Section 5.8.

5.2 COLUMN AXIAL STRENGTH

Table 5.1 compares the maximum axial load resisted by each specimen (P_{max}) to the predicted axial load capacity of the confined core for each specimen. Any contribution of the concrete cover to the predicted column strength is ignored in predicting the axial load capacity, since it is assumed that the cover concrete has spalled away and therefore carries no load when P_{max} is reached. Two predicted axial load strengths are presented for each column. One strength is calculated based on the compressive strength of the day-of-test field-cured

cylinders (P_c), and one is calculated based on the compressive strength of the cored cylinder (P_{ccore}). The predicted strengths are based on Equations 4.1 and 4.2, respectively. The contribution of the confined concrete to the predicted axial capacity of the column is calculated from Equation 2.7 (Martinez et al. 1982, 1984). Equation 2.7 includes a correction factor for the spacing of the spiral reinforcement. This correction factor ($1-s/d_c$) reduces the effectiveness of the confinement as the pitch (s) increases relative to the core diameter (d_c).

It is difficult to draw definitive conclusions from Table 5.1, in part because of the differences in compressive strengths of the cored cylinders as compared to the field-cured cylinders.

To examine the results, it is useful to begin first with low-strength concrete specimens, L1 and L2. For these specimens, the field-cured cylinder and the cored cylinder concrete compressive strength values were about the same. Thus, the two predicted values in Table 5.1 are about the same. Table 5.1 shows good agreement between the observed and predicted strengths of Specimen L2. The agreement of observed and predicted axial strengths for Specimen L1, while not as good as L2, is still reasonably close.

It is interesting to note that the low-strength concrete columns did not exhibit a strength generally higher than that predicted by Equations 4.1 and 4.2. Martinez et al. (1982, 1984) noted for their tests that the contribution of the confined concrete to the ultimate strength of the column was higher than predicted by Equation 2.7, because the cover concrete in these specimens did not completely

spall away and was thus still effective in carrying some load at peak resistance. In the large-scale specimens tested in this study, however the cover concrete was likely to have been completely ineffective in carrying any axial load at peak resistance.

Equations 4.1 and 4.2 also gave reasonably good agreement between observed and predicted column axial strengths for the M-Series specimens. This is particularly true if $f_{c\text{-field}}$ is used to compute the contribution of the confined concrete f_{cc} to the column axial capacity. If $f_{c\text{-core}}$ is used to compute f_{cc}, then Equation 4.2 seems to under predict the strengths of the columns, i.e. the equation is conservative.

An evaluation of whether Equation 2.7 is appropriate for the H-Series specimens seems to depend somewhat on whether the concrete compressive strength is taken as $f_{c\text{-field}}$ or $f_{c\text{-core}}$. If $f_{c\text{-field}}$ is used to predict f_{cc}, then Equation 4.1 is unconservative, as the ratio P_{max}/P_c varies between 0.86 and 0.71. Better agreement is obtained between the observed and predicted strengths if $f_{c\text{-core}}$ is used to compute f_{cc}.

5.3 COLUMN DUCTILITY

5.3.1 Definition of Ductility

Two definitions for column displacement ductility were adopted for this report: (1) ductility based on the displacement at first spiral fracture; and, (2) ductility based on the displacement at an axial load equal to 85% of P_{max}. The two

ductility values were calculated as a ratio between a maximum displacement and an initial displacement corresponding to an approximation of the limit of elastic behavior. Figure 5.1 shows how each of the displacements were determined. Both definitions of column ductility required an estimate of the displacement at the limit of elastic behavior, Δ_1, which is obtained as follows. A best-fit line to the linear portion of the load-displacement graph for each specimen was obtained by linear regression analysis. This line was then extrapolated to intersect with the maximum load sustained by the column (P_{max}). The displacement corresponding to this intersection was labelled Δ_1. The displacement at the first spiral fracture was labelled Δ_{SF}. Next, the load corresponding to 85% of P_{max} was intersected with the descending portion of the load-deflection curve. The displacement at this point was labelled Δ_{85}. The 85% factor was arbitrarily selected for comparison purposes; other values could also have been used. A resistance equal to 85% of the peak resistance seemed to be a reasonable limit at which to consider the column as having maintained its peak resistance.

The ratio of Δ_{SF} to Δ_1 is equal to the ductility at first spiral fracture (Equation 5.1), and the ratio of Δ_{85} to Δ_1 is equal to the ductility at 85% of P_{max} (Equation 5.2). In some instances, μ_{SF} was equal to μ_{85}, since the two displacements, Δ_{SF} and Δ_{85} were equal.

$$\mu_{SF} = \frac{\Delta_{SF}}{\Delta_1} \tag{5.1}$$

$$\mu_{85} = \frac{\Delta_{85}}{\Delta_1} \qquad (5.2)$$

Each of the displacement values Δ_1, Δ_{SF}, and Δ_{85} are shown on the load-displacement graphs in Chapter 4. Table 5.2 summarizes, the maximum load, 85% of the maximum load, the values Δ_1, Δ_{SF}, and Δ_{85}, and the ductilities as defined in Equations 5.1 and 5.2 for all the specimens.

Table 5.2 shows that, in general, the H-Series specimens (H1, H2, and H3) exhibited lower ductilities (for both definitions of ductility) relative to the L- and M-Series specimens. The M-Series specimens possessed a higher ductility than both the L- and H-Series specimens. This apparent increase in ductility occurred because the M-Series specimens contained a volumetric ratio of spiral reinforcement based on a concrete compressive strength of 69 MPa (10 ksi). However, the actual compressive strengths were in the range of 52.7 MPa (6.48 ksi) to 52.7 MPa (7.64 ksi). Thus the M-Series specimens were over-confined in so far as the ACI 318 Code provisions are concerned. The result of this over confinement is an increase in ductility.

The ductilities of Specimens M3 and H3 vary considerably depending on which definition of ductility is used. For Specimen M3, μ_{SF} is equal to 7.04, and μ_{85} is equal to 2.99; and for Specimen H3, μ_{SF} is equal to 5.12, and μ_{85} is equal to 2.93. The reason for the discrepancy between the two ductility values can be seen in the load-displacement graphs for both specimens (Figures 4.21 and 4.38).

Neither column was able to maintain its peak resistance and instead quickly decreased in resistance to 85% of P_{max}. This reduction in axial resistance decreased the value of Δ_{85}, which decreased the ductility, μ_{85}.

Table 5.3 compares the column ductilities in terms of the three test variables; concrete compressive strength, longitudinal steel ratio, and spiral steel size/pitch. The ratio of the ductilities of the first specimen to the second specimen (i.e. L1/H1) are shown in the third and forth columns of the table. These ratios, are calculated from Equations 5.3 and 5.4, respectively.

$$R_{SF} = \frac{\mu_{SF}}{\mu_{SF}} \tag{5.3}$$

$$R_{85} = \frac{\mu_{85}}{\mu_{85}} \tag{5.4}$$

The following sections describe the influence of each of the test variables on column ductility by comparing the ratios defined above.

5.3.2 Influence of Concrete Compressive Strength

In Table 5.3 the ductilities of the low-strength concrete specimens are compared to the ductilities of the high-strength concrete specimens. The longitudinal steel ratio is held constant for each of the comparisons. The ratios are all greater than 1.0, indicating that the low-strength concrete specimens exhibited

greater ductility than the high-strength concrete specimens. This relationship between concrete strength and column ductility is true for both definitions of ductility.

This decrease in column ductility is graphically represented in Figures 5.1, 5.2, and, 5.3. In these graphs, the axial load is normalized with respect to P_{max}, and the axial displacement is normalized with respect to Δ_1, respective to each column. Figure 5.2 compares Specimens L1 and H1, Figure 5.3 compares Specimens L2 and H2, and Figure 5.4 compares Specimens L2 and H3. For each of the two specimens in these comparisons the longitudinal steel ratios are equal. From these figures, it can be seen that the H-series specimens displayed less ductility than the L-Series specimens. However, it must be noted that while the H-Series specimens displayed less ductility, they actually had a greater displacement capacity than the L-Series specimens. This difference in displacement capacity can be seen on the axial load versus axial displacement graphs from Chapter 4. The ductility represented in Figures 5.2, 5.3, and 5.4 is dependent on the value defined for the limiting elastic displacement, Δ_1, and could therefore change with a change in this defined displacement.

5.3.3 Influence of Longitudinal Reinforcement

Table 5.3 also compares the ductilities of the specimens with a lower longitudinal steel ratio to the ductilities of the specimens with a higher longitudinal

steel ratio. The concrete strengths and spiral reinforcement details are the same with each of these comparisons.

This table shows that all the ductility ratios are greater than 1.0, except R_{85} for the low-strength concrete specimens (L2/L1). Table 5.3 suggests that, in general, the 8-#8 bar columns exhibited greater ductility than the 16-#9 bar columns. This was an unexpected result since it was suggested by some of the earlier research that a greater amount of longitudinal reinforcement would contribute to more effective confinement and thus more ductility (see Section 2.4.2). It may be, however, that the columns with a greater amount of longitudinal reinforcement placed a greater demand on the spiral reinforcement causing failure at an overall lower column ductility. This is discussed further in Sections 5.6 and 5.7.

Figures 5.5, 5.6, and 5.7 graphically display the relationships between the column ductilities described above in the low-, medium-, and high-strength concrete specimens, respectively. In each of the figures, the compressive strength of the concrete and the amount of spiral reinforcement remains constant. Again, the trend in these comparisons based on the definitions of ductility presented in Section 5.3 is that the columns with less longitudinal reinforcement displayed greater ductility.

It is also noted in Figures 5.5, 5.6, and 5.7 that the columns with a greater amount of longitudinal reinforcement (L1, M1, H1) though exhibited less overall ductility, do seem to maintain a greater fraction of P_{max} during that portion of the

response when the column is deforming at a relatively constant axial load. This is discussed further in Section 5.5.

5.3.4 Influence of Spiral Reinforcement Size/Pitch

In Table 5.3 the ductilities of the specimens with a larger spiral pitch and larger spiral diameter are compared to the ductilities of the specimens with a reduced spiral pitch and smaller spiral diameter. The two spiral reinforcement bars used were a #5 bar at a 64 mm (2.5 in) pitch and a #4 bar at a 41 mm (1.625 in) pitch. The volumetric ratio of spiral reinforcement, the longitudinal steel ratio, and the concrete strength are constant within each comparison. All of the ductility ratios are greater than 1.0 with the exception of the ratio at first spiral fracture for the high-strength concrete specimens, where R_{SF} was equal to 0.95. This ratio is approximately equal to one.

The comparisons in Table 5.3 suggest that, in general, the specimens with a larger spiral pitch and larger spiral diameter exhibit greater ductility. This may simply be the result of the larger spiral bars having greater strain capacity than the smaller spiral bars. Thus, fracture of the spiral was delayed, leading to increased values of μ_{SF} and μ_{85} for the columns made with the larger diameter spirals. This possibility is difficult to confirm since complete stress-strain curves were not available for the spiral reinforcements.

Figures 5.8 and 5.9 graphically show the differences in the column ductilities as described above. Figure 5.8 compares the M-Series specimens, and Figure 5.9

compares the H-Series specimens. Again in both of these graphs the axial load and the axial displacements for each specimen are normalized with respect to P_{max} and Δ_1, respectively. These figures clearly show the decrease in column ductility when the spiral pitch is 41 mm (1.63 in) as compared to 64 mm (2.5 mm) for the M-Series specimens (Figure 5.8). The difference in ductility is not as apparent for the H-Series specimens (Figure 5.9).

5.4 BEHAVIOR OF CONCRETE COVER

Table 5.4 compares the maximum axial load resisted by each column (P_{max}) to the axial load corresponding to first observed cracking of the concrete cover (P_{FCR}). The load at first cracking is considered to be an approximate value since first cracking was only visually observed during the column tests from a distance of approximately 7.6 m (10 ft). It is possible that cracking occurred at lower loads but the first crack was not immediately detected. Table 5.4 shows that the higher strength concrete columns experienced first cracking of the cover concrete at a lower load relative to peak load. This earlier cracking in the concrete cover may indicate that the cover may also have become ineffective in carrying load earlier in the response for these columns.

During the experiments, the concrete covers on the high-strength and medium-strength concrete specimens were observed to fall away from the columns in large sheets (Figure 5.10(a)). This is in contrast to the low-strength concrete specimens where the cover concrete broke away in smaller pieces (Figure

5.10(b)). The separation of the cover concrete from the core in high-strength concrete columns may be explained as an instability problem. In the higher strength specimens, large cracks formed early in the loading, and widened as the core concrete expanded laterally Figure 5.10(c)). Many of these cracks propagated the entire length of the column and divided the cover into long sections around the circumference of the column (Figure 5.10(d)). As the column was displaced further, the sections of cover concrete separated from the core and the sheets buckled outward and fell from the column (Figure 5.10(e)).

Figures 5.10(f) and (g) show a low-strength concrete specimen and a high-strength concrete specimen after testing. From these figures it is seen that a large portion of the concrete cover still remains intact in the low-strength concrete specimen, whereas most of the cover concrete spalled off the column in the high-strength concrete specimen.

It is not clear what causes earlier cracking in the concrete cover in high-strength concrete columns. One possibility is that the more brittle nature (lower ultimate strain capacity) of higher strength concrete may lead to this earlier cracking. A second possibility is that the greater amount of spiral reinforcement required in a high-strength concrete column creates a natural plane of separation between the spiral reinforcement and the cover concrete. This allows the cover concrete to separate more easily from the core concrete.

5.5 DISCUSSION OF THE LOAD-DISPLACEMENT CURVES

The load-displacement curves for each specimen are shown in the individual test summaries in Chapter 4. Comparisons of these curves reveals several interesting features about column behavior.

The specimens reinforced with 8-#8 bars (L2, M2, M3, H2, H3) displayed different post peak load-displacement responses compared to the specimens reinforced with 16-#9 bars (L1, M1, H1). Figure 5.11 shows the load-displacement curves of specimens which contained 16-#9 bars, L1, M1, and H1. All 3 specimens reached and maintained a maximum load until the first spiral fracture occurred. Figure 5.12 shows selected specimens which were reinforced with 8-#8 bars (L2, M2, H3). This figure as compared to Figure 5.11 clearly shows the difference in the post peak responses. Up to maximum axial load, the 8-#8 bar specimens behaved in a similar manner to the 16-#9 bar specimens. However, after reaching maximum load, the 8-#8 bar specimens did not maintain the peak value of load, but instead dropped in axial load resistance.

By comparing the load-displacement curves of the specimens with large spiral steel spacing, Specimens M1, H1, M2 and H2, to the specimens with reduced spiral steel spacing, Specimens M3 and H3, a difference in the descending branches of the load-displacement curves is observed. Figure 5.13 shows the load-displacement curves for selected specimens with a spiral pitch of 64 mm (2.5 in) (M1 and H1), and Figure 5.14 shows the load-displacement curves for the specimens with a spiral pitch of 41 mm (1.63 in) (M3 and H3). Figure 5.13

shows that the specimens with a larger spiral size and pitch displayed a large decrease in axial load resistance when a spiral fracture occurred. In this figure, the large decrease in resistance is seen as a distinct drop from one data point to the next. Two to three spiral fractures were typically observed in these specimens. Figure 5.14 shows that the specimens with a smaller spiral sized and pitch exhibited several small decreases in axial load resistance as each of the spiral fractures occurred. Typically 10 to 14 spiral fractures were observed in these specimens.

5.6 FRACTURE OF SPIRAL REINFORCEMENT

Figures 5.15(a)-(c) show the locations of spiral fractures on the L-Series specimens. These columns were reinforced with #3 spirals at 44 mm (1.75 in) pitch. These columns had 2 to 3 spiral fractures each of which were contained within the failure region at the top 1/3 of the column.

Figures 5.15(d)-(f) show the locations of spiral fractures on the columns reinforced with #5 spirals at a 63.5 mm (2.5 in) pitch (Specimens M1,M2, H1, H2). The spiral fractures were contained within the failure region and occurred at the locations of buckled longitudinal bars. Figures 5.15(g)-(i) show the locations of spiral fractures on the columns reinforced with #4 spirals at a 41 mm (1.63 in) pitch (Specimens M3 and H3). These spiral fractures were also contained within the failure region and also occurred at the locations of buckled longitudinal bars.

As noted above, in many instances in the M- and H-Series specimens, it

appeared as though the spirals fractured directly over a longitudinal bar. This can be seen in Figures 5.15(d)-(i). It appeared as though when the spirals were subjected to tension from expansion of the concrete core, they were also subjected to bending as they kinked around the longitudinal bars. This combined state of stress precipitated spiral fractures directly over the longitudinal reinforcement. A similar situation may have occurred in the L-Series specimens, though this is not as readily seen in Figures 5.15(a)-(c).

5.7 FAILURE MODES

Two types of failure modes were observed among the eight specimens tested: (1) bulging until spiral fracture; and, (2) formation of an inclined failure plane.

Figures 4.5(e) and 4.10(b) illustrate the mode of failure in the low strength concrete specimens, L1 and L2. Both of these specimens failed in a bulging failure mode located in the top 1/3 of the column. The failure modes of the M- and H-Series specimens were characterized by the formation of an inclined failure plane. The failure planes of the M-Series specimens M1, M2, and M3 are shown in Figures 4.15(h), 4.20(f), and 4.25(j), respectively. The failure planes of the H-Series specimens H1, H2, and H3 are shown in Figures 4.31(f), 4.37(d), and 4.43(h), respectively. These inclined failure planes typically extend from the top 1/3 of the column to the middle of the column, with the exception of Specimens H2 and H3. The failure plane of Specimen H3 was concentrated in the lower half of

the specimen, and extended from the bottom 1/3 of the column to the middle of the column. Specimen H2 did not exhibit a large inclined plane failure. Only a small inclined plane existed at the very top of the column. The failure in the column was concentrated in this region. It is unclear whether the failed appearance of Specimen H2 was influenced by the failure of the capping compound during testing.

In general (with the exception of Specimen H2), the appearance of each column that exhibited an inclined failure plane had certain similar features. Each failure plane intersected the column at an angle that would create an elliptical failure surface through the column. Many of the spiral fractures were concentrated in two regions, namely the top and bottom of the intersection of the failure plane with the column surface. Many of the buckled bars occurred along the failure surface between these two end regions.

In the specimens with the inclined failure plane, the sequence of events that accompanied failure is not completely clear. It is suspected that the inclined failure plane formed first, shortly after the peak column resistance was reached. Continued applied axial displacement then caused relative movement of the two column sections along this plane. This caused the longitudinal bars, acting as dowels, to resist sliding along the failure plane. This dowel action would increase the force on the spirals. Once the spirals fractured, the longitudinal bars were then unrestrained and buckled under the action of continued sliding along the failure plane.

As noted earlier, the columns reinforced with 16 longitudinal bars were able to maintain their peak resistances with continued axial displacement much more effectively than the columns reinforced with 8 longitudinal bars. It may be that 16 bars were more effective as dowels in restraining relative movement of the column sections along the failure plane. The decrease in capacity after peak load in the 8-bar columns may be the result of the initial formation of the failure plane in the column that could not be effectively restrained by the 8 longitudinal bars.

5.8 SUMMARY AND CONCLUSIONS

The results of the eight columns tested in this study were presented in Chapter 4 and are discussed in this chapter. The tests were performed to evaluate the axial load behavior of spirally-reinforced high-strength concrete columns. The influence of the three test variables on column strength and ductility were evaluated: concrete compressive strength, longitudinal steel ratio, and spiral steel size/pitch. The following conclusions are made from the eight column tests:

1. A comparison was made between the maximum axial load resisted by each specimen and the predicted axial load capacity of the confined core for each specimen. The following equation by Martinez et al. (1982, 1984) was used to estimate the strength enhancement for the core concrete:

$$f_{cc} = 0.85 f_c' + 4.0 f_2 (1 - \frac{s}{d_c}) \qquad (2.7)$$

Both the field-cured cylinder and cored cylinder concrete compressive strengths were used to compute the predicted strengths (see Equations 4.1 and 4.2), since these concrete strengths were observed to differ considerably, particularly for the high-strength concrete specimens.

It was found that the suitability of the equation presented by Martinez et al. depends on whether the field-cured or cored cylinder concrete compressive strength values are used. If the field-cured strengths $f_{c\text{-}field}$ are used to predict the strength of the confined core, Equation 2.7 can be used to accurately predict column strengths from 34.5 MPa to 52.7 MPa (5 ksi to 7.64 ksi). However, this equation over predicts the column strengths and is therefore unconservative when $f_{c\text{-}field}$ ranges from 75.8 MPa to 82.7 MPa (11.0 ksi to 12.0 ksi). If instead the cored cylinder strengths $f_{c\text{-}core}$ are used to predict the compressive strength of the confined core, then Equation 2.7 provides reasonable agreement to the experimental results.

2. The compressive strength of the concrete was found to influence column ductility. Two displacement ductility values are defined in this report, one based on the displacement at first spiral fracture, and one based on the displacement corresponding to an axial load equal to 85% of P_{max}. For both definitions of ductility, the higher strength concrete columns displayed less ductility than the lower strength concrete columns. This suggests that more than the minimum amount of spiral reinforcement currently prescribed by

the ACI 318 Code is needed for high-strength concrete columns to achieve the same ductility as provided in the low-strength concrete columns.

3. Two types of failure modes were observed among the eight specimens tested in this research: (1) bulging until the first spiral fracture; and, (2) formation of an inclined failure plane. The mode of failure seems to depend on the concrete strength. For the columns tested in this research, a bulging type failure mode was observed in the specimens with $f_{c\text{-field}}$ around 34.5 MPa (5 ksi), and an inclined failure plane developed in columns with $f_{c\text{-field}}$ around 51.7 MPa (7.5 ksi) and greater.

4. The amount of reinforcement impacted the behavior of the columns in two related ways. First, it was found that, in general, the 8-#8 longitudinal bar columns exhibited greater ductility than the 16-#9 longitudinal bar columns. This was a surprising result since it was expected that a greater amount of longitudinal reinforcement would contribute to more effective confinement and thus more overall ductility. It was noted in many of the tests that the spiral reinforcement would fracture directly over a longitudinal bar. It may be that more longitudinal reinforcement did in fact contribute to more effective confinement, but that this also placed a greater demand on the spiral reinforcement, and thus caused an overall reduction in column ductility.

The second way in which the amount of longitudinal reinforcement impacted the behavior of the columns was in the ability of the columns to maintain their peak values of resistance for increasing axial displacements. It was found that the 16-#9 longitudinal bar columns were able to maintain their peak resistances with continued axial displacement much more effectively than the columns with 8-#8 longitudinal bars. For the low-strength concrete columns, this may be a reflection of more effective confinement provided by the greater amount of longitudinal reinforcement. In addition, for the medium- and high-strength concrete columns, it is thought that the 16-#9 longitudinal bars are more effective as dowels in restraining an inclined failure mode that develops in these columns.

5. For the columns tested in this research, a decrease in the size and pitch of the spiral reinforcement, while maintaining a constant volume of spiral reinforcement, lead to a decrease in the ductility of the column. This result, however, may be attributed to the differences in strain capacity of the different size spiral reinforcement used.

6. The higher strength concrete columns experienced first cracking of the concrete cover at a lower load relative to peak load. It is thought that the larger volume of spiral reinforcement may provide a natural plane of separation between the cover concrete and the core.

		Cored Concrete Strength		Field-Cured Concrete Strength	
Specimen	P_{max} (MN)	P_{ccore} (MN)	P_{max}/P_{ccore}	P_c (MN)	P_{max}/P_c
L1	11.70	12.76	0.92	12.70	0.92
L2	9.53	9.58	0.99	9.44	1.01
M1	16.99	15.97	1.06	17.14	0.99
M2	13.86	12.83	1.08	14.05	0.99
M3	14.50	12.89	1.12	14.10	1.03
H1	17.45	18.27	0.96	20.40	0.86
H2	13.12	15.34	0.86	18.35	0.71
H3	15.21	15.01	1.01	18.27	0.83

0.004448 MN=1 kip

Table 5.1 Comparison of observed and predicted column axial strengths.

Specimen	P_{max} (MN)	$0.85P_{max}$ (MN)	Δ_1 (mm)	Δ_{SF} (mm)	Δ_{85} (mm)	μ_{SF}	μ_{85}
L1	11.70	9.95	4.3	27.6	27.6	6.40	6.40
L2	9.53	8.10	3.6	29.4	19.0	8.12	5.26
M1	16.99	14.44	7.4	51.3	51.3	6.95	6.95
M2	13.86	11.78	6.4	56.8	56.8	8.87	8.87
M3	14.50	12.32	7.2	50.3	21.4	7.04	2.99
H1	17.45	14.83	10.4	43.3	47.4	4.17	4.57
H2	13.12	11.15	8.4	41.2	41.2	4.87	4.87
H3	15.21	12.93	7.9	40.4	23.1	5.12	2.93

25.4 mm=1 in
0.004448 MN=1 kip

Table 5.2 Computed column ductilities at first spiral fracture and at 85% of P_{max}.

Test Variable	Specimens	$R_{SF}=\mu_{SF} / \mu_{SF}$	$R_{85}=\mu_{85} / \mu_{85}$
Concrete Strength (low/high)	L1/H1	1.53	1.40
	L2/H2	1.67	1.15
	L2/H3	1.59	1.79
Longitudinal Steel Ratio (1.65% / 4.2%)	L2/L1	1.27	0.82
	M2/M1	1.28	1.28
	H2/H1	1.17	1.07
Spiral Steel Size/Pitch (64 mm/41 mm)	M2/M3	1.26	2.97
	H2/H3	0.95	1.66

Table 5.3 Comparison of ductility ratios with regard to test variables.

Specimen	P_{FCR} (MN)	P_{max} (MN)	P_{FCR}/P_{max}
L1	10.95	11.70	0.94
L2	8.53	9.53	0.90
M1	11.45	16.99	0.67
M2	10.20	13.86	0.74
M3	11.10	14.50	0.77
H1	11.26	17.45	0.65
H2	8.90	13.12	0.68
H3	11.28	15.21	0.74

0.004448 MN=1 kip

Table 5.4 Comparison of column axial load at first observed cracking (P_{FCR}) of the concrete cover with the maximum axial load of the column (P_{max}).

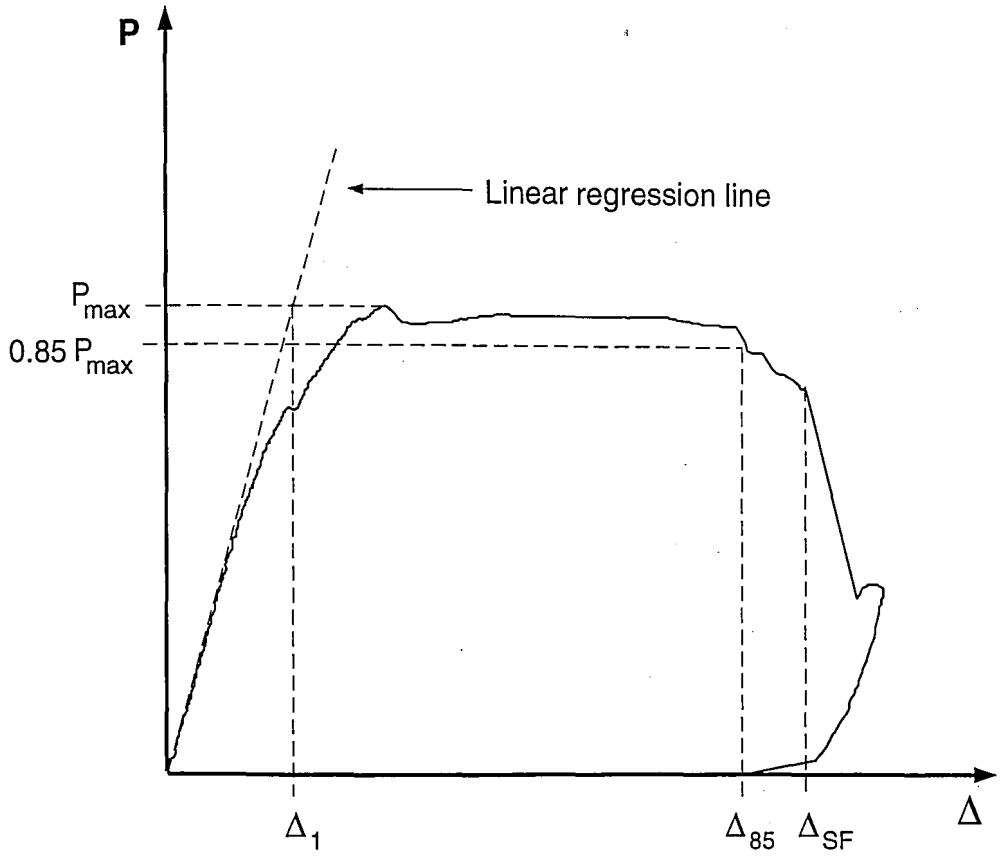

Figure 5.1 Measurement of displacements to calculate column ductilities.

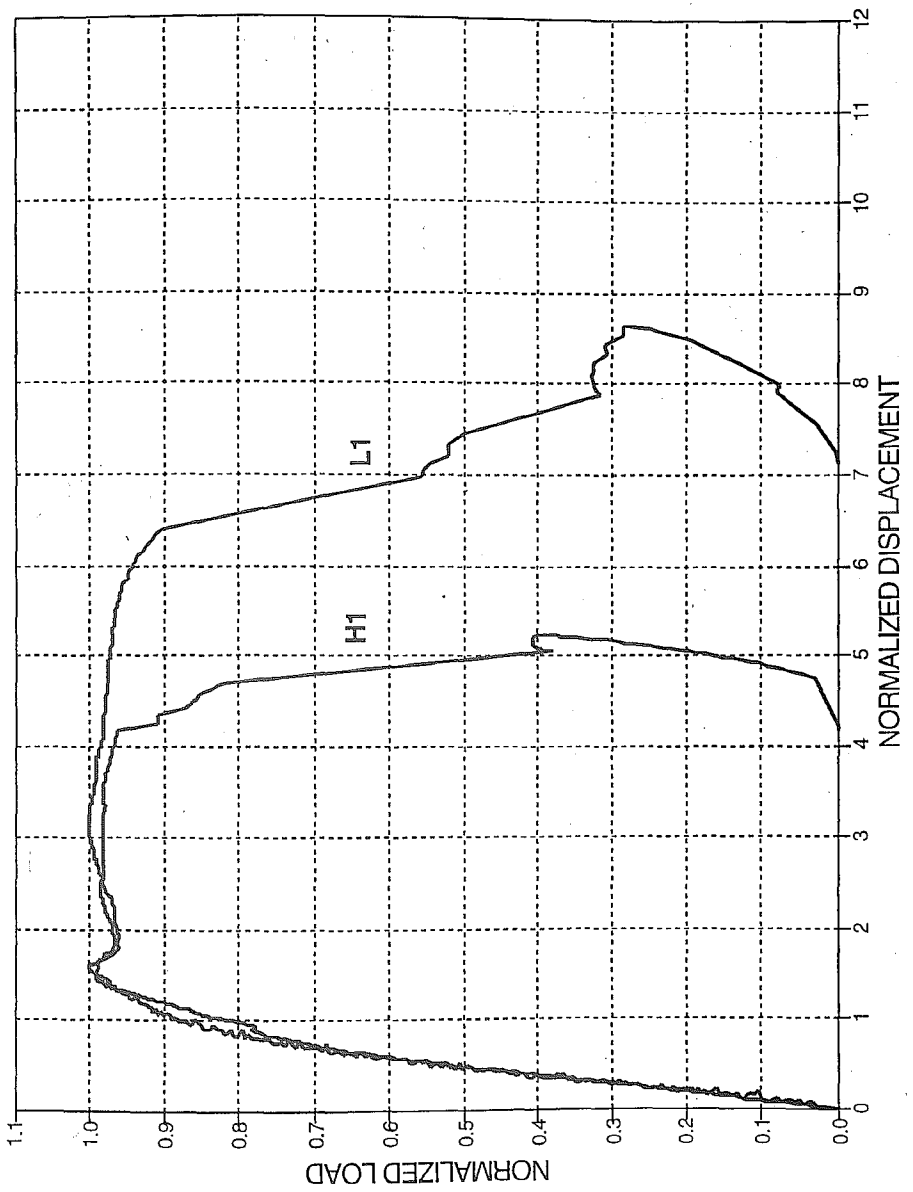

Figure 5.2 Normalized load and displacement-L1 and H1.

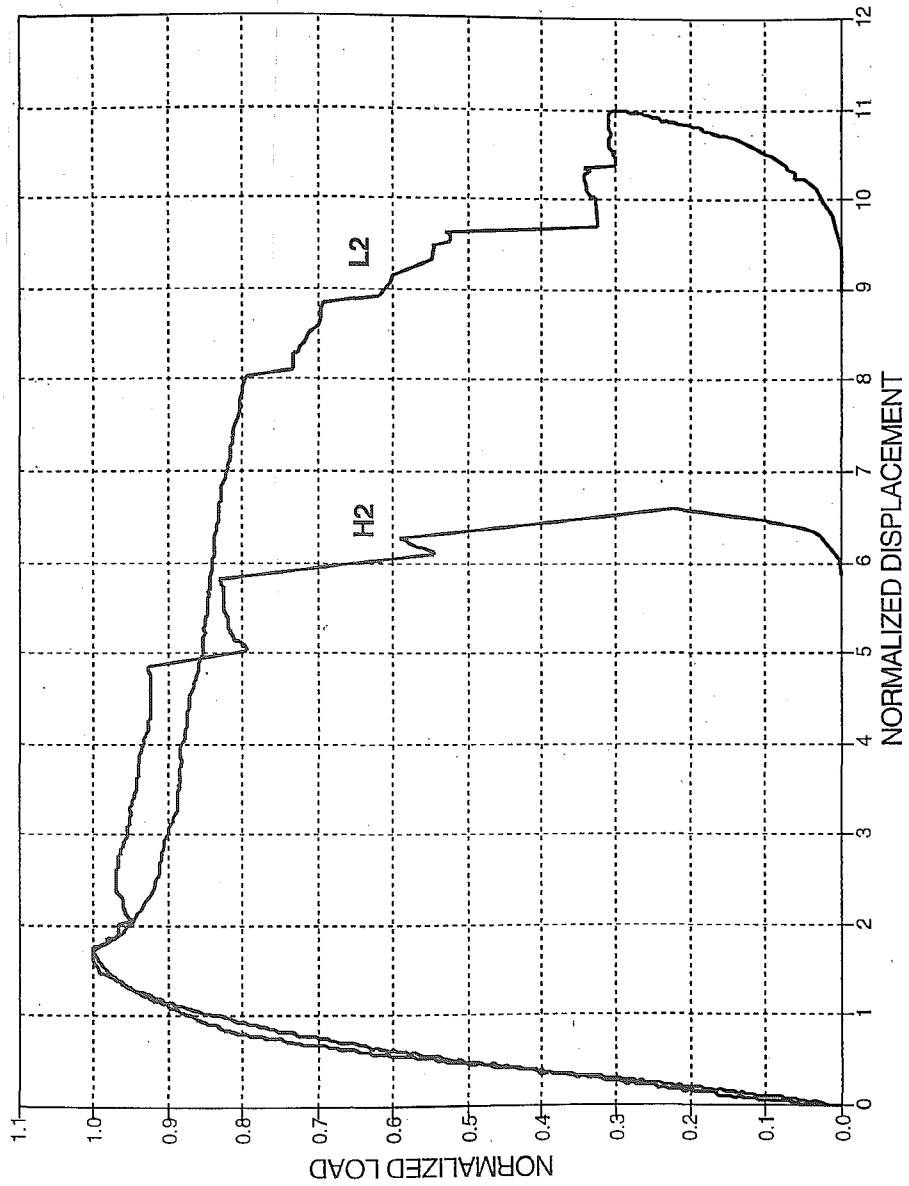

Figure 5.3 Normalized load and displacement-L2 and H2.

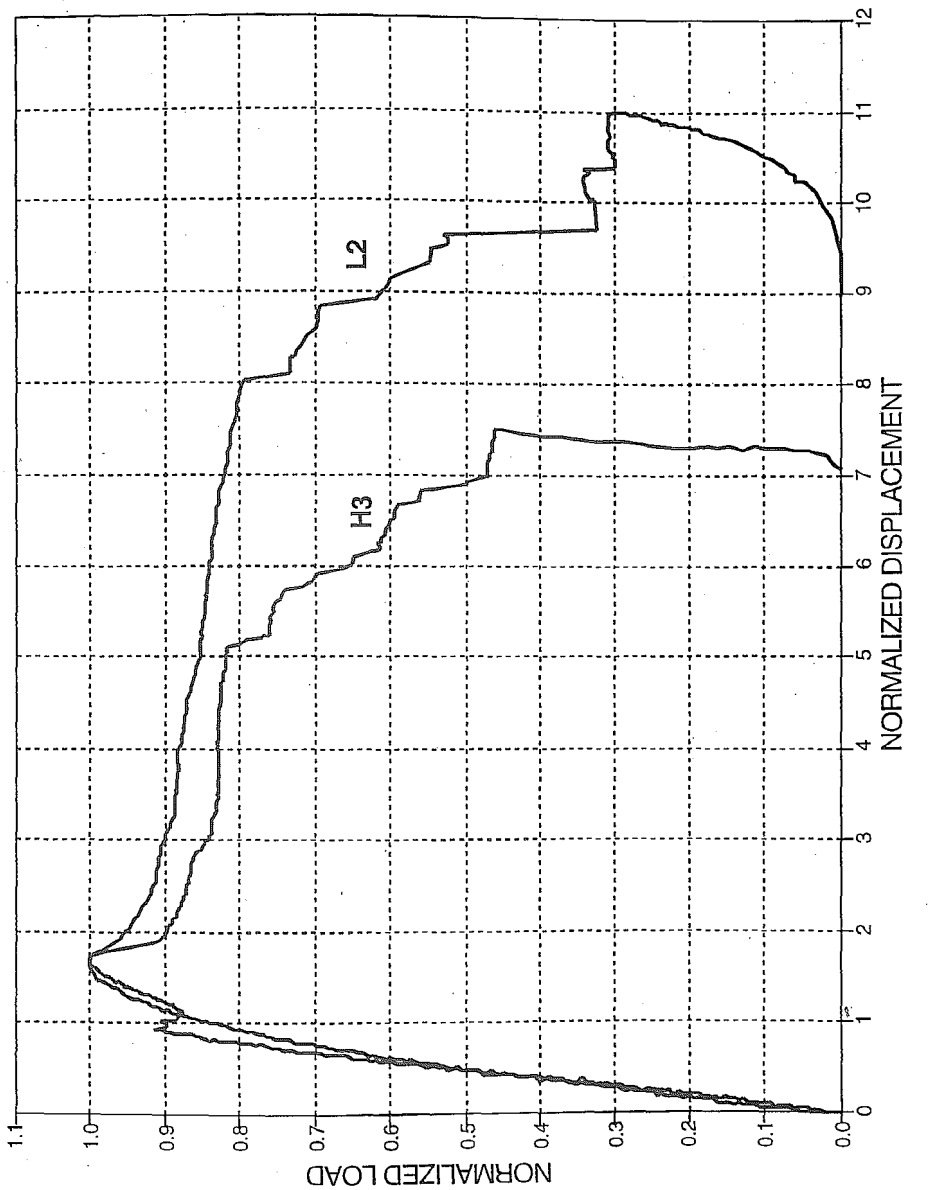

Figure 5.4 Normalized load and displacement-L2 and H3.

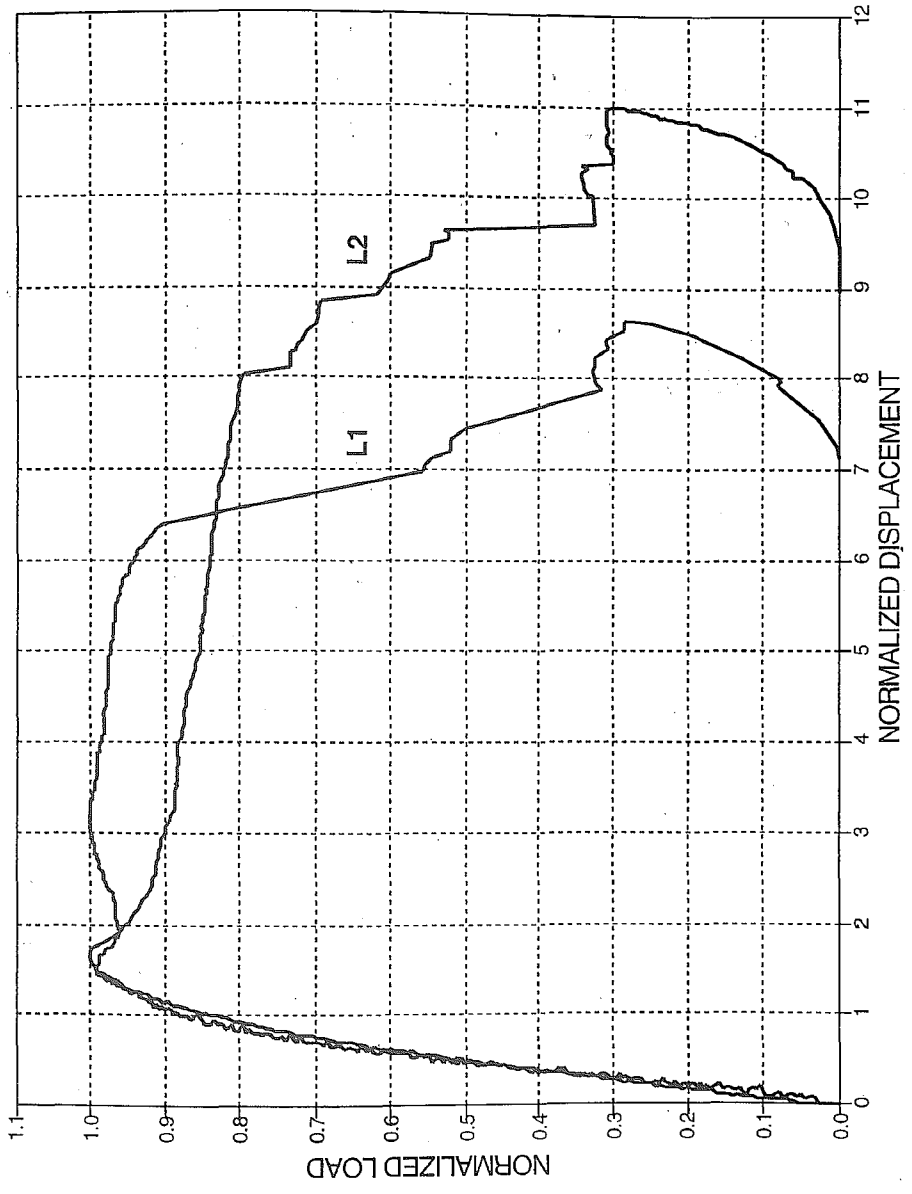

Figure 5.5 Normalized load and displacement-L2 and L1.

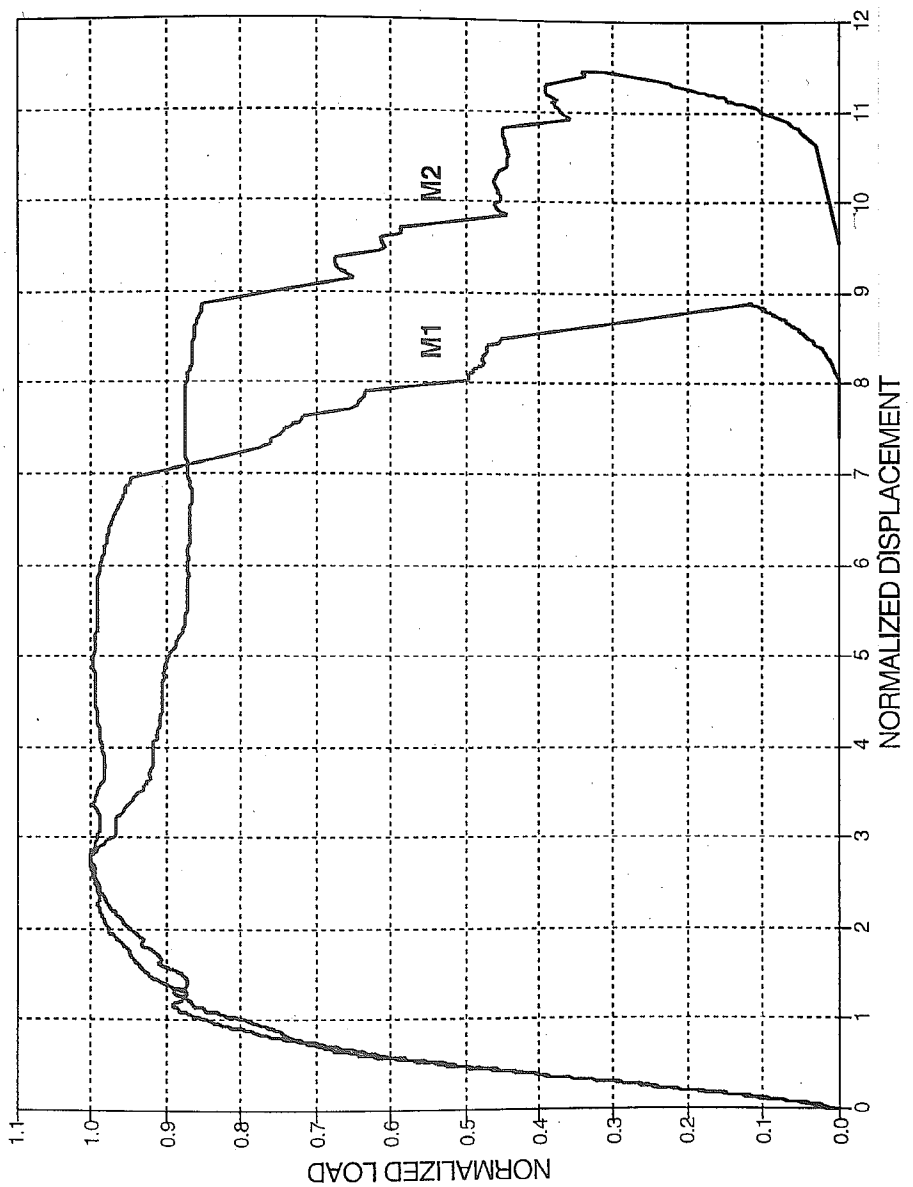

Figure 5.6 Normalized load and displacement-M2 and M1.

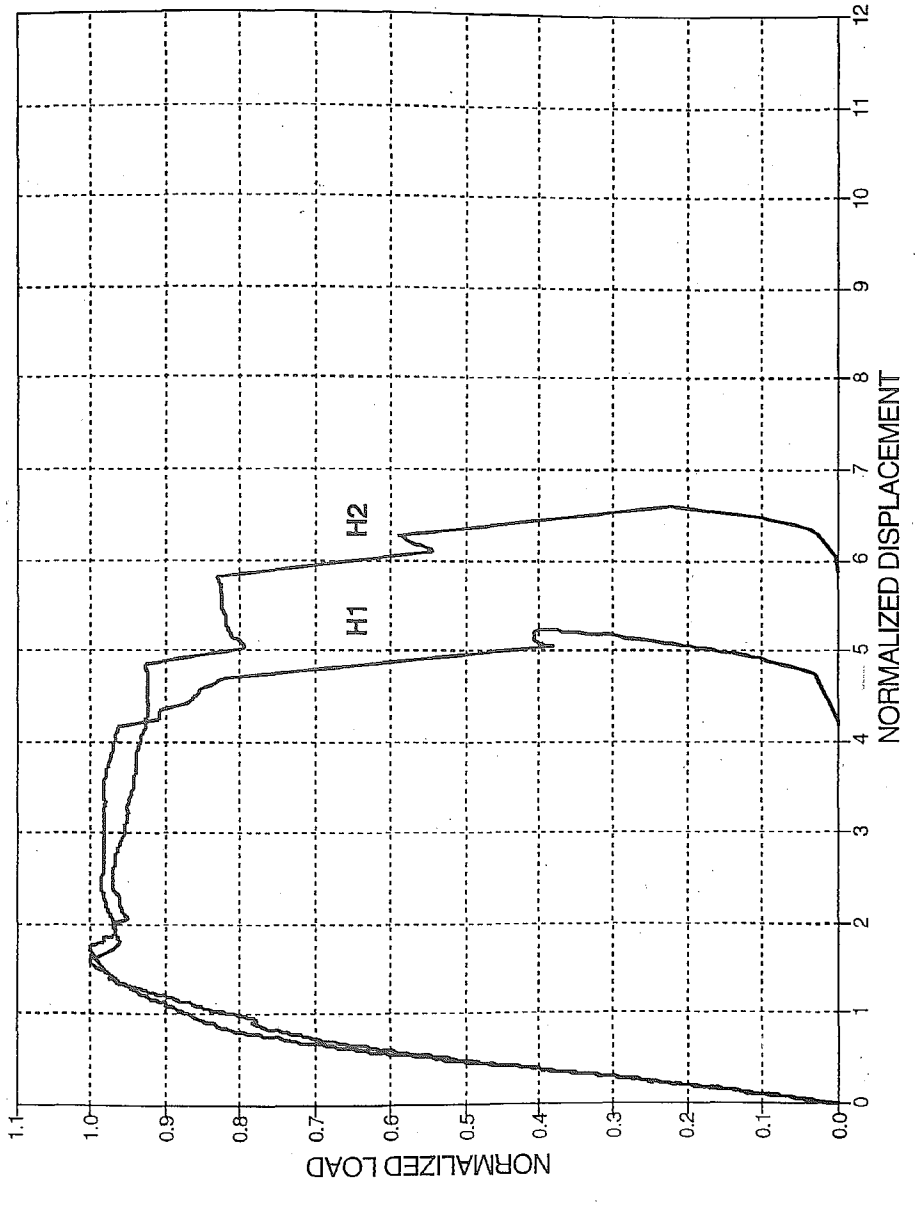

Figure 5.7 Normalized load and displacement-H2 and H1.

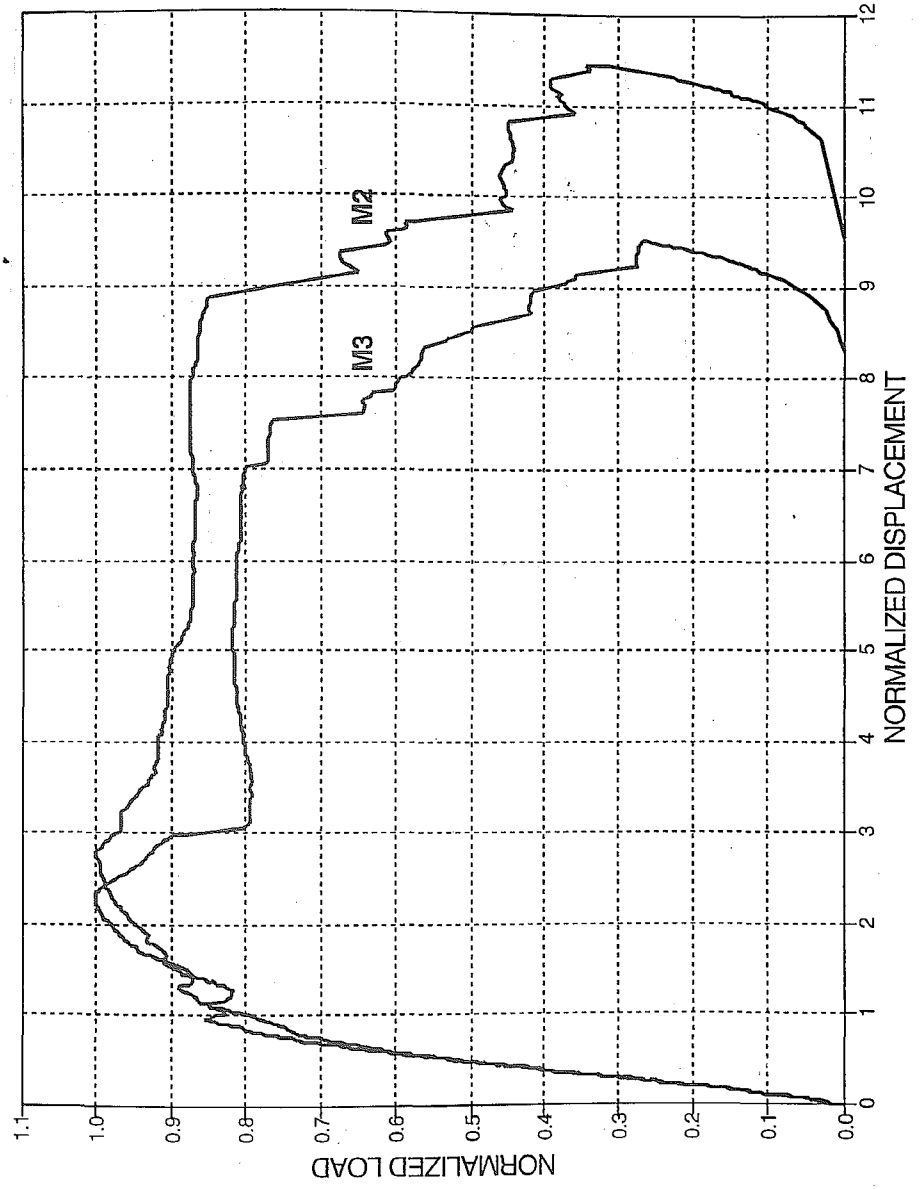

Figure 5.8 Normalized load and displacement-M2 and M3.

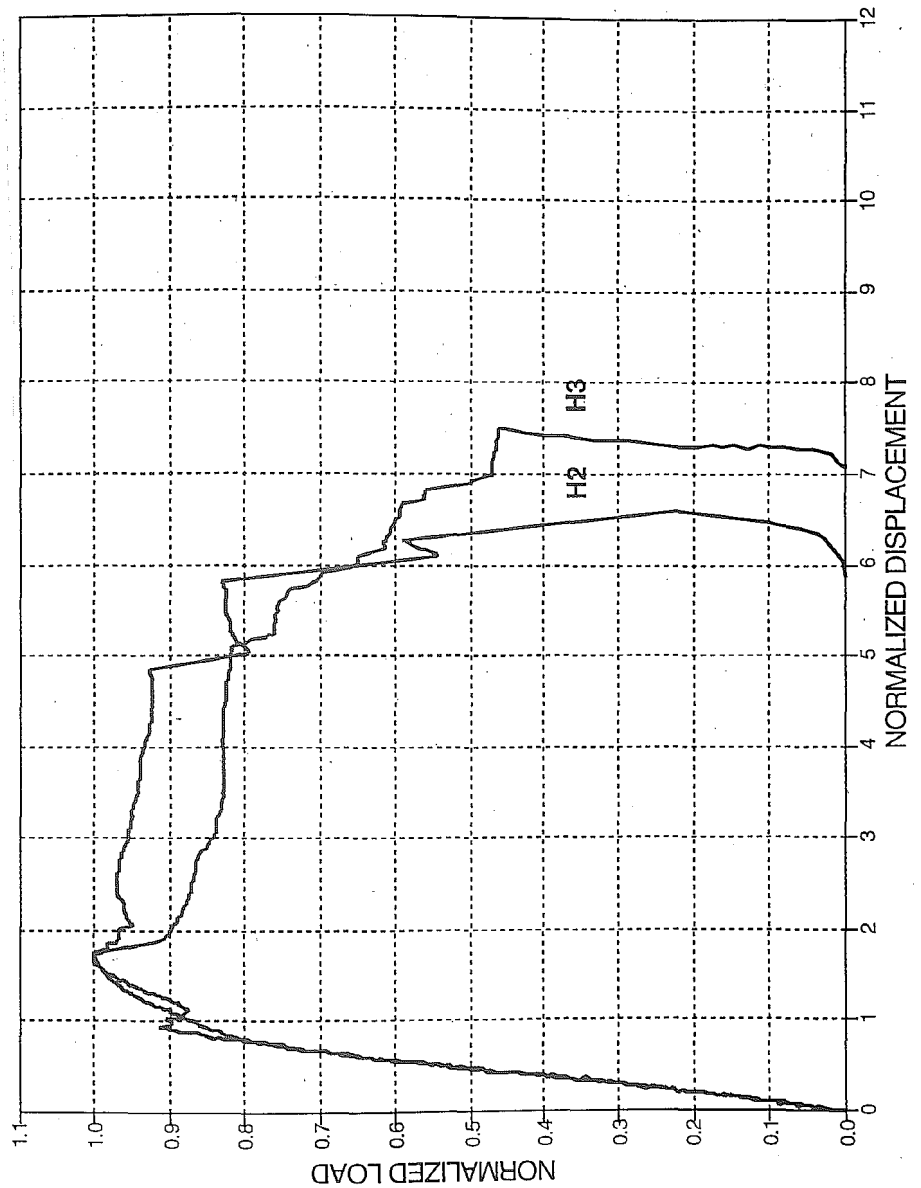

Figure 5.9 Normalized load and displacement-H2 and H3.

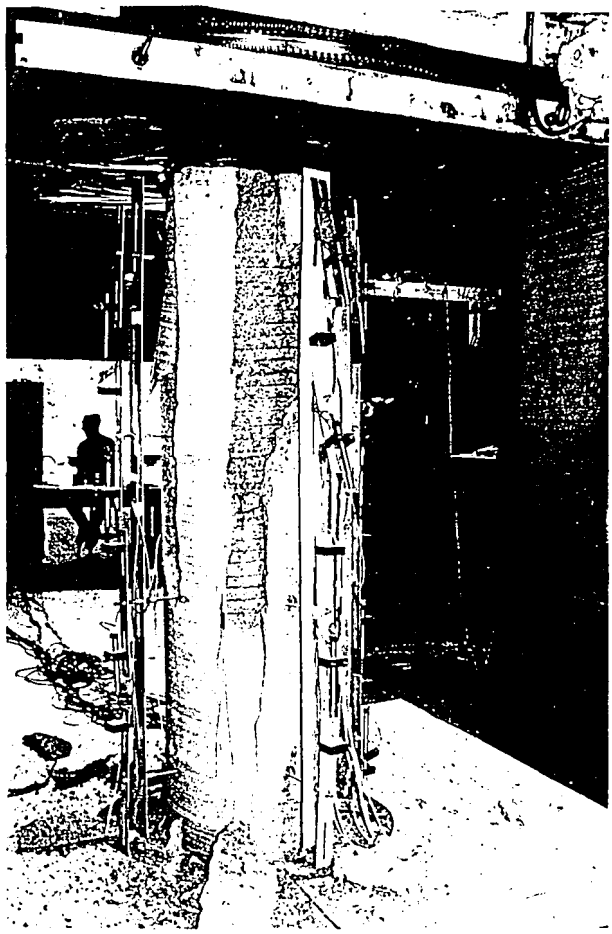

Figure 5.10(a) Series of photographs depicting the behavior of the cover concrete: (a) M-Series specimen.

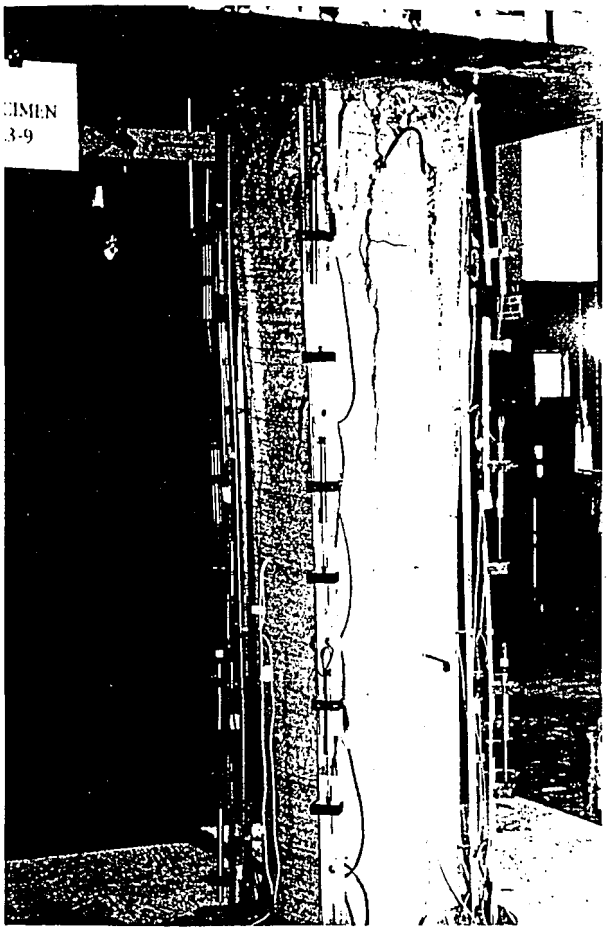

Figure 5.10(b) Series of photographs depicting the behavior of the cover concrete: (b) L-Series specimen.

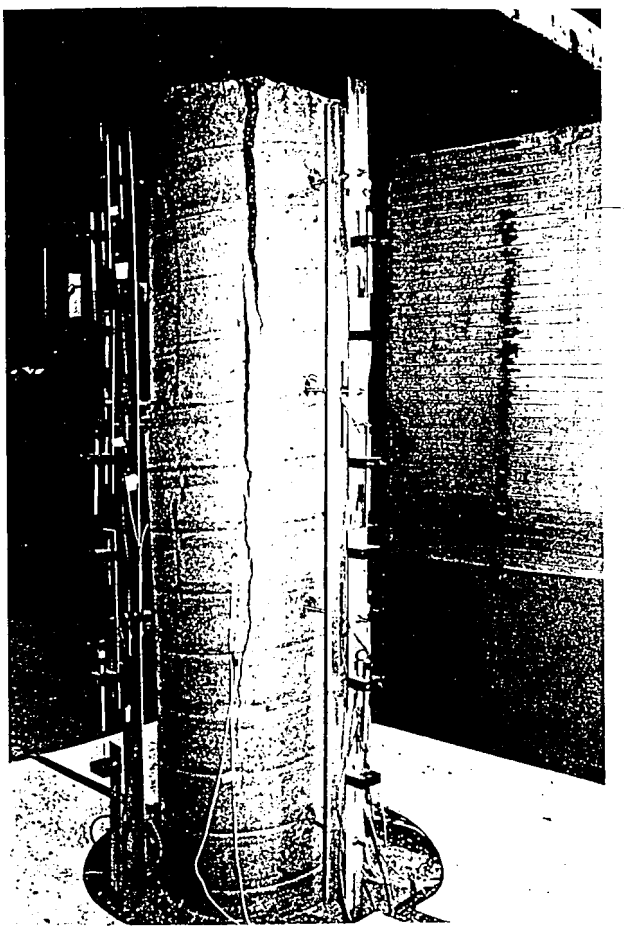

Figure 5.10(c) Series of photographs depicting the behavior of the cover concrete: (c) progression of cracking during testing, M-Series.

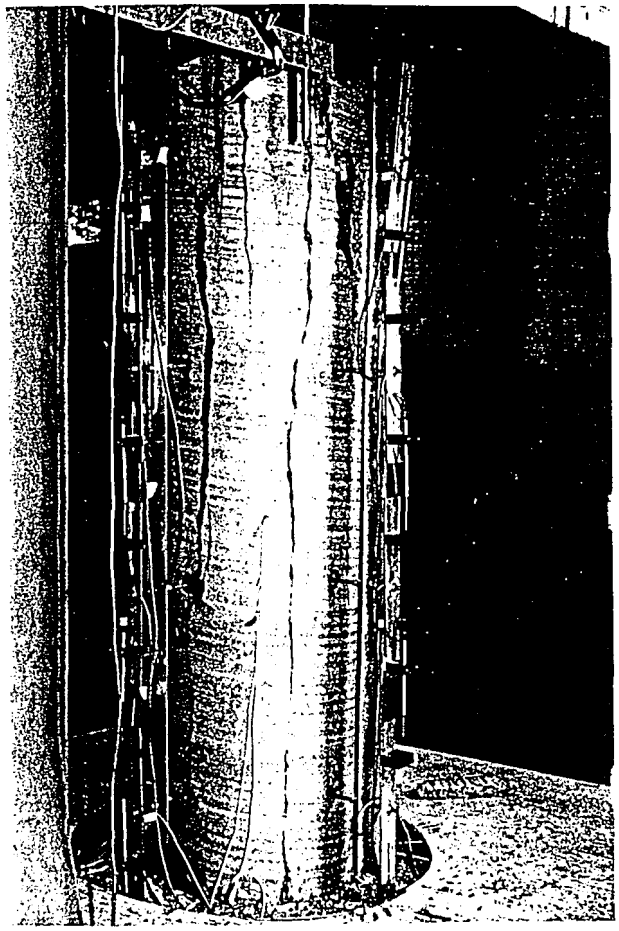

Figure 5.10(d) Series of photographs depicting the behavior of the cover concrete: (d) progression of cracking during testing, M-Series.

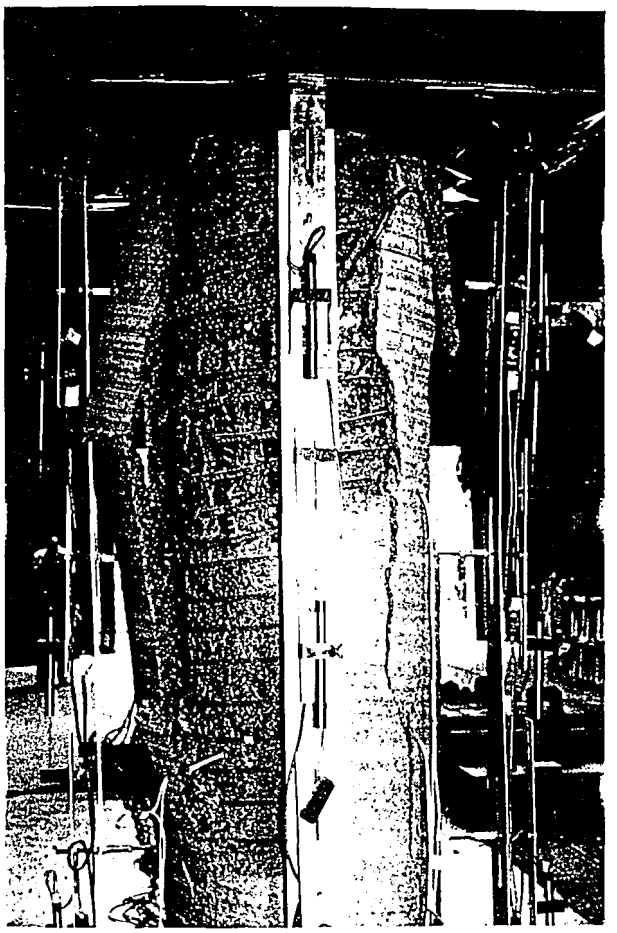

Figure 5.10(e) Series of photographs depicting the behavior of the cover concrete: (e) progression of cracking during testing, M-Series.

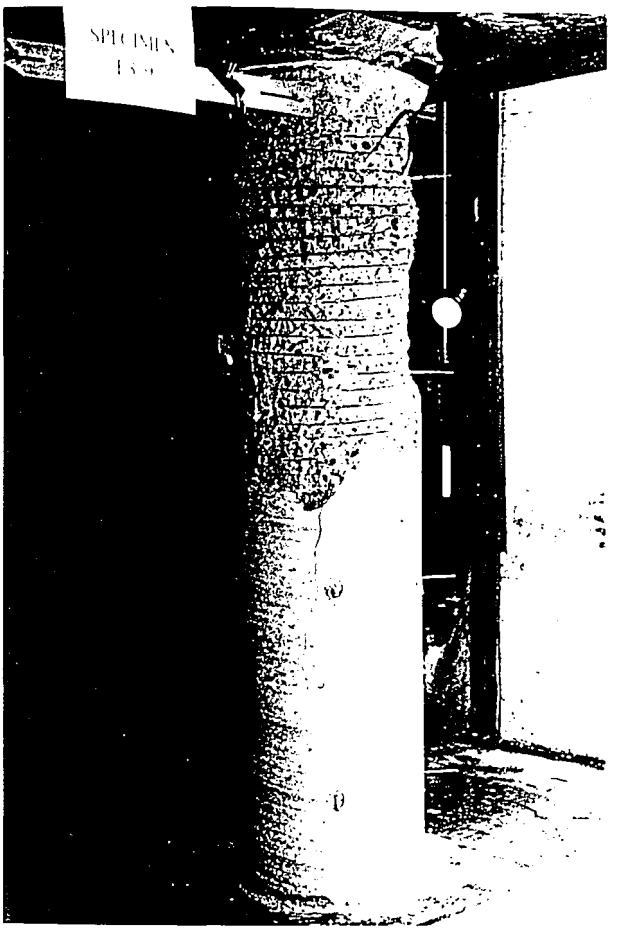

Figure 5.10(f) Series of photographs depicting the behavior of the cover concrete: (f) L-Series specimen at end of test.

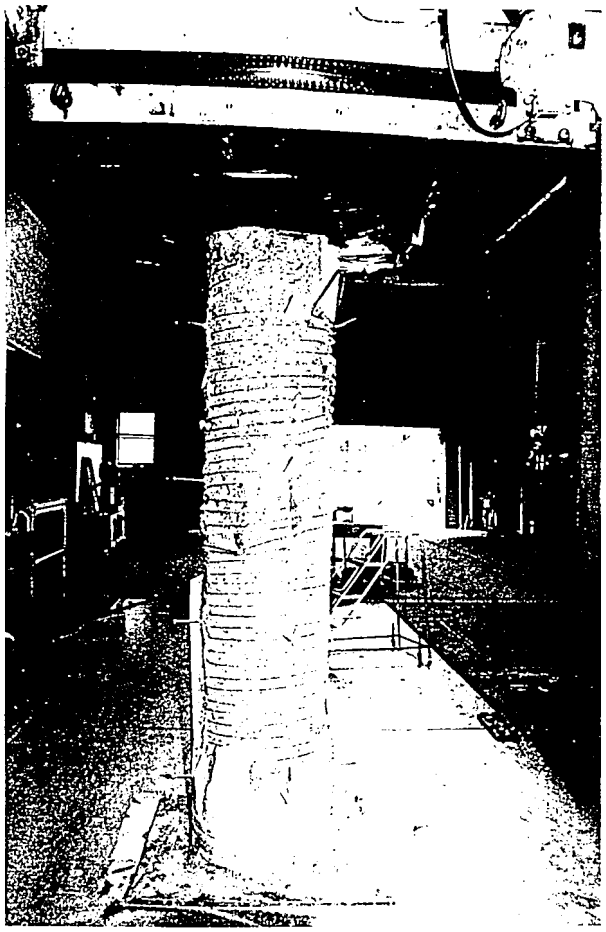

Figure 5.10(g) Series of photographs depicting the behavior of the cover concrete: (g) M-Series specimen at end of test.

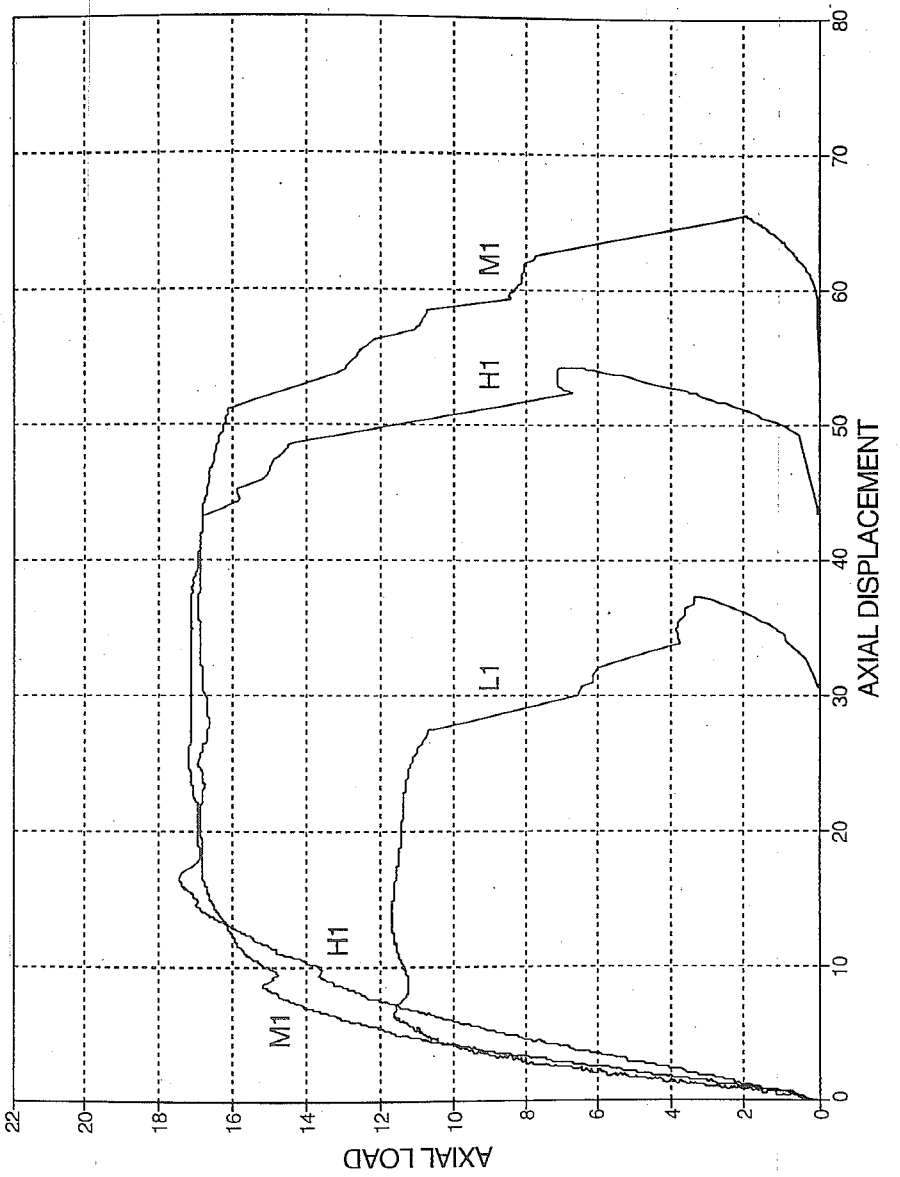

Figure 5.11 Axial load versus axial displacement of columns reinforced with 16-#9 longitudinal bars, Specimens L1, M1, and H1.

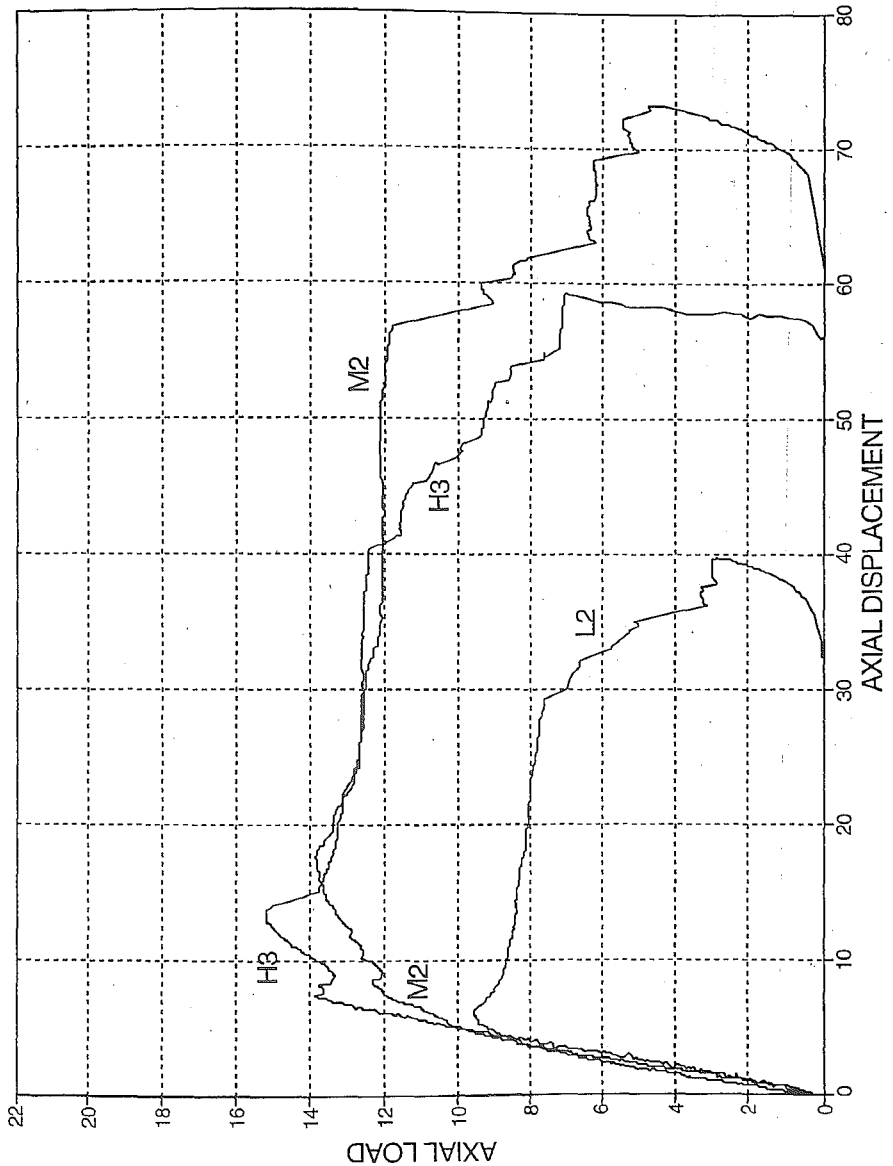

Figure 5.12 Axial load versus axial displacement of columns reinforced with 8-#8 longitudinal bars, Specimens L2, M2, and H3.

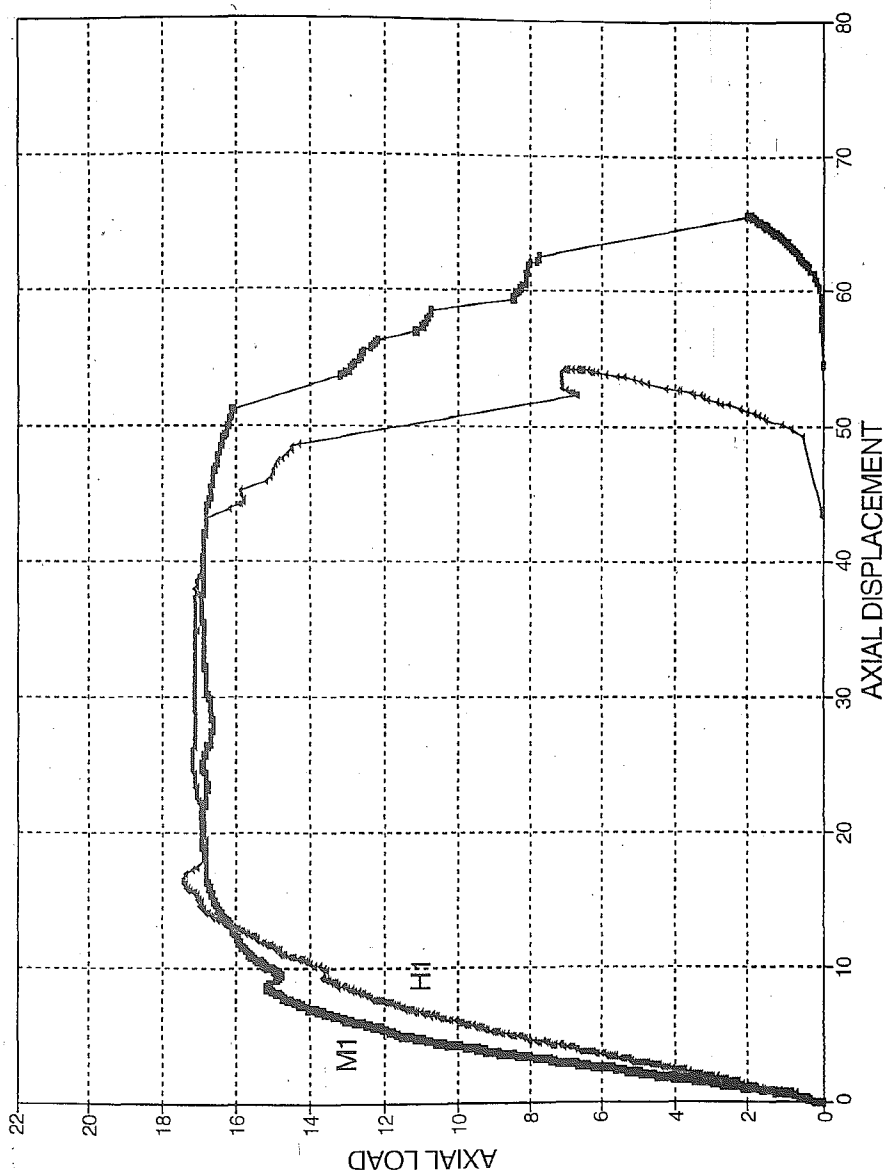

Figure 5.13 Axial load versus axial displacement of columns with a spiral pitch of 64 mm (2.5 in), Specimens M1, and H1.

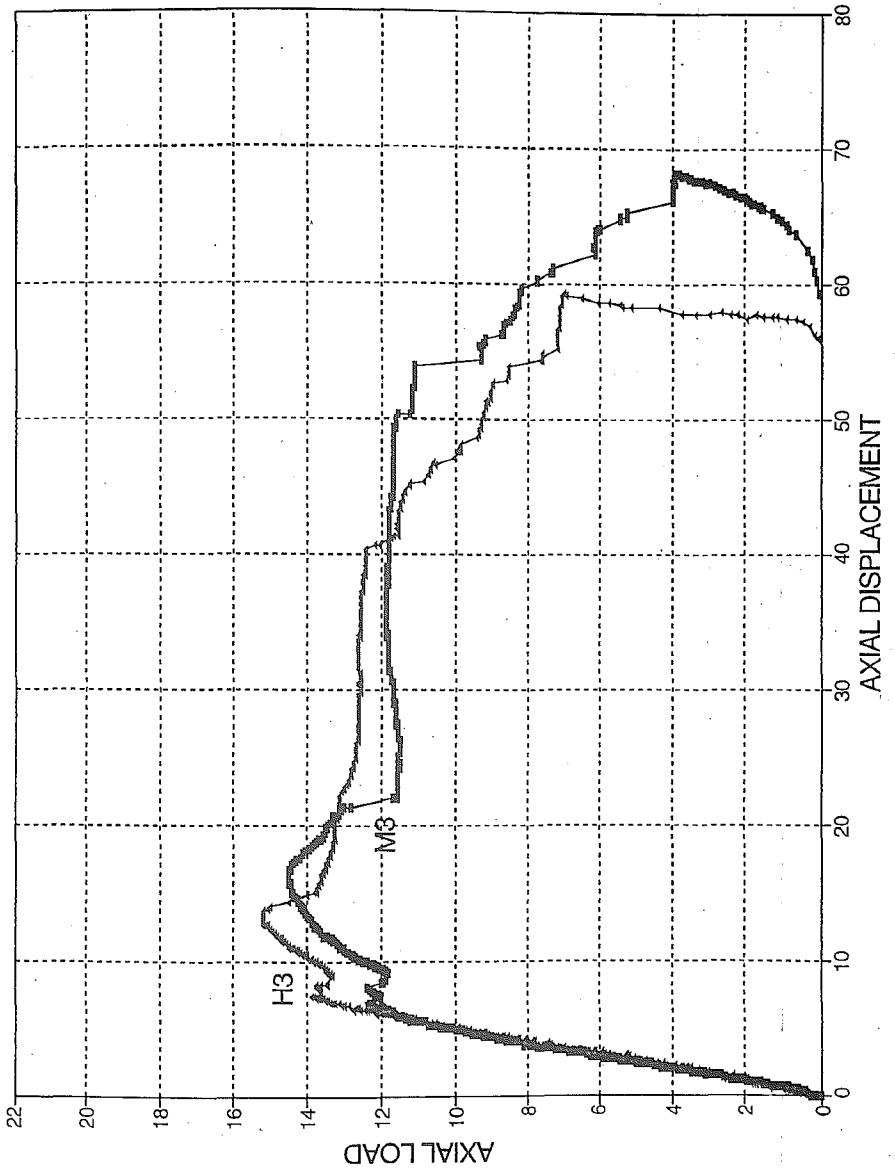

Figure 5.14 Axial load versus axial displacement of columns with a spiral pitch of 41 mm (1.63 in), Specimens M3, and H3.

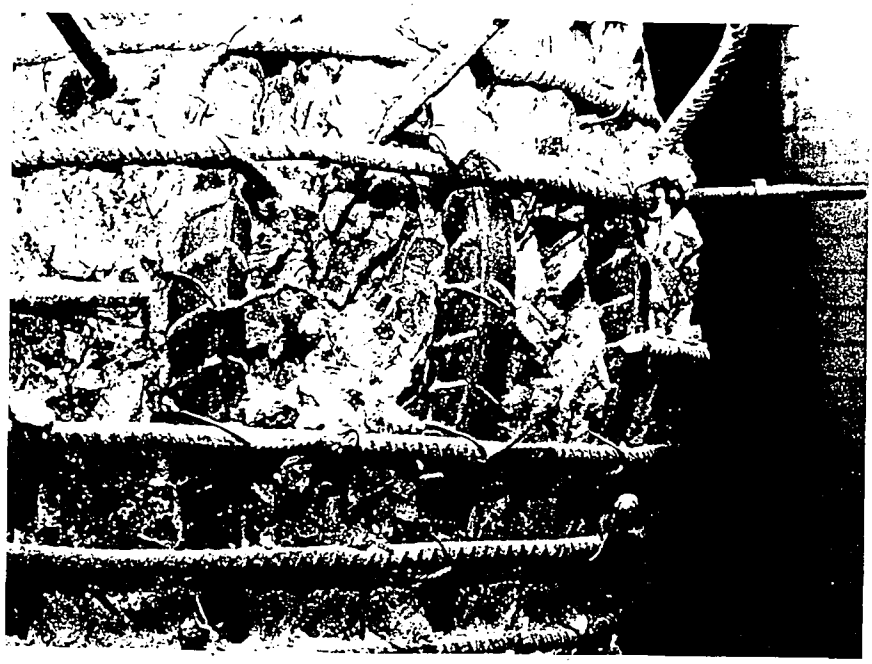

Figure 5.15(a) Photographs depicting the behavior of the spiral reinforcement: (a) L-Series specimen.

Figure 5.15(b) Photographs depicting the behavior of the spiral reinforcement: (b) L-Series specimen.

Figure 5.15(c) Photographs depicting the behavior of the spiral reinforcement: (c) L-Series specimen.

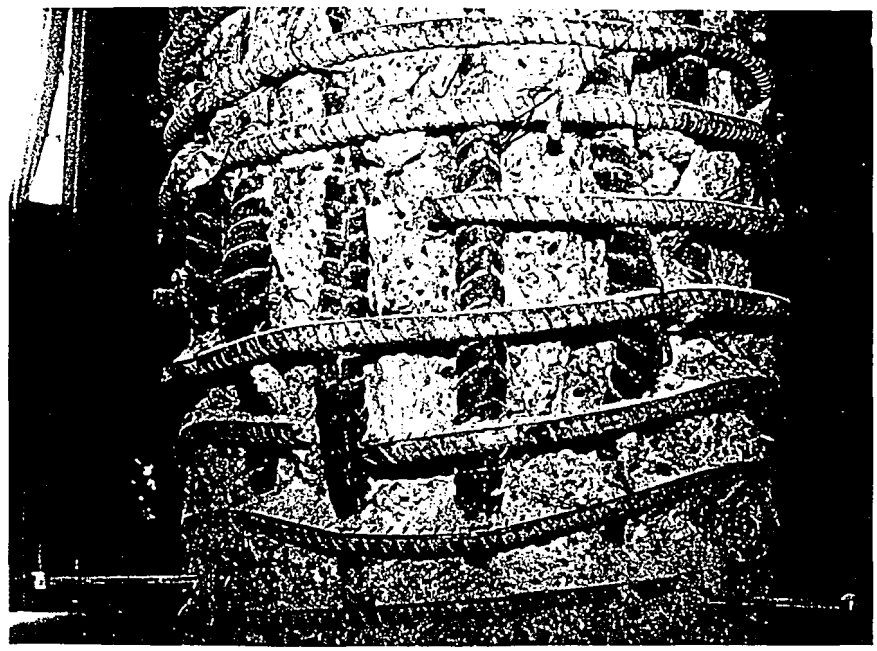

Figure 5.15(d) Photographs depicting the behavior of the spiral reinforcement: (d) M-Series specimen.

Figure 5.15(e) Photographs depicting the behavior of the spiral reinforcement: (e) M-Series specimen.

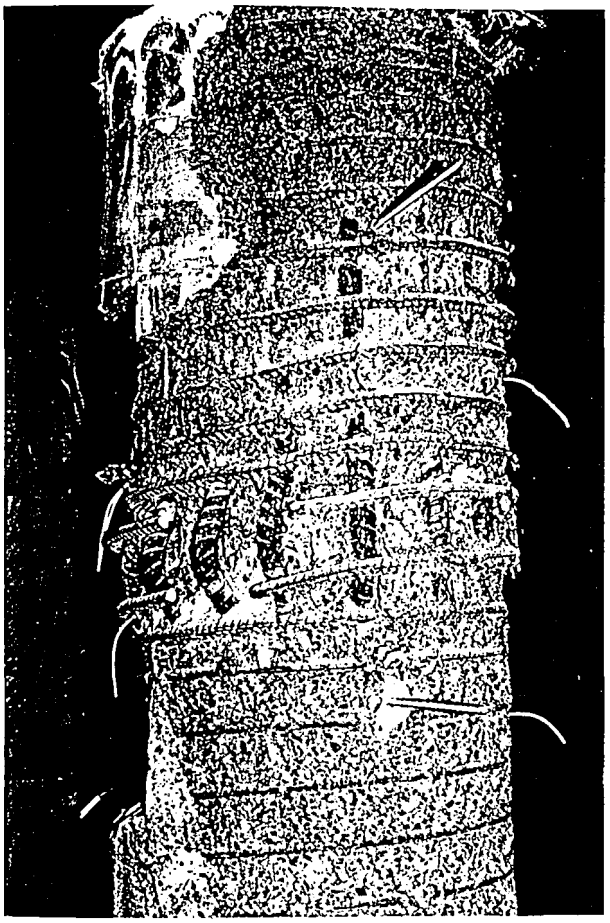

Figure 5.15(f) Photographs depicting the behavior of the spiral reinforcement: (f) H-Series specimen.

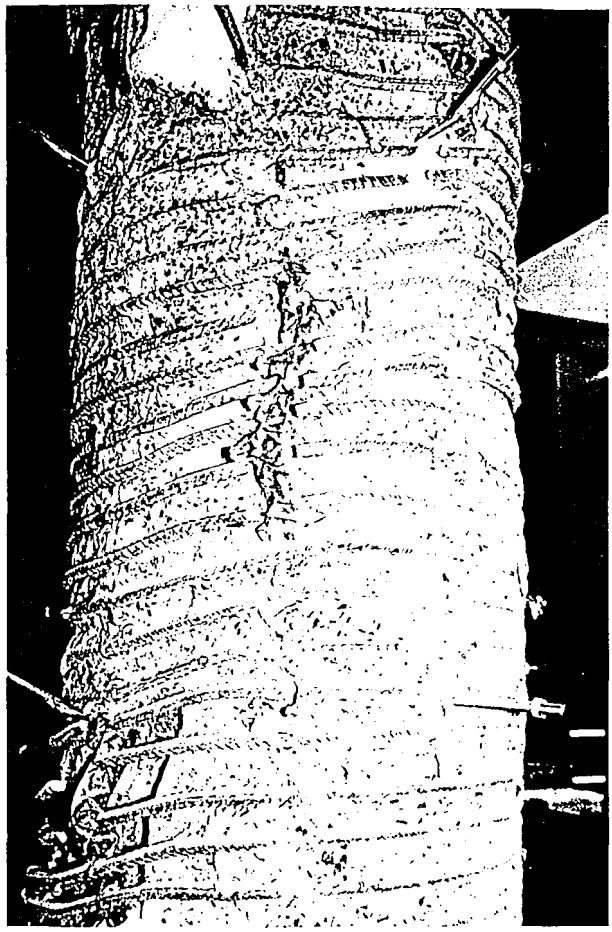

Figure 5.15(g) Photographs depicting the behavior of the spiral reinforcement: (g) M-Series specimen.

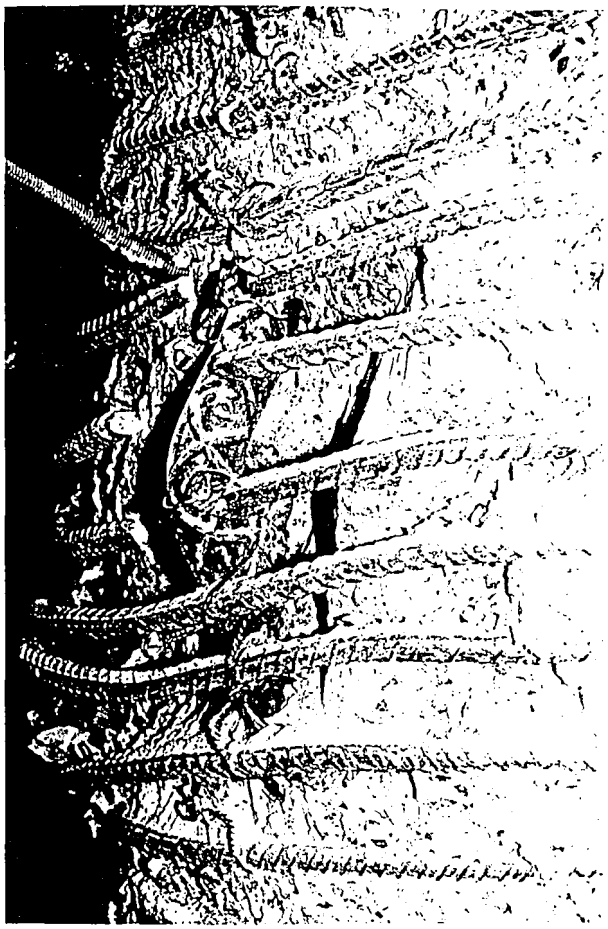

Figure 5.15(h) Photographs depicting the behavior of the spiral reinforcement: (h) M-Series specimen.

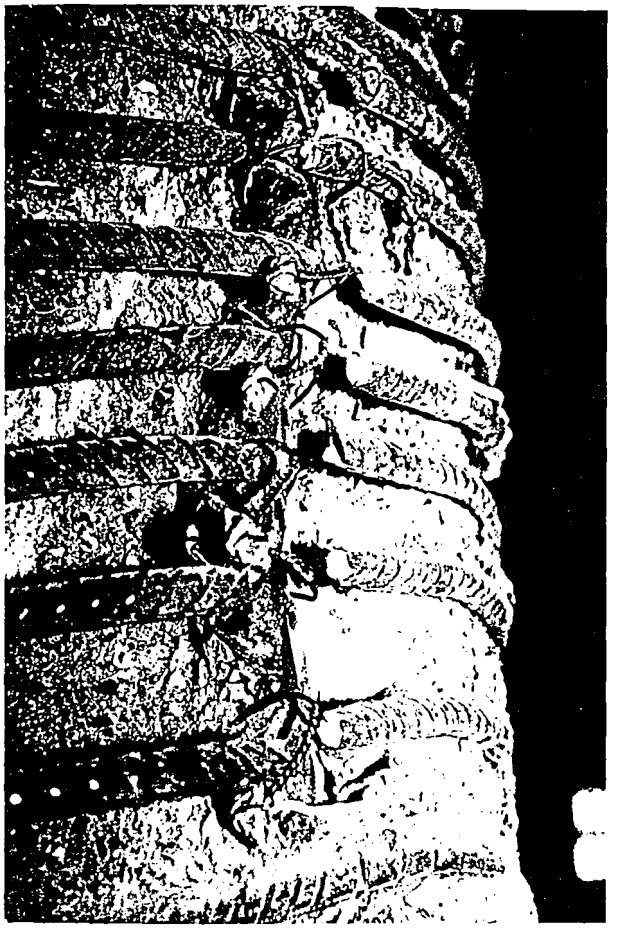

Figure 5.15(i) Photographs depicting the behavior of the spiral reinforcement: (i) M-Series specimen.

CHAPTER 6

SUMMARY, CONCLUSIONS, AND FUTURE RESEARCH

6.1 INTRODUCTION

This chapter summarizes the findings and conclusions from this research. Also included in this chapter is a list of areas which need further research in the future. Section 6.2 summarizes the experimental program. Section 6.3 presents the conclusions from this research, and Section 6.4 outlines areas for future research.

6.2 SUMMARY

Eight large-scale spirally-reinforced columns designed according to ACI 318 Code provisions were tested under concentric axial compression to evaluate the behavior of spirally-reinforced high-strength concrete columns. The experimental program was developed to specifically evaluate the influence of concrete compressive strength, longitudinal reinforcement ratios, and spiral reinforcement size/pitch on column strength and ductility. The results of these 8 tests are presented in Chapter 4 and discussed in Chapter 5.

6.3 CONCLUSIONS

The following conclusions are made from the 8 column tests:

1. A comparison was made between the maximum axial load resisted by each specimen and the predicted axial load capacity of the confined core for each specimen. The following equation by Martinez et al. (1982, 1984) was used to estimate the strength enhancement for the core concrete:

$$f_{cc} = 0.85 f_c' + 4.0 f_2 (1 - \frac{s}{d_c}) \qquad (2.7)$$

Both the field-cured cylinder and cored cylinder concrete compressive strengths were used to compute the predicted strengths (see Equations 4.1 and 4.2), since these concrete strengths were observed to differ considerably, particularly for the high-strength concrete specimens.

It was found that the suitability of the equation presented by Martinez et al. depends on whether the field-cured or cored cylinder concrete compressive strength values are used. If the field-cured strengths $f_{c\text{-field}}$ are used to predict the strength of the confined core, Equation 2.7 can be used to accurately predict column strengths from 34.5 MPa to 52.7 MPa (5 ksi to 7.64 ksi). However, this equation over predicts the column strengths and is therefore unconservative when $f_{c\text{-field}}$ ranges from 75.8 MPa to 82.7 MPa (11.0 ksi to 12.0 ksi). If instead the cored cylinder strengths $f_{c\text{-core}}$ are used to predict the compressive strength of the confined core, then Equation 2.7 provides reasonable agreement to the experimental results.

2. The compressive strength of the concrete was found to influence column ductility. Two displacement ductility values are defined in this report, one based on the displacement at first spiral fracture, and one based on the displacement corresponding to an axial load equal to 85% of P_{max}. For both definitions of ductility, the higher strength concrete columns displayed less ductility than the lower strength concrete columns. This suggests that more than the minimum amount of spiral reinforcement currently prescribed by the ACI 318 Code is needed for high-strength concrete columns to achieve the same ductility as provided in the low-strength concrete columns.

3. Two types of failure modes were observed among the eight specimens tested in this research: (1) bulging until the first spiral fracture; and, (2) formation of an inclined failure plane. The mode of failure seems to depend on the concrete strength. For the columns tested in this research, a bulging type failure mode was observed in the specimens with $f_{c\text{-field}}$ around 34.5 MPa (5 ksi), and an inclined failure plane developed in columns with $f_{c\text{-field}}$ around 51.7 MPa (7.5 ksi) and greater.

4. The amount of reinforcement impacted the behavior of the columns in two related ways. First, it was found that, in general, the 8-#8 longitudinal bar columns exhibited greater ductility than the 16-#9 longitudinal bar columns. This was a surprising result since it was expected that a greater

amount of longitudinal reinforcement would contribute to more effective confinement and thus more overall ductility. It was noted in many of the tests that the spiral reinforcement would fracture directly over a longitudinal bar. It may be that more longitudinal reinforcement did in fact contribute to more effective confinement, but that this also placed a greater demand on the spiral reinforcement, and thus caused and overall reduction in column ductility.

The second way in which the amount of longitudinal reinforcement impacted the behavior of the columns was in the ability of the columns to maintain their peak values of resistance for increasing axial displacements. It was found that the 16-#9 longitudinal bar columns were able to maintain their peak resistances with continued axial displacement much more effectively than the columns with 8-#8 longitudinal bars. For the low-strength concrete columns, this may be a reflection of more effective confinement provided by the greater amount of longitudinal reinforcement. In addition, for the medium- and high-strength concrete columns, it is thought that the 16-#9 longitudinal bars are more effective as dowels in restraining an inclined failure mode that develops in these columns.

5. For the columns tested in this research, a decrease in the size and pitch of the spiral reinforcement, while maintaining a constant volume of spiral reinforcement, lead to a decrease in the ductility of the column. This result,

however, may be attributed to the differences in strain capacity of the different size spiral reinforcement used.

6. The higher strength concrete columns experienced first cracking of the concrete cover at a lower load relative to peak load. It is thought that the larger volume of spiral reinforcement may provide a natural plane of separation between the cover concrete and the core.

6.4 FUTURE RESEARCH

Future research needs to be performed on additional columns to better understand the behavior of large-scale spirally-reinforced high-strength concrete columns. The following is a list of areas of research which will augment the research presented in this report:

1. Investigate the effects of spiral pitch on column ductility in columns reinforced with a high longitudinal steel ratio to prove that the results seen in this study are true for both longitudinal reinforcement ratios.

2. Investigate the difference between member strength and cylinder strength in high-strength concrete specimens to provide a better understanding of the material strengths of the columns in order to predict axial load capacities.

3. Investigate the influence of the number of longitudinal bars on the ductility of the column, and on the shape of the load-displacement curve. This is to determine if more longitudinal reinforcement actually places a greater demand on the spiral reinforcement, thereby reducing the overall ductility of the column. In addition, this will also determine if more longitudinal reinforcement is more effective in restraining the inclined failure mode in the higher strength concretes.

4. Investigate the effects of concrete strengths greater than 69 MPa (10 ksi) on the strength and ductility of columns designed with the ACI spiral.

REFERENCES

ACI Committee 318, "Building Code Requirements for Reinforced Concrete (ACI 318-89) and Commentary ACI 318R-89," ACI, Detroit, 1989.

ACI Committee 363, "State-of-the-Art Report on High Strength Concrete," *Journal of the American Concrete Institute*, ACI, Vol. 81, No. 4, July-August 1984, pp. 364-411.

ACI Committee 363, "State-of-the-Art Report on High Strength Concrete," *Journal of the American Concrete Institute*, Report ACI 363R-92, September 1992, 55 pp.

Annual Book of ASTM Standards, "Standard Practice for Making and Curing Concrete Test Specimens in the Field," C 31-90, ASTM, Philadelphia.

Annual Book of ASTM Standards, "Standard Method of Obtaining and Testing Drilled Cores and Sawed Beams of Concrete," C 42-77, ASTM, Philadelphia.

Annual Book of ASTM Standards, "Practice for Capping Cylindrical Concrete Specimens," C 617, ASTM, Philadelphia.

Ahmad, S. H., and Abdel-Fattah, H., "A Rational Model for the Stress-Strain Relationship of Circular Hoop-Confined Concrete," *Magazine of Concrete Research,* Vol. 43, No. 154, March 1991, pp. 23-28.

Ahmad, S. H., and Shah, S. P., "Stress-Strain Curves of Concrete Confined by Spiral Reinforcement," *Journal of American Concrete Institute*, ACI, Vol. 79, No. 6, November-December 1982, pp. 484-490.

Ahmad, S. H., and Shah, S. P., "Complete Triaxial Stress-Strain Curves for Concrete," *Journal of Structural Engineering,* ASCE, Vol. 108, No. 4, April 1982, pp. 728-742.

Azizinamini, A., Paultre, P., and Saatcioglu, M., "High-Strength Concrete Columns: State of the Knowledge," ASCE Structures Congress, 1993, pp. 444-449.

Bartlett, F. M., MacGregor, J. G., "Effect of Core Length-to-Diameter Ratio on Concrete Core Strengths," *American Concrete Institute Materials Journal*, ACI, Vol. 91, No. 4, July-August 1994, pp. 339-348.

Bjerkeli, L., Tomaszewicz, A., and Jensen, J. J., "Deformation Properties and Ductility of High-Strength Concrete," *Utilization Of High-Strength Concrete-Second International Symposium*, SP-121, ACI, Detroit, 1990, pp. 215-238.

Chan, W. W. L., "The Ultimate Strength and Deformation of Plastic Hinges in Reinforced Concrete Frameworks," *Magazine of Concrete Research*, Vol. 7, No. 21, November 1955, pp. 121-132.

Considere, A., "Resistance a la Compression du Beton Arme et du Beton Frette," Genie Civil, 1903. Also, translation "Experimental Researches on Reinforced Concrete," Moisseiff, L. S., McGraw-Hill Book Company, 1906.

Galeota, D., Giammatteo, M. M., and Marino, R., "Strength and Ductility of Confined High Strength Concrete," *Proceedings of 10th World Conference on Earthquake Engineering,* Madrid, Vol. 5, 1992, pp. 2609-2613.

Hatanaka, S., and Tanigawa, Y., "Lateral Pressure Requirements for Compressive Concrete," *Proceedings of 10th World Conference on Earthquake Engineering,* Madrid, Vol. 5, 1992, pp. 2603-2608.

Itakura, Y., and Yagenji, A., "Compressive Test on High-Strength R/C Columns and Their Analysis Based on Energy Concept," *Proceedings of 10th World Conference on Earthquake Engineering,* Madrid, Vol. 5, 1992, pp. 2599-2602.

Iyengar, K. T. S. R., Desayi, P., Reddy, K. N., "Stress-Strain Characteristics of Concrete Confined in Steel Binders," *Magazine of Concrete Research*, Vol. 22, No. 72, September 1970, pp. 173-184.

Iyengar, K. T. S. R., Desayi, P., Reddy, T. S., "Equation for Stress-Strain Curve of Concrete Confined in Circular Steel Spiral," *Materials and Structures, Research and Testing*, Vol. 11, No. 65, September-October, 1978.

Mander, J. B., Priestley, M. J. N., and Park, R., "Observed Stress-Strain Behavior of Confined Concrete," *Journal of Structural Engineering,* ASCE, Vol. 114, No. 8, August 1988, pp. 1827-1849.

Mander, J. B., Priestley, M. J. N., and Park, R., "Theoretical Stress-Strain Model for Confined Concrete," *Journal of Structural Engineering,* ASCE, Vol. 114, No. 8, August 1988, pp. 1804-1826.

Martinez, S., Nilson, A. H., and Slate, F. O., "Spirally Reinforced High-Strength Concrete Columns," *Journal of American Concrete Institute,* ACI, Vol. 81, No. 5, September-October 1984, pp. 431-442.

Martinez, S., Nilson, A. H., Slate, F. O., "Spirally-Reinforced High Strength Concrete Columns," Research Report No. 82-10, Department of Structural Engineering, Cornell University, Ithaca, New York, August 1982, 255 pp.

MacGregor, J. G., *Reinforced Concrete Mechanics and Design*, Prentice Hall, Enlgewood Cliffs, New Jersey,1988.

Mielich, K., Pessiki, S., "Spirally-Reinforced High Strength Concrete Columns," Final Report, Research Experience for Undergraduates (REU) Program, ATLSS Center/Lehigh University, Summer 1991, 39 pp.

Nagashima, T., Sugano, S., Dimura, H., and Ichidawa, A., "Monotonic Axial Compression Test on Ultra-High-Strength Concrete Tied Columns," *Proceedings of 10th World Conference on Earthquake Engineering,* Madrid, Vol. 5, 1992, pp. 2983-2988.

Nilson, A. H., and Winter, G., *Design of Concrete Structures*,McGraw-Hill, Inc., New York, New York, 11th ed., 1991.

Razvi, S. R., and Saatcioglu, M., "Strength and Deformability of Confined High-Strength Concrete Columns," *American Concrete Institute Structural Journal*, ACI, Vol. 91, No. 6, Novemver-December 1994, pp. 678-687.

Richart, F. E., Brandtzaeg, A., Brown, R. L., "A Study of the Failure of Concrete under Combined Compressive Stresses," University of Illinois Engineering Experiment Station Bulletin No. 185, Urbana, November 1928.

Richart, F. E., Brandtzaeg, A., Brown, R. L., "The Failure of Plain and Spirally Reinforced concrete in Compression," University of Illinois Engineering Experiment Station Bulletin No. 190, Urbana, April 1929, 73 pp.

Saatcioglu, M. and Razvi, S. R., "Behavior of Confined High-Strength Concrete Columns," Proceedings from the 1993 CSCE/CPCA Structural Concrete Conference, Toronto, Ontario, May 19-21, 1993, pp. 37-50.

Saatcioglu, M., and Razvi, S. R., "Strength and Ductility of Confined Concrete," *Journal of Structural Engineering,* ASCE, Vol. 118, No. 6, June 1992, pp. 1590-1607.

VITA

Annette M. Pieroni was born in Reading, Pennsylvania on the 17th of April, 1971 and raised in Schnecksville, Pennsylvania. She is the fifth child of Ralph and Mirella Pieroni. After graduating from Parkland Senior High School in Orefield Pennsylvania in May of 1989, she attended the Pennsylvania State University in State College. She earned the degree of Bachelor of Science in Civil Engineering from Penn State in May of 1993. In September of that year she began her graduate education at Lehigh University, where she conducted her research at the Center for Advanced Technology for Large Structural Systems.

END OF TITLE